

The chromatin remodeller Chd7 and the calcium ATPase Serca2 - adding new facets to the role of Notch in Hematopoiesis and T-ALL

THÈSE N° 6615 (2015)

PRÉSENTÉE LE 15 MAI 2015

LA FACULTÉ DES SCIENCES DE LA VIE

UNITÉ DU PROF. RADTKE

PROGRAMME DOCTORAL EN APPROCHES MOLÉCULAIRES DU VIVANT

ÉCOLE POLYTECHNIQUE FÉDÉRALE DE LAUSANNE

POUR L'OBTENTION DU GRADE DE DOCTEUR ÈS SCIENCES

PAR

Monique COERSMEYER

acceptée sur proposition du jury:

Prof. O. Hantschel, président du jury

Prof. F. Radtke, directeur de thèse

Prof. M. Lütolf, rapporteur

Prof. M. Manz, rapporteur

Dr A. Wilson, rapporteuse



ÉCOLE POLYTECHNIQUE
FÉDÉRALE DE LAUSANNE

Suisse
2015

Abstracts

Project I: Chd7 Deficiency does not affect N1-driven T-ALL Induction and Maintenance nor impair Hematopoiesis

Notch1 has been shown to be a key driver in pediatric T-cell acute lymphoblastic leukemia (T-ALL), and over-expression of the intracellular domain of Notch1 (NICD) in murine bone marrow (BM) progenitors induces T-ALL. Previous work in the lab identified the chromatin-remodeling enzyme Chd7 to be highly over-expressed in aggressive versus pre-malignant disease. The aim of this project was to study if Chd7 is required during T-ALL initiation and disease maintenance as well as to characterize its role in the hematopoietic system under physiological and stress conditions. Therefore, *Chd7* conditional knock out (cKO) animals were crossed with the MxCre deleter to ablate *Chd7* specifically in BM progenitors. *Chd7* deficiency did not induce any overt phenotype in the hematopoietic system, when studied under “steady” state or stress conditions in competitive BM chimeras, upon serial transplantation or due to 5-FU-mediated hematopoietic stem cell (HSC) mobilization. In addition, Chd7 was studied in (i) the retroviral MigR1-NICD and (ii) in the genetic RNIC murine T-ALL induction models. In both models MxCre, targeting BM progenitors, and CD4Cre transgenic mice, targeting thymic progenitors at the DN3b-DN4 stage of maturation, were used to inactivate *Chd7*. Chd7 proved to be dispensable in the initiation and maintenance of murine Notch1-driven T-ALL. Similarly, knock down of *CHD7* in human T-ALL did not impact on survival or proliferation of T-ALL cell lines. Therefore, we can rule out a role of Chd7 during late-stage leukemogenesis in Notch1-induced murine and human T-ALL.

Project II: Serca2, a putative drug target to fight Notch1-driven T cell acute lymphoblastic leukemia, and its role in Hematopoiesis

Aberrant activation of Notch signalling has been implicated in many different aspects of human cancer such as hyperproliferation, invasiveness and angiogenesis. Therefore, the Notch signalling pathway represents a bona fide drug target. We and Roti *et al.* performed a chemical compound screen and identified Cyclopiazonic acid (CPA) to be a potent Notch inhibitor. Biological target of this compound is the Sarco/Endoplasmic Reticulum ATPase2 (Serca2) that is involved in calcium homeostasis within the cell. Recently, it was shown that Serca2 regulates Notch1 (N1) receptor maturation and inhibition of Serca ATPases, using thapsigargin, blocks T-ALL progression in xenografts (Roti *et al.*, 2013). The putative global effects of Serca2 inhibition on hematopoiesis have, however, not been addressed in this study.

Aim of this study was to characterize the function of Serca2 in the hematopoietic system. Therefore, we crossed *Serca2* conditional knock out (cKO) with MxCre recombinase Tg mice to ablate *Serca2* function in BM progenitors. *Serca2* haploinsufficiency did not lead to any overt phenotype under physiological or competitive conditions studied upon 5-FU administration, serial transplantation and in mixed BM chimeras. In contrast, *Serca2*^{ΔMxCre} chimeras showed (i) impaired long-term reconstitution capacity upon transplantation, (ii) a severe reduction of total BM, splenic and thymic cellularity and (iii) an enrichment of Lineage-CD117⁺Sca1⁺ (KLS) cells,

the cell pool that contains HSCs. Mature lineages were highly apoptotic, while KLS cells were not majorly affected by apoptosis. These cells resided predominantly in G₀ phase of the cell cycle (Hoechst-Ki-67 staining) and exhibited significantly slower cycling kinetics (CFSE division tracking). In addition, *Serca2*^{AMxCre} KLS cells were functionally impaired as they formed significantly less and smaller colony forming units (CFUs) *in vitro*. Deregulated intracellular calcium levels can lead to an accumulation of unfolded proteins in the ER, a phenomenon called ER stress. In order to resolve ER stress, the cell activates the unfolded protein response (UPR), thereby inducing chaperones to counter-balance the impaired folding capacity. In case of unresolved ER stress, however, the cell undergoes apoptosis. We demonstrate that mature hematopoietic lineages up-regulate UPR-associated and pro-apoptotic genes, while KLS cells, in contrast, show unperturbed expression of these genes. In addition, we performed *in vitro* experiments, inhibiting *Serca* function in MACS enriched Lin⁻ BM cells via thapsigargin (TH) treatment. Upon prolonged treatment, TH induced severe apoptosis in the overall cell population, while KLS accumulated and were blocked in the G₀ phase of the cell cycle, closely mimicking *Serca2* LOF *in vivo*.

Therefore, we showed for the first time, that targeting *Serca2* in the BM leads to (i) induction of apoptosis in mature lineages through activation of UPR, while (ii) KLS are, to some extent, more resistant to ER stress and undergo cell cycle arrest. We therefore question the therapeutic approach of targeting *Serca2* in Notch1-driven T-ALL due to severe side effects induced by *Serca2* inactivation in the BM.

Keywords: Notch, T-ALL, Chd7, *Serca2*, HSC

Zusammenfassung

Projekt I: Chd7 Inaktivierung beeinflusst weder die Entstehung noch Erhaltung Akuter T-Zell Lymphoblastischer Leukämie oder Hämatopoese

Akute T-Zell Lymphoblastische Leukämie (T-ALL) betrifft hauptsächlich Kinder und Jugendliche und liegt in mehr als 50% der Fälle einer Überaktivierung des Notch Signalwegs zu Grunde. Experimentell wurde in Mäusen gezeigt, dass Expression der intrazellulären Domäne des Notch1 Rezeptors (NICD) nach Transplantation zu T-ALL Entwicklung führt. In einer früheren Studie wurden solche murinen T-ALL Modelle verglichen, um Kandidaten-Moleküle zu identifizieren, die potenziell mit Notch in der Entwicklung von T-ALL kooperieren. Chd7, ein Chromatin remodellierendes Enzym, wurde dabei in aggressiver (*RNIC⁺/Δ^{Lck}Cre*) im Vergleich zu milder Vorläufer (*RNIC⁺/Δ^{Mx}Cre*) T-ALL identifiziert.

Ziel dieser Doktorarbeit war es die Funktion von Chd7 in T-ALL aber auch im hämatopoietischen System generell zu studieren. Transgene konditionelle knock out (cKO) Mäuse für *Chd7* wurden mit *MxCre* gekreuzt, um *Chd7* spezifisch im Knochenmark zu deletieren. Chd7 spielte keine Rolle in der Regulierung von Hämatopoese unter physiologischen oder „Stress“ Bedingungen, wie serielle Transplantation oder 5-FU Injektionen gezeigt haben. Chd7 wurde ebenfalls in den zwei unterschiedlichen (i) Retroviralen MigR1-NICD und (ii) Genetischen RNIC T-ALL Initiationsmodellen studiert. Weder die Inaktivierung von *Chd7* in BM Progenitoren (*MxCre*), noch die Deletion in Progenitoren im Thymus (*CD4Cre*) haben eine Rolle bei der Entwicklung von T-ALL in diesen Modellsystemen gespielt. Ebenso hatte die Inaktivierung von *Chd7* weder Konsequenzen für T-ALL im genetischen RNIC Modell, noch in etablierten humanen T-ALL Zelllinien. Somit zeigen unsere Studien, dass Chd7 keine bedeutende Rolle in der Entwicklung von T-ALL spielt.

Projekt II: Die Rolle von Serca2, einem potenziellen Zielmolekül zur Therapie von Notch1-induzierter Akuter T-Zell Lymphoblastischer Leukämie, in Hämatopoese

In vielen Krebsarten ist die Notch Signalkaskade überaktiviert, was auf das Wachstum, die Metastasierung und den Metabolismus einer Krebszelle unterstützend wirkt. Deshalb stellt der Notchrezeptor ein prominentes Zielmolekül auf der Suche nach neuen Therapiemöglichkeiten in der Krebsforschung dar. In unserer Forschungsgruppe wurde ein initialer Arzneimittel Screen durchgeführt, um neue chemische Moleküle, die Notch-inhibierende Wirkung haben, zu identifizieren. Zeitgleich folgten Roti *et al.* unserem Beispiel und führten einen ähnlichen Screen durch, um Inhibitoren für Notch aber auch Gen-Kandidaten zu finden, die mit onkogenem Notch interagieren. Interessanter Weise haben beide Ansätze zur Identifikation derselben Moleküle geführt, der cyclopiazonic acid (CPA) und Thapsigargin (TH), die die Funktion von Kalzium ATPasen des Sarko/Endoplasmatischen Retikulums (Sercas) hemmen. Als Notch Interaktionspartner wurde Serca2 aus der Familie der Sercas als potenzielles intermediäres Zielmolekül identifiziert, um Notch in akuter T-Zell Leukämie (T-ALL) zu inhibieren (Roti *et al.*).

Diese Studien zeigten zwar, dass *Serca2* in der Tat den Notch1 Rezeptor strukturell reguliert und sich *Serca2* Inhibierung positiv auf T-ALL Fortschreitung auswirkt, allerdings wurde nicht geklärt, welche potenziellen globalen Nebenwirkungen eine Inhibierung von *Serca2* auf das blutbildende System haben kann.

Daher war es Ziel dieser Doktorarbeit, die Funktion von *Serca2* im hämatopoietischen System zu untersuchen. Mit Hilfe von transgenen Mäusen, die es erlauben das *Serca2* Gen spezifisch im Knochenmark zu deletieren, haben wir die Rolle von *Serca2* unter normalen homeostatischen Bedingungen aber auch unter hämatologischem Stress studiert. Deletion von einem *Serca2* Allele führte dabei zu keinem merklichen Phänotyp im hämatopoietischen System; ebenso nicht unter kompetitiven Bedingungen wie zum Beispiel nach 5-FU Injektionen oder serieller Transplantation. In Kontrast dazu, führt der Verlust von beiden *Serca2* Allelen zu einem drastischen Phänotyp: (i) *Serca2*-defiziente Knochenmarkszellen sind nicht nachhaltig transplantierbar; (ii) lymphoide Organe wie der Thymus, die Milz aber auch das Knochenmark weisen verringerte Zellzahlen auf während (iii) hämatopoietische Stammzellen (HSC) anormal hoch sind in ihrer Anzahl. Nähere Analysen zeigten, dass ausdifferenzierte Effektorzellen des Immunsystems stark apoptotisch waren, während die vorwiegend in der Phase G_0 des Zellzyklus vorzufinden waren (Ki-67-Höchst Färbung) oder *in vitro* vergleichend langsamer proliferierten (CFSE Färbung).

Ein unbalanzierter Kalziumgehalt im Inneren der Zelle kann dazu führen, dass Proteine im ER nicht mehr effizient ihre dreidimensionale Struktur einnehmen können. Es kommt zur fehlerhaften Faltung der Proteine, was der Zelle eine "Stress"-Meldung sendet. Daraufhin, wird der Signalweg der Unfolded Protein response (UPR) aktiviert, um der fehlerhaften Proteinfaltung entgegen zu wirken. Ist dies allerdings ohne Erfolg, entscheidet sich die Zelle für den programmierten Zelltod (Apoptose). Gen Expressions Analysen zeigten, dass differenzierte hämatopoietische Zellen sensitiver auf *Serca2* Inaktivierung reagieren und apoptotisch waren im Gegensatz zu HSCs, die im Zellzyklus in der Phase G_0 "blockiert" sind. Komplementäre Studien *in vitro* demonstrierten, dass das potenzielle Krebsmedikament TH ähnliche Effekte auf wild-typ (WT) Knochenmarkszellen hat. Somit zeigen wir in dieser Arbeit, dass *Serca2* ein bedenkliches neues Zielmolekül in der Krebstherapie darstellt, da Inhibierung von *Serca2* im hämatopoietischen System zu starken Nebenwirkungen führt.

Schlüsselworte: Notch, T-ALL, Chd7, *Serca2*, HSC

Acronyms and Abbreviations

BM	bone marrow
bp	base pairs
CD	cluster of differentiation
cDNA	complementary desoxyribonucleic acid
CDS	coding sequence
CFU	colony forming unit
CFSE	carboxyfluorescein succinimidyl ester
CHD	Chromodomain-helicase-DNA-binding
cKO	conditional knockout
DN	dominant negative
DNA	desoxyribonucleic acid
DP	double positive
ER	endoplasmatic reticulum
FACS	fluorescence activated cell sorting
FC	fold change
FSC	forward scatter
GOF	gain-of-function
GSI	γ secretase inhibitor
HBSS	Hank's balanced salt solution
HSC	Hematopoietic stem cell
IFN α	interferon alpha
IRES	internal ribosome entry site
kb	kilo base (=1000 bp)
kDa	kilo Dalton
KO	knockout
LOF	loss-of-function
lox	locus of crossing over
LT-HSC	long-term repopulating HSC
mRNA	messenger RNA
NGFR	nerve growth factor receptor

NICD	Notch1 intracellular domain
PBL	peripheral blood lymphocyte
PCR	polymerase chain reaction
PIC	polyinosinic:polycytidylic acid
qRT-PCR	quantitative real time PCR
RNA	ribonucleic acid
RT	room temperature
SD	standard deviation
SERCA	Sarco-endoplasmatic reticulum ATPase
shRNA	small hairpin RNA
SM	staining medium
SSC	side scatter
T-ALL	T cell acute lymphoblastic leukemia
TCR	T cell receptor
UPR	unfolded protein response
UTR	untranslated region
WBC	white blood cell
WT	wild type

Gene Nomenclature

<i>Chd7, Serca2</i>	mouse gene, cDNA, mRNA
Chd7, Serca2	mouse protein
<i>CHD7, SERCA2</i>	human gene, cDNA, mRNA
CHD7, SERCA2	human protein

Table of Contents

ABSTRACTS	I
ZUSAMMENFASSUNG	III
ACRONYMS AND ABBREVIATIONS	VII
GENE NOMENCLATURE	VIII
TABLE OF CONTENTS	IX
1 INTRODUCTION	1
1.1 HEMATOPOIESIS AND THE IMMUNE SYSTEM.....	1
1.2 HSCs IN THE ADULT HEMATOPOIETIC SYSTEM	3
1.3 T CELL DEVELOPMENT IN THE THYMUS.....	6
1.4 THE CANONICAL NOTCH SIGNALLING PATHWAY.....	6
1.4.1 Notch Signalling in Hematopoietic Stem Cells.....	9
1.4.2 Notch Signalling in T Cell and MZB Cell Development.....	10
1.4.3 Notch Signalling in T cell Acute Lymphoblastic Leukemia (T-ALL).....	11
1.5 CHROMATIN REMODELLERS AS REGULATORS OF GENE EXPRESSION	12
1.5.1 Chromodomain-Helicase-DNA binding Proteins	15
1.5.2 Identification of Chd7 in a Microarray Screen comparing early versus late-stage Notch1-driven T-ALL.....	17
1.5.3 Chd7 in Development and Disease.....	20
1.6 CALCIUM SIGNALLING	22
1.6.1 Calcium Levels, ER stress and Unfolded Protein Response.....	23
1.6.2 Calcium Signalling and ER Stress in Hematopoietic Stem Cells.....	26
1.6.3 Identification of Serca2 as potential Drug Target in Notch1-driven T-ALL	27
1.6.4 Sarco-Endoplasmatic Reticulum Calcium ATPases (Sercas).....	28
1.6.5 Serca2 in Development and Disease.....	29
2 OBJECTIVES OF THIS WORK	35
2.1 PART I: ROLE OF CHD7 IN THE HEMATOPOIETIC SYSTEM AND IN T-ALL.....	35
2.2 PART II: ROLE OF SERCA2 IN THE HEMATOPOIETIC SYSTEM	35
3 RESULTS – PART I: ROLE OF CHD7 IN HEMATOPOIESIS & T-ALL	37

3.1	VALIDATION OF POTENTIAL MEDIATORS COOPERATING WITH NOTCH1 IN T-ALL	37
3.2	FUNCTIONAL CHARACTERIZATION OF CHD7 IN HEMATOPOIESIS.....	38
3.2.1	Chd7 Deficiency does not affect Hematopoiesis under Steady State Conditions.....	38
3.2.2	Chd7 Deficiency does not affect on Hematopoiesis under Competitive Conditions upon Serial Transplantation.....	41
3.3	CHD7 DEFICIENCY DOES NOT AFFECT NOTCH1-DRIVEN MURINE T-ALL	47
3.3.1	Chd7 is highly expressed in murine Notch-driven T-ALL	47
3.3.2	Chd7 Deficiency does not affect T-ALL Initiation	48
3.4	CHD7 DEFICIENCY DOES NOT AFFECT NOTCH1-DRIVEN HUMAN T-ALL.....	54
3.4.1	Chd7 is expressed in human T-ALL cells	54
3.4.2	Chd7 does not regulate Cell Cycle, Apoptosis or Proliferation of human T-ALL cells	55
4	DISCUSSION PART I: ROLE OF CHD7 IN HEMATOPOIESIS & T-ALL	59
4.1	VALIDATION OF POTENTIAL MEDIATORS COOPERATING WITH NOTCH1 IN T-ALL	59
4.2	FUNCTIONAL CHARACTERIZATION OF CHD7 IN HEMATOPOIESIS.....	60
4.3	CHD7 DOES NOT AFFECT NOTCH1-DRIVEN MURINE T-ALL.....	61
4.4	CHD7 DOES NOT AFFECT NOTCH1-DRIVEN HUMAN T-ALL.....	63
5	RESULTS – PART II: ROLE OF SERCA2 IN HEMATOPOIESIS	65
5.1	EXPRESSION OF SERCA FAMILY MEMBERS IN THE HEMATOPOIETIC SYSTEM.....	66
5.2	CONSEQUENCES OF SERCA2 HAPLOINSUFFICIENCY IN THE HEMATOPOIETIC SYSTEM	67
5.3	CONSEQUENCES OF SERCA2 LOF IN THE HEMATOPOIETIC SYSTEM.....	67
5.3.1	Genetic Ablation of Serca2 impairs Hematopoiesis.....	68
5.3.2	Genetic Ablation of both Serca2 alleles leads to Apoptosis of Mature Lineages due to ER stress and activation of UPR.....	73
5.3.3	Genetic Ablation of Serca2 negatively affects the HSC compartment.....	75
5.3.4	Enrichment of KLS in Serca2 cKO Animals 1 week post MxCre Induction is not due to Interferon α -induced Mobilization of HSCs	77
5.3.5	Serca2-deficient KLS form less and smaller CFUs	82
5.3.6	Serca2-deficient KLS cells are not driven into Apoptosis but have a Cell Cycle Defect	83
5.4	THAPSIGARGIN TREATMENT MIMICS SERCA2 LOF <i>IN VITRO</i>	90
5.4.1	Thapsigargin induces Apoptosis of Total MACS enriched Lineage negative Cells <i>in vitro</i>	91
5.4.2	Thapsigargin induces an enrichment of the KLS population <i>in vitro</i>	92

5.4.3 Thapsigargin does not induce Apoptosis in KLS cells but deregulates their Cell Cycle *in vitro* 93

6	DISCUSSION PART II: ROLE OF SERCA2 IN HEMATOPOIESIS	97
6.1	FUNCTIONAL CHARACTERIZATION OF LOSS OF ONE SERCA2 ALLELE IN THE HEMATOPOIETIC SYSTEM	
	97	
6.2	FUNCTIONAL CHARACTERIZATION OF SERCA2 LOSS OF FUNCTION IN THE HEMATOPOIETIC SYSTEM	
	98	
6.3	THAPSIGARGIN TREATMENT MIMICS SERCA2 LOF <i>IN VITRO</i>	102
7	MATERIAL AND METHODS	106
7.1	MOUSE WORK	106
7.1.1	Experimental Mice.....	106
7.1.2	Poly(I)-poly(C): Preparation and Administration	107
7.1.3	5-FU: Preparation and Administration.....	107
7.1.4	Generation of Single Cell Suspensions from Isolated Organs	107
7.1.5	Generation of Bone Marrow Chimeras	108
7.1.6	Isolation of Peripheral Blood Lymphocytes (PBL)	108
7.1.7	White Blood Cell Count.....	109
7.2	FLOW CYTOMETRY ANALYSIS	109
7.2.1	Cell Surface Staining	109
7.2.2	Cell Sorting.....	109
7.2.3	Automated Cell Sorting using Magnetic Beads (AutoMACS).....	109
7.2.4	Cell Cycle Analysis (Ki67 vs. Hoechst)	110
7.2.5	CFSE Cell Division Assay	110
7.2.6	Apoptosis Analysis (Annexin V vs. 7-AAD or DAPI).....	110
7.2.7	Calcium Flux Assay.....	110
7.3	CELL CULTURE/ <i>IN VITRO</i> EXPERIMENTS	111
7.3.1	Culture of Lineage Negative Bone Marrow Cells.....	111
7.3.2	Retroviral Infection of Bone Marrow Cells	111
7.3.3	Thapsigargin Treatment	111
7.3.4	Colony Forming Unit (CFU) Assay	112
7.3.5	Culture of murine and human T-ALL cells	112
7.3.6	Lentiviral Infection of T-ALL cell lines.....	112
7.4	MOLECULAR BIOLOGY TECHNIQUES	112
7.4.1	DNA Preparation from Cells and Tissues	112

7.4.2	RNA Isolation from Cells and Tissues	113
7.4.3	Reverse Transcription	113
7.4.4	Quantitative Real Time RT-PCR.....	114
7.5	PROTEIN METHODS.....	114
7.5.1	Preparation of Whole Cell Extracts	114
7.5.2	Preparation of Nuclear Extracts	114
7.5.3	SDS-Polyacrylamide Gel Electrophoresis & Western Blot Analysis.....	115
APPENDICES		117
7.6	FUNCTIONAL CHARACTERIZATION OF LOSS OF ONE SERCA2 ALLELE IN THE HEMATOPOIETIC SYSTEM 125	
7.6.1	Serca2 Haploinsufficiency does not affect Hematopoiesis under Steady State Conditions.....	125
7.6.2	Serca2 Haploinsufficiency does not affect Hematopoiesis under Stress	128
REFERENCES.....		144
ACKNOWLEDGEMENTS		155
CURRICULUM VITAE.....		157

1 Introduction

1.1 Hematopoiesis and the Immune System

Hematopoiesis is the process by which all cell types of the blood and immune system are generated. The hematopoietic system consists of more than 10 different cell types, with each fulfilling specialized functions. Blood cells can be broadly divided into red blood cells (erythrocytes), important for oxygen transport; platelets, which function in blood clotting; and white blood cells (leukocytes), which comprise innate and adaptive immunity. Although diverse, all different cell types within the hematopoietic system arise from a single pluripotent cell, the hematopoietic stem cell (HSC).

During mammalian development, the first and primitive form of hematopoiesis (from embryonic day 7.5; E 7.5) takes place in the extra-embryonic yolk sac and later in intra-embryonic sites such as the allantois and placenta. Primitive hematopoiesis functions to rapidly produce erythroid progenitors in order to guarantee sufficient oxygen supply for the developing fetus. HSCs begin to arise only during the second or definitive wave of hematopoiesis (E 8.5), which takes place in the aorta-gonad-mesonephros (AGM) region (Muller et al., 1994). Once starting to circulate in the blood stream, HSCs migrate from the AGM into the fetal liver at E10 (Ema and Nakauchi, 2000), which represents the major site for HSC expansion during embryonic development. Shortly after, HSCs start to populate the thymus (E11.5) and spleen (E12.5) and shortly before birth the bone marrow (BM), which is the primary site of hematopoiesis in the adult (Wang and Wagers, 2011).

In the adult, the long-term (LT) repopulating HSC is unique in its ability to undergo self-renewal and to continuously give rise to immature progenitor cells (Figure 1). During hematopoietic differentiation, LT-HSCs give rise to multipotent progenitors (MPPs) with limited self-renewal and transient but multilineage reconstitution potential. These MPPs subsequently differentiate into oligo-potent progenitors, such as the common myeloid progenitor (CMP); megakaryocyte/erythroid progenitor (MEP); granulocyte/macrophage progenitor (GMP) and common lymphoid progenitor (CLP). CLPs have the potential to give rise to mature effector dendritic cells (DCs), T cells, natural killer (NK) cells and B cells. CMPs are hierarchically above MEPs and GMPs but can also immediately give rise to DCs. MEPs differentiate into erythroid progenitors (Ep) and megakaryocyte progenitors (MkP) to give rise to mature erythrocytes and

platelets, respectively. GMPs differentiate into mature myeloid lineages such as granulocytes and macrophages.

Flow cytometric analysis is frequently used for the identification and classification of the distinct HSC, progenitor and mature hematopoietic lineages (Figure 1 left). Each of the above mentioned cell types express specific cell surface antigens, which can be used during flow cytometry as “markers” to identify even small and rare populations, which are frequently characterized by the expression of multiple markers. Upon flow cytometric analysis, fluorochrome-coupled antibodies against these cell surface markers are passing through a laser stream, thereby exciting the fluorochrome and emitted a signal at a discrete wavelength. Cell populations can thereby not only be identified but also collected (Fluorescence activated cell sorting; FACS). The system applied for identifying cell surface markers thereby allowing the immunophenotyping of HSCs and hematopoietic cells is called cluster of differentiation (CD).

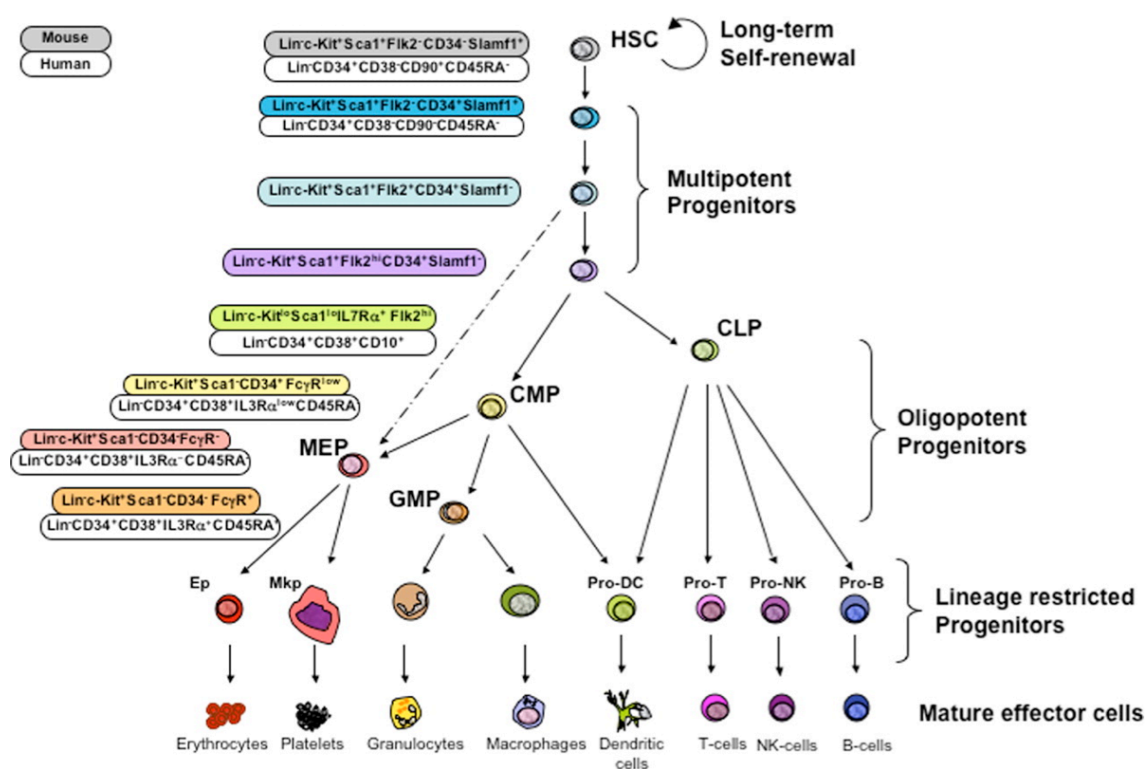


Figure 1: Model of the hematopoietic developmental hierarchy. At the top of the hematopoietic developmental hierarchy stands the rare and unique long-term (LT-) HSC, which can through asymmetric division self-renew but also give rise to multipotent progenitors (MPPs). These cells have limited self-renewal capacity and but differentiate into all short-lived mature blood cells. Therefore, MPPs give rise to oligo-potent progenitors, such as the common myeloid progenitor (CMP), megakaryocyte/erythroid progenitor (MEP) granulocyte/macrophage progenitor (GMP) and common lymphoid progenitor (CLP). CLPs first differentiate to give rise to mature effector dendritic cells (DCs), T cells, natural killer (NK) cells and B cells. MEPs differentiate into erythroid progenitors (Ep) and mekaryocyte progenitors (Mkp) to give rise to mature erythrocytes and platelets. GMPs differentiate into mature myeloid lineages like granulocytes and macrophages. Cell surface markers used for isolation are indicated on the **left** for human (**top**) and mouse (**bottom**) for each stem and progenitor cell. Adapted from (Bryder et al., 2006).

Mature oxygen-transporting erythrocytes express markers such as Ter119 and CD71, with early erythroblasts being Ter119⁺CD71⁺ and mature erythrocytes Ter119⁺CD71⁻. Myeloid-derived granulocytes (CD11b⁺Gr1⁺) include monocytes, neutrophils and eosinophiles; phagocytic cell types specialized in defending the system from infection in a non-specific manner in innate immunity. The cytotoxic lymphoid-derived NK cells cooperate with myeloid cells by destroying compromised host cells that have been infected with a virus or have been transformed during tumorigenesis. In contrast, mature T (CD4⁺ and CD8⁺ single positive; SP) and B (B220⁺IgM⁺) cells are effectors of the adaptive immune system. B cells are specialized in antigen recognition and differentiate into plasma cells, which produce and secrete antibodies specific to the activating antigen. T cells, however, recognize antigens presented by the major histocompatibility complex (MHC) on the surface of infected cells through their T cell receptor (TCR). Antigens of the MHC class I (all nucleated cells) are recognized by the CD8 co-receptor of cytotoxic T cells, which consequently target the infected cell to undergo apoptosis. In contrast, antigens of the MHC class II are recognized by the CD4 co-receptor, expressed by helper T cells, which in turn produce cytokines in order to activate CD8 “killer” T cells and macrophages for uptake of cellular debris.

1.2 HSCs in the Adult Hematopoietic System

Within the BM, HSCs reside in a specialized microenvironment composed of different cell types, extracellular elements and contains secreted factors adapted to the needs of this rare cell population, which is called the stem cell niche. The stem cell niche guarantees all necessary cues for the HSC to maintain self-renewal and differentiation potential. The crucial role of the stem cell niche for HSC function has long been recognized. For instance, studies in steel-Dickie mice, harbouring a mutated form of the membrane-bound stem cell factor (SCF), showed that in absence of SCF within the niche, HSC maintenance *in vivo* is severely impaired (McCulloch et al., 1965). Due to the observation that mainly two cell types, osteoblasts and endothelial cells, are crucial components of the BM niche, it is hypothesized that the niche contains two compartments: The endosteal and the perivascular niche. In the endosteal niche, rare and dormant LT-repopulating HSCs are in close physical contact with osteoblasts that line the endosteal surface of the bone, while more differentiated HSCs and hematopoietic progenitors are predominantly residing in the central and more vascularized regions of the BM. Within the vascular HSC niche, a large pool of CD150⁺ self-renewing HSCs resides in close proximity to endothelial cells of sinusoids. These HSCs are believed to more actively replenish the

hematopoietic system via intermediate multi-potent progenitors, in particular in response to injury (Wilson and Trumpp, 2006).

Phenotypically HSCs have been well defined based on the expression of particular cell surface antigens and can be classified by flow cytometry. HSCs reside in the immature lineage negative (Lin⁻), not yet committed or differentiated, fraction of cells within the BM and express high levels of stem cell antigen 1 (Sca1) and stem cell factor (SCF) receptor, c-kit (CD117) (Bryder et al., 2006; Uchida and Weissman, 1992). Given these expression characteristics, the overall HSC compartment is therefore often referred to as LSK (Lin⁻Sca1⁺c-kit⁺) fraction; in this work termed “KLS”. Consisting of rare hematopoietic cell types, the KLS population only accounts for approximately 0.5% of total BM cells (Morrison and Weissman, 1995). However, within the KLS fraction, only a small population of cells harbors true stem cell potential, e.g. the LT-HSCs. This population is defined as CD34⁻, while all MPP subsets are CD34⁺. The signalling lymphocyte activation molecule (SLAM) markers CD150 and CD48 and also CD135 (Fms-like tyrosine kinase 3; Flt3 receptor) allow further enrichment for pure HSCs (Kiel et al., 2005). Based on a combination of these markers and their cell cycle behavior, KLS can be further sub-fractionated into LT-HSCs (CD150⁺CD48⁻CD34⁻CD135⁻), which differentiate into MPP1 cells (CD150⁺CD48⁻CD34⁺CD135⁻), giving rise to MPP2 cells (CD150⁺CD48⁺CD34⁺CD135⁻), which consequently differentiate into MPP3 cells (CD150⁻CD48⁺CD34⁺CD135⁻) and up-regulation of CD135 defines the last MPP population (MPP4; CD150⁻CD48⁺CD34⁺CD135⁺) (Figure 2) (Wilson et al., 2008). Upon cell cycle analysis, LT-HSCs were demonstrated to primarily reside in G₀ phase of the cell cycle (>70%), which accounts for their quiescent state, whereas less than 10% of more differentiated MPPs (KLSCD34⁺) are found quiescent.

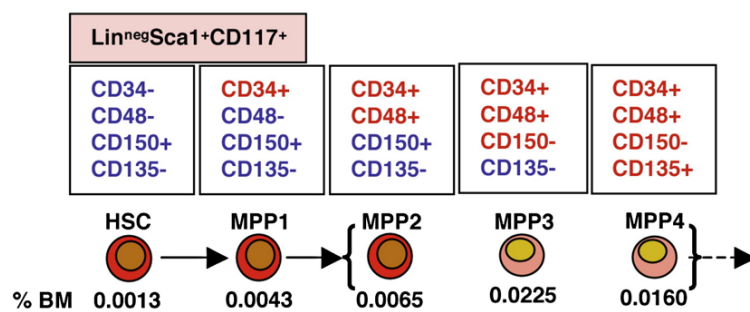


Figure 2: The five major KLS subpopulations. Differential expression of CD34, the signalling lymphocyte activation molecules (SLAM) CD48 and CD150, and CD135 (Flt3 receptor) allows the phenotypic classification of 5 major subsets within the KLS compartment. The most quiescent KLS subset is the CD34⁻CD48⁻CD150⁺CD135⁻ population, which accounts for only 0.0013% of cells within the BM. Based on cell surface expression, relative cell cycle status and their abundance the five subsets HSC to MPP4 are put in hierarchical order. Adapted from (Wilson et al., 2008).

Furthermore, HSC were functionally subcategorized by efflux studies using rhodamine 123 or with Hoechst 33342 dye, which demonstrated that only the rare LT-HSC possess multi-drug resistant pumps, such as MDR1 or ABC transporter G family member 2 (ABCG2). Therefore, these HSCs fall into the side population, which is able to efficiently efflux dyes such as Hoechst 3334 via these transporters. This is also of importance in the context of hematologic malignancies, as leukemic stem cells are resistant to conventional chemotherapy due to the action of these multi-drug resistant pumps.

Functional existence of LT-HSCs was proven by studies demonstrating that a single transplanted HSC could fully reconstitute the hematopoietic system of lethally irradiated mice (Ema et al., 2005; Matsuzaki et al., 2004; Osawa et al., 1996; Trumpp et al., 2010; Wilson et al., 2008). The Long-term reconstitution (LTR) capacity of HSCs can be further assessed using serial transplantation assays, in which transplanted LT-HSCs are forced to replenish the entire hematopoietic system in sequentially transplanted recipient mice. True LT-HSCs are capable of self-renewal and multi-lineage differentiation for up to three rounds of serial transplantation (Domen and Weissman, 1999). However, under homeostatic conditions, up to 70% of LT-HSCs are dormant. These cells reside preferentially in the G_0 phase of the cell cycle and divide only five times per life time as shown in BrdU label retaining studies (Wilson et al., 2008). However, dormant HSCs can be successfully activated and “pushed” into cycle by BM injury or extracellular cues, such as granulocyte colony-stimulating factor (G-CSF), interferon- α (INF α) or 5-fluorouracil (5-FU). For instance, stimulation of HSCs and progenitor cells with recombinant G-CSF leads to HSC mobilization without negatively affecting the HSC pool even upon repeated administration (de Kruijf et al., 2007). A study by Esser *et al.* demonstrated that upon treatment with INF α , dormant HSCs exit G_0 phase and enter the cell cycle (Essers et al., 2009). This was shown to be dependant on increased phosphorylation of STAT1 and AKT1, up-regulation of INF α and increased expression of Sca1. Reciprocal experiments in HSCs derived from *INF α R* KO mice, which lack the INF $\alpha\beta$ receptor, *STAT1* cKO mice and *Sca1* cKO mice proved insensitive to INF α -mediated mobilization and hence STAT1 and Sca1 are essential during this process. Furthermore, (i) combinatorial treatment with INF α to prime HSC mobilization followed by 5-FU, a chemotherapeutic agent, administration and (ii) chronic INF α exposure were demonstrated to lead to HSC loss. Another means to challenge and mobilize quiescent is via 5-FU administration. 5-FU is a pyrimidine analogue that is frequently used in the treatment of cancer as it (i) inhibits thymidylate synthase, thereby blocking thymidine synthesis and (ii) incorporates into newly synthesized DNA leading to cell cycle arrest and apoptosis (Lerner and Harrison, 1990). By targeting proliferating cells, mature lineages of myeloid and lymphoid origin are rapidly reduced, resulting in the mobilization of the HSC compartment.

1.3 T cell Development in the Thymus

During T cell development, early thymic progenitors (ETPs), which arise from HSCs within the BM, migrate into the thymus whereby they progress through different stages T cell maturation to become mature CD4⁺ or CD8⁺ single positive (SP) T cells. The earliest thymic progenitors are negative for CD4 and CD8, therefore referred to as double negative (CD4⁻CD8⁻, DN) thymocytes. DN thymocytes can be further subdivided by the differential expression of CD25 and CD44 into DN1 (CD44⁺CD25⁻CD117^{hi}), DN2 (CD44⁺CD25⁺), DN3 (CD44⁻CD25⁺) and DN4 (CD44⁻CD25⁻) immature T cells, whereby cells progress from DN1 to DN4. At the DN2 stage, T cell progenitors up-regulate genes important during T cell maturation and selection, such as the recombination activating genes 1 and 2 (*RAG1* and *RAG2*) required for the rearrangement of T cell receptor (TCR) genes and the CD3 chain as part of the TCR complex. Only a small subset activates TCR rearrangement of the γ and δ loci to become TCR $\gamma\delta$ (2%). This transition phase between DN2 and DN3 is called the TCR β selection checkpoint at which progenitors are committed to the T cell lineage and can no longer differentiate into any other lineage. Upon down-regulation of CD25, DN3 cells progress to the DN4 stage, followed by an immature single positive CD8 (CD8 iSP) stage, at which cells express low levels of surface TCR β and CD8 (CD8⁺ SP). Extensive proliferation and expression of CD4 leads to the CD4⁺CD8⁺ double positive (DP) stage, at which T cell progenitors express intermediate levels of TCR β and account for approximately 80% of immature T cells. DP cells undergo TCR α rearrangement and then these progenitors undergo final maturation through positive and negative selection. During negative selection, self-reactive thymocytes, which express their TCRs that recognize “self”-peptides presented by MHC molecules in the thymic epithelium, undergo apoptosis and are thereby eliminated from the thymus. During positive selection, functional T cells, which are able to interact with molecules of the major histocompatibility complex (MHC) presented by thymic epithelial cells, survive to become either mature CD4⁺ SP helper T cells (MHC class II) or CD8⁺ SP cytotoxic T cells (MHC class I).

1.4 The Canonical Notch Signalling Pathway

The Notch pathway is evolutionary conserved and regulates key cellular processes such as proliferation, differentiation and cell fate specification within self-renewing organs including the hematopoietic system, the gut and the skin. In 1917, Thomas Hunt Morgan described a strain of the fruit fly *Drosophila melanogaster* that exhibited notches at the margins of their wing blades (Morgan, 1917). These notches were the phenotypic outcome of a partial loss in a gene cloned in the mid 1980's and named Notch (Kidd and Young, 1986; Wharton et al., 1985).

Notch signalling is a cell-to-cell communication pathway, which relies on the physical interaction between a signal-sending cell, expressing a Notch ligand at the cell surface, and a signal-receiving cell, which expresses the transmembrane bound Notch receptor. There exists only one transmembrane Notch receptor in *Drosophila*, which can be activated via interaction with two different membrane-bound ligands called Delta and Serrate (Figure 3 top). In mammals, there are four Notch receptors, Notch (N) 1 to 4, that are bound by five different ligands called Jagged 1 and 2 (homologs of Serrate) and Delta-like (Dll) 1, 3 and 4, which are homologs of Serrate (Figure 3 bottom).

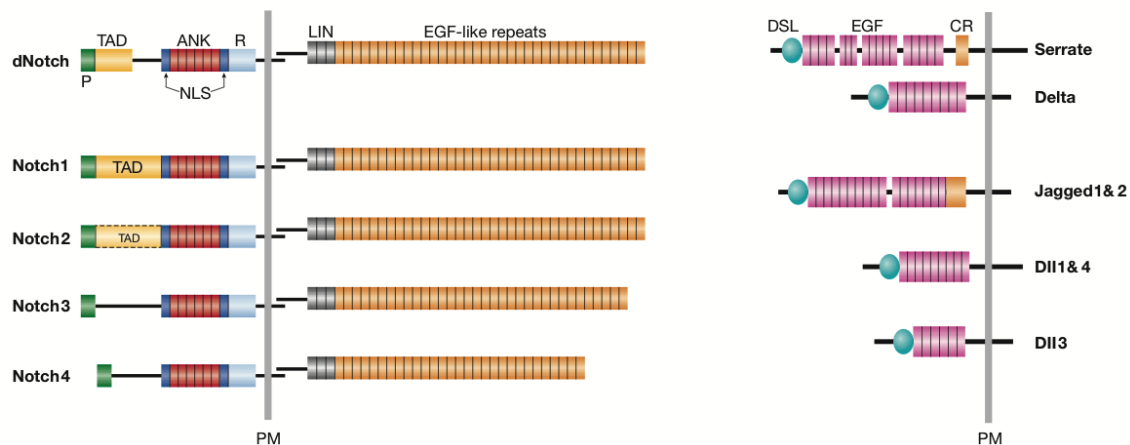


Figure 3: Notch receptors and their ligands. In *Drosophila* there exists only one Notch receptor (dNotch), which is bound by two transmembrane ligands Serrate and Delta. In mammals, there exist the four Notch receptors Notch1-4 that can be bound by the five different ligands Jagged 1 and 2 (homologues of Serrate) and Delta-like (Dll) 1, 3 and 4, which are homologues of Delta. **Left**, Notch receptors are expressed at the cell surface as heterodimeric proteins, whose extracellular portion contains 29-36 epidermal growth factor (EGF)-like repeats, being important for ligand binding and ligand specificity. These are followed by 3 cystein-rich LIN-repeats, preventing signalling in absence of a ligand, and a heterodimerization domain (HD). The intracellular Notch domain is composed of the RAM domain (R) and six ankyrin repeats (ANK), both important for protein interaction, followed by 2 nuclear localization signals (NLS), a transactivation domain (TAD, absent in N3 and N4) and a PEST sequence (P). **Right**, Similarly, Notch ligands are also expressed as membrane-bound proteins. All ligands harbor an amino-terminal DSL domain (Delta, Serrate and Lag2) followed by EGF-like repeats. Serrate and Jagged ligands possess a cysteine-rich (CR) domain adjacent to the EGF-like repeats. Both receptors and ligands span the plasma membrane. Adapted from (Radtke et al., 2005).

Notch receptors are expressed at the cell surface as heterodimeric proteins, whose extracellular portion contains 29-36 epidermal growth factor (EGF)-like repeats. These repeats are important for ligand binding and ligand specificity. These are structurally followed by 3 cystein-rich LIN-repeats, preventing signalling in absence of a ligand, and a heterodimerization domain (HD). The intracellular Notch domain is composed of the RBP-associated molecule (RAM) domain (R) and six ankyrin repeats (ANK), both important for protein interactions, followed by 2 nuclear localization signals (NLS), a transactivation domain (TAD, absent in N3 and N4) and a peptide sequence, rich in proline, glutamic acid, serine and threonine (PEST;P). Similarly, Notch ligands

are also expressed as membrane-bound proteins spanning the plasma membrane. All ligands share an amino-terminal DSL domain (Delta, Serrate and Lag2) followed by EGF-like repeats. Serrate and Jagged ligands possess a cysteine-rich (CR) domain adjacent to the EGF-like repeats. Newly synthesized Notch receptor proteins are proteolytically cleaved in the Golgi apparatus by a furin-like convertase at cleavage site S1 before being trafficked towards the cell membrane, where they form heterodimers (Figure 4). Upon ligand receptor interaction, two sequential proteolytic cleavages are carried out by metalloproteases of the ADAM family (tumor necrosis factor- α -converting enzyme; TACE) at S2 in the extracellular part of the receptor and by a multi-protein complex exhibiting a proteolytic γ -secretase activity at S3 in the intracellular part. Consequently, the Notch intracellular domain (NICD) is released and shuttles into the nucleus where it binds to the transcription factor CSL, also known as CBF-1 in humans, suppressor of hairless in *Drosophila* and RBPJ κ in the mouse. Further recruitment of co-activators of the mastermind-like family (MAML1-3) results in the formation of an activated transcriptional complex and expression of Notch target genes is launched. Among Notch target genes, members of the Hairy enhancer of split (*Hes*) or Hairy related (*Hey* or *Hrt*) gene families of basic-helix-loop-helix (bHLH) transcriptional repressors are best characterized (Jarriault et al., 1995; Jarriault et al., 1998; Wendorff et al., 2010). Additional Notch target genes include the cell cycle regulator, cyclin dependent kinase 1 inhibitor *Cdkn1a* (p21) (Rangarajan et al., 2001), *Deltex1* (Matsuno et al., 1995) and *c-myc* (Palomero et al., 2006).

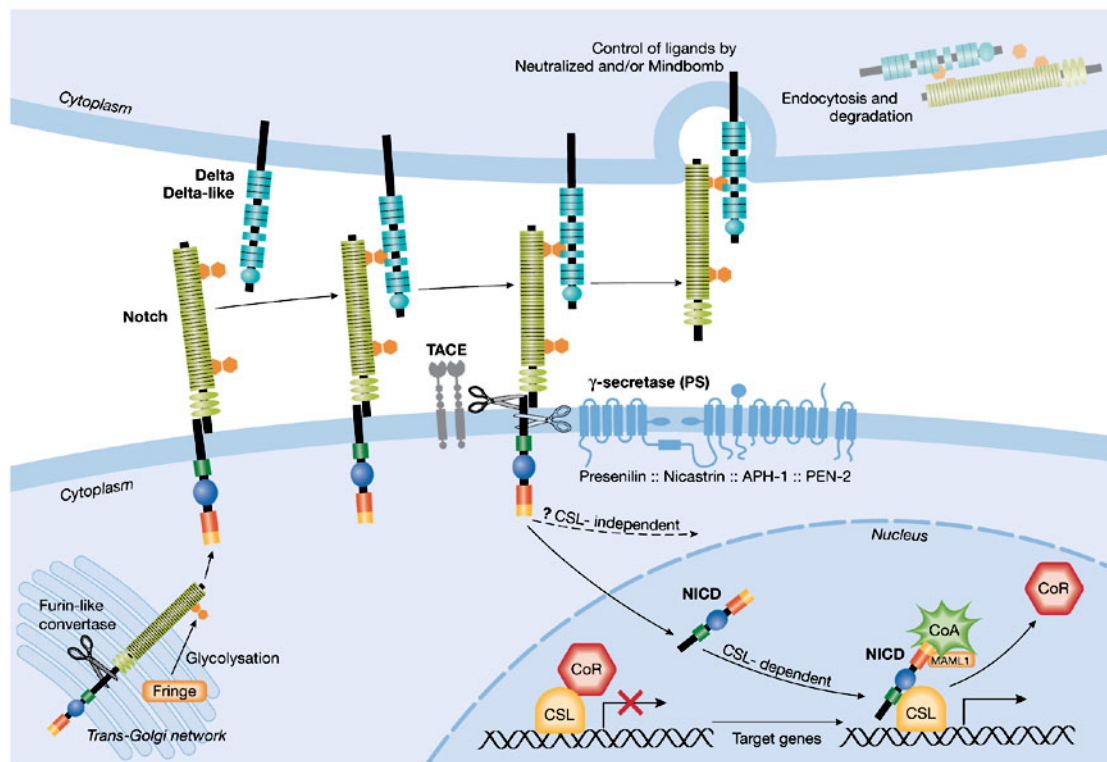


Figure 4: Notch signalling. Notch precursor receptors are cleaved in the Golgi apparatus by a furin-like convertase before trafficking towards the cell membrane, where they form heterodimers. Glycosyltransferases of the Fringe family mediate glycosylation of the EGF repeats of the receptor, thereby regulating receptor-ligand specificity. Upon receptor-ligand interaction, two proteolytic cleavages take place, (i) the metalloprotease TACE (tumor necrosis factor α -converting enzyme) cleaves within the extracellular domain, followed by (ii) cleavage within the transmembrane domain mediated by the γ -secretase complex, which is composed of presenilins such as Nicastrin, APH-1 and PEN-2. This results in release of the intracellular domain (NICD), which translocates into the nucleus to form a transcriptional complex with CSL, master-mind like proteins (MAML1) and other co-activators (CoA), thereby replacing transcriptional co-repressors (CoR). As a result expression of Notch target genes is launched. Adapted from (Radtke et al., 2005).

1.4.1 Notch Signalling in Hematopoietic Stem Cells

Notch receptors and ligands are widely expressed in HSCs and in cells within the HSC niche. Therefore, Notch signalling was proposed to regulate hematopoiesis. While N1 signalling was shown to be dispensable in primitive hematopoiesis within the yolk sac, germline mutant embryos deficient for *N1* or *RBPJ κ* failed to generate intraembryonic HSCs (Robert-Moreno et al., 2008). However, the impaired development of definitive hematopoiesis in these mice may be due to a cell-autonomous effect or as a secondary effect due to perturbed vasculogenesis. Further studies in conventional KO mice for *Jagged1* demonstrated that expression of this ligand is essential for HSC numbers in the AGM, without, however, perturbing the integrity of the arterial system (Robert-Moreno et al., 2008).

In contrast, whether Notch1 plays a physiological role in the maintenance and self-renewal of HSCs is still a matter of debate. Jagged 1 was proposed to be important in the HSC stem cell niche

since parathyroid hormone-related protein-receptor (PTHPR) expression by osteoblasts resulted in increased numbers of Jagged1-expressing osteoblasts. This in turn correlated with higher numbers of HSCs, suggesting that Jagged1 may support HSC self-renewal (Calvi et al., 2003). However, Jagged1-mediated Notch signalling was demonstrated to be dispensable for the maintenance of HSCs using a conditional gene targeting approach in BM and HSC niche cells (Mancini et al., 2005). Since Jagged2 was reported to be also expressed in the HSC stem cell niche, Jagged2 may compensate for loss of Jagged1 function. In addition, a study demonstrated differential Jagged2 expression in hematopoietic and endothelial cells (Tsai et al., 2000). Over-expression of Jagged2 promoted HSC proliferation and survival *in vitro* in the absence of growth factors. Therefore, Tsai *et al* propose Jagged2 to be a regulator of hematopoiesis.

In addition, Maillard et al. demonstrated that impairment of canonical Notch signalling using a dominant-negative (dn) of MAML as well as the conditional inactivation of RBPJ κ does not result in a block of HSC maintenance (Maillard et al., 2008). This suggests that Notch signalling is dispensable for HSC maintenance. Hence, the controversial outcome of these studies still questions whether Notch signalling plays a role in definitive hematopoiesis.

1.4.2 Notch Signalling in T Cell and MZB Cell Development

Notch signalling in the hematopoietic system has been best characterized in the context of T cell development in the thymus. Fiorini *et al.* demonstrated that developing thymocytes express Notch1 and Notch2 receptors (Fiorini et al., 2009), while thymic epithelial cells express the ligands Dll1, Dll4 and Jagged 2 (Felli et al., 1999).

In 1999, the *Notch1* conditional knock out (cKO) mouse was generated and crossed with the INF type I-responsive MxCre recombinase in order to study the role of Notch in the hematopoietic system (Radtke et al., 1999). Upon ablation of *N1* in BM progenitors, the majority of hematopoietic lineages remained unaffected. T cell development however, was severely impaired in *N1* cKO mice as immature T cells were blocked at the DN1 stage (Lin⁻CD4⁻CD8⁻CD25⁻CD44⁺), which was accompanied by an accumulation of immature B cells (IgM⁺B220⁺CD19⁺) within the thymus. Therefore, this study demonstrated, for the first time that Notch is important for regulating T versus B lineage commitment decisions in hematopoietic progenitors.

Although three different Notch ligands are expressed by the thymic epithelium, *in vitro* culture experiments suggested that Dll1 may be physiological ligand for N1 in the thymus (Schmitt et al., 2004). Only later, Koch *et al.* studied the conditional ablation of Dll1 and Dll4 in thymic epithelial cells (TECs) in order to identify the physiological ligand for N1 in the thymus. Upon ablation of Dll4 but not Dll1, thymocytes were blocked at the DN1 stage of T cell development and

immature B cells accumulated in the thymus. These results were confirmative of the phenotype observed in BM-specific *N1* cKO mice, also leading to ectopic B cell at the expense of T cell development in the thymus. Therefore, Dll4 is the essential Notch ligand to induce Notch signalling upon interaction with thymic progenitors that express N1 (Koch et al., 2008).

The second well characterized role for Notch signalling in the hematopoietic system involves mature B cell differentiation. Marginal zone B cells (MZB) are rapidly recruited in early adaptive immune responses against blood-borne antigens in a T cell-independent manner. Thereby the production of antibodies is mounted in order to defend the body from pathogens. First studies in *RBPJ κ* cKO mice crossed with the B cell specific *CD19* Cre revealed impaired development of MZB cells (B220⁺IgM⁺CD21^{hi}CD23^{lo}) with a concomitant increase in follicular zone B cells (B220⁺IgM⁺CD21^{int}CD23^{hi}) in the spleen (Tanigaki et al., 2002). Similarly, upon conditional ablation of *N2* or *Dll1*, MZB cells were negatively affected. This study hence provided evidence that N2 and Dll1 are the physiological Notch receptor ligand pair, responsible for MZB lineage specification (Hozumi et al., 2004; Saito et al., 2003). Furthermore, downstream of N2-Dll1 signalling, members of the MAML family of transcriptional co-activators have been studied in the context of MZB cell specification. Chimeric *MAML1* KO mice exhibited a block in MZB development, while the thymic compartment remained mainly unaffected. This suggested, that a sole member of transcriptional co-activators, MAML1, regulates MZB specification in the spleen, while in the thymus other members may compensate for MAML1 deficiency (Wu et al., 2007).

1.4.3 Notch Signalling in T cell Acute Lymphoblastic Leukemia (T-ALL)

The first link between the Notch pathway and cancer was established in 1987, when Reynolds and colleagues discovered the chromosomal translocation t(7;9) (q34;q34.3) in a small subset (<1%) of patients suffering from T-cell acute lymphoblastic leukemia (T-ALL) (Reynolds et al., 1987). This translocation leads to the expression of a dominant active form of N1 since the intracellular domain of the Notch receptor (NICD) is juxtaposed to the enhancer of the T cell receptor β (TCR β). As a result, developing T cells constitutively express NICD and are thereby transformed to become leukemic (Ellisen et al., 1991). Experimentally, work by Pear *et al.* demonstrated that retroviral overexpression of NICD in isolated BM progenitors leads to the development of T-ALL upon transplantation in lethally irradiated recipient mice (Pear et al., 1996a). Leukemic cells generated in this retroviral T-ALL induction model phenotypically resemble human T-ALL due to their clonal origin of immature transformed T cells. Hence this study provided first experimental proof that aberrant N1 signalling is causative for T-ALL. Therefore, the retroviral induction model is frequently used as a means to study T-ALL *in vivo*

(Pear et al., 1996a). The aberrant expression of Notch1 in T-ALL gained more importance with the land marking study by Weng *et al.* (Weng et al., 2004). They sequenced 96 primary human T-ALL samples and T-ALL cell lines and identified activating mutations in the heterodimerization (HD) and PEST domains of the Notch1 receptor in more than 50% of the cases (Figure 5).

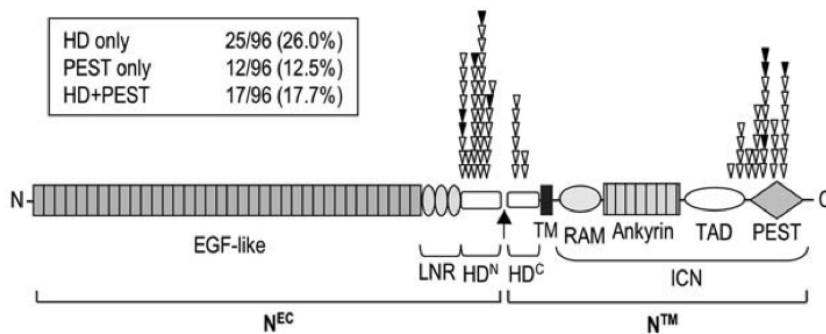


Figure 5: Notch1 mutations in the HD and PEST domains identified in human T-ALL. Schematic representation of the Notch1 receptor with its extracellular domain (N^{EC}), harbouring EGF-like repeats, LIN/Notch repeats and parts of the heterodimerization domain (HD). The transmembrane portion of N1 with the C-terminal HD domain, transmembrane domain (TM), ankyrin repeats, transactivation domain and PEST domain. The by DNA sequencing identified mutations affect the extracellular HD domain at the N- (HD^N) or C-terminal (HD^C) part, the transmembrane PEST domain or both HD and PEST at the same time. These mutations lead to aberrant Notch pathway activation due to ligand-independent signalling (HD domain) or delayed NICD degradation (PEST domain). Adapted from (Weng et al., 2004).

Mutations affecting the HD domain lead to ligand-independent Notch pathway activation. This is due to the altered conformation of the negative regulatory region (NRR), which in turn exposes the S2 site for cleavage even in absence of Notch receptor-ligand interaction. Mutations within the PEST domain in contrast, negatively affect the degradation of NICD mediated by FBW7 E3 ligase, thereby leading to prolonged availability for signalling. In addition, it was demonstrated that the occurrence of mutations affecting both the HD and the PEST domain, further enhance Notch pathway activation as shown by a luciferase Notch reporter assay. Consequently, this work also proposed targeting the Notch signalling pathway as therapeutic approach to treat T-ALL in patients (Weng et al., 2004).

1.5 Chromatin Remodellers as Regulators of Gene Expression

In eukaryotic cells, the genetic information containing DNA is compacted into chromatin. The fundamental subunit of chromatin is the nucleosome, which consists of 146 bp of DNA wrapped around an octamer of four core histones, in general a H3/H4 tetramer and two H2A/H2B dimers, forming a beads-on-a-string-structure (Strahl and Allis, 2000). The nucleosomal units are then folded into higher-order chromatin fibres (Luger and Richmond, 1998). Once thought of

as static, non-participating structural elements, it is now evident that histones are integral and dynamic components of the gene transcription machinery (Strahl and Allis, 2000) (Figure 6).

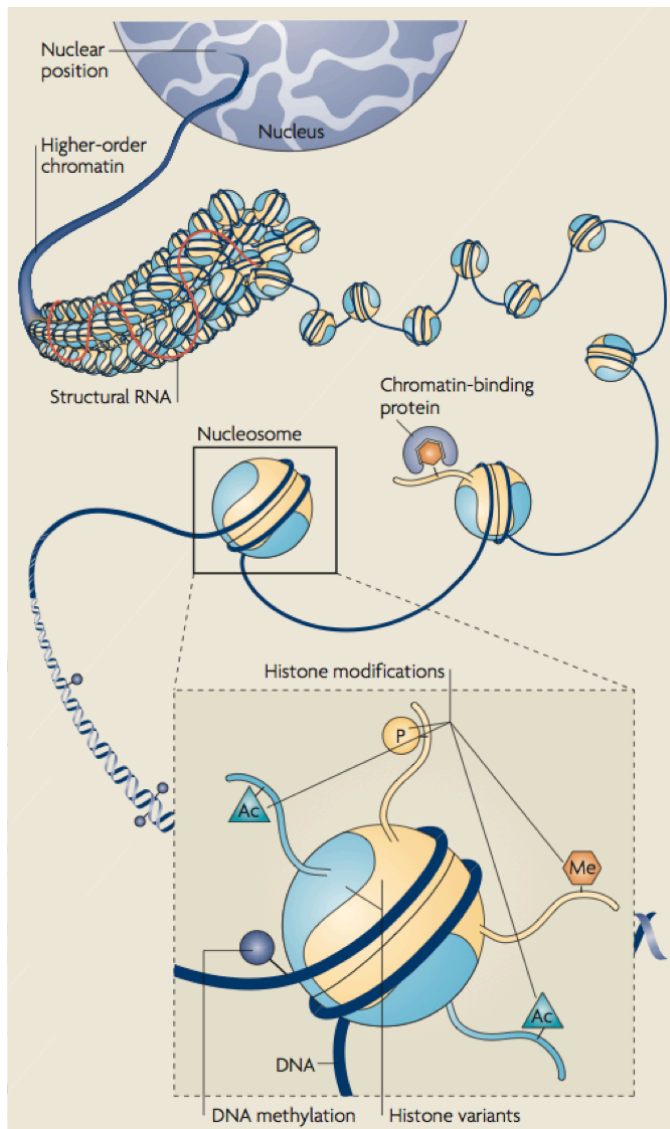


Figure 6: Epigenetic regulation of gene expression. In eukaryotes the genetic information, encoded by the DNA, is compacted into chromatin. Chromatin fibers consist of DNA wrapped around an octamer of core histones (nucleosome), thereby building a “beads-on-a-string-structure”. Histone tails produce out from the nucleosome and serve as docking sites for epigenetic marks. These tails are also recognized by chromatin-binding proteins, which physically slide nucleosomes along the DNA, thereby opening (euchromatin) or closing (heterochromatin) the chromatin structure. In addition, the DNA can be methylated thereby regulating accessibility for the transcriptional machinery. Adapted from CNS Spectr. 2010;15(4):220-230.

Histone tails protrude out of the nucleosome and are subjected to diverse covalent post-translational modifications. These include acetylation, phosphorylation, methylation, ubiquitination, sumoylation and ADP-ribosylation (Luger and Richmond, 1998). These histone modifications act sequentially or in combination to form the “histone code”. Histone

modifications directly influence chromatin structure, thereby regulating access to the DNA. In addition, specific histone modifications or combinations thereof serve as recognition motifs for chromatin binding proteins to bring about distinct downstream events (Strahl and Allis, 2000). Thereby, the information content of the genome is extended beyond the DNA sequence (Jenuwein and Allis, 2001). In general, histone acetylation favors gene activation. Histone methylation has different effects, depending on the site of the methylated residue, e.g. H3K4 promotes transcriptional activation, while H3K27 represses transcription.

Therefore, it is not solely the DNA sequence that determines gene expression but also epigenetic modifications. Per definition, epigenetic regulators alter the activities and the abilities of a cell without affecting and mutating the sequence of the DNA (Lund and van Lohuizen, 2004). These epigenetic alterations include (i) DNA methylation, (ii) histone modifications and (iii) chromatin

remodelling, which are stable over rounds of cell division and get hence inherited (Mai et al., 2005). DNA methylation, mediated by DNA methyltransferases (DNMTs), is the best-characterised epigenetic mark and occurs on cytosines directly located 5' to a guanosine, which are called CpG dinucleotides or CpG islands. These DNMTs can be over-expressed due to activating mutations in human cancer cells (Szyf and Detich, 2001). As a result, CpG-rich promoters are hypermethylated, leading to transcriptional inactivation of the respective genes, as binding of the transcription machinery is impaired. In contrast, in some cases proto-oncogenes can become over-expressed due to DNA hypomethylation. Furthermore and most importantly for this work, DNA methylation is associated with chromatin remodelling that promotes the formation of a condensed chromatin structure, the heterochromatin. For instance, promoter hypermethylation is associated with particular combinations of histone marks including (i) deacetylation of the histone H3 and H4, (ii) loss of H3 lysine K4 (H3K4) trimethylation, (iii) H3K9 methylation and (iv) H3K27 trimethylation. Hence, DNA methylation works in concert with another epigenetic key mechanism, the chromatin remodelling. During chromatin remodelling (i) covalent post-translational modifications of histones and (ii) ATP-dependent chromatin remodelling complexes, which either move, eject or restructure nucleosomes, regulate the accessibility of the underlying DNA. This accessibility can either be enhanced, leading to an open chromatin structure (euchromatin) or it can be blocked, resulting in a closed chromatin environment (heterochromatin). Through the modulated accessibility of the DNA, certain genes get silenced or activated.

Histone modifications act as docking sites for ATP-dependant chromatin remodelling complexes. These are multi-subunit complexes, which physically slide nucleosomes along the DNA strand, thereby regulating the accessibility of the DNA. In eukaryotic cells, there exist chromatin-remodelling complexes of the (i) Chromodomain-Helicase-DNA-binding (CHD), switching defective sucrose-non fermenting (SWI/SNF), (iii) imitation switch (ISWI) and (iv) inositol requiring 80 (INO80) family (Figure 7). All chromatin-remodelling enzymes share a conserved ATPase domain, but are unique in their flanking domains.

The CHD family is defined by the presence of two tandem chromodomains, N-terminal of the ATPase domain. Additional structural motifs are used to further divide the CHD family into the subfamilies CHD1, Mi-2 and CHD7 (Flaus et al., 2006; Sims and Wade, 2011).

SWI/SNF remodellers are characterized by presence of an N-terminally located HSA (helicase-SANT) domain, which is known to recruit actin and actin-related proteins; and a C-terminally located bromo domain, suggested to bind to acetylated lysines on histone tails. SWI/SNF enzymes form multi-subunit complexes containing 8 or more proteins and slide and evict nucleosomes from DNA, but lack chromatin assembly activities.

ISWI family ATPases harbor a C-terminal SANT domain adjacent to a SLIDE domain (SANT-like ISWI), which together form a nucleosome recognition module that binds to DNA and unmodified H4 tails (Clapier and Cairns, 2009).

In contrast to the other remodellers, members of the INO80 family possess a dimeric ATPase domain, which functions as a scaffold for interaction with the RuvB-like proteins, which primarily bind around holliday junctions to promote their migration during homologous recombination (West, 1997).

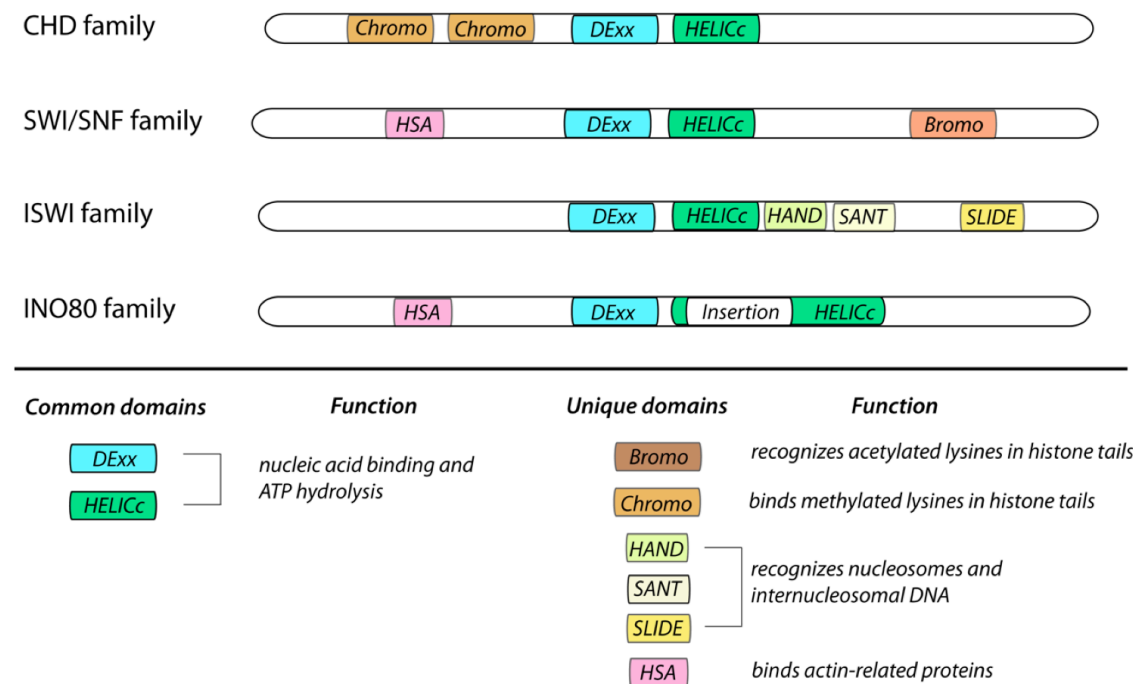


Figure 7: Chromatin remodelling enzymes. Chromatin remodellers can be classified into members of Chromodomain-Helicase-DNA-binding (CHD), switching defective sucrose-non-fermenting (SWI/SNF), imitation switch (ISWI) and inositol requiring 80 (INO80) families. All chromatin-remodelling enzymes share the ATPase domain, but are unique in their flanking domains. Adapted from Biochemistry, Genetics and Molecular Biology » "Chromatin Remodelling", book edited by Danuta (Radzioch).

In summary, the chromatin environment and the recruitment of chromatin-associated proteins determine the "on" versus "off"- transcriptional state of a gene.

1.5.1 Chromodomain-Helicase-DNA binding Proteins

CHD chromatin remodelling enzymes contribute to the dynamic changes in chromatin structure during transcription, recombination, repair and replication. Structurally, CHD chromatin remodelling complexes are characterized by the presence of two N-terminal chromodomains, a DNA-dependant ATPase domain of the SNF2 superfamily and, in some cases, a DNA-binding domain. The ATPase domain carries out ATP hydrolysis, which provides the energy necessary

for either the sliding of histone octamers (Becker and Horz, 2002) or the displacement of histones (Durr et al., 2006; Pazin and Kadonaga, 1997).

Members of the CHD family of chromatin remodellers are subdivided into (i) CHD1/CHD2, CHD3-5/Mi-2 and (iii) CHD6-9 subfamilies (Figure 8). Subfamily I, comprising CHD1 and CHD2, is conserved from yeast to human and regulates (i) nucleosome spacing and (ii) chromatin assembly. CHD1 primarily functions in the maintenance of mouse embryonic stem cells (Gaspar-Maia et al., 2009) and CHD2 regulates mammalian development as well as DNA damage responses, demonstrating tumor suppressive functions (Nagarajan et al., 2009).

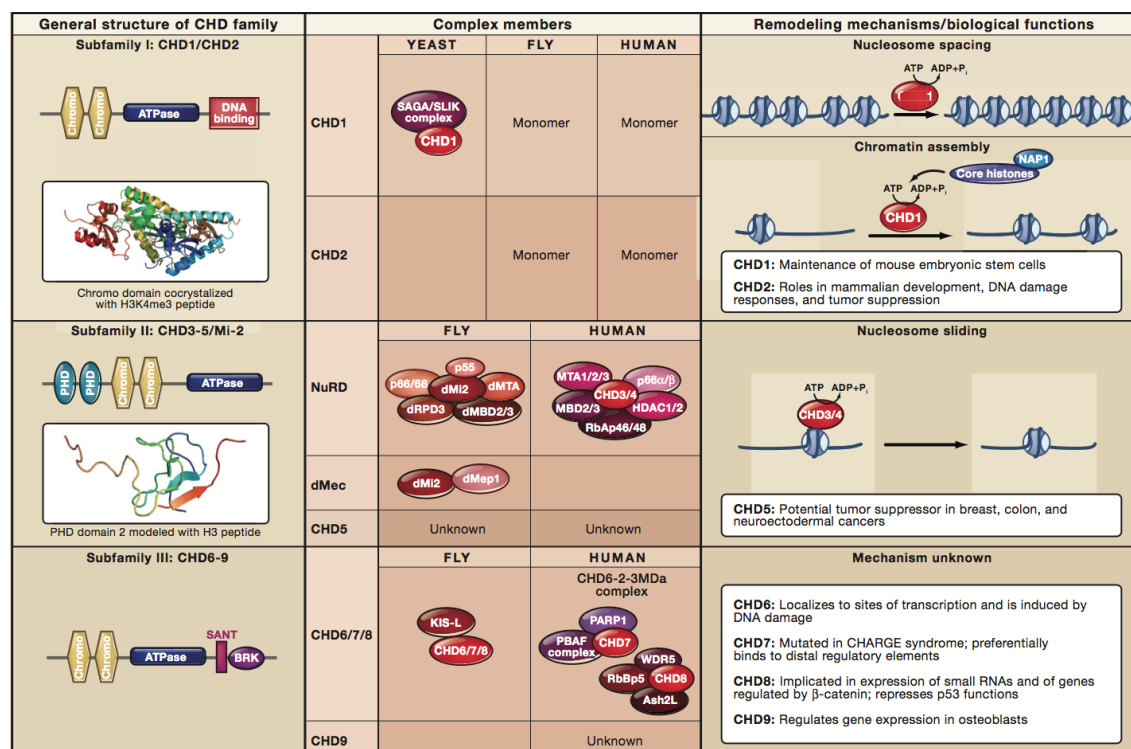


Figure 8: CHD family of chromatin remodelling enzymes. Characterization and classification of the 3 subfamilies of CHD proteins. Subfamily I comprises CHD1 and CHD2; CHD3-5/Mi-2 belong to subfamily II and subfamily III consists of CHD6, 7, 8 and 9. **Left**, General structure of CHD members according to their classification into subfamilies. **Middle**, Conservation of CHD members from yeast over fly to human, depicted for each family member. **Right**, Remodelling and biological functions of the different CHD proteins. Adapted from (Sims and Wade, 2011).

Subfamily II includes CHD3, CHD4 and CHD5/Mi-2, and is characterized by two N-terminal PHD finger domains, initially identified as Cys₄-His-Cys₃ motifs in the plant homeodomain, adjacent to the chromodomains. Another distinct feature is the significantly different chromodomain sequence, which allows interaction with histone tails. The members CHD3 and CHD4 are integral subunits of the Mi2-NuRD histone deacetylase complex in flies and in humans, with the PHD fingers being essential for interaction with HDCA1 and for modified histone tails (Zhang et al.,

1998). The main functions of these complexes are to modulate transcription, to regulate chromatin assembly during DNA replication and to regulate DNA repair. Therefore, CHD3 and CHD4 are ubiquitously expressed. In contrast, CHD5 is predominantly expressed in neuronal tissue (Egan et al., 2013), but its interaction partners remain still undefined. Interestingly, CHD5 was reported to be a tumor suppressor in breast, colon and neuroectodermal cancers (Bagchi et al., 2007; Esteller, 2007; Mokarram et al., 2009; Mulero-Navarro and Esteller, 2008), giving another link between the actions of a chromatin-remodelling enzyme and cancer.

The subfamily III chromatin remodelling enzymes consists of the four members: CHD6, CHD7, CHD8 and CHD9. These are homologs of a single *Drosophila* Trithorax protein Kismet, which is important for the regulation of *Hox* genes, body segmentation and transcriptional elongation (Daubresse et al., 1999). DNA damage was reported to “induce” CHD6, stimulating its recruitment and interaction with other yet unidentified co-factors at transcriptional start sites. CHD7 preferentially binds to distal regulatory chromatin regions (Schnetzer et al., 2010) and is frequently associated with CHARGE syndrome, a disease affecting multiple organs (Vissers et al., 2004). In contrast, CHD8 was shown to interact with CHD7 and represses p53 function and induction of apoptosis during mammalian development (Nishiyama et al., 2009). Finally, expression of CHD9 has been implicated in regulating gene expression in osteoblasts. Interestingly, members of all CHD subfamilies were shown to be deregulated in gastric and colorectal cancers, linking aberrant chromatin remodelling to cancer pathogenesis (Kim et al., 2011).

1.5.2 Identification of Chd7 in a Microarray Screen comparing early versus late-stage Notch1-driven T-ALL

A previous research project in the lab focused on identifying the developmental stage at which T cell progenitors or developing T cells can give rise to T-ALL via constitutive over-expression of the Notch 1 intracellular domain (NICD). Therefore, mouse models, in which specific NICD over-expression from the Rosa26 locus is induced at discrete stages of T cell development, were generated (Figure 9; courtesy of Caroline Poisson). MxCre recombinase was used to induce NICD over-expression in BM progenitors and two thymic-specific Cre lines were used in order to target thymic progenitors at the DN2-DN3a stage (LckCre) and at the DN3b-DN4 stage (CD4Cre) of T cell maturation for NICD over-expression. This allowed identifying more precisely the stage of T cell development at which T-ALL can be induced and closer mimicked the human disease, which arises presumably in the thymus.

In brief, over-expression of NICD in hematopoietic progenitors in the BM ($RNIC^{+/\Delta MxCre}$) resulted in a lethal, non-transplantable polyclonal early-stage T-ALL. NICD over-expression at early stages of T cell development (DN2 to DN3a stage; LckCre) induced a transplantable T-ALL that is also metastatic in non-lymphoid tissues. In contrast, NICD over-expression beyond the TCR β selection checkpoint mediated by CD4Cre did not lead to T-ALL development. Thus, the over-expression of NICD in T cell progenitors gives rise to a true T-ALL only up to the DN3a stage of T cell development, as shown in Figure 9.

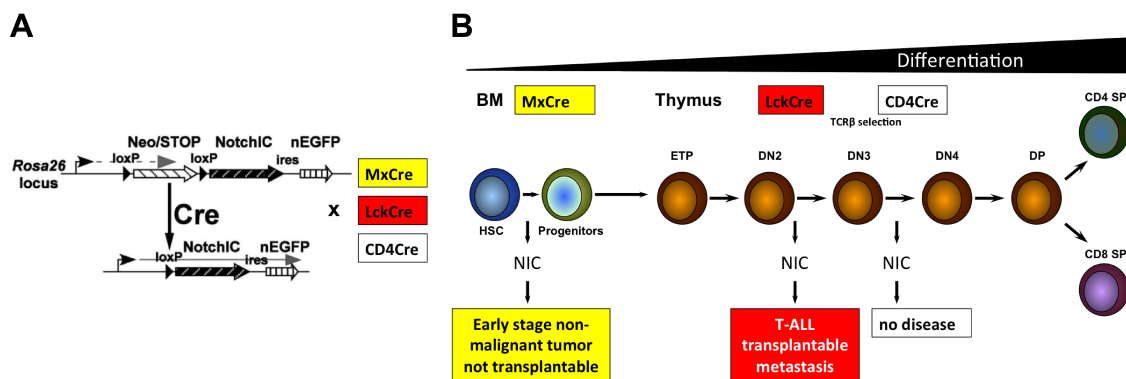


Figure 9: Murine stage-specific RNIC Disease Models. The RNIC transgenic mouse was crossed to different tissue- and lineage stage-specific Cre recombinases in order to specifically over-express NICD in the BM (MxCre), at the DN2-DN3a (LckCre) or at the DN3b-DN4 stage of T cell development in the thymus. **A**, Schematic representation of the RNIC model, in which Cre recombinase activation leads to excision of the loxP-site flanked STOP cassette preceding NICD ires eGFP, resulting in NICD expression from the Rosa26 locus. **B**, Overview of disease outcome upon NICD over-expression at different stages of T cell development: MxCre-targeted BM progenitors give rise to an early stage non-malignant, non-transplantable disease; LckCre-targeted DN2-DN3a thymic progenitors give rise to aggressive, transplantable and metastatic T-ALL; CD4Cre targeted DN3b-DN4 thymic progenitors do not give rise to T-ALL upon NICD over-expression. Courtesy of Caroline Poisson (Poisson, 2011).

Microarray data have been generated comparing the $RNIC^{+/\Delta MxCre}$ early stage T-ALL DP cells with the $RNIC^{+/\Delta LckCre}$ late stage tumor cells in order to identify a gene expression signature for T-ALL aggressiveness and metastatic potential (Poisson, 2011). In total, the expression of 190 genes was significantly modulated with 73 genes being down-regulated and 117 up-regulated in late-stage $RNIC^{+/\Delta LckCre}$ T-ALL versus $RNIC^{+/\Delta MxCre}$ early stage non-malignant T-ALL. Pre-malignant MxCre-induced T-ALL cells clustered well in their gene expression signature with physiologic, non-malignant DP thymocytes, while LckCre-mediated T-ALL showed a distinct profile, as shown in the heat map, depicting the top 50 up- and down-regulated genes identified (Figure 10).

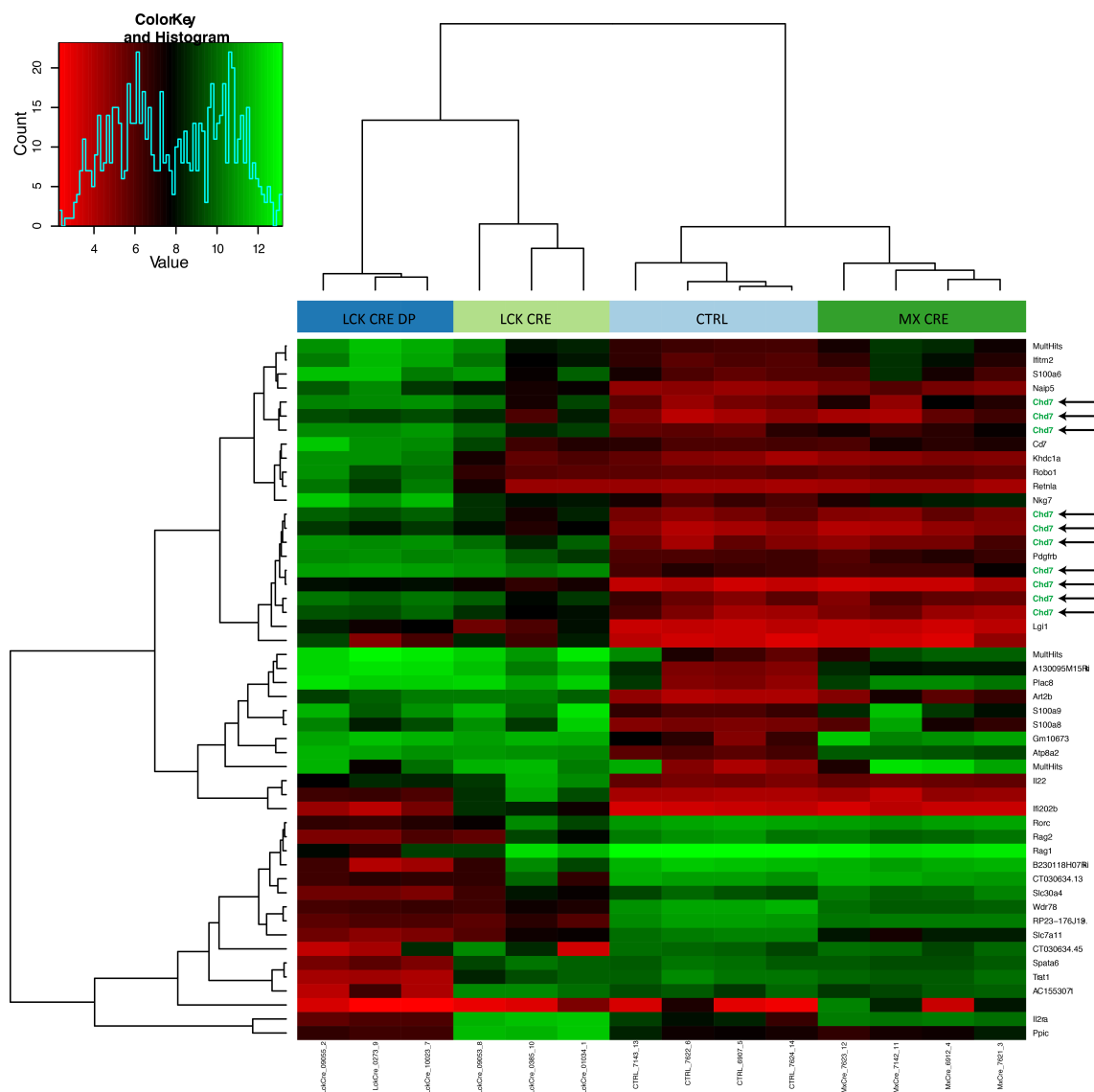


Figure 10: Top 50 differentially regulated gene candidates in late-stage metastatic versus early-stage Notch1-driven T-ALL. Heatmap depicting top gene candidates up-regulated (green) and down-regulated (red) in late-stage *RNIC⁺/ΔLckCre* and early stage *RNIC⁺/ΔMxCre* T-ALL tumors compared to physiologic CD4⁺CD8⁺ DP thymocytes (Ctrl). *Chd7* is identified as the highest up-regulated gene in late-stage metastatic T-ALL (LckCre) versus early stage pre-malignant T-ALL (MxCre) and is detected by multiple probe sets on the Affymetrix gene chip. Courtesy of Caroline Poisson (Poisson, 2011).

Chromodomain-helicase-DNA-binding protein 7, *Chd7*, was identified in the microarray as the highest over-expressed gene in late stage T-ALL with a maximal fold change expression of 26-fold compared to the early stage *RNIC⁺/ΔMxCre* T-ALL cells. Furthermore, it was identified multiple times by independent probe sets on the GeneChip (Figure 10). In addition, *Chd7* LOF had not been studied in the context of cancer at the time this PhD project was initiated. Therefore, this

candidate was selected for in-depth *in vitro* and *in vivo* validation for a potential role in hematopoiesis and T-ALL development.

1.5.3 Chd7 in Development and Disease

Chd7 is an ATP-dependant chromatin-remodelling enzyme that is expressed mostly during embryonic development (Hurd et al., 2007). For dynamic chromatin regulation, Chd7 preferentially binds to distant regulatory elements within chromatin, as demonstrated by chromatin immunoprecipitation studies (ChIP-chip) in (i) human colorectal carcinoma, (ii) human neuroblastoma cells and (iii) mouse embryonic stem (ES) cells, which were either un- or differentiated (Schnetz et al., 2009). Although Chd7 localizes to discrete chromatin locations specific for each cell type, histone H3 methylated at lysine 4 (H3K4me) is a common recognition site, which is similar to those of gene enhancer elements. This suggests that Chd7 may function in enhancer-mediated transcription of genes during embryonic development.

Loss-of-function mutations in the Chd7 encoding gene are frequently associated with CHARGE syndrome, a multi-organ disorder that affects the eye, heart, general growth and development. CHARGE stands for coloboma, heart defect, atresia choanae (also known as choanal atresia), retarded growth and development, genital abnormality, and ear abnormality. The severity of malformations vary within patients, however infants diagnosed with CHARGE syndrome often present with life-threatening conditions. Up to 60-80% of CHARGE patients carry mutations in *Chd7*; these mutations were initially identified to lie in a 2.3-Mb spanning microdeletion on chromosome 8q12, leading to the generation of pre-mature stop codons, missense mutations or mutations at the intron-exon boundary affecting the *Chd7* locus (Vissers et al., 2004).

In addition to the multi-organ defects, a small cohort of CHARGE syndrome patients also suffer from severe T-cell deficiency, linking Chd7 function to T-cell development and in T-cell mediated immunity (Writzl et al., 2007). These observations may support the potential role of Chd7 in driving aggressiveness in T-ALL, which arises from transformed immature T cell progenitors.

To study Chd7 *in vivo*, *Chd7* knock out animals were generated, however these mice are embryonic lethal at embryonic day 10.5 (E 10.5) (Hurd et al., 2007). In contrast, heterozygous gene-trapped reporter *Chd7(Gt/+)* male and female mice are viable and exhibit variable degrees of head-bobbing and circling, consistent with vestibular dysfunction. Paint-filling and beta-galactosidase staining of E12.5 and E14.5 embryos confirmed Chd7 expression in CHARGE-syndrome affected organs such as the brain, ear, heart and craniofacial structures. Therefore, *Chd7 (Gt/+)* reporter mice are a valuable means to study this disease *in vivo* (Hurd et al., 2007). The same research group also generated *Chd7* conditional knock out (cKO) animals in order to

study *Chd7* function beyond embryogenesis (Hurd et al., 2012). Conditional *Chd7* targeting in the subventricular zone neural stem cell niche and in the inner ear resulted in abnormal proliferation of the stem cells within this niche and malformations in the inner ear (Hurd et al., 2012). Further studies, inducing *Chd7* ablation in the developing eye, ear, nose, pharyngeal pouch, forebrain (Foxg1Cre) and gut (Wnt1Cre) demonstrated that *Chd7* is essential for craniofacial and tracheal development (Micucci et al., 2014).

In addition, preliminary data generated by the laboratory of Leonard Zon identified *Chd7* as a cell autonomous regulator of chromatin in HSCs performing a reverse genetic screen to find chromatin factors required for HSC induction in zebrafish (Hsuan-Ting Huang, 2010). Their work demonstrated that *Chd7*-deficient *Tg(c-myb:GFP)* cells transplanted into *Tg(Imo2:DsRed)* blastomeres resulted in more chimeric embryos compared to controls, indicating that *Chd7* may have a role in repressing HSC formation during zebrafish embryogenesis. Similarly, *Chd7* was identified as a regulator of adult hematopoiesis in a screen for Runx1-Cbfb interaction partners in the regulation of HSCs (Hsu J, 2011). In murine adult hematopoiesis, VaviCre-mediated *Chd7* deficiency does not cause any lineage specification defects but *Chd7*-deficient BM cells have a competitive advantage in reconstituting T cell numbers compared to controls. Therefore, the group of Nancy Speck suggested that *Chd7* may play a role in the regulation of the generation of mature T cells under competitive conditions (Hsu J, 2011).

These observations are supported by a study by Bajpai *et al.*, which demonstrated that another stem cell type, namely human neural crest-like stem cells, require *Chd7* for migration (Bajpai et al., 2010). Therefore, we speculated that *Chd7* may play a role in driving leukemic cell invasion into other non-hematopoietic tissues.

In addition, some studies have proposed *Chd7* as a cancer-related gene. A study by Engelen *et al.* identified *Chd7* as transcriptional co-factor for Sox2 performing proteomic and genomic screens (Engelen et al., 2011). *Chd7* and Sox2 were demonstrated to physically interact, to share similar genome-binding sites as well as common target genes, such as the Notch target *Jagged1*, the Wnt target *Gli3* and *Mycn*. These genes in turn were reported mutated in diseases that affect multiple organs similar to CHARGE syndrome, thereby linking the deregulation of *Jagged1*, *Gli3* and *Mycn* by the Sox2-*Chd7* complex with disease outcome. Furthermore, *Jagged1*-expression was strongly down-regulated in the inner ear of *Chd7*-haploinsufficient embryos, linking *Chd7* function with Notch signalling (Engelen et al., 2011).

Chd7 GOF had only been reported in one disease setting, at the beginning of this project. The group of PJ Campbell set out to identify novel driver mutations in human small-cell lung cancer by performing massive parallel sequencing of 3 representative small-cell lung cancer cell lines. Within the identified 22,910 somatic substitutions, Campbell *et al.* discovered (i) an in frame

tandem duplication affecting exons 3-8 of the CHD7 encoding gene and (ii) *PVT1-CHD7* fusion genes, indicating that *CHD7* may be frequently rearranged in small-cell lung cancer (Pleasant et al., 2010).

This was the first evidence *Chd7* may play a role in cancer development at the starting point of the project. Recently, however, *Chd7* GOF was reported in pancreatic ductal adenocarcinoma (PDAC) (Colbert et al., 2014). In this study, *Chd7* was identified as DNA damage responsive gene, which, once silenced, conferred sensitization to gemcitabine treatment in PDAC cells. The authors therefore postulate *Chd7* as a novel biomarker to evaluate and further improve PDAC treatment.

In summary, *Chd7* is a chromatin remodeller that acts in concert with different co-factors to regulate chromatin structure, thereby allowing the dynamic regulation of genes important for the development of multiple organs. Being frequently mutated in CHARGE syndrome, *Chd7* was only recently identified having potential roles in hematopoiesis and being aberrantly activated in cancer. Therefore, the chromatin remodeller *Chd7* was chosen in this thesis as prime candidate to study its role in hematopoiesis and T-ALL development.

1.6 Calcium Signalling

Calcium signalling is involved in many different temporally and spatially tightly regulated processes within the cell. These include contraction, metabolism, apoptosis, transcription, proliferation and/or hypertrophic growth. Ca^{2+} is therefore one of the most, if not the most, versatile intracellular signal. Given the many functions of calcium signalling calcium levels within the cell must be tightly controlled. Therefore, a well adjusted balance between the uptake of Ca^{2+} into the cytoplasm for signalling purposes and its removal from the cytosol by buffers, pumps and exchangers after signalling needs to be maintained (Berridge et al., 2003). The uptake of Ca^{2+} is mediated via either voltage-sensitive; store-operated or receptor-operated channels, while the plasma membrane Ca^{2+} ATPase (PMCA) and $\text{Na}^{+}/\text{Ca}^{2+}$ exchanger (NCX) are responsible for the clearance of Ca^{2+} from the cytosol (Figure 11). Within the cell, formation of second messengers and release of intracellular calcium from the sarcoplasmic/endoplasmic reticulum (SR/ER) make Ca^{2+} available for downstream events. The ER is a multifunctional organelle essential for the synthesis, folding, and processing of secretory and transmembrane proteins. Members of the SERCA family of SR/ER Ca^{2+} ATPases reside in the ER membrane and remove Ca^{2+} from the cytosol for storage within the ER lumen, which has high Ca^{2+} levels reaching the millimolar range. Thereby Serca pumps function to maintain a constant Ca^{2+} supply available for signalling events but also maintain “physiological” levels of approximately 100 nM

Ca^{2+} in the cytosol. This is counteracted by the removal of Ca^{2+} from the ER by inositol-1,4,5-trisphosphate receptors (Ins(1,4,5)P₃Rs) and ryanodine receptors (RYRs), as well as Ca^{2+} -binding proteins, such as calreticulin and calsequestrin that reside in the ER lumen and thereby regulate the relative abundance of Ca^{2+} . In mitochondria, Ca^{2+} also plays important roles in regulating cellular outcomes, such as differentiation, cell survival and apoptosis. Mitochondrial Ca^{2+} supply is guaranteed by the electrophysiological uptake through a Ca^{2+} uniporter, whereas Ca^{2+} removal from the mitochondrion is mediated either via a Na^+/H^+ -dependant Ca^{2+} -exchanger or via the opening of permeability transition pores (PTP) (Figure 11) (Orrenius et al., 2003).

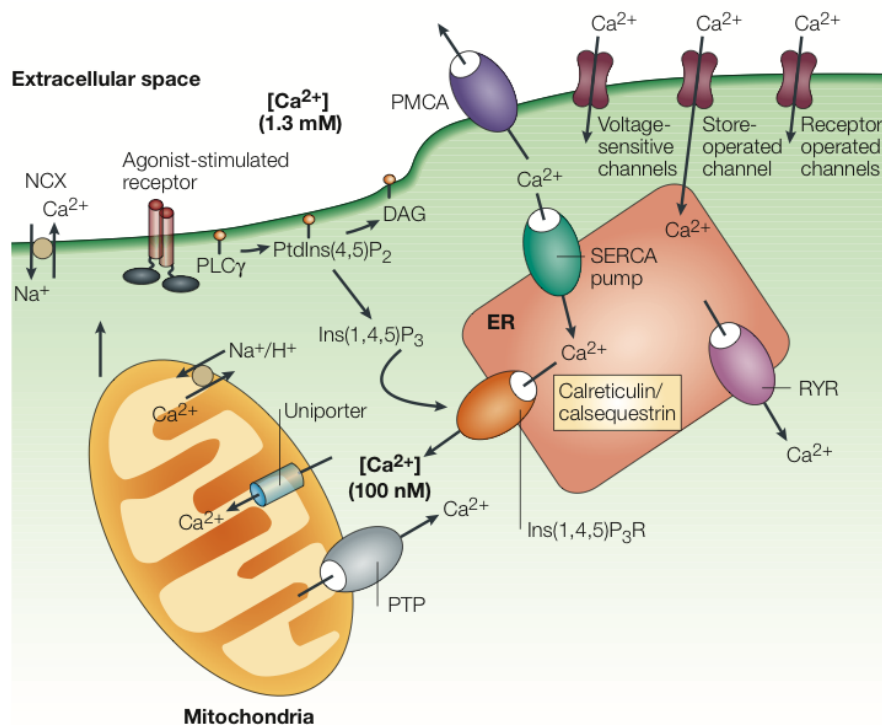


Figure 11: The regulation of intracellular Ca^{2+} compartmentalization. Ca^{2+} supply within the cell is regulated by several pumps and exchangers located in the cell membrane and in intracellular organelles. Ca^{2+} uptake is mediated via voltage-sensitive, store-operated or receptor-mediated channels located within the outer cell membrane. In contrast, the plasma membrane Ca^{2+} ATPase (PMCA) and $\text{Na}^+/\text{Ca}^{2+}$ exchanger (NCX) remove Ca^{2+} from the cytosol by pumping it into the extracellular space. Within the ER, sarcoplasmic/endoplasmic reticulum (SR/ER) Ca^{2+} ATPases pump Ca^{2+} under hydrolysis of ATP into the ER lumen. This is counteracted by the removal of Ca^{2+} by inositol-1,4,5-trisphosphate (Ins(1,4,5)P₃) receptors (Ins(1,4,5)P₃Rs) and ryanodine receptors (RYRs) in the ER membrane. In addition, Ca^{2+} -binding proteins, such as calreticulin and calsequestrin residing in the ER lumen regulate the relative abundance of Ca^{2+} . Adapted from (Orrenius et al., 2003).

1.6.1 Calcium Levels, ER stress and Unfolded Protein Response

Calcium homeostasis within the cell is guaranteed by the interplay between several ATP-dependent calcium pumps; ion channels and exchangers; as well as receptor-mediated second

messenger uptake of Ca^{2+} . Therefore, aberrant activation or inactivation of components of the calcium signalling network can have detrimental effects for the cell.

Alterations in intracellular calcium levels (exceeding ≈ 100 nM) but also inhibition of N-glycosylation were demonstrated to cause an accumulation and aggregation of unfolded proteins in the ER. In response to this “danger” signal, chaperones are induced to resolve the presence of unfolded proteins; a phenomenon termed unfolded protein response (UPR) or ER stress (Sidrauski et al., 1998). In mammals, the UPR is mediated by three major and parallel signalling branches, mediated by (i) the ER-resident transmembrane protein kinase-endoribonucleases (RNase) IRE1, (ii) the protein RNA-like ER kinase PERK and (iii) a family of type II transmembrane transcription factors, with ATF6 being its most prominent member (Figure 12).

In brief, PERK phosphorylates eukaryotic initiation factor (eIF2a) in order to suppress general protein translation (Ron and Walter, 2007). IRE1 activation leads to recruitment of several signaling molecules that can engage inflammatory and survival-related signals, and activation of its RNase domain leads to the splicing and production of an active transcription factor called X box-binding protein 1 (XBP-1) (Todd et al., 2008). ATF6 translocates to the Golgi apparatus, where it is processed by two proteases to become an active transcription factor (Chen et al., 2002). Taken together, the three arms of the UPR act to (i) reduce general protein translation, (ii) stimulate protein degradation and (iii) increase folding capacity to cope with ER stress (Figure 12). Therefore, the UPR is a key response mechanism activated in order to resolve ER stress.

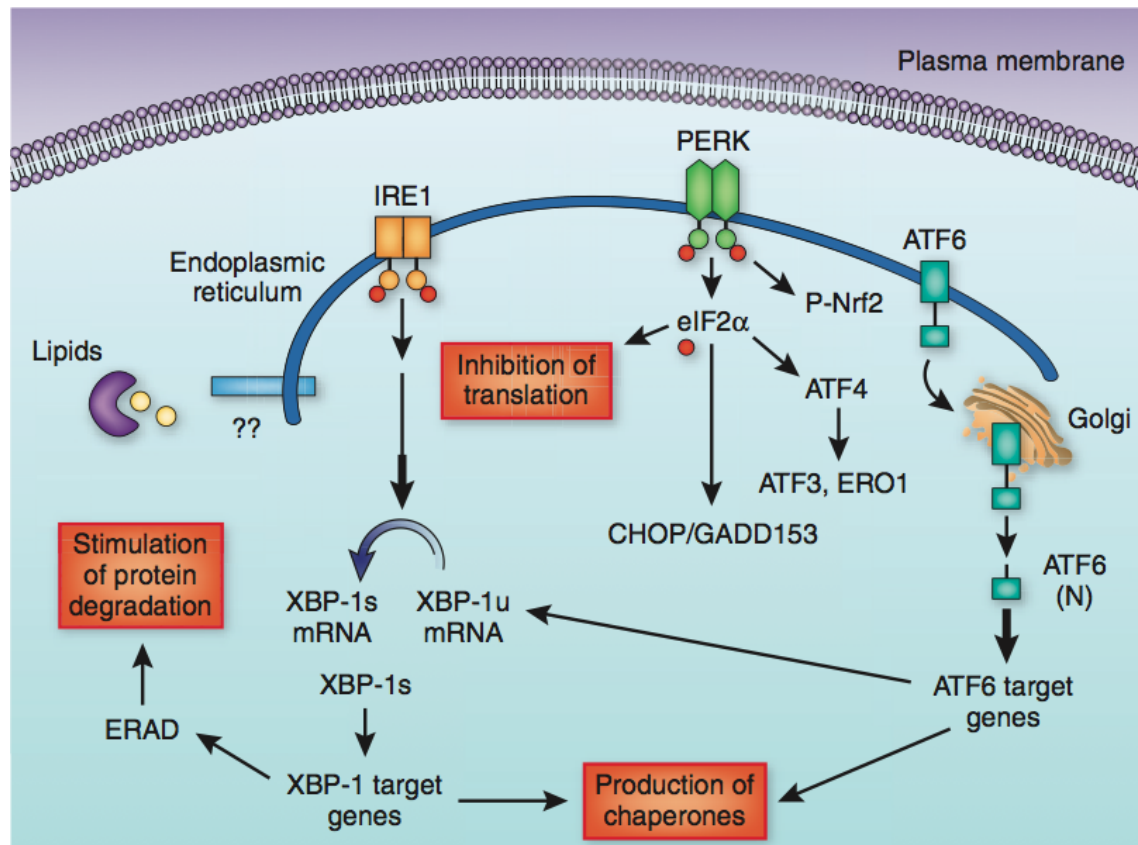


Figure 12: Canonical unfolded protein response (UPR). The canonical UPR is mediated by the three UPR sensors PERK, IRE1a and ATF6. PERK mainly functions in phosphorylating eIF2 α to attenuate general protein translation, but can also regulate the activity of several transcription factors such as ATF4, ATF3 and nuclear factor E2-related factor-2 (Nrf2). Upon autophosphorylation, the RNase activity of IRE1a results in the production of the active spliced XBP-1, leading to the expression and production of ER chaperones and components of the ER-associated degradation (ERAD) process. Consequently, ATF6 moves to the Golgi apparatus, where it is proteolytically processed to become an active transcription factor. Taken together, activation of the three branches results in expression of chaperone proteins and XBP-1, thereby (i) inhibiting translation, (ii) facilitating protein degradation and (iii) producing of ER chaperones and other molecules that restore the ER folding environment. Adapted from (Hotamisligil, 2010).

But, if this stress cannot be resolved successfully after UPR induction, apoptosis is initiated (Ron and Walter, 2007). This process, however, is poorly understood and there are studies proposing different mechanisms for apoptosis induction in response to ER stress. For instance, deregulated calcium levels within the cell were demonstrated to negatively impact on the translocation of the pro-apoptotic proteins BAX and BAK from the ER to the mitochondria (Scorrano et al., 2003). Further evidence suggests that IRE-mediated activation of Jun N-terminal kinase (JNK) may contribute to apoptosis by phosphorylating and thereby inactivating the anti-apoptotic protein BCL-2 (Urano et al., 2000). In addition, PERK-mediated phosphorylation of eIF2 α was demonstrated to contribute to apoptosis by inhibiting the synthesis of pro-survival proteins and in induction of the CCAAT/enhancer-binding protein homologous protein, downstream of PERK, may repress expression of BCL2 (McCullough et al., 2001). This was confirmed in *CHOP*^{-/-}

mice, in which a negative feedback loop leads to eIF2 α dephosphorylation, which in consequence favours recovery of protein synthesis.

Further studies in mice suggested that ER-stress induced apoptosis is mediated via caspase 12 (Nakagawa and Yuan, 2000), whose cleavage is activated through tumor necrosis factor receptor signalling.

There exist different chemicals to induce and study ER stress *in vitro*. The chemical thapsigargin (TH), a sesquiterpene lactone isolated from the plant *Thapsia garganica*, was demonstrated to inhibit SERCA pumps, thereby causing ER store depletion of Ca²⁺ and consequently inducing ER stress and apoptosis (Jiang et al., 1994). In contrast, tunicamycin, a mixture of homologous nucleoside antibiotics, inhibits N-linked glycosylation and is therefore also frequently used to induce ER stress and UPR (Chan and Egan, 2005).

1.6.2 Calcium Signalling and ER Stress in Hematopoietic Stem Cells

Hematopoietic stem cells have also been studied in the context of calcium signalling. The group of DT Scadden identified expression of the Calcium sensing receptor (CaR) on HSCs as crucial requirement for their proper migration from fetal liver into the endosteal BM niche. Notably, fetal liver *CaR*-deficient HSCs were normal in numbers and were found in circulation in spleen and BM, however their capacity to constantly lodge to the endosteal niche was severely impaired. Therefore, *CaR* was shown to critically retain HSCs in close proximity to the endosteal surface in the BM niche (Adams et al., 2006). Consequently, pharmacological modulation of CaR using the agonist Cinacalcet led to increased primitive hematopoietic cell activity *in vitro*, such as enhanced growth and migration towards the chemotactic stimulus stromal cell derived factor 1 α . This is confirmative of the studies in *CaR* KO animals and gives the modulation of this receptor a rationale for the treatment of HSC during stem cell therapy, thereby enhancing lodgement towards into the BM niche (Lam et al., 2011).

In addition, the group of Means AR (Kitsos et al., 2005) studied the role of calmodulin-dependant protein kinase IV (CaMKIV) in HSC biology in *CaMKIV* KO animals. Notably, KLS cells deficient for *CaMKIV* are significantly reduced in numbers and are impaired in their reconstitutive capacity in serial transplantation assays. This KLS cell failure in response to *CaMKIV* deficiency was due to apoptosis induction via CBP and Bcl2, hence linking deregulated calcium levels with HSC homeostasis and survival. This demonstrated further evidence that calcium signalling is crucial for HSC function.

Recently, the lab of John Dick performed single cell sequencing on lineage-depleted umbilical cord blood populations and thereby identified a gene signature for UPR-responsive genes

enriched in HSC compared to progenitors (Laurenti et al., 2013). Therefore, Van Galen *et al.* set out to address the effect of the UPR on human HSCs (hHSCs) under stress conditions (van Galen et al., 2014). In this study, ER stress mediated via (i) inhibition of N-glycosylation by tunicamycin and (ii) calcium imbalance provoked by deregulation of Serca function was studied in hHSCs and progenitor cells. Analysis of gene expression of candidates implicated in all three branches in the UPR demonstrated that hHSCs activated preferentially the PERK branch of UPR, followed by the induction of apoptosis. In contrast, progenitor subsets rather showed adaptive responses to UPR promoting cell survival rather than apoptosis. Hence “stressed” hHSCs rather committed apoptosis compared to more differentiated progenitors, thereby protecting the hematopoietic system from propagation of damaged or mutated genetic information. Reciprocal experiments, overexpressing the co-chaperone ERDJ4 in hHSCs, which functions downstream of PERK, led to an increase in HSC repopulation capacity in xenograft models. Thereby, a first link between ER stress/UPR and HSC function was established (van Galen et al., 2014).

1.6.3 Identification of Serca2 as potential Drug Target in Notch1-driven T-ALL

Aberrant Notch1 pathway activation is frequently linked to T-ALL and therefore, there exists a strong need to identify novel inhibitors of Notch in order to ameliorate treatment regimens apart from conventional therapy such as chemo- and radiotherapy in this hematological tumor. Therefore, a co-culture based chemical compound screen was performed in house (Lehal, 2011) to identify molecules with inhibitory potential against Notch (Figure 13 A). In this assay, HeLa cells, stably expressing either the DL4 ligand or the N1 receptor, were cultured in close proximity in order to induce Notch signaling. A co-transfected luciferase reporter construct, harboring multiple CSL binding sites, was utilized as read out for Notch pathway activation, and hence served as means to quantify inhibitory effects of the screened compounds on the Notch pathway. With the use of this screening approach, cyclopiazonic acid (CPA), which targets calcium pumps of the Serca family, was identified (Lehal, 2011).

Similarly, in a recent study Roti *et al.* performed a (i) Notch1 “loss-of-function” (LOF) screen combined with (ii) a Notch “gain-of-function” (GOF) screen in order to identify Notch inhibitory compounds on the one hand and proteins, which may regulate Notch, on the other hand (Roti et al., 2013) (Figure 13 B). Pursuing the chemical compound screen in Notch-activated DND41 T-ALL cells, led to the identification of the compounds thapsigargin (TH) and strikingly also CPA, both targeting the calcium ATPases of the Serca family. Furthermore, overexpression of cDNA clones from an open reading frame library was performed in U2OS osteosarcoma cells These

expressed a mutated form of the N1 receptor hence displaying oncogenic activity, and were used to find potential Notch cooperating molecules in T-ALL. Using this approach, Serca2, the biological target of TH and CPA, was confirmed.

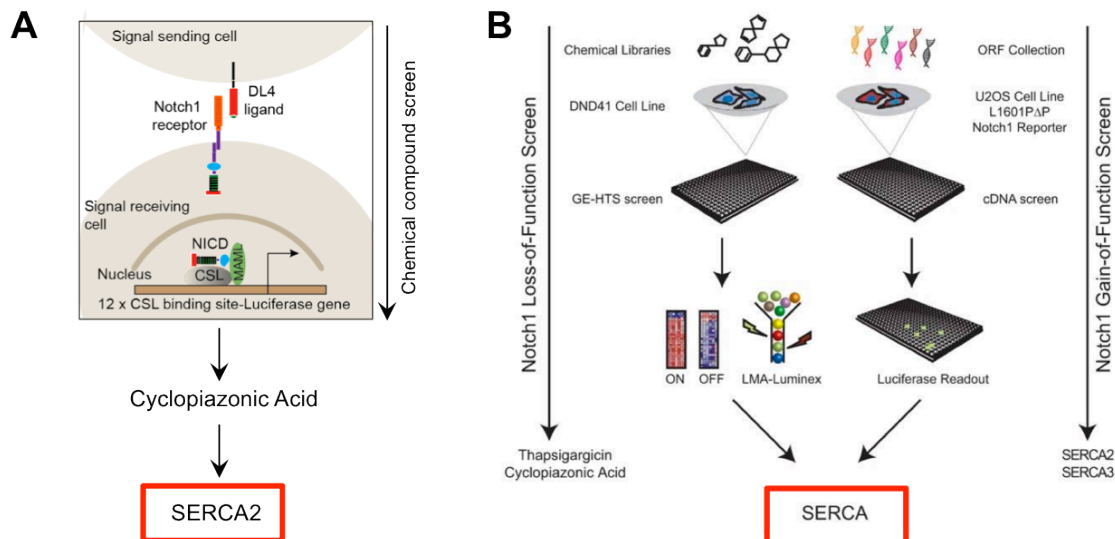


Figure 13: Identification of SERCA2 as a potential drug target in Notch-1 driven T-ALL. Three independent screening approaches led to identification of the chemical compounds Thapsigargin and CPA, which specifically target SERCA2, a Calcium ATPase in the ER membrane. **A**, Co-culture-based chemical compound screen performed in house to discover novel inhibitors for DL4-Notch1 mediated Notch signaling in HeLa cells (Lehal, 2011). **B**, (**left**), Notch1 loss of function screen in DND41 T-ALL cells and (**right**) Notch 1 gain of function screen in Notch-mutated U2OS cells performed by Stegmaier *et al.* to identify chemical Notch inhibitors and cooperating partners of mutated Notch1 (Roti *et al.*, 2013).

Rajwinder Lehal studied CPA treatment of leukemic cell lines in the context of his PhD thesis and confirmed that CPA blocks Notch pathway activation in the co-culture system and down-regulates Notch target genes (Lehal, 2011). The study by Roti *et al.* addressed the function of Serca2 for N1 receptor maturation and proved TH treatment detrimental for T-ALL cell engraftment in xenografts, thereby proposing Serca2 as a potential drug target in Notch-driven T-ALL (Roti *et al.*, 2013).

Given the identification of CPA as a putative drug to treat N1-driven T-ALL, we set out to characterize the function of its biological target, Serca2, in hematopoiesis to better understand (i) how deregulation of intracellular calcium signalling may impact on hematopoietic lineages and (ii) to decipher the mode of action of CPA in treatment of T-ALL.

1.6.4 Sarco-Endoplasmatic Reticulum Calcium ATPases (Sercas)

Serca pumps are responsible for the accumulation of Ca^{2+} in the SR/ER lumen and therefore have important function in the regulation of intracellular calcium levels. The mobilisation of $[\text{Ca}^{2+}]_i$

from intracellular organelles is highly specialized in cardiac and skeletal muscle cells and Serca ATPases are mainly studied in the context of muscle contraction and heart biology. In brief, Ca^{2+} transport from the cytosol into the SR causes relaxation of muscle cells, while high cytosolic Ca^{2+} levels in contrast lead to muscle excitation.

The Serca family of Ca^{2+} ATPases comprises the three members Serca1, Serca2 and Serca3, which are evolutionary highly conserved but localized on different chromosomes. Serca isoforms are diverse in their nature due to alternative splicing predominantly affecting their COOH-terminus. At present, 7 mammalian Serca isoforms have been identified, which can be subclassified into Serca1a-b, Serca2 a-c and Serca3a-c.

The first subfamily of Serca pumps is specific for the SR in fast-twitch skeletal muscle and both isoforms Serca1a and Serca1b are regulating the uptake of Ca^{2+} into the SR. Autosomal recessive (LOF) mutations in *SERCA1* are linked to Brody disease, a rare inherited muscle disorder characterized by stiffness and cramps due to exercise-induced impairment of muscle relaxation (Prasad et al., 2004). Generation of *Serca1* KO mice by conventional gene targeting revealed that *Serca1 null* mice develop normally after birth, but die due to an aberrant Ca^{2+} uptake and hypercontracture injury to the diaphragm muscles. Furthermore, it was demonstrated that neither *Serca2* nor *Serca3* compensate for *Serca3* LOF, which is confirmative of the lethality of *Serca1* KO animals (Pan, 2003). Serca2 family members are important for calcium transport into the ER and similarly show differential expression depending on the isoform. *Serca2*, being focus of this thesis, will be discussed in the next section. In contrast to Serca1 and Serca2, Serca3 has 3 splice variants (Serca3a-c), which vary in their C-termini. Serca3 members, initially thought to be expressed only in a limited number of tissues such as endothelial cells and pancreatic β -cells (Prasad et al., 2004), were recently demonstrated expressed in cardiomyocytes. However, mice deficient for *Serca3* develop normally and do not display any gross developmental abnormalities other than mild defects in Ca^{2+} uptake detected in vascular endothelial cells (Buckley and Whorton, 1997).

1.6.5 Serca2 in Development and Disease

The Serca2a protein is prominently expressed in cardiac and slow-twitch muscle and was first cloned in 1985 (MacLennan et al., 1985). In contrast, the isoform Serca2b is expressed in all tissues, including heart and smooth muscle, and is the main non-cardiac ER Ca^{2+} ATPase with house keeping function and differs from Serca2a in its C-terminus (Figure 14). Structurally, both Serca2a and b are anchored to the ER membrane by its 10 transmembrane helices, which are intersected by a β -strand domain between loop 2-3 and by the phosphorylation and nucleotide

binding domains between loop 4-5. While both the N- and C-terminal segments of Serca2a are exposed to the cytoplasm, the C-terminus of Serca2b enters into the ER lumen. In both of these isoforms, the active site for ATP hydrolysis is located within the phosphorylation and nucleotide binding domains and the transmembrane domain, containing Ca^{2+} binding sites, builds the channel for Ca^{2+} transport from the cytosol into the ER (Figure 14).

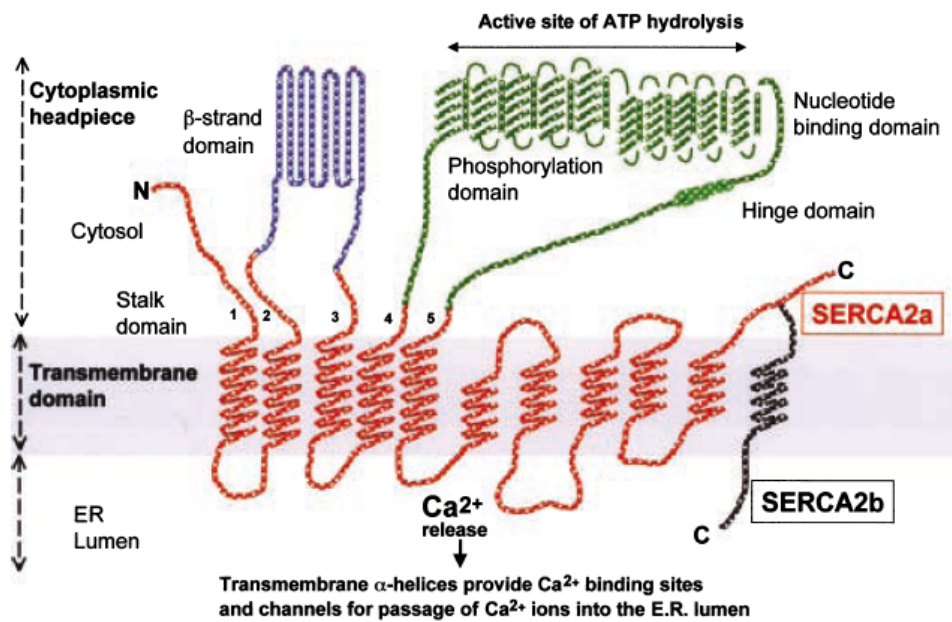


Figure 14: Structure of Serca2a and Serca2b residing in the ER membrane. Serca2 is anchored to the ER membrane by its 10 transmembrane helices, which are intersected with a β -strand domain between loop 2-3 and the phosphorylation and nucleotide binding domains between loop 4-5. The active site for ATP hydrolysis is formed in the phosphorylation and nucleotide binding domains. The transmembrane domain, containing Ca^{2+} binding sites, builds the channel for Ca^{2+} transport from the cytosol into the ER. Both the N- and C-terminal segments of Serca2a are exposed to the cytoplasm, while the C-terminus of Serca2b enters into the ER lumen. Adapted from (Dhitavat et al., 2004).

In 2003, another isoform, Serca2c, was identified in monocytes. Serca2c is ubiquitously expressed and arises from the Serca2a isoform but displays a short intronic sequence located between exons 20 and 21. Furthermore, structurally the Serca2c protein was predicted to possess a truncated C-terminus containing a short but unique peptide stretch (Gelebart et al., 2003). However, to date, little is known about this isoform of the Serca2 family.

In general, upon hydrolysis of one ATP molecule, Serca2 pumps two Ca^{2+} ions into the SR/ER, thereby working against the 1:7000 calcium gradient, that is established from the cytosol over the SR/ER (Shannon and Bers, 1997). Ample evidence suggests however, that in neutral pH, two H^{+} ions are exported out of the SR/ER per two Ca^{2+} ions transported into this compartment, speculating that Serca2 may function as a Ca^{2+} - H^{+} antiporter (Kuhlbrandt, 2004; Niggli and Sigel, 2008).

In order to study the function of *Serca2* *in vivo*, conventional and conditional *Serca2* KO animals have been generated. *Serca2 null* mice die *in utero* due to cardiac defects caused by severely reduced Ca^{2+} levels in the SR. SERCA2 heterozygous mice (*Serca2*^{+/-}) mice are viable but display impaired cardiac contractility and relaxation, suggesting that *Serca2* function is crucial for sequestration of Ca^{2+} within cardiac cells and their intracellular compartments (Periasamy et al., 1999). In contrast, conditional *Serca2* ablation in cardiomyocytes in the adult leads to only a mild heart dysfunction (Andersson et al., 2009).

In 1993, the chromosomal locus 12q23-24.1, encoding SERCA2, was linked to Darier's disease for the first time (Bashir et al., 1993; Craddock et al., 1993). Darier's disease patients mainly present missense mutations in a single copy of the SERCA2 encoding gene *ATP2A2*, thereby attributing it a role as haploinsufficient tumor suppressor in this pathologic setting. Darier's disease is an autosomal-dominant skin disease in humans characterized by keratinized squamous epithelial cells (Sakuntabhai et al., 1999). However, since these patients do not display with any heart malfunction, the functional copy of the residual *SERCA2* allele can compensate for its counter partner. Interestingly, mice heterozygous for *SERCA2* (*SERCA2*^{+/-}) develop squamous cell carcinoma of the skin (Prasad et al., 2004), which is confirmative of the identification of *ATP2a2* as the Darier's disease-causing gene. Taken together, these studies demonstrate a gene dosage effect for *SERCA2* in regulating skin homeostasis.

Studies in our laboratory identified CPA as potential Notch inhibitor, through targeting SERCA2 (Lehal, 2011). Lehal Rajwinder demonstrated that CPA significantly down-regulates Notch pathway activation in the co-culture based screening system and as a consequence Notch target gene expression (*Hes1*, *Deltex*, *c-myc*) is similarly reduced in human T-ALL cells. Furthermore, *Hes1* down-regulation was due to impaired recruitment of NICD to CSL/RBPJ κ binding sites within the *Hes1* promoter. When treating human T-ALL cells lines with CPA, Rajwinder Lehal demonstrated that most Notch-driven leukemic cells were sensitive to CPA, resulting in a proliferation block upon treatment. Preliminary *in vivo* data demonstrated that CPA does not induce goblet cell metaplasia in mice, a well described *N1* and *N2* double LOF phenotype in the gut (Riccio et al., 2008). These data supported *in vitro* results and suggest that CPA primarily negatively impacts on *N1* rather than *N2* signalling.

Similarly, work by Roti et al. linked over-activation of SERCA2 with T-ALL, thereby giving first evidence, that *SERCA2* GOF is linked to cancer development (Roti et al., 2013). In this study the chemical compounds TH and CPA were identified as Notch inhibitory drugs, targeting SERCA2. Inhibition of SERCA by TH led to down-regulation of Notch target genes like *MYC*, *DELTEX1* and *HES1*, confirming that SERCA was a valid target in *N1* driven T-ALL. Furthermore, Roti et al.

demonstrated growth-inhibitory effects of TH in human T-ALL cells *in vitro* as well as in Xenografts, which display decreased tumor volume when treated with TH. This was demonstrated to be due to impaired Notch receptor maturation specifically in N1-mutated T-ALL cells, which displayed lower NICD levels in response to TH treatment and therefore, SERCA2 was proposed to be a possible therapeutic target in T-ALL.

2 Objectives of this work

2.1 Part I: Role of Chd7 in the Hematopoietic system and in T-ALL

Aberrant Notch1 pathway activation is reported in more than 50% of T-ALL patients. Treatment regimens include chemotherapy in concert with radiotherapy, however the incidence of relapse in patients is extremely high. Therefore, there exists a strong need to not only specifically inhibit the Notch signalling pathway but to also identify molecular players that cooperate with Notch in T-ALL development. Microarray analysis performed by a former student in the lab, PhD Caroline Poisson, identified the chromatin-remodelling enzyme Chromodomain Helicase DNA-binding protein 7, Chd7, as such a potential partner cooperating with Notch in T-ALL maintenance. Aim of this work was to assess whether genetic ablation of *Chd7* would improve or accelerate disease outcome in murine and human Notch1-driven T-ALL. In addition, given the identification of *Chd7* in late-stage T-ALL, we set out to characterize the role of *Chd7* in the hematopoietic system under physiological and competitive conditions.

2.2 Part II: Role of Serca2 in the Hematopoietic system

Aberrant Notch signaling has been implicated in many different aspects of human cancer such as hyperproliferation, invasiveness and angiogenesis. Therefore, the Notch signaling pathway represents a bona fide drug target. We and Roti *et al.* have performed chemical compound screenings and identified Cyclopiazonic acid (CPA) to be a potent Notch inhibitor (Lehal, 2011; Roti et al., 2013). Biological target of this compound is the Sarco/Endoplasmic Reticulum ATPase2 (Serca2) that is involved in calcium homeostasis within the cell.

Aim of this study was to characterize the function of Serca2 in the hematopoietic system in order to better understand the mode of action of CPA in the treatment of T-ALL. Therefore, we generated BM specific Serca2-deficient chimeric mice that either lacked one or both functional alleles of *Serca2* and assessed the impact of *Serca2* loss of function (LOF) on the hematopoietic system under physiologic and competitive conditions. In addition and more relevant to the clinic, we studied the effect of the proposed anti-cancer drug Thapsigargin, a non-competitive Serca ATPase inhibitor and CPA analogue, on BM progenitor and HSC biology.

3 Results – Part I: Role of Chd7 in Hematopoiesis & T-ALL

3.1 Validation of Potential Mediators cooperating with Notch1 in T-ALL

Based on the microarray study performed by a former PhD student, Caroline Poisson (unpublished data), we set out to validate potential mediators that may co-operate with Notch1 in T-ALL (Poisson, 2011). The top 40 up- and down-regulated candidate genes identified to be differentially regulated between early-stage non-malignant *RNIC⁺/ΔMxCre* and late-stage metastasizing *RNIC⁺/ΔLckCre*-induced T-ALL were validated by qRT-PCR. Data achieved during this microarray validation can be found in the Appendix section I. The chromatin remodeller Chd7 was selected for study in this thesis because it was (i) the highest over-expressed gene in late stage tumors out of 117 gene candidates (Figure 15 A and B) and (ii) *Chd7* gain-of-function effects in cancer were until then only identified by one research group but not studied.

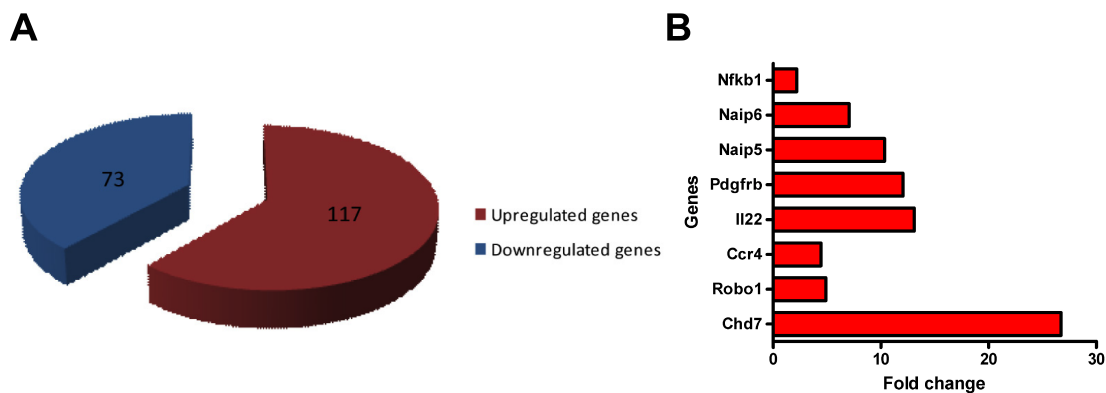


Figure 15: Chd7 is the highest over-expressed gene in late-stage T-ALL compared to pre-malignant T-ALL. A, Pie chart of differentially expressed genes identified in late-stage metastatic T-ALL (*RNIC⁺/ΔLckCre*) versus pre-malignant (*RNIC⁺/ΔMxCre*) T-ALL. **B,** Top up-regulated gene candidates in late-stage T-ALL compared to early-stage T-ALL (set to 1). Chd7 is the highest up-regulated gene in *RNIC⁺/ΔLckCre* T-ALL with a maximal expression change of 26-fold normalized to *RNIC⁺/ΔMxCre* pre-malignant T-ALL. Courtesy of Caroline Poisson (Poisson, 2011).

Since *Chd7* was highly expressed in late-stage Notch1-driven T-ALL, we wanted to investigate the function of Chd7 first in normal hematopoiesis followed by its putative function in the context of T-ALL development and maintenance.

3.2 Functional Characterization of Chd7 in Hematopoiesis

To study the role of Chd7 during hematopoiesis, *Chd7^{ΔMxCre}* mice were generated by crossing the *Chd7^{lox/lox}* cKO strain (Hurd et al., 2010) with the INF type I-responsive MxCre recombinase, which efficiently targets BM progenitors.

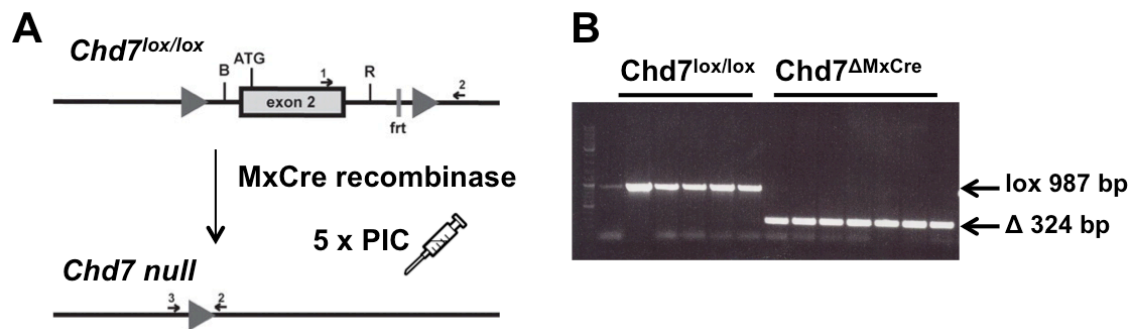


Figure 16: Strategy for conditional *in vivo* inactivation of *Chd7* in the BM. **A**, Schematic representation of the genetically modified murine *Chd7* locus, in which the ATG-encoding exon 2 is flanked by loxP sites. Activation of MxCre recombinase by administration of PIC leads to the generation of a *Chd7 null* allele in BM cells. **B**, Deletion PCR analysis demonstrating a 987 bp lox band and a 324 bp deletion band amplified from genomic DNA isolated from *Chd7^{lox/lox}* or *Chd7^{ΔMxCre}* BM cells.

MxCre-mediated *Chd7* conditional deletion was induced via administration of Poly(I):Poly(C) (PIC) every second day over 10 days, resulting in excision of the ATG-encoding exon 2 in the murine *Chd7* locus (Figure 16 A). Four weeks post PIC induction, deletion efficiency was confirmed by PCR analysis of DNA isolated from BM of *Chd7^{ΔMxCre}* or *Chd7^{lox/lox}* mice: Excision of the loxP-site flanked exon 2 resulted in amplification of a 324 bp deletion (Δ) band as compared to a 987 bp amplicon from the *Chd7* floxed locus (Figure 16 B).

3.2.1 Chd7 Deficiency does not affect Hematopoiesis under Steady State Conditions

It was previously reported that CHD7 is important for stem cell biology (Bajpai et al., 2010) and it was hypothesized that Chd7 may negatively regulate T cell numbers (Hsu J, 2011). Therefore, we characterized all hematopoietic lineages in absence or presence of *Chd7* with a primary focus on HSCs and T cells. Conditional loss of *Chd7* utilizing the MxCre recombinase was found to have no effect on the HSC compartment. Figure 17 shows representative FACS plots of (A) the Lineage-c-kit⁺Sca1⁺ (KLS) population enriched for HSCs and progenitor cells that was further analyzed for expression of the markers CD135 and CD34, which allow the classification into

long-term HSC (LT-HSC, CD135-CD34⁻), short-term HSC (ST-HSC, CD135-CD34⁺) and multi-potent progenitors (MPP, CD135⁺, CD34⁺).

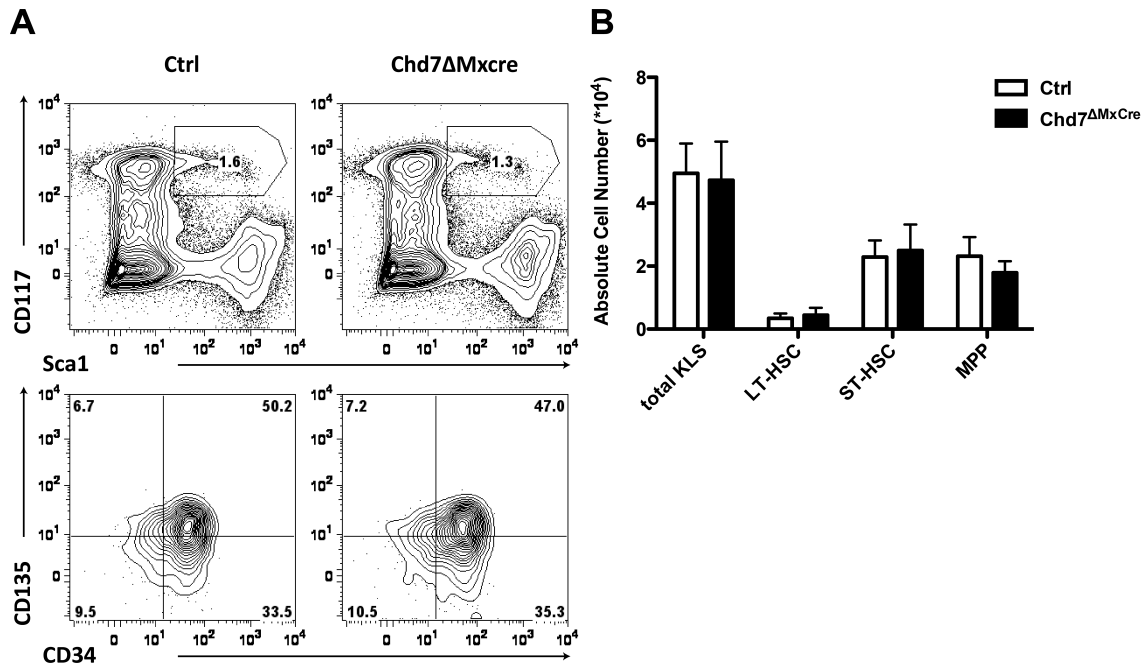


Figure 17: *Chd7* Deficiency does not perturb hematopoietic development. *Chd7*^{ΔMxCre} and *Chd7*^{lox/lox} (Ctrl) BM cells were analysed for the KLS compartment 5 weeks post MxCre induction. **A upper panel**, Representative FACS plots showing Ctrl and *Chd7*^{ΔMxCre} Lineage-CD117⁺Sca1⁺ (KLS) cells and **lower panel**, Ctrl and *Chd7*^{ΔMxCre} LT-HSCs (KLS, CD135⁻CD34⁻), ST-HSCs (KLS, CD135⁻CD34⁺) and MPPs (KLS, CD135⁺CD34⁺). **B**, Absolute cell numbers of total KLS and HSC subpopulations depicted in **A**. Error bars represent mean ± SD, n = 5 (Ctrl) and n = 5 (*Chd7*^{ΔMxCre}).

Upon analysis of the HSC compartment five weeks post PIC induction, no significant differences in (i) percentages (Figure 17 A) and (ii) absolute numbers (Figure 17 B) of total KLS, LT-HSCs, ST-HSCs and MPPs were found between *Chd7*-competent and *Chd7*-deficient cells.

Furthermore, we hypothesized that *Chd7* may regulate T cell development given that Notch is crucial for T lineage commitment (Radtke et al., 1999) and that *Chd7* was identified as highly up-regulated in late-stage N1-driven T-ALL compared to pre-malignant T-ALL. Therefore, we analyzed the thymi of *Chd7*^{ΔMxCre} and *Chd7*^{lox/lox} Ctrl 5 weeks post MxCre activation focusing on T cell progenitors at the DN stages and immature and mature αβ and γδ T cells. However, *Chd7*-deficient hematopoietic progenitors gave rise to normal numbers of T cell progenitors at double negative stages DN1 to DN4 (Figure 18 A) as well as immature CD4⁺CD8⁺ DP and mature CD4⁺SP, CD8⁺ SP effector T cells (Figure 18 B) and TCRγδ T cells as shown in Figure 18 C.

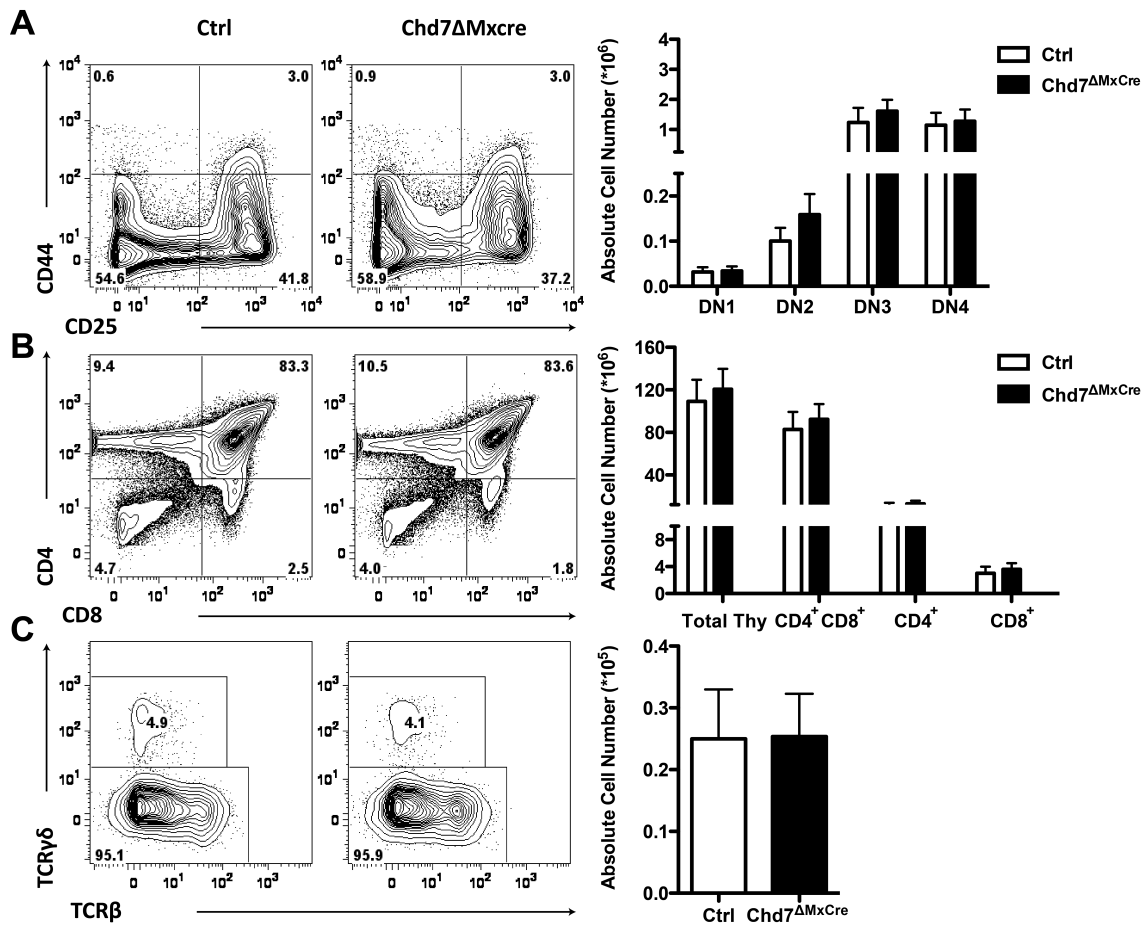


Figure 18: *Chd7* deficiency does not affect T cell development in the thymus. *Chd7* Δ MxCre and *Chd7*^{lox/lox} (Ctrl) thymi were analysed 5 weeks post MxCre induction. **A, left panel**, Representative FACS analysis showing Ctrl and *Chd7* Δ MxCre CD4-CD8-Lin⁻ thymocytes stained with anti-CD25 and anti-CD44 antibodies to distinguish DN1 (CD44⁺CD25⁻), DN2, (CD44⁺CD25⁺), DN3 (CD44⁻CD25⁺) and DN4 stages (CD44⁻CD25⁻) of maturation and **right panel** corresponding absolute cell numbers. **B, left panel**, Representative FACS plots showing cell surface expression of CD4 and CD8 in *Chd7*^{lox/lox} (Ctrl) and *Chd7* Δ MxCre mice, and **right panel** corresponding absolute cell numbers. **C, left panel**, Representative FACS plots showing cell surface expression of TCR $\gamma\delta$ and TCR β , gated on CD4-CD8⁻ thymocytes, and **right panel** corresponding absolute cell numbers. Error bars represent mean \pm SD, n = 5 (Ctrl) and n = 5 (*Chd7* Δ MxCre).

In addition, given the importance of Notch signalling in the development of marginal zone B (MZB) cells in the spleen (Tanigaki et al., 2002), we also investigated whether *Chd7* plays a role in MZB differentiation. No significant differences in the percentage (Figure 19 A), nor in absolute cell numbers of MZB cells (Figure 19 B) was observed in *Chd7*-competent or *Chd7*-deficient cells. However, similarly, other mature hematopoietic lineages in the periphery such as B cells (B220⁺), overall T cells (TCR β ⁺) and CD4⁺ SP or CD8⁺ SP T cells were also not affected by genetic ablation of *Chd7* as depicted in Figure 19 B.

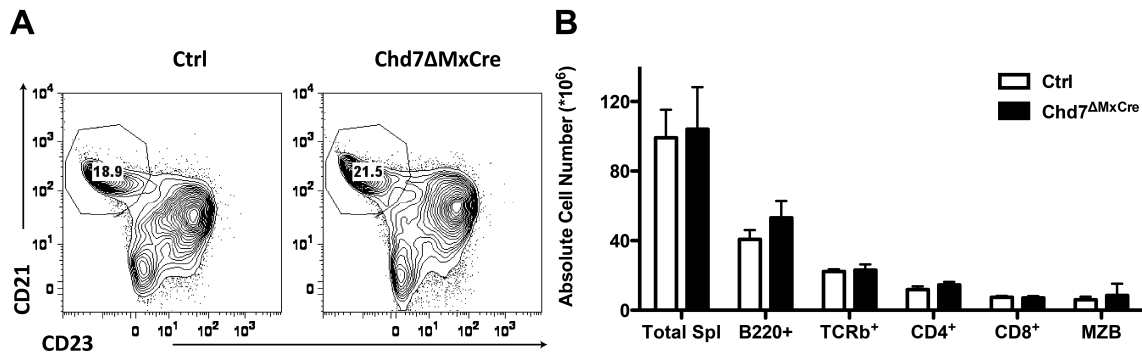


Figure 19: *Chd7* deficiency does not affect mature lineages or marginal zone B cells in the spleen. *Chd7*^{ΔMxCre} and *Chd7*^{lox/lox} (Ctrl) spleens were analysed 5 weeks post MxCre induction. **A**, Representative FACS plots showing Ctrl and *Chd7*^{ΔMxCre} marginal zone B cells, gated for B220⁺IgM⁺CD21⁺CD23⁻. **B**, Absolute cell numbers of total splenic cellularity, B cells (B220⁺), T cells (TCRb⁺, CD4⁺, CD8⁺) and marginal zone B cells (MZB) in the spleen of Ctrl (n = 5) and *Chd7*^{ΔMxCre} (n=5) mice. Error bars represent mean ± SD.

3.2.2 *Chd7* Deficiency does not affect on Hematopoiesis under Competitive Conditions upon Serial Transplantation

Genetic ablation of *Chd7* did not result in any overt phenotype in the hematopoietic system under physiologic conditions. However, previous data generated by the group of Nancy Speck indicated that *Chd7*-deficient BM cells had a competitive advantage in T cell reconstitution compared to wild type cells, when serially transplanted into lethally irradiated recipients (Hsu J, 2011). This suggested a role for *Chd7* in restraining T cell numbers in the adult. Furthermore, work by the Zon lab suggested that *Chd7* regulates HSC induction in the zebrafish, as *Chd7*-deficient progenitor cells transplanted into blastomeres induced less chimeric embryos compared to Ctrl (Huang HT, 2010).

These results suggested that *Chd7* may play a role in regulating hematopoiesis under competitive conditions. Therefore, we set out to study whether loss of *Chd7* renders HSCs more or less sensitive to stress conditions. This was performed in the 5-FU *in vivo* challenging system and by generation of primary and secondary competitive BM chimeras.

3.2.2.1 *Chd7* Deficiency does not render Hematopoietic Stem Cells more susceptible to 5-FU-mediated Exhaustion

Hematopoietic stem cells possess the capacity to self-renew but also to maintain homeostasis by differentiation in order to replenish the entire pool of all mature cell types in the blood in response to injury. The chemotherapeutic agent 5-FU depletes all cycling cells within the BM, thereby stimulating HSC proliferation (Lerner and Harrison, 1990). Therefore, 5-FU is frequently administered to study HSC mobilization in response to stress *in vivo*. 5-FU was administered bi-weekly in *Chd7*-competent and *Chd7*-deficient chimeras over a period of 12 days and animals were analysed for the HSC compartment. *Chd7*-competent BM chimeras (n = 10) had a median

survival of 11 days as compared to Ctrl mice (n = 10) with a 10 day-median survival (Figure 20 A) demonstrating that *Chd7* deficiency does not confer a survival advantage in this *in vivo* challenging system. In response to 5-FU treatment, total BM cellularity (Figure 20 B) and the percentage of mobilized donor-derived CD45.2⁺Lin⁻CD117⁺Sca1⁺ HSCs (Figure 20 C) in *Chd7*-deficient (n = 4) and Ctrl (n = 5) mice were comparable.

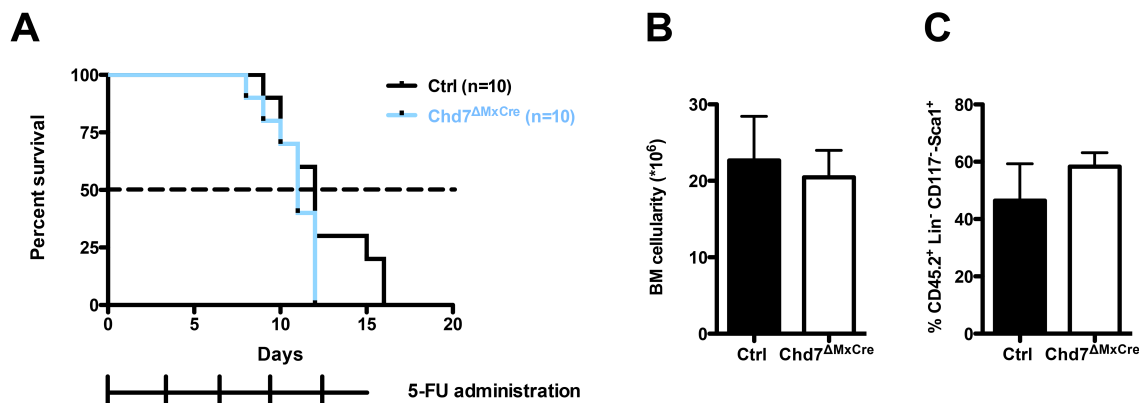


Figure 20: Chd7 deficiency does not render hematopoietic stem cells more susceptible to exhaustion. Three weeks post MxCre induction *Chd7*^{lox/lox} (Ctrl) and *Chd7*^{ΔMxCre} mice were treated with 5-FU twice per week over 12 days. **A**, Kaplan-Meier survival curve of 5-FU treated BM chimeras with *Chd7*^{ΔMxCre} (n = 10) mice depicted in blue and Ctrl (n = 10) mice depicted in black. Arrows indicate 5-FU injections. Median survival was calculated using Log-rank Mantel-Cox test. **B**, Absolute number of total BM cells and **C**, Percentage of HSCs (KLS; Lin⁻CD117⁺Sca1⁺) from control and indicated cKO mice. Error bars represent mean ± SD.

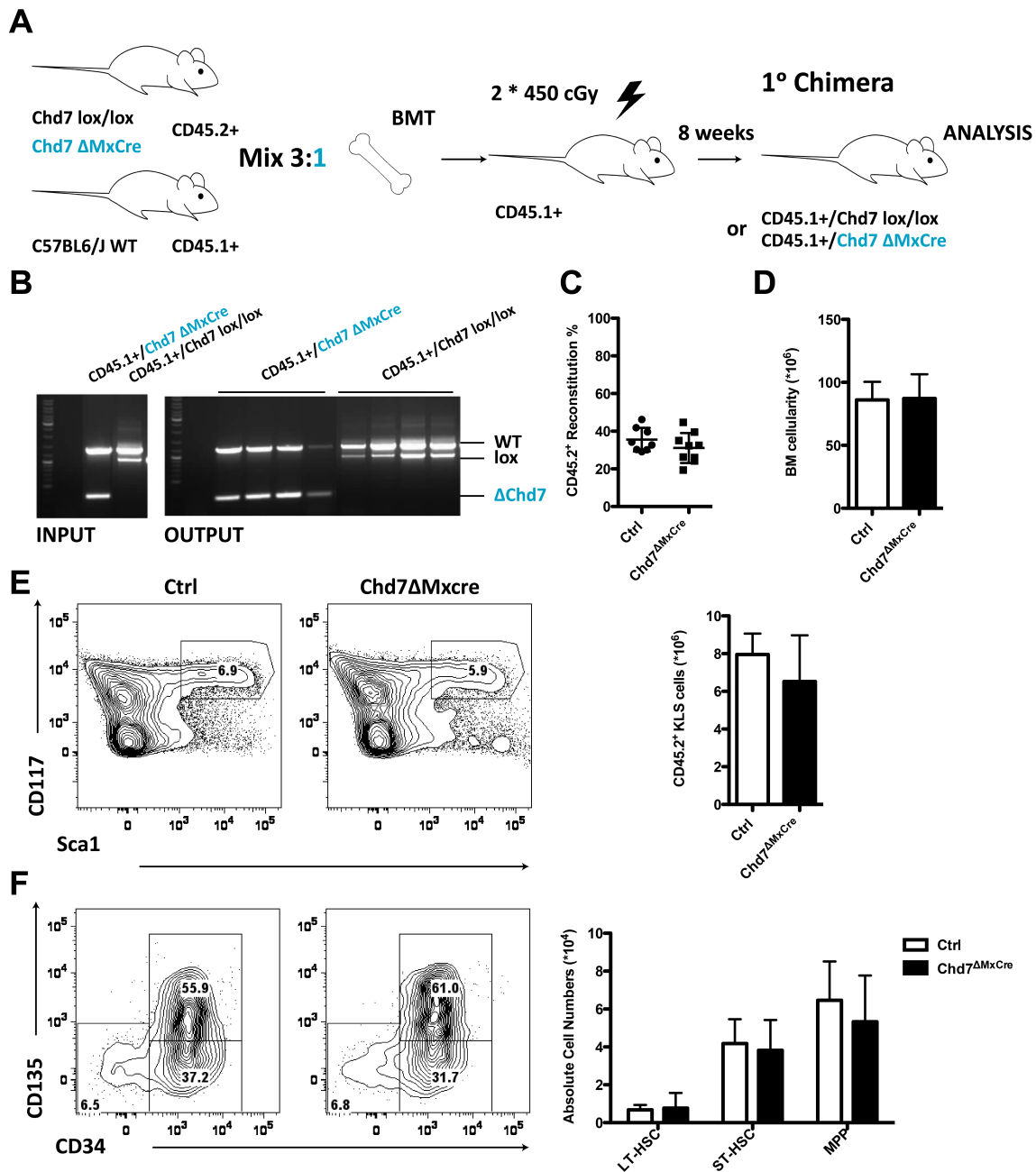
Taken together, these data indicate that *Chd7* does not render HSCs more susceptible to exhaustion upon 5-FU mediated stress.

3.2.2.2 *Chd7* Deficiency does not render Hematopoietic Stem Cells more competent in Primary Competitive BM Chimeras

Chd7 deficiency did not affect the “fitness” of HSCs upon ablation of mature cycling hematopoietic lineages and the hereby-induced mobilization of the quiescent HSC pool to replenish the blood system after repetitive 5-FU administration *in vivo*. To assess another form of stress, we investigated the ability of *Chd7*-deficient BM cells to reconstitute the hematopoietic system under competitive conditions. Therefore, competitive BM chimeras were generated by mixing CD45.1⁺ WT C57BL6/J BM cells with either CD45.2⁺ *Chd7*^{ΔMxCre} or *Chd7*^{lox/lox} (Ctrl) BM cells in a 3:1 ratio and transplanting into lethally irradiated CD45.1⁺ recipients (Figure 21 A) and the short-term reconstitution was assessed 8 weeks post transplantation. DNA from input BM (Figure 21 B, left panel) and from BM of analysed chimeras (Figure 21 B, right panel) was analysed for the ratio of *Chd7* WT and *Chd7*-deleted or *Chd7*^{lox/lox} cells by PCR. Three to one ratio of WT versus *Chd7*-competent or *Chd7*-deficient hematopoietic reconstitution was maintained

short-term post transplantation (Figure 21 C) as indicated by the percentage CD45.2⁺ cells in PBLs of chimeric mice.

When analysing Chd7 competitive BM chimeras, we focussed on the stem cell compartment given the importance of Chd7 in regulating the transcriptional program in human neural crest derived stem cells and thereby enhancing migratory properties in these cells (Bajpai et al., 2010). Overall, the total BM cellularity of *Chd7*-competent and *Chd7*-deficient mixed BM chimeras was comparable (Ctrl = $86.12 \pm 5.04 * 10^6$ cells; *Chd7*^{ΔMxCre} = $87.13 \pm 6.4 * 10^6$ cells, 21 D). Similarly, the percentage and absolute numbers of KLS (Lin⁻CD117⁺Sca1⁺) remained comparable between these cohorts (21 E). Subfractionation of the KLS compartment into LT-HSCs (CD135⁻CD34⁻), ST-HSCs (CD135⁻CD34⁺) and MPPs (CD135⁺, CD34⁺) also demonstrated no apparent effect of *Chd7* deficiency on these subpopulations of the stem cell pool (21 F). In addition, thymi of chimeric mice were analysed, however *Chd7* deficiency did not affect T cell development in these mice (data not shown). Taken together, these data indicate that Chd7 does not confer any advantage or disadvantage in the short-term repopulation of the hematopoietic system of lethally irradiated recipients in primary 3:1 competitive BM chimeras.



3.2.2.3 Chd7 Deficiency does not affect HSCs in Secondary Competitive BM Chimeras

We demonstrated that *Chd7* deficiency does not affect short-term HSC reconstitutive capacity in primary mixed BM chimeras. However certain genes, such as *p21*, only functionally regulate HSC self-renewal and multilineage reconstitution potential upon multiple rounds of serial transplantation (Siu et al., 2014). Therefore, we wanted to investigate whether *Chd7* ablation may affect HSC function upon serial transplantation as inducer of hematological stress. Secondary mixed BM chimeras were generated by pooling BM from *Chd7*^{ΔMxCre} : CD45.1⁺ (n = 3) and *Chd7*^{lox/lox} : CD45.1⁺ (Ctrl, n = 3) primary chimeras, which had similarly engrafted, and performed serial transplantation into lethally irradiated recipient mice (Figure 22 A). Successful engraftment of donor-derived BM was monitored in PBLs 4 weeks post transplantation and the BM of chimeric mice was analysed focusing on the HSC compartment 10 weeks after transplantation.

Deletion PCR analysis of input BM demonstrated the maintenance of 3:1 ratio of WT and deleted *Chd7* or *Chd7* lox band at the time of transplantation (Figure 22 B) and flow cytometric analysis of CD45.2⁺ donor-derived cells confirmed similar reconstitution between *Chd7*^{ΔMxCre} and Ctrl chimeras (Figure 22 C).

No significant differences in (i) total BM cellularity (Figure 22 D), nor in (ii) the KLS compartment (Figure 22 E) were detected in *Chd7*-competent and *Chd7*-deficient secondary competitive BM chimeras. However, *Chd7*^{ΔMxCre} secondary chimeras contained significantly more LT-HSCs (KLS CD135⁺CD34⁻) compared to control chimeras (Figure 22 F) with *Chd7*^{ΔMxCre} chimeras containing $3.36 \pm 1.08 * 10^4$ LT-HSCs (n = 7) compared to $0.88 \pm 0.15 * 10^4$ LT-HSCs in control chimeras (n = 8). This increase in LT-HSCs did however not translate into significant differences for ST-HSCs or MPPs, including more mature lineages such as T cells (data not shown).

Taken together, our work suggests that *Chd7* does not play a major role in regulating hematopoiesis under normal and 5FU-mediated stress conditions and in competitive repopulation assays and if so, only under strong competition against C57BL6/J WT cells, however, without significant benefit for the recipient host.

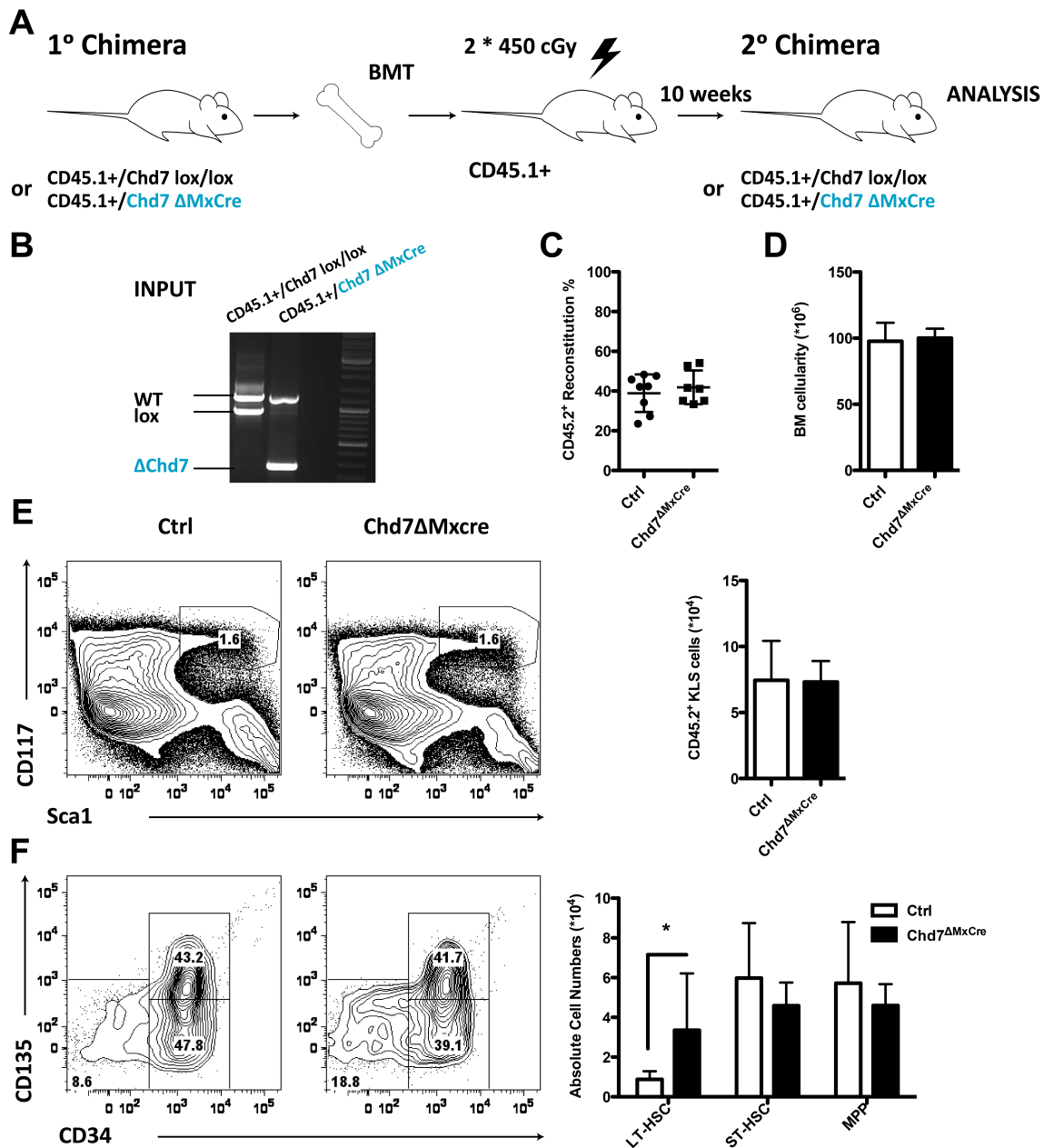


Figure 22: *Chd7* deficiency does affect the short-term repopulation capacity of HSCs under competitive conditions in secondary mixed BM chimeras. **A**, Schematic representation of the generation of *Chd7*^{ΔMxCre} and *Chd7*^{lox/lox} (Ctrl) secondary 3:1 mixed BM chimeras. **B**, Deletion PCR analysis of input DNA pooled from total BM of either Ctrl or *Chd7*^{ΔMxCre} primary mixed BM chimeras. **C**, Percentage of CD45.2⁺ reconstitution in PBLs 4 weeks post ATBM. **D**, Total BM cellularity of secondary 3:1 chimeras. **E**, **left panel**, Representative FACS plots of CD45.2⁺ Ctrl and *Chd7*^{ΔMxCre} KLS cells with **right panel**, absolute cell numbers depicted. **F**, **left panel**, Representative FACS plots of CD45.2⁺ Ctrl and *Chd7*^{ΔMxCre} LT-HSCs (KLS, CD135⁻CD34⁺), ST-HSCs (KLS, CD135⁻CD34⁺) and MPPs (KLS, CD135⁺CD34⁺) with **right panel**, absolute cell numbers depicted. *Chd7*^{ΔMxCre}: CD45.1⁺ (n = 7) and Ctrl: CD45.1⁺ (n = 8) BM cells were analysed 10 weeks post MxCre induction. Error bars represent mean ± SD (* p < 0.05).

3.3 Chd7 Deficiency does not affect Notch1-driven murine T-ALL

Previous work demonstrated that *Chd7* is highly expressed in late-stage Notch1-driven T-ALL (*RNIC⁺/ΔLckCre* model) compared to non-metastasizing pre-malignant precursor T-ALL cells (*RNIC⁺/ΔMxCre* model). A study by Bajpai *et al.* demonstrated that human neural crest like stem cells require CHD7 for normal migration. If this Chd7 function would also be conserved in the context of Notch-driven T-ALL, then Chd7 could promote leukemic cell invasion into non-hematopoietic tissues. To test this hypothesis, we first assessed *Chd7* expression levels in T-ALL cells generated in the genetic *RNIC⁺/ΔMxCre* and *RNIC⁺/ΔLckCre* mouse models.

In addition, we also studied the role of Chd7 by LOF experiments in murine Notch1-driven T-ALL. These studies were performed using two different murine T-ALL models: (i) the RNIC model, in which Chd7 was initially identified and in (ii) a retroviral MigR1-NICD BM transduction model. MxCre and CD4Cre transgenic mice were crossed into the retroviral T-ALL transduction model to inactivate *Chd7* in either BM cells or at DN3b-DN4 stages of T cell maturation. MxCre and LckCre transgenic mice were crossed into the genetic RNIC model to ablate *Chd7* function in BM progenitors or in T cells at the earlier DN2-DN3a stage of T cell development.

3.3.1 Chd7 is highly expressed in murine Notch-driven T-ALL

Microarray analysis performed on *RNIC⁺/ΔMxCre* versus *RNIC⁺/ΔLckCre* T-ALL tumors demonstrated that *Chd7* was the highest over-expressed gene in late stage T-ALL tumors compared with early stage tumours (26-fold increased expression, Figure 23 A, courtesy of Caroline Poisson). Therefore, we selected this candidate for in-depth *in vitro* and *in vivo* validation. In agreement with previous findings, *Chd7* was highly up-regulated in BM samples of T-ALL-bearing *RNIC^{ΔLckCre}* mice and in cell lines generated from these mice compared to primary early stage *RNIC^{ΔMxCre}* T-ALL (Figure 23 B). While primary *RNIC^{ΔLckCre}*-derived leukemic cells showed a mean expression of 26.12 ± 9.54 FC compared and normalized to T-ALL cells derived from pre-malignant *RNIC^{ΔMxCre}* T-ALL (set to 1), cultured murine T-ALL cell lines derived from these mice had a mean FC *Chd7* expression of 13.78 ± 4.80 (Figure 23 B), suggesting that *Chd7* is expressed at higher levels *in vivo* than *in vitro*.

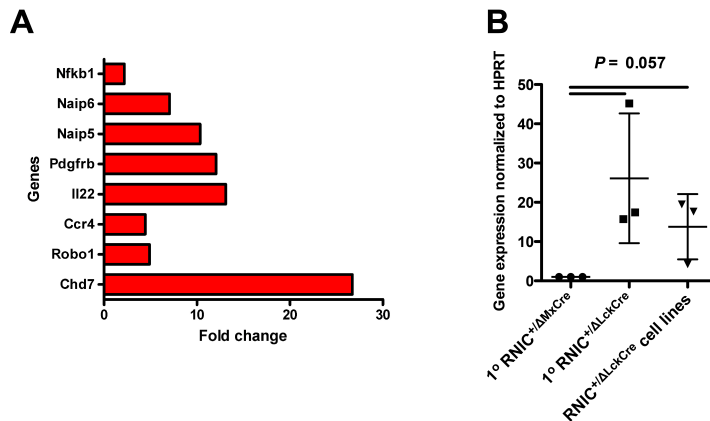


Figure 23: *Chd7* is highly expressed in aggressive metastasizing late stage versus early stage murine Notch1-driven T-ALL. **A**, Top gene candidates up-regulated in late (*RNIC^{+/ΔLckCre}*) versus early stage (*RNIC^{+/ΔMxCre}*) murine Notch1-driven T-ALL identified by PhD Caroline Poisson. **B**, *Chd7* relative gene expression assess by qRT-PCR in cDNA derived from independent primary *RNIC^{+/ΔLckCre}* T-ALL cells and *RNIC^{+/ΔLckCre}*-derived cell lines compared to primary *RNIC^{+/ΔMxCre}* T-ALL cells isolated from BM. Error bars represent mean \pm SD, $n = 3$.

Taken together, we confirmed over-expression of *Chd7* in late-stage T-ALL tumors and therefore set out to study the role of *Chd7* in T-ALL development *in vivo*.

3.3.2 *Chd7* Deficiency does not affect T-ALL Initiation

Aberrant Notch pathway activation is frequently observed in T-ALL (Ellisen et al., 1991; Weng et al., 2004) and over-expression of NICD via retroviral infection of BM progenitor cells leads to T-ALL development with 100% penetrance (Pear et al., 1996b). We utilized this well-established T-ALL induction model to assess whether conditional ablation of *Chd7* may have beneficial or detrimental effects on hematopoietic cells driven towards leukemia.

3.3.2.1 *Chd7* Deficiency does not affect T-ALL Initiation in the Retroviral *Chd7^{ΔMxCre}* NICD-NGFR Model

Bone marrow of *Chd7^{ΔMxCre}* or *Chd7^{lox/lox}* (Ctrl) mice was harvested 4 weeks after induction of MxCre by administration of PIC and enrichment for lineage negative BM cells was performed using MACS technology. *Chd7^{ΔMxCre}* or Ctrl Lin⁻ BM cells were retrovirally infected with MigR1-NICD-ires-NGFR to induce stable expression of NICD fused to an internal ribosomal entry site followed by the cDNA encoding the Nerve Growth Factor Receptor (NGFR). Upon *in vitro* culture for three days, infected NICD-expressing BM cells were transplanted into lethally irradiated recipient mice in order to give rise to T-ALL (Figure 24 A). *Chd7*-deficient NICD-NGFR over-expressing chimeras ($n = 5$) had a median survival of 79 days compared with a 67-day median survival in Ctrl chimeras ($n = 7$), indicating that *Chd7* does not impact on T-ALL induction in this retroviral model (Figure 24 B). In addition, PCR analysis confirmed efficient deletion of *Chd7* in

BM cells of tumor-bearing chimeras (Figure 24 C). Flow cytometric analysis of CD45.2⁺NICD-NGFR⁺ T-ALL cells revealed no phenotypic difference in CD4⁺ CD8⁺ cell surface expression between *Chd7*-competent and *Chd7*-deficient cells (Figure 24 D). *Chd7*-competent and *Chd7*-deficient BM progenitors over-expressing NICD had comparable relative and absolute numbers of abnormal CD4⁺CD8⁺ DP and CD8⁺ SP cells in (i) the BM (Figure 24 E) and (ii) in peripheral organs such as the spleen (Figure 24 G). Similarly, total BM cellularity (Figure 24 F) as well as total splenic cellularity (Figure 24 H) was comparably increased in *Chd7*-competent and *Chd7*-deficient chimeras due to CD45.2⁺NGFR⁺ T-ALL cell expansion.

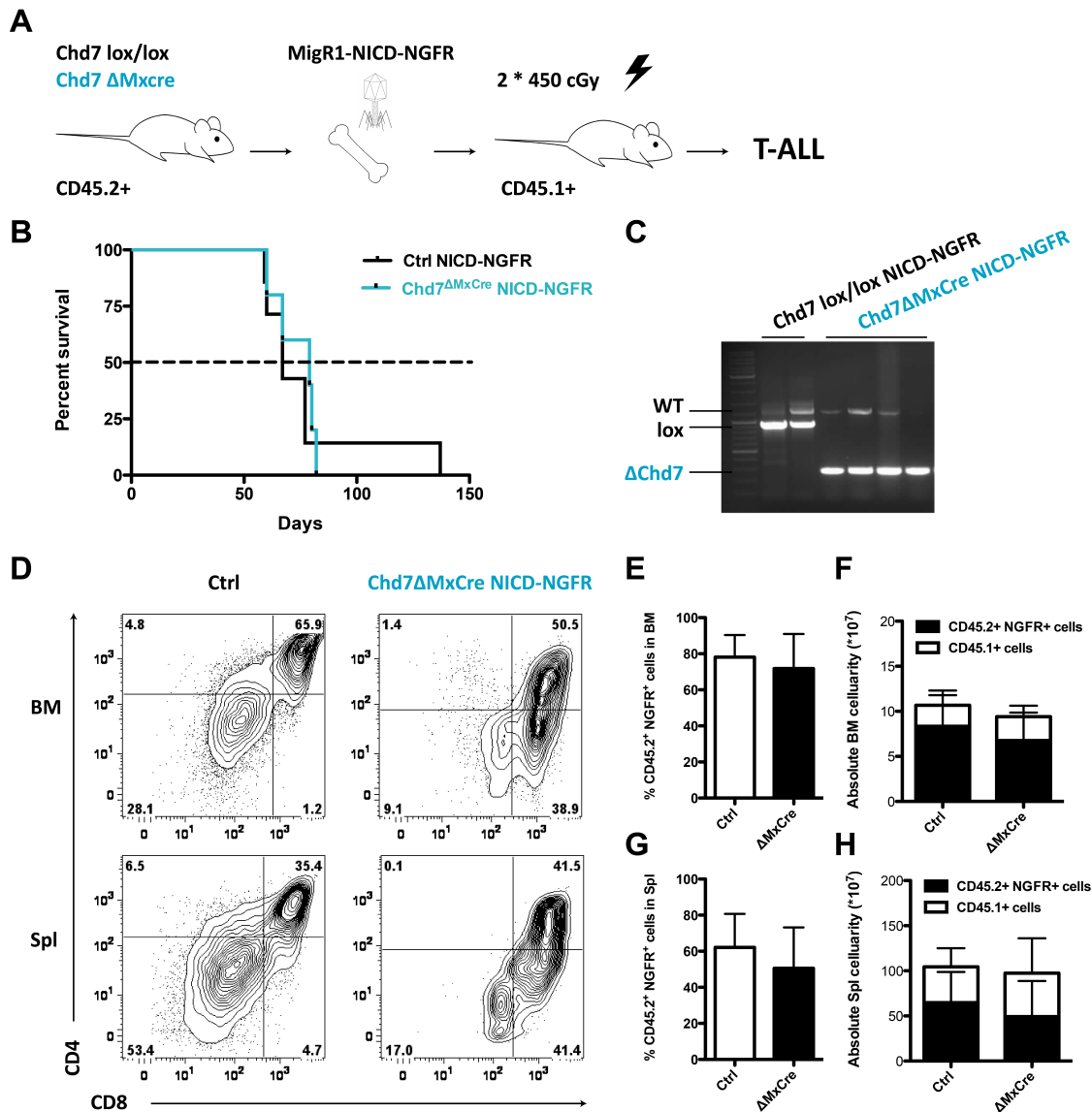


Figure 24: *Chd7* deficiency does not alter T-ALL induction in the murine MxCre-mediated MigR1-NICD model. A, Schematic representation of *Chd7* Δ MxCre MigR1-NICD-NGFR T-ALL induction model. B, Kaplan-Meier survival curve of *Chd7* Δ MxCre MigR1-NICD-NGFR chimeras (n = 5) depicted in blue and Ctrl (n = 7) chimeras depicted in black. Median survival was calculated using Log-rank Mantel-Cox test. C, *Chd7* deletion PCR analysis on BM cells from T-ALL bearing mice. Representative FACS plots for cell surface expression of CD4 and CD8 in *Chd7* Δ MxCre MigR1-NICD-NGFR and Ctrl T-ALL cells in the BM and spleen (D). Bar diagrams depicting percentage of CD45.2⁺NGFR⁺ T-ALL cells in BM (E) and spleen (G). Total BM (F) and splenic (H) cellularity calculated for CD45.1⁺ WT and CD45.2⁺NGFR⁺ T-ALL cells in chimeras.

Collectively, these data demonstrate that loss of *Chd7* does not detectably influence induction of T-ALL in the retroviral NICD BM transduction model using the MxCre deleter.

3.3.2.2 Chd7 Deficiency does not affect T-ALL Initiation in the Retroviral *Chd7*^{ΔCD4Cre} NICD-NGFR Model

To test whether ablation of *Chd7* at a somewhat later developmental stage, once Notch has induced the development of pre-leukemic cells, may influence disease outcome, we used *Chd7*^{ΔCD4Cre} transgenic mice. The CD4 Cre recombinase is activated in thymic progenitor cells at the DN3b-DN4 stage of differentiation beyond the TCR β checkpoint, up to which Notch signalling is required for T lineage specification. Crossing *Chd7* cKO mice with CD4Cre transgenic mice generated *Chd7*^{ΔCD4Cre} and T-ALL was induced in *Chd7*-deficient and Ctrl cells via retroviral infection of BM progenitors with MigR1-NICD-NGFR as previously described (Figure 25 A).

Chd7^{ΔCD4Cre}-MigR1-NICD chimeric mice (n = 6) had a median survival of 67.5 days in comparison with 74.5 days in Ctrl chimeras (n = 8, Figure 25 B). In addition, PCR analysis confirmed efficient deletion of *Chd7* in BM cells of T-ALL-bearing chimeras (Figure 25 C). Flow cytometric analysis of CD45.2⁺NICD-NGFR⁺ T-ALL cells revealed no phenotypic difference between CD4⁺ CD8⁺ cell surface expression on *Chd7*-competent and *Chd7*-deficient T-ALL cells in the BM and spleen (Figure 25 D). Comparable expansion of abnormal CD4⁺CD8⁺ DP and CD8⁺ SP cells in (i) the BM (Figure 25 E) and (ii) in the spleen (Figure 25 G) was observed in both cohorts. Similarly, total BM cellularity (Figure 25 F) as well as total splenic cellularity (Figure 25 H) were comparably increased in *Chd7*-competent and *Chd7*-deficient chimeras due to CD45.2⁺NGFR⁺ T-ALL cell expansion.

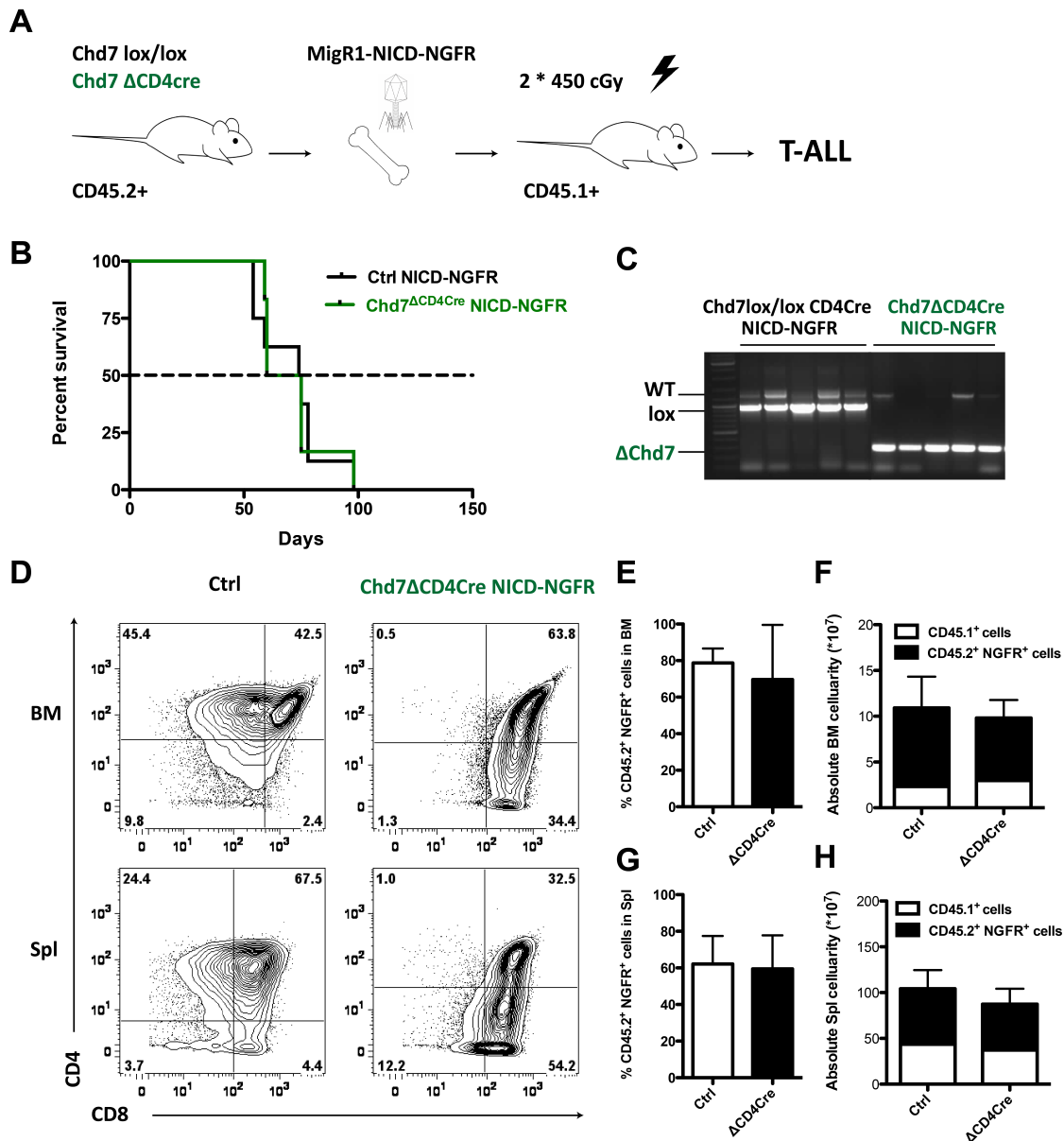


Figure 25: *Chd7* deficiency does not alter T-ALL induction in the murine CD4Cre-mediated MigR1-NICD model. **A**, Schematic representation of *Chd7*^{ΔCD4Cre} MigR1-NICD-NGFR T-ALL induction model. **B**, Kaplan-Meier survival curve of *Chd7*^{ΔCD4Cre} MigR1-NICD-NGFR chimeras (n = 6) depicted in green and Ctrl (n = 8) chimeras depicted in black. Median survival was calculated using Log-rank Mantel-Cox test. **C**, *Chd7* deletion PCR analysis on T-ALL bearing mice. Representative FACS plots for cell surface expression of CD4 and CD8 in *Chd7*^{ΔCD4Cre} MigR1-NICD-NGFR and Ctrl T-ALL cells in the BM and spleen (**D**). Bar diagrams depicting percentage of CD45.2+NGFR⁺ T-ALL cells in BM (**E**) and spleen (**G**). Total BM (**F**) and splenic (**H**) cellularity calculated for CD45.1⁺ WT and CD45.2+NGFR⁺ T-ALL cells in chimeras.

Taken together, these data suggest that *Chd7* does not influence T-ALL initiation when deleted in thymic progenitor cells at the DN3b-DN4 stage of maturation.

3.3.2.3 Chd7 Deficiency does not affect T-ALL initiation in the Genetic MxCre or LckCre-driven RNIC Chd7 Models

Chd7 was originally identified in the genetic RNIC T-ALL model, which differs from the NICD retrovirally induced T-ALL model as NICD is expressed from the Rosa26 locus. To exclude the possibility that we missed a possible Chd7 function due to the experimental system used, we also performed *Chd7* LOF experiments using the genetic RNIC T-ALL model. Therefore, we generated the *Chd7*^{lox/lox} *RNIC*^{+/ Δ MxCre} (early stage T-ALL) and *Chd7*^{lox/lox} *RNIC*^{+/ Δ LckCre} (late-stage T-ALL) mice.

Bone marrow chimeras reconstituted with *RNIC*^{+/ Δ Chd7 Δ MxCre} BM were generated to simultaneously over-express NICD and delete *Chd7* within the BM compartment (Figure 26 A). PIC-mediated MxCre activation led to T-ALL development in both *Chd7*-competent and *Chd7*-deficient mice. However, no significant difference in the overall survival of T-ALL-bearing chimeras was found with *RNIC*^{+/ Δ Chd7 Δ MxCre} mice exhibiting a median survival of 105 days (n = 9) and *RNIC*^{+/ Δ MxCre} mice a median survival of 95 days (n = 7), Figure 26 B.

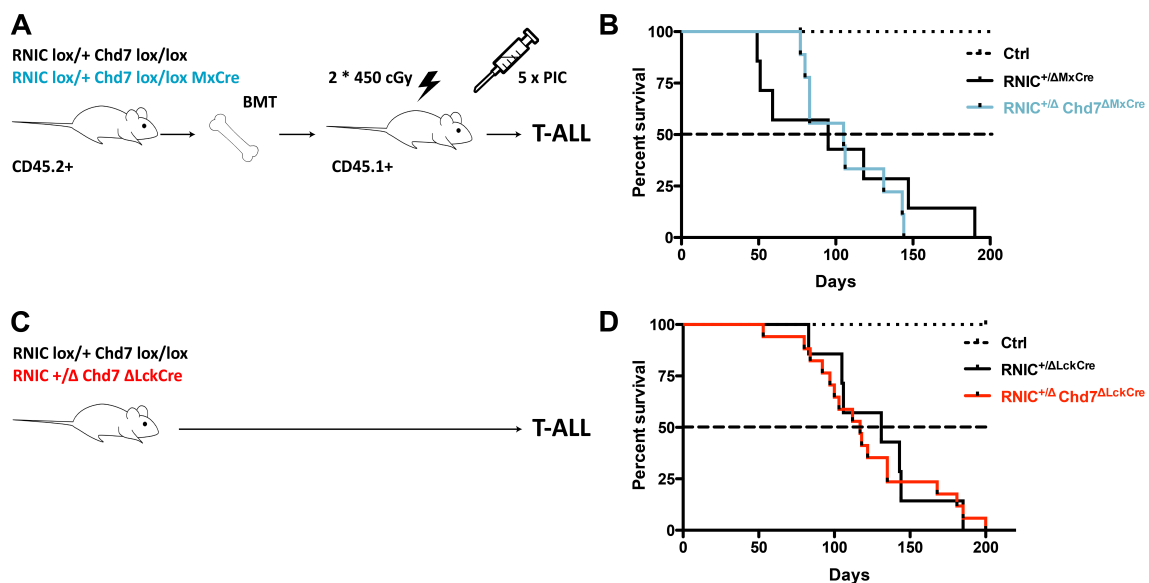


Figure 26: **A**, Schematic representation of *RNIC*^{+/ Δ Chd7 Δ MxCre} T-ALL induction model. **B**, Kaplan-Meier survival curve of *RNIC*^{+/ Δ Chd7 Δ MxCre} chimeras (n = 7) depicted in blue and Ctrl (n = 9) chimeras shown in black. **C**, Schematic representation of the *RNIC*^{+/ Δ Chd7 Δ CD4Cre} T-ALL induction model. **D**, Kaplan-Meier survival curve of *RNIC*^{+/ Δ Chd7 Δ CD4Cre} tumor mice (n = 17) depicted in red and Ctrl (n = 7) mice shown in black. Median survival was calculated using Log-rank Mantel-Cox test.

T-ALL development in the *RNIC*^{+/ Δ Chd7 Δ LckCre} model was monitored in the non-chimeric (physiological) setting (Figure 26 C), since activation of the LckCre deleter is restricted to the thymic compartment. Median survival of both cohorts was not significantly altered by

conditional ablation of Chd7 (Ctrl = 131 days, n = 7 and *RNIC^{+/Δ}Chd7^{ΔLckCre}* = 117 days, n = 17) as shown in Figure 26 D.

In summary, we have shown that conditional deletion of *Chd7* in NICD-over-expressing BM progenitors, as well as in thymic progenitors at the DN2-DN3a stage of differentiation, does not impact on T-ALL development. This observation raises the question whether Chd7 may be compensated by other members of the Chd family of chromatin remodellers or may be up-regulated in late-stage T-ALL tumors as a defense mechanism in order to counteract leukemogenic cues induced by NICD.

3.4 Chd7 Deficiency does not affect Notch1-driven human T-ALL

Although our studies using mouse models of T-ALL did not indicate a major contribution of Chd7 in Notch-driven T-ALL development, its putative role in human T-ALL remained to be investigated.

3.4.1 Chd7 is expressed in human T-ALL cells

Several human T-ALL cell lines that harbor Notch activating mutations such as KOPTK1, RPMI, HPB-ALL, DND41, T-ALL1 and CUTL1 were screened for the expression of CHD7 mRNA (Figure 27 A) and protein (Figure 27 B). *CHD7* expression was detected in HPB-ALL, DND41 and CUTL1 cell lines, with HPB-ALL showing least and CUTL1 showing highest expression. In contrast, *CHD7* was expressed at very low levels in KOPTK1 and RPMI cells, as depicted in Figure 27 A. *CHD7* was also expressed in the Notch-independent B lymphocyte-derived cell line, Raji, at the mRNA but not at the protein level, indicating that CHD7 expression can be regulated independently of Notch signaling.

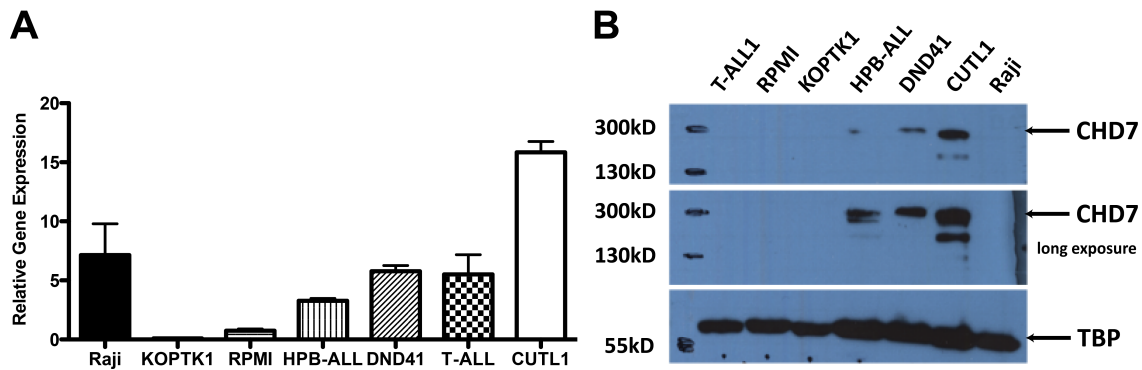


Figure 27: CHD7 is expressed in human T-ALL cells at different levels. **A**, Quantitative RT-PCR for *CHD7* expression levels in human T-ALL cell lines KOPTK1, RPMI, HPB-ALL, DND41, T-ALL1 and CUTL1. The Notch-independent B cell line Raji served as internal control. **B**, Representative western blot for CHD7 (300 kD) expression in human T-ALL cell lines. Tata-box binding protein (TBP; 55 kD) served as internal loading control for nuclear proteins.

3.4.2 Chd7 does not regulate Cell Cycle, Apoptosis or Proliferation of human T-ALL cells

Chd7 was identified as highly up-regulated gene in late-stage versus pre-malignant Notch – driven murine T-ALL and we hence wanted to address whether *CHD7* deficiency would affect survival and growth of established human T-ALL cell lines, which more closely resemble the human cancer situation. Since CHD7 was most abundantly expressed in HPB-ALL, DND41 and CUTL1 T-ALL cells, these Notch-dependent cell lines were selected to study the effect of *CHD7* LOF on human T-ALL cell lines *in vitro*. *CHD7* KD was performed using either (i) a non-inducible shRNA lentiviral vector in HPB-ALL cells or (ii) a doxycycline-inducible RFP⁺ shRNA lentiviral vector in DND41 and CUTL1 cells that both specifically target *CHD7* mRNA for degradation. DND41 cells showed most efficient *CHD7* KD in presence of doxycycline with 25% residual *CHD7* levels, whereas *CHD7* mRNA could only be reduced to about 40% in HPB-ALL and 50% in CUTL1 (Figure 28 A). These results were confirmed by the reduction in CHD7 protein expression in treated HPB-ALL and CUTL1 cell lines (Figure 28 B).

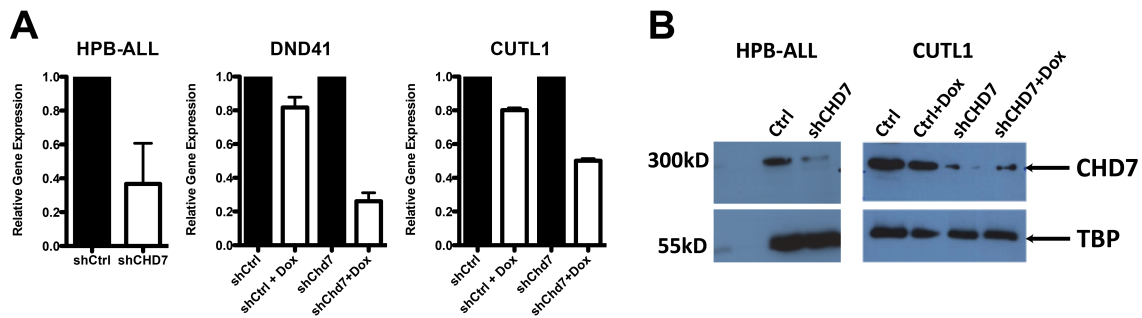


Figure 28: CHD7 knock down in human T-ALL cell lines HPB-ALL, DND41 and CUTL1. **A**, Quantitative RT-PCR for *CHD7* expression in human T-ALL cell lines HPB-ALL, DND41 and RPMI stably expressing lentiviral shRNA constructs. **B**, Representative western blot for CHD7 (300 kD) expression in human T-ALL cell lines HPB-ALL and CUTL1 expressing shCtrl or shCHD7 lentiviral vectors one week post puromycin selection. Tata-box binding protein (TBP; 55 kD) served as internal loading control for nuclear proteins.

In order to test to functional outcome of *CHD7* KD we synchronized the cells by serum starvation and performed apoptosis and cell cycle analysis over a time course of 5 to 7 days after release into serum-containing medium.

No significant differences in i) the percentage (Figure 29 B), nor in ii) the absolute number of apoptotic cells (Annexin-V+7AAD[±] cells) was observed in all three studied *CHD7* KD cell lines (Figure 29 C-E) over a time course of 5 or 7 days respectively post synchronization. The cell cycle of DND41 and CUTL1 cells was unperturbed by *CHD7* KD (Figure 29 I, J). shRNA-mediated KD of *CHD7* in HPB-ALL cells caused a transient G₁ arrest at early time points post synchronization (Figure 29 G & H). However, similar to DND41 and CUTL1 cell lines, *CHD7* KD did not significantly impair the proliferation of HPB-ALL cells over time (Figure 29 K-M).

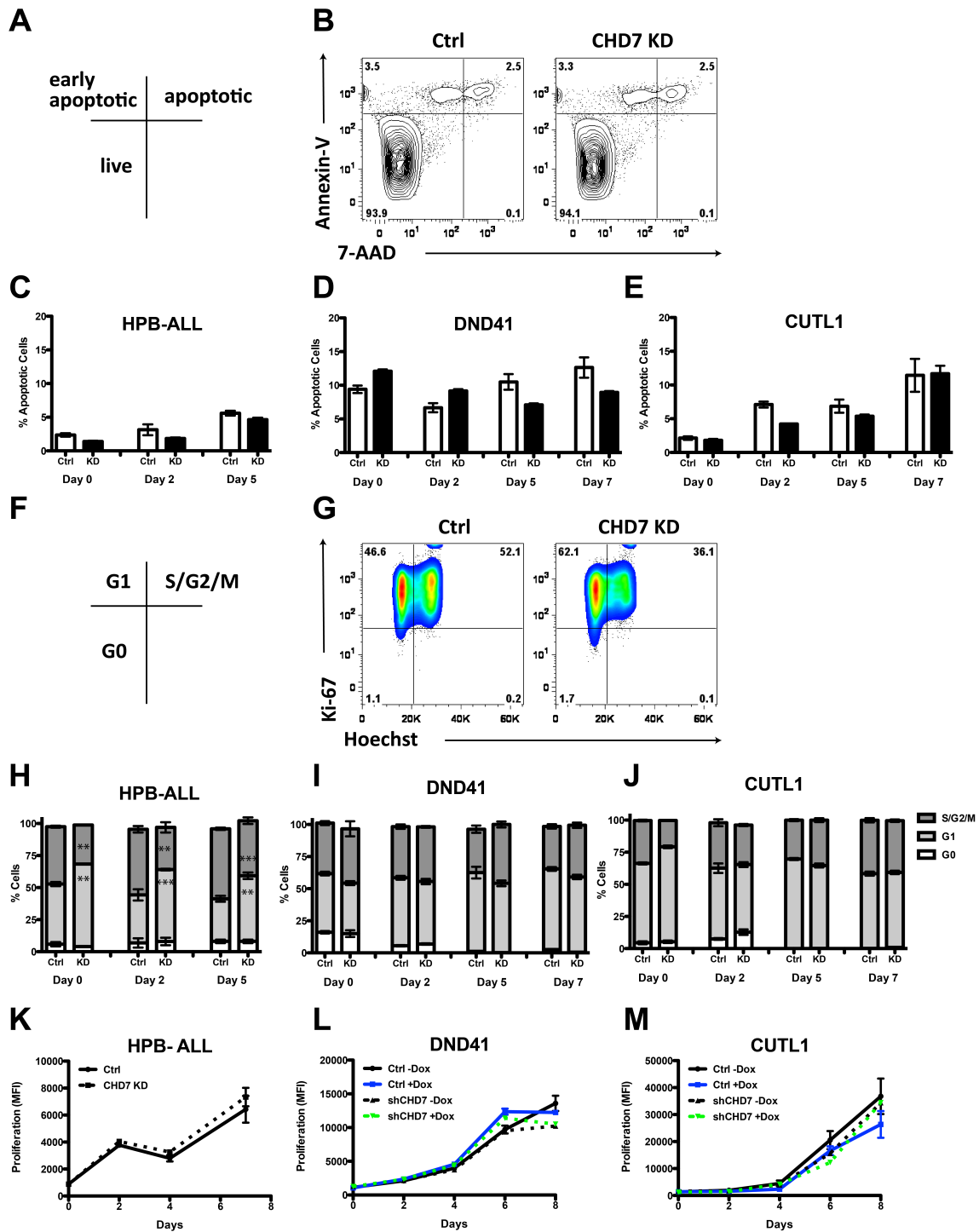


Figure 29: CHD7 knock down does not alter apoptosis, cell cycle or proliferation in human T-ALL cell lines HPB-ALL, DND41 and CUTL1. **A**, Gating strategy to distinguish live from early apoptotic and late apoptotic cells. **B**, Representative FACS plots depicting Annexin-V versus 7-AAD staining in HPB-ALL cells stably expressing shCHD7 or shCtrl (Ctrl) at 2 days post synchronisation. Percentage of apoptotic cells in HPB-ALL (**C**), DND41 (**D**) and CUTL1 (**E**) CHD7 knock down cells compared to ctrl. **F**, Gating strategy to identify cells in G₀, G₁ and S/G₂/M cell cycle phases **G**, Representative FACS plots depicting staining for Ki-67 versus Hoechst in HPB-ALL cells stably expressing shCHD7 or shCtrl. Quantification of cell cycle kinetics in HPB-ALL (**H**), DND41 (**I**) and CUTL1 (**J**) CHD7 knock down cells over 5 or 7 days respectively. Proliferation of HPB-ALL (**K**), DND41 (**L**) and CUTL1 (**M**) cells, stably expressing shCtrl and shCHD7 shRNAs, measured by Alamar Blue assay. Error bars represent mean ± SD, n = 3.

Overall, these data indicate that KD of *CHD7* does not affect (i) the viability, (ii) the cell cycle or (iii) the growth of human T-ALL cell lines. Therefore, in conclusion, CHD7 does not seem to majorly affect the maintenance of established human T-ALL cells lines.

4 Discussion Part I: Role of Chd7 in Hematopoiesis & T-ALL

4.1 Validation of Potential Mediators cooperating with Notch1 in T-ALL

Aberrant Notch pathway activation was firstly linked to T-ALL in 1987, when the chromosomal translocation t(7;9), leading to expression of NICD under the control of the TCR β enhancer, was identified in a small subset of T-ALL patients (Ellisen et al., 1991; Reynolds et al., 1987). Furthermore, it was experimentally demonstrated that NICD overexpression in BM progenitors induces T-ALL upon transplantation into lethally irradiated recipient mice (Pear et al., 1996b). The landmark study by Weng *et al.* identified activating mutations in the HD and PEST domain of N1, thereby initiating ligand-independent signalling and delayed decoy of NICD, when sequencing 96 primary human T-ALL samples and T-ALL cell lines. This provided further evidence that hyperactivated Notch signalling is strongly linked to T-ALL and proposes the Notch pathway as therapeutic target in this malignancy (Weng et al., 2004).

A previous research project in the lab aimed at identifying genes that would cooperate with N1 in the transformation of T cell progenitors to give rise to aggressive metastatic T-ALL. Therefore, mouse models have been generated to specifically over-express NICD at different stages of T cell maturation with the outcome that targeted BM progenitors give rise to pre-malignant T-ALL, while only DN2-DN3a thymocytes are fully responsive to oncogenic Notch and give rise to late-stage T-ALL. Performing microarray based screening, the chromatin remodelling enzyme Chd7 was identified as highly up-regulated gene in late stage metastatic N1-driven T-ALL (*RNIC⁺/ Δ Lck^{Cre}*) compared to early stage pre-malignant T-ALL (*RNIC⁺/ Δ Lck^{Cre}*).

Aim of my thesis was the validation of this gene candidate in the context of T-ALL development and normal hematopoiesis. When initiating the project, Chd7 had not been functionally studied in the context of cancer. However, one study (Pleasant et al., 2010) identified a duplication in the *CHD7* locus and the occurrence of two *PVT1-CHD7* fusion genes when screening human small-cell lung cancer cells for mutations via next-generation sequencing. This was the first study, linking aberrant expression of *CHD7* with tobacco exposure-induced development of small-cell lung cancer. Only recently, Colbert *et al.* reported Chd7 overexpression in pancreatic cancer and therefore proposed Chd7 as a potential biomarker (Colbert et al., 2014). We

demonstrated that *Chd7* was 26-fold higher expressed in late-stage versus pre-malignant T-ALL (Poisson, 2011) and confirmed these data when screening independent primary murine T-ALL samples derived from the *RNIC⁺/ΔLckCre* and *RNIC⁺/ΔMxCre* models. Furthermore, *Chd7* expression was still elevated in murine cell lines derived from the same genetic T-ALL induction models. Therefore, during T-ALL progression *Chd7* may similarly be proposed as biomarker to delineate stage and severity of T-ALL. We did not identify *Chd7* up-regulation in pre-malignant *RNIC⁺/ΔMxCre* T-ALL versus physiological immature CD4⁺CD8⁺ DP T cells, suggesting that *Chd7* expression and/or function may be correlated with only later events during leukemogenesis. This rules out that *Chd7* expression may be applicable as biomarker during early stage T-ALL. Colbert and colleagues published that *Chd7* ablation sensitizes pancreatic tumors to gemcitabine treatment (Colbert et al., 2014). Therefore, *Chd7* inactivation or silencing by inhibiting its ATPase function with a competitive inhibitor may have additive effects to conventional chemotherapy in T-ALL patients. However, this is purely speculative, since we did not use chemotherapeutic drugs in order to perform and test different treatment regimens in our murine N1-driven T-ALL models. In addition, *Chd7* function in cancer progression in solid pancreatic ductal adenoma carcinomas may be strikingly different compared to downstream effects of Notch during leukemogenesis.

4.2 Functional Characterization of Chd7 in Hematopoiesis

Epigenetic regulators such as chromatin remodelling enzymes can modulate gene transcription beyond the information encoded in the DNA. They are powerful enzymes, which slide nucleosomes along the DNA, thereby compacting chromatin into heterochromatin or opening it up into euchromatin, which is accessible for transcription machinery. CHD7 is strongly linked to CHARGE syndrome (Vissers et al., 2004), in which loss of one functional *CHD7* allele affects multiple organs, such as the eye, the ear, the heart as well as the genital and urinary tract. A minority of CHARGE syndrome patients were reported to suffer from congenital T cell immunodeficiency (Chopra et al., 2009; Hoover-Fong et al., 2009), suggesting that CHD7 may regulate adaptive T-cell mediated immune responses in these patients. However, these studies are only descriptive case reports, not delineating any functional impact of CHD7 on T cell biology. Preliminary data generated by the Zon and Speck labs postulated a role for *Chd7* hematopoiesis. In zebrafish, *Chd7*-deficient HSCs gave rise to more chimeric embryos upon transplantation into blastomeres compared to *Chd7*-competent HSCs, suggesting that *Chd7* suppresses HSC formation during zebrafish embryogenesis (Huang HT, 2010). In contrast, Nancy Speck demonstrated that VavCre-mediated *Chd7* inactivation does not lead to any overt phenotype in the BM. However, under competitive conditions *Chd7*-deficiency led to increased T

cell numbers as studied in serial transplantation experiments (Hsu J, 2011). We studied MxCre-mediated *Chd7* ablation in BM progenitors, which in contrast to VavCre, is activated after embryogenesis. We did not observe any lineage specification defects in HSC or mature hematopoietic lineages, which supports the findings by Nancy Speck. Upon analysis of the T cell compartment, we did not observe abnormal accumulation of DN1 thymic progenitors nor ectopic accumulation of B cells in the thymus as described for *N1* LOF (Radtke et al., 1999). Upon analysis of the spleen, *Chd7*^{ΔMxCre} MZB cell numbers were comparable to control, indicating that *Chd7* deficiency does not phenocopy *N2* LOF (Saito et al., 2003). Upon serial transplantation of BM from competitive *Chd7*-deficient and *Chd7*-competent chimeras, similarly the HSC and T cell compartment were not significantly affected. However, in secondary chimeras numbers of CD45.2⁺LT-HSCs were slightly increased in *Chd7*^{ΔMxCre} chimeras compared to controls but this did not translate into any competitive advantage during multi-lineage reconstitution. Therefore, *Chd7* does not play a role in regulating hematopoiesis under “steady state” or competitive conditions studied in this thesis. However, we cannot rule out a potential compensatory mechanism by the other 8 members of the CHD family of chromatin remodellers, in order to counter-balance a putative hematopoietic transcriptional program in absence of *Chd7*.

4.3 *Chd7* does not affect Notch1-driven murine T-ALL

Bajpai *et al.* demonstrated that CHD7 is essential during the formation of multipotent migratory neural crest cells in both humans and *Xenopus* (Bajpai et al., 2010). This transient ectodermal cell population is transcriptionally reprogrammed by CHD7 in order to differentiate and migrate throughout the body to form the peripheral nervous system, craniofacial bones and cartilages and cardiac structures. During this developmental process, CHD7 was demonstrated to cooperate with the transcription factors SOX9, TWIST and SLUG. TWIST and SLUG are known mediators of the epithelial-to-mesenchymal transition (EMT), a process often aberrantly activated during tumor cell invasion (De Craene and Berx, 2013). Therefore, we speculated that *Chd7* may render leukemic cells more aggressive and enhance their invasion properties in our Notch1-driven T-ALL models. Consequently, we addressed the question, whether conditional inactivation of *Chd7* in murine models of Notch1-driven T-ALL may affect development of this disease. Therefore, we studied the absence of *Chd7* in the (i) retroviral T-ALL induction model, using the BM-specific MxCre and the thymus-specific CD4Cre and in (ii) the genetic RNIC T-ALL induction model, in which *Chd7* had been originally identified. Retroviral transformation of *Chd7*-deficient BM progenitors with MigR1-NICD and subsequent transplantation into lethally irradiated recipient mice (*Chd7*^{ΔMxCre} MigR1-NICD induction model) did not confer any survival

advantage or disadvantage to the recipient mice but demonstrated similar T-ALL development. Phenotypically, *Chd7*-competent and *Chd7*-deficient T-ALLs were comparable with the expansion of CD45.2⁺NGFR⁺CD4⁺CD8⁺ DP cells within the BM and the spleen. Similarly, over-expression of NICD in DN3b-DN4 thymocytes in the *Chd7*^{ΔCD4Cre} MigR1-NICD induction model did not ameliorate nor accelerate T-ALL survival outcome. Furthermore, abnormal proliferation of immature NICD-transformed T cells was similar in both cohorts, with the majority of cells being CD4CD8 DP and CD8 iSPs, which is a hallmark of experimentally induced T-ALL via over-expression of NICD. In addition, we wanted to exclude the possibility that we missed a possible *Chd7* function due to the experimental system used. Therefore, we studied *Chd7* conditional inactivation in the *RNIC*^{+/ΔMxCre} (early stage T-ALL) and *RNIC*^{+/ΔLckCre} (late-stage T-ALL) models, in which *Chd7* was initially identified. Similarly, NICD over-expression from the Rosa26 locus upon deletion of *Chd7* in the BM (MxCre) or in thymic progenitors (LckCre) did not impair nor accelerate T-ALL development, hence supporting our studies in the retroviral MigR1-NICD induction model.

In conclusion and in contrast to our hypothesis, *Chd7* is not important for T-ALL induction and does not affect T-ALL cell invasion into the spleen. However, *Chd7* belongs to a large family of chromatin remodellers, which counts nine members. It is possible that in absence of *Chd7* other family members may compensate for its loss to drive a transcriptional leukemic program downstream of N1 in T-ALL.

On the other hand, is it tempting to speculate whether *Chd7* may be up-regulated in more aggressive T-ALL in order to counteract the transforming potential of NICD. In that scenario however, the absence of *Chd7* should have conferred a survival disadvantage compared to control chimeras and T-ALL cells should have expanded more rapidly. Reciprocal experiments, over-expressing *Chd7* cDNA in immature BM progenitors, may shed more light into the function of *Chd7* during malignant transformation and T-ALL progression. This approach was initially pursued but was experimentally challenging since the murine *Chd7* coding sequence spans 8.9 kb, resulting in expression of a 300 kD protein. Upon successful cloning, we were unfortunately not able to transiently or lentivirally express *Chd7* cDNA in T-ALL suspension or adherent cells (data not shown). As an experimental alternative, the generation of *Chd7* knock in animals would have allowed to study the role of *Chd7* over-activation in pre-malignant T-ALL by crossing these mice with the *RNIC*^{+/ΔMxCre} model. Unfortunately, *Chd7* GOF studies in the context of T-ALL were experimentally challenging and not possible in the given time frame.

4.4 Chd7 does not affect Notch1-driven human T-ALL

CHD7 over-expression was reported in solid tumors like PDAC and NSCLC in humans (Colbert et al., 2014). Since *Chd7* was identified as highly over-expressed candidate gene in late-stage versus pre-malignant murine T-ALL, we set out to characterize CHD7 expression human N1-driven T-ALL cell lines. HPB-ALL, DND41 and CUTL1 expressed high CHD7 mRNA and protein levels. Therefore, these cell lines were chosen for *CHD7* KD studies *in vitro*. Sufficient shRNA-mediated KD of *CHD7* was achieved in all three cell lines. Overall, *CHD7* KD T-ALL cells were not apoptotic, nor displayed a significantly deregulated cell cycle to translate into proliferative advantage or disadvantage as compared to *CHD7* competent cells. However *CHD7* KD levels were ranged between 50-80% depending on the cell line studied. Residual *CHD7* levels may account for the unaffected growth and survival of human *CHD7* KD T-ALL cell lines. In conclusion, CHD7 does not impact on survival of established human T-ALL cell lines under the experimental conditions studied herein. These results are confirmative of the results achieved when studying Chd7 function in murine NICD-driven T-ALL models.

5 Results – Part II: Role of Serca2 in Hematopoiesis

Serca2 was identified to be a suitable drug target in Notch1-driven T-ALL by two independent screening approaches: i) Roti *et al.* initiated a chemical compound screen and identified thapsigargin and CPA as potential drugs to inhibit Notch via targeting of Serca2 and this target was further confirmed when over-expressing cDNA clones from an ORF library to identify proteins that may regulate a truncated and leukemic N1 receptor (Roti *et al.*, 2013); ii) Previous work in our lab by Rajwinder Lehal led to the identification of CPA as a Notch inhibitor in a co-culture-based chemical compound screen (Lehal, 2011). Rajwinder Lehal showed, that CPA blocks Notch pathway activation in a concentration-dependant manner (Figure 30 A), resulting in the down-regulation of the Notch target genes *Hes1*, *cmyc* and *Deltex1* (*Dtx1*) (Figure 30 B).

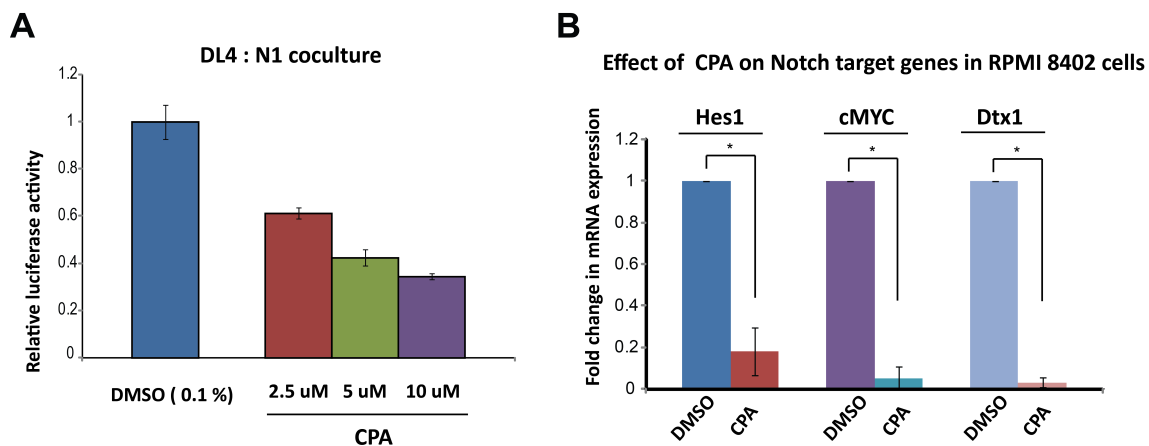


Figure 30: CPA treatment blocks Notch pathway activation and down-regulates Notch target genes. **A**, Co-cultured Dll4- and N1-expressing HeLa cells were treated with increasing concentrations of CPA, which blocks Notch pathway activation in a dose-dependant manner. **B**, Quantitative RT-PCR on cDNA from CPA-treated human RPMI 8402 T-ALL cells for Notch target genes *Hes1*, *cMYC* and *Deltex1* (*Dtx1*). Courtesy of Rajwinder Lehal.

Furthermore, Roti *et al.* showed that Serca2 regulates the maturation of the Notch receptor and that inhibition of Serca ATPases in T-ALL xenografts significantly ameliorates disease outcome (Roti *et al.*, 2013). Although this work shows that Serca2 is indeed regulating N1, the work did not address, whether Serca2 function is specific for Notch, or may have additional function within the hematopoietic system. This is of importance since Serca2 has been suggested as a potential novel drug target to fight Notch-driven T-ALL. Therefore, we set out to study the impact of *Serca2* ablation on the hematopoietic system, mainly to address whether i) *Serca2* deficiency may recapitulate the Notch LOF effects on T and MZB cell development and ii) to assess whether a Serca2 inhibitor may be an applicable therapeutic approach for the treatment of T-ALL, as previously suggested.

5.1 Expression of *Serca* Family Members in the Hematopoietic System

The *Serca* family of calcium ATP-ases comprises three members that are expressed in a tissue-specific fashion: *Serca1* is expressed predominantly in skeletal muscle, all three isoforms of *Serca2* (a-c) are widely expressed in smooth muscle and nonmuscle tissues and *Serca3* is expressed in most tissues (Prasad et al., 2004).

Therefore, we first set out to analyse the gene expression pattern of the *Serca* family members *Serca1*, *Serca2* (isoforms a and b) and *Serca3* among different hematopoietic lineages (Figure 31). Stem and progenitor subsets such as KLS cells, MPP2s (KLSCD150⁺CD48⁺), MPP3-MPP4s (KLSCD150⁻CD48⁺) and overall CD117⁺Sca1⁻ progenitors, further subfractionated into common myeloid progenitors (CMPs; Lin⁻CD117⁺Sca1⁻CD34⁺D16/32^{int}), granulocyte macrophage progenitors (GMPs; Lin⁻CD117⁺Sca1⁻CD34⁺CD16/32^{hi}) and myeloid erythroid progenitors (MEPs; Lin⁻CD117⁺Sca1⁻CD34⁻CD16/32^{lo}) were sorted from total BM of 8 weeks old C57BL6/J WT mice.

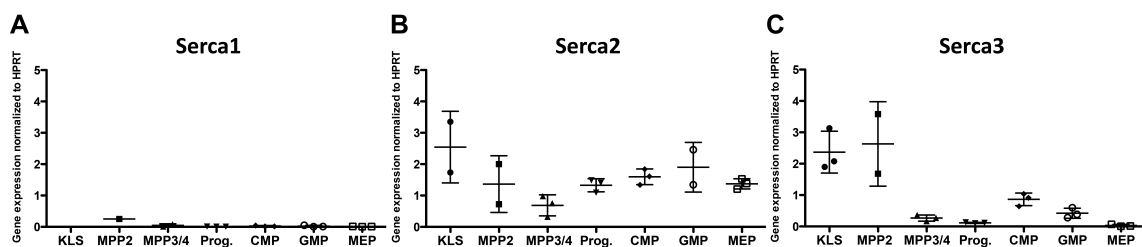


Figure 31: *Serca* family member expression in WT hematopoietic stem and progenitor cells. Relative gene expression of *Serca1* (A), *Serca2* (B) and *Serca3* (C) in sorted BL6/J WT KLS cells, MPP2s, MPP3-MPP4s, CD117⁺Sca1⁻ progenitors, common myeloid progenitors (CMPs; Lin⁻CD117⁺Sca1⁻CD34⁺D16/32^{int}), granulocyte macrophage progenitors (GMPs; Lin⁻CD117⁺Sca1⁻CD34⁺CD16/32^{hi}) and myeloid erythroid progenitors (MEPs; Lin⁻CD117⁺Sca1⁻CD34⁻CD16/32^{lo}) normalized to expression of HPRT (set to 1). Experiment performed in at least biological duplicates. Error bars represent mean ± SD.

Quantitative RT-PCR analysis demonstrated that *Serca2* and *Serca3* are expressed in KLS cells. However, *Serca2* was expressed at higher levels in progenitors than *Serca3* (Figure 31 B, C). *Serca1* expression was not detectable in any of the hematopoietic subsets (Figure 31 A). These results are confirmative of the published expression data for members of the *Serca* family.

5.2 Consequences of *Serca2* Haploinsufficiency in the Hematopoietic System

Serca2 haploinsufficiency is strongly linked to Darier's Disease in humans, in which LOF mutations affecting one *Serca2* allele result in keratinized epithelial cells, leading to the formation of crusty patches on the skin (Sakuntabhai et al., 1999).

Therefore, we wondered whether conditional ablation of one *Serca2* allele may affect hematopoiesis. We studied *Serca2* haploinsufficiency under homeostatic conditions and under hematological stress, induced by 5-FU treatment and competitive as well as serial transplantation assays (data shown in Appendix section 7.6). However, conditional inactivation of one *Serca2* allele in the BM did not cause any defects in hematopoietic differentiation or hematopoietic maintenance under these physiologic and competitive conditions.

5.3 Consequences of *Serca2* LOF in the Hematopoietic System

Since *Serca2* was proposed to be a therapeutic target in Notch-driven T-ALL (Roti et al., 2013), we set out to study the physiological role of *Serca2* in the hematopoietic system via conditional deletion in BM cells using the MxCre recombinase. In *Serca2* cKO mice, the translational start site containing exon 2 as well as exon 3 are flanked by loxP sites, resulting in a *Serca2 null* allele upon Cre recombinase activation following administration of PIC (Figure 32 A).

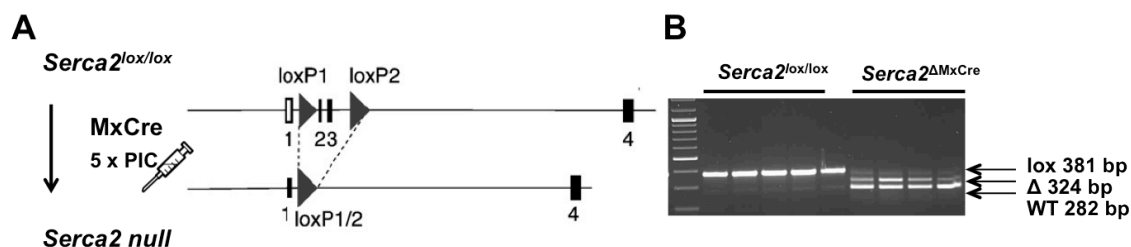


Figure 32: Strategy for *in vivo* conditional inactivation of *Serca2* in the BM. **A**, Schematic representation of the genetically modified murine *Serca2* locus, in which the ATG-encoding exon 2 and exon 3 are flanked by loxP sites. Activation of the efficient BM-deleter strain MxCre recombinase by administration of PIC leads to the generation of a *Serca2 null* allele in BM cells. **B**, Deletion PCR analysis demonstrating a 381 bp lox band, a 324 bp deletion band (Δ) and a 282 bp WT band amplified from genomic DNA isolated from *Serca2*^{lox/lox} or *Serca2* ^{Δ MxCre} BM cells from chimeras.

Efficient (> 90%) conditional *Serca2* deletion was confirmed by PCR analysis on DNA from BM cells of *Serca2*-deficient chimeras: MxCre-mediated excision of exon 2 and 3 out of the murine *Serca2* locus led to amplification of a 324 bp deletion band (Δ), whereas the genetically modified *Serca2*^{lox/lox} locus would yield in a 381 bp band (lox) and WT murine *Serca2* locus (residual CD45.1⁺ WT cells from recipient) a smaller 282 bp amplicon (Figure 32 B).

5.3.1 Genetic Ablation of *Serca2* impairs Hematopoiesis

We questioned whether ablation of both functional *Serca2* alleles may impact on hematopoiesis and therefore generated *Serca2*^{ΔMxCre} and *Serca2*^{lox/lox} (Ctrl) chimeras by transplanting CD45.2⁺ *Serca2*^{lox/lox} MxCre or Ctrl BM into lethally irradiated CD45.1⁺ hosts. Analysis of CD45.2⁺ cells in the peripheral blood of non-competitive chimeric mice indicated that reconstitution of *Serca2*^{ΔMxCre} chimeras was significantly impaired compared to Ctrl chimeras. PBL analysis of chimeric mice (Figure 33 A) over a time course of 8 weeks post PIC administration indicated a progressive loss of donor-derived CD45.2⁺ cells in *Serca2*-deficient chimeras compared to *Serca2*-competent chimeras (Figure 33 B). For example, 5 weeks post MxCre activation only 70.05 ± 3.35% CD45.2⁺ cells were present in PBLs of *Serca2*-deficient chimeras (n = 4) compared to 98.50 ± 0.18% in *Serca2*-competent chimeras (n = 5). Reduction in CD45.2⁺ cells (35.30 ± 1.45%, n = 3) in the PBLs of *Serca2*-deficient chimeras was most prominent at 8 weeks post MxCre activation compared to *Serca2*-competent chimeras (98.53 ± 0.49%, n = 4).

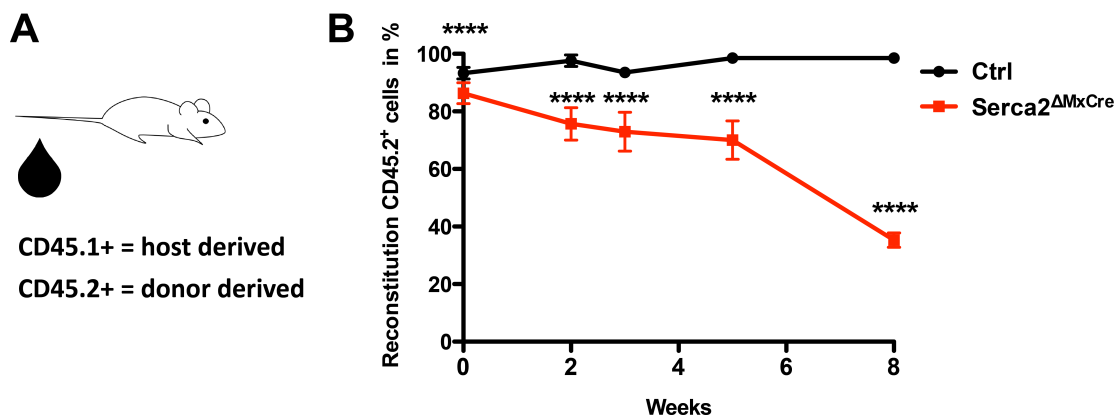


Figure 33: *Serca2*-deficient CD45.2⁺ peripheral blood cells get outcompeted from residual host-derived CD45.1⁺ C57BL6/J WT cells over time. Peripheral blood analysis of *Serca2*^{ΔMxCre} versus *Serca2*^{lox/lox} (Ctrl) was performed to assess reconstitution efficiency over a time course of 8 weeks. **A**, Schematic depicting congenic markers CD45.1⁺ derived from residual host cells and CD45.2⁺ donor-derived cells. **B**, PBL analysis for CD45.2⁺ reconstitution over 8 weeks. Error bars represent mean ± SD (**** p < 0.0001).

These data indicate that homozygous loss of *Serca2* negatively affects reconstitutive capacity of BM cells in lethally irradiated recipients. These results raised the question whether *Serca2* may play a role in regulating rather mature hematopoietic lineages or the HSC compartment.

To address this question, the BM compartment of *Serca2*-competent and *Serca2*-deficient chimeras was analysed at 1, 4 and 8 weeks post PIC administration. Analysis of mature hematopoietic lineages in the BM demonstrated that the absolute numbers of B, myeloid and erythroid cells were significantly reduced in *Serca2*-deficient chimeras, compared with Ctrl

chimeras, at all time points analysed (Figure 34 A-C). This likely contributed to the overall significant reduction in total BM cellularity.

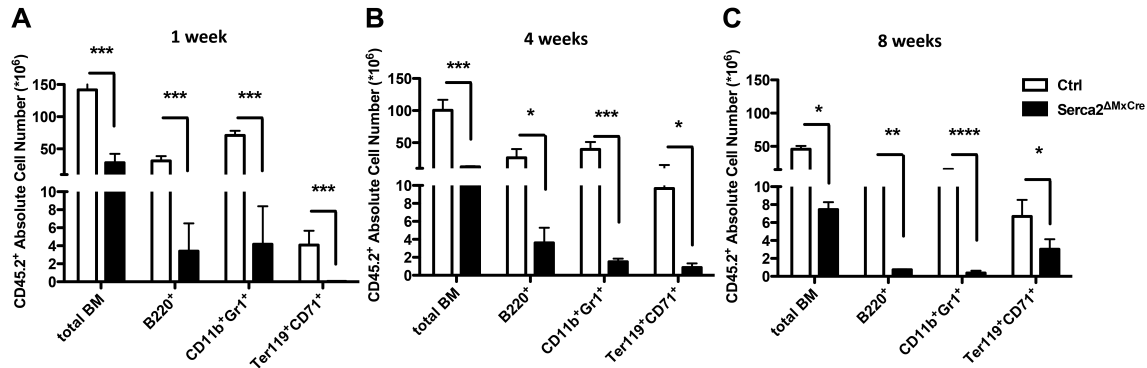


Figure 34: *Serca2* deficiency negatively affects hematopoietic development in the BM. Bone marrow of *Serca2*^{ΔMxCre} and *Serca2*^{lox/lox} (Ctrl) chimeras was analysed at 1, 4 and 8 weeks post MxCre induction. **A**, Absolute cell numbers for total BM cellularity, B220⁺ B cells, CD11b⁺Gr1⁺ myeloid cells and Ter119⁺CD71⁺ erythroid cells analysed at 1 week (**A**), 4 weeks (**B**) and 8 weeks post MxCre induction (**C**). Error bars represent mean ± SD (* p < 0.05; ** p < 0.01, *** p < 0.001, **** p < 0.0001).

In the thymus, CD45.2⁺ donor cells were out-competed by residual CD45.1⁺ host-derived cells in *Serca2*-deficient chimera (Figure 35 A). Overall, total thymic cellularity progressively reduced from $19.20 \pm 8.84 \times 10^6$ cells at 1 week (n = 6, Figure 35 C) to $0.16 \pm 0.14 \times 10^6$ cells at 3 weeks (n = 3, Figure 35 D) post *Serca2* conditional deletion compared to $128.30 \pm 14.83 \times 10^6$ (n = 4) or $76.36 \pm 16.20 \times 10^6$ (n = 3) cells, at the equivalent time points in Ctrl chimeras. Phenotypic analysis of CD4 and CD8 cell surface expression (Figure 35 B) demonstrated progressive reduction in the percentage of immature CD4⁺CD8⁺ DP thymocytes and a corresponding increase in mature CD4⁺ and CD8⁺ SP cells, compared to Ctrl chimeras.

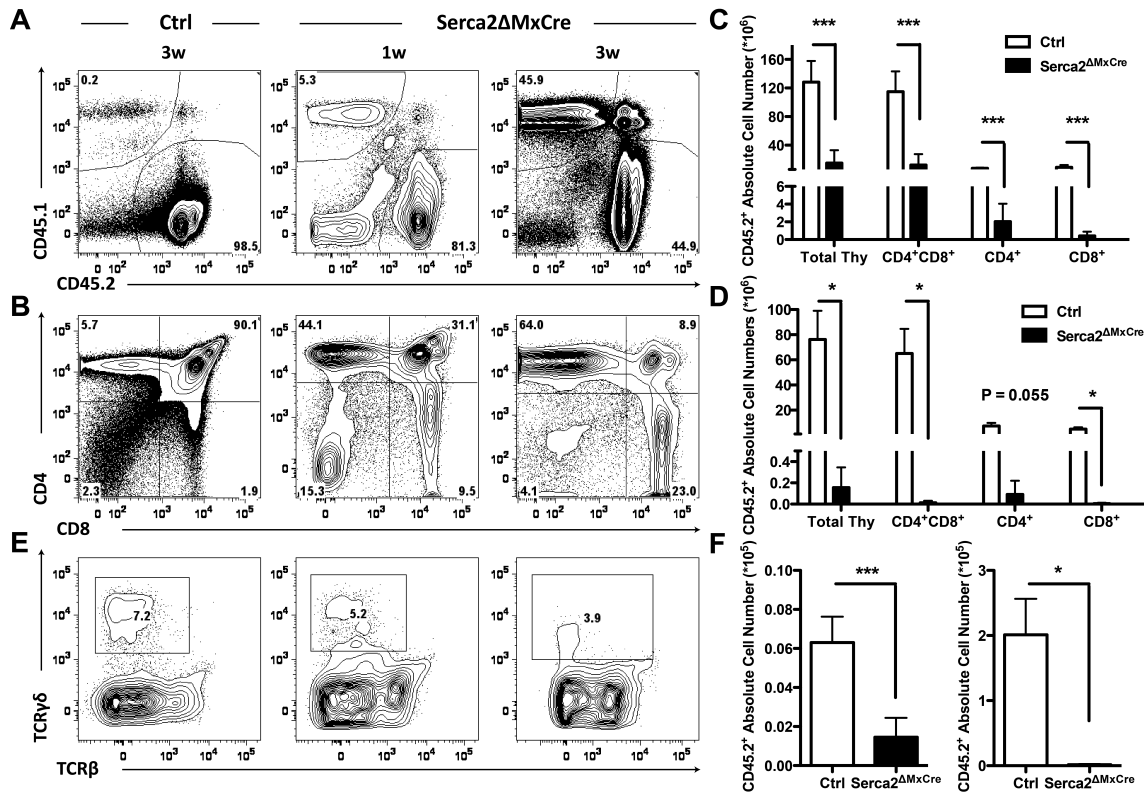


Figure 35: *Serca2* deficiency negatively affects T cell numbers in the thymus. Thymi of *Serca2*^{ΔMxCre} and *Serca2*^{lox/lox} (Ctrl) chimeric mice were analysed 1 and 3 weeks post MxCre induction. **A**, Representative FACS plots showing cell surface expression of congenic markers CD45.1 and CD45.2 in Ctrl and *Serca2*^{ΔMxCre} chimeric mice. **B**, Representative FACS plots showing cell surface expression of CD45.2⁺CD4 and CD45.2⁺CD8 in Ctrl and *Serca2*^{ΔMxCre} chimeric mice. Corresponding absolute cell numbers for total thymic cellularity, mature CD45.2⁺CD4⁺CD8⁺, CD45.2⁺CD4⁺ and CD45.2⁺CD8⁺ T cells are shown for time points 1 week (**C**) and 3 weeks (**D**). **E**, Representative FACS plots showing cell surface expression of TCRγδ and TCRβ, gated on CD45.2⁺CD4⁺CD8⁻ thymocytes and corresponding absolute cell numbers depicted in **F**. Absolute cell numbers are derived from Ctrl (n = 5) and *Serca2*^{ΔMxCre} (n = 5) mice. Error bars represent mean ± SD (* p < 0.05; ** p < 0.01, *** p < 0.001).

Serca2 conditional inactivation also negatively affected the percentage (Figure 35 E) and absolute numbers (Figure 35 F) of TCRγδ T cells compared to Ctrl chimeras.

In addition, thymic progenitors progressing through the DN stages of T cell maturation were analysed. The (i) percentages (Figure 36 A) and (ii) absolute numbers (Figure 36 B) of immature thymic progenitors (DN1-DN4) were also significantly reduced in *Serca2*-deficient chimeras (n = 5) compared to Ctrl chimeras (n = 5).

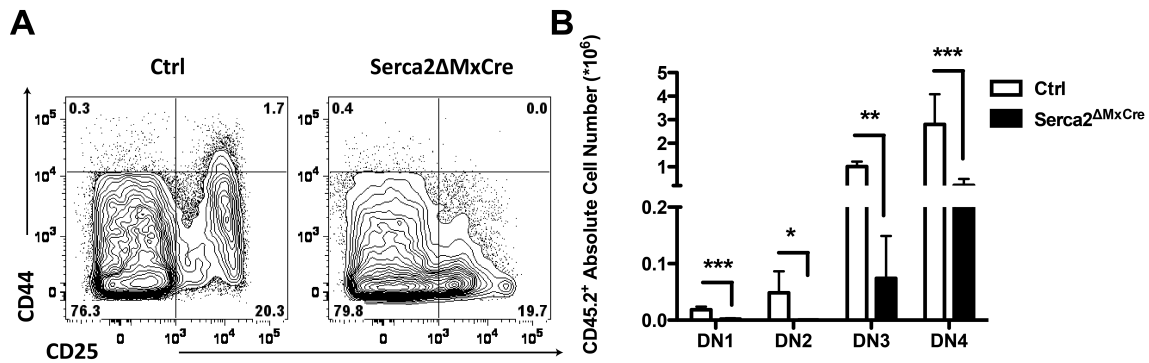


Figure 36: *Serca2* deficiency negatively affects T cell progenitors in the thymus. Thymi of *Serca2* Δ MxCre and *Serca2*^{lox/lox} (Ctrl) chimeric mice were analysed 1 week post MxCre induction. **A**, Representative FACS analysis showing Ctrl and *Serca2* Δ MxCre CD4⁺CD8⁻Lin⁻ thymocytes stained with anti-CD25 and anti-CD44 antibodies to distinguish DN1 (CD44⁺CD25⁻), DN2 (CD44⁺CD25⁺), DN3 (CD44⁻CD25⁺) and DN4 stages (CD44⁻CD25⁻) of maturation. Corresponding absolute cell numbers (n = 5+5) are shown in **B**. Error bars represent mean \pm SD (* p < 0.05; ** p < 0.01, *** p < 0.001).

Upon analysis of the spleen at 1 w (Figure 37 A) and 4 weeks (Figure 37 B) post MxCre activation, we observed that total splenic cellularity and absolute numbers of mature peripheral T and B cells were likewise strongly reduced in *Serca2*-deficient compared to *Serca2*-competent chimeras.

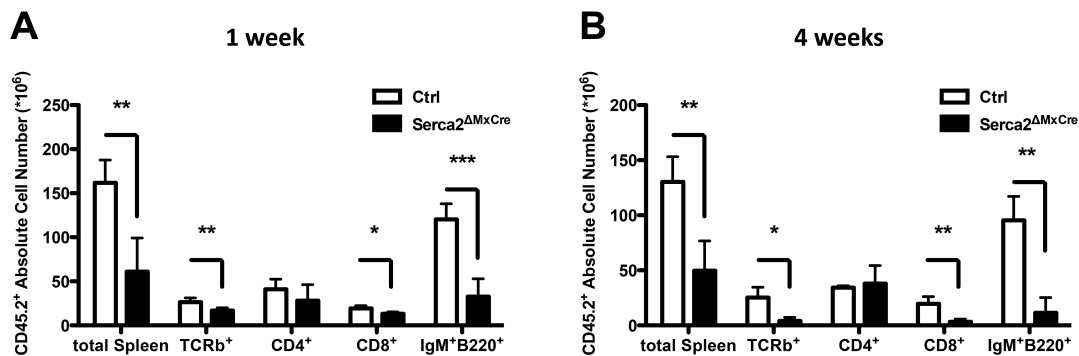


Figure 37: *Serca2* deficiency negatively affects splenic cellularity and mature peripheral T and B cells. Spleens of *Serca2* Δ MxCre and *Serca2*^{lox/lox} (Ctrl) chimeric mice were analysed 1 and 4 weeks post MxCre induction. Total splenic cellularity and absolute cell numbers of TCRb⁺, CD4⁺ and CD8⁺ T cells and IgM⁺B220⁺ B cells in *Serca2* Δ MxCre (n = 4) and Ctrl (n = 4) chimeras at 1 week (**A**) and 4 weeks (**B**) post MxCre induction. Error bars represent mean \pm SD (* p < 0.05; ** p < 0.01, *** p < 0.001).

In order to address the hypothesis whether conditional inactivation of *Serca2* in the BM may phenocopy *N2* LOF, we analysed the spleens of 1 week deleted *Serca2* Δ MxCre and Ctrl chimeras for MZB cells. Interestingly, percentages of *Serca2*-deficient MZBs (B220⁺IgM⁺CD21^{hi}CD23^{int}) were significantly increased at the expense of the follicular B cell population (B220⁺IgM⁺CD21^{int}CD23^{hi}) (Figure 38 A). This relative increase did, however, not reflect in absolute numbers as the overall splenic cellularity was reduced, affecting all other mature B cell

numbers. In contrast, the relative enrichment of MZBs was levelled out in absolute cell numbers due to the reduction in splenic cellularity in absence of *Serca2* (Figure 38 B).

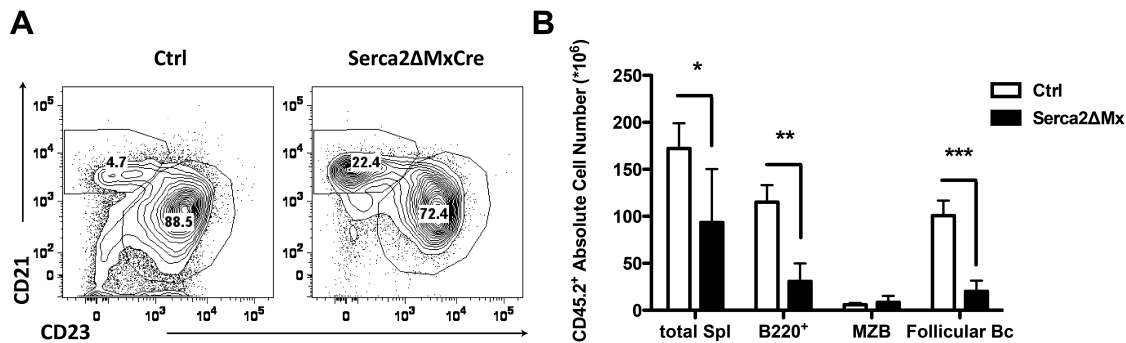


Figure 38: *Serca2* deficiency leads to a relative enrichment of MZB cells, while negatively affecting other mature B cell populations. Spleens of *Serca2*^{ΔMxCre} and *Serca2*^{lox/lox} (Ctrl) chimeric mice were analysed 1 post MxCre induction. **A**, Representative FACS analysis of spleen cells stained with anti-CD21 and anti-CD23 gated on CD45.2⁺B220⁺IgM⁺ population **(B)** Total splenic cellularity and absolute cell numbers of B220⁺, MZB and Follicular B cells in *Serca2*^{ΔMxCre} (n = 4) and Ctrl (n = 4) chimeras at 1 week post MxCre induction. Error bars represent mean ± SD (* p < 0.05; ** p < 0.01, *** p < 0.001).

Collectively, these data suggest that conditional *Serca2* ablation globally affects mature hematopoietic lineages within the BM; T cell development in the thymus; and peripheral mature T and B cells in the spleen. Relative enrichment of MZB cells upon *Serca2* inactivation suggests that *Serca2* may regulate not only N1 but also N2.

Serca2, pumps Ca²⁺ from the cytosol into the ER and its function is therefore crucial for calcium homeostasis within the cell (Berridge et al., 2003). Therefore, we set out to characterize the effect of *Serca2* LOF on calcium levels within peripheral mature T and B cells by measuring calcium flux with the ratiometric Ca²⁺ indicator Indo1 (Figure 39). In brief, calcium baseline levels were measured over time and calcium flux was induced by addition of ionomycin, a cell membrane permeabilizing agent. Baseline calcium levels were defined as INDO-1 ratio before adding ionomycin, while intracellular Ca²⁺ store release was measured as increase in INDO-1 ratio upon ionomycin stimulation.

Analysis of calcium flux by peripheral T (Figure 39 A) and B cells (Figure 39 B) in chimeras demonstrated that (i) baseline levels of intracellular Ca²⁺ were significantly elevated in *Serca2*-deficient mice compared to Ctrl chimeras (Figure 39 C) and (ii) intracellular ER calcium stores of *Serca2*-deficient cells released significantly less Ca²⁺ (Figure 39 D). These results demonstrate that calcium flux is deregulated in *Serca2*-deficient hematopoietic cells, giving a functional proof of concept for the cKO animals studied. This is in agreement with previously published work, in which thapsigargin-treated cells show similar calcium flux kinetics (Takemura et al., 1989).

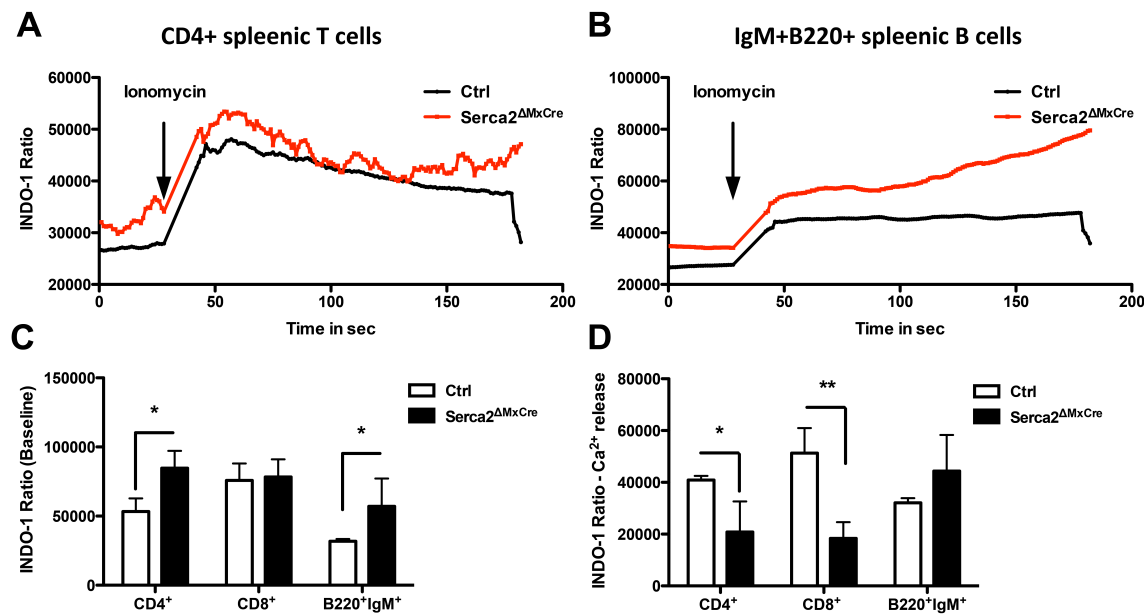


Figure 39: Calcium kinetics are deregulated in *Serca2*-deficient mature splenic T and B cells. T and B cells of *Serca2*^{ΔMxCre} and *Serca2*^{lox/lox} (Ctrl) spleens were isolated 8 weeks post MxCre induction and loaded with INDO-1. Calcium kinetics were measured over time and ionomycin was added to induce flux. Representative calcium flux responses in *Serca2*^{ΔMxCre} and Ctrl CD4⁺ T cells (A) and IgM⁺B220⁺ B cells (B) shown as ratio Indo-violet versus Indo-blue (INDO1 ratio). Quantification of Indo1 baseline levels (C) and Ca²⁺ release (D) depicted for *Serca2*^{ΔMxCre} (n = 3) and Ctrl (n = 3) mice. Error bars represent mean ± SD (* p < 0.05; ** p < 0.01). Experiment performed in collaboration with Danny Labes at the UNIL flow facility.

Taken together, we demonstrated that ablation of both alleles of *Serca2* in the BM led to a severe reduction of total BM (Figure 34), total thymic (Figure 35) and total splenic cellularity (Figure 37), indicating that *Serca2* is likely important for the survival of the herein studied cell types in these compartments. This raised the question whether *Serca2* ablation may negatively affect cell survival via induction of apoptosis.

5.3.2 Genetic Ablation of both *Serca2* alleles leads to Apoptosis of Mature Lineages due to ER stress and activation of UPR

We demonstrated that *Serca2* ablation in the hematopoietic system using MxCre leads to a severe reduction in total BM cellularity (Figure 34). Analysis of apoptosis (Figure 40 A) in lineage-committed BM cells (CD45.2⁺Lin⁺) revealed that *Serca2*-deficient cells are significantly more apoptotic than *Serca2*-competent cells (46.96 ± 3.75% in *Serca2*^{ΔMxCre} versus 16.84 ± 1.49% in Ctrl chimeras, Figure 40 B, C).

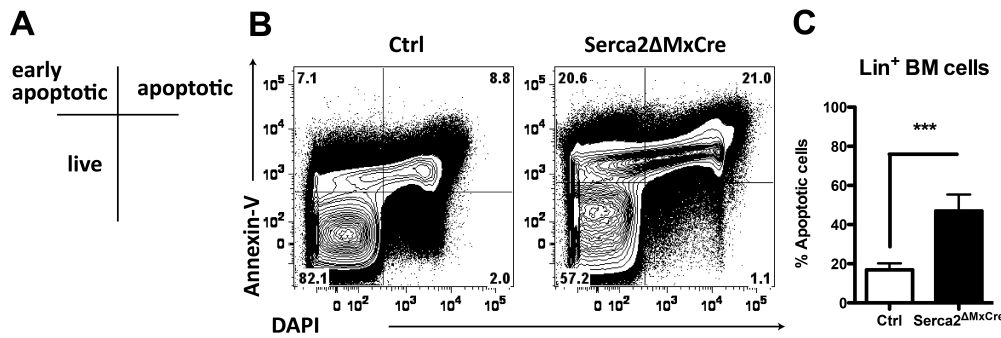


Figure 40: Serca2-deficient mature BM cells activate apoptosis. *Serca2*-deficient lineage positive cells were analysed for apoptosis one week post MxCre induction. **A**, Gating strategy to distinguish live from early apoptotic and apoptotic cells. **B**, Representative FACS plots depicting apoptosis staining for Annexin-V versus DAPI, gated on the overall CD45.2⁺ Lin⁺ population of *Serca2*^{lox/lox} (Ctrl) versus *Serca2* Δ MxCre animals. **C**, Quantification of the percentage of apoptotic cells in CD45.2⁺ Lin⁺ BM cells in *Serca2* Δ MxCre versus *Serca2*^{lox/lox} mice (n = 5 + 5). Error bars represent mean \pm SD (***) p < 0.001).

Imbalance of calcium levels within the cell can lead to the induction of the unfolded protein response (UPR), promoting apoptosis if chaperone proteins cannot counteract the protein misfolding in the ER. We hypothesized that *Serca2* deficiency may induce UPR and thereby activate apoptosis in Lin⁺ cells. Unfolded protein response genes *Ern2/Ire1*, encoding one of the three upstream UPR sensors, and *Hspa5/Grp78*, encoding the chaperone Hspa5 of the heat shock family, were found to be up-regulated in *Serca2*-deficient compared to *Serca2*-competent Lin⁺ BM cells (Figure 41 A). In agreement with our hypothesis, pro-apoptotic genes including *Bad*, *Bax* and *Bim* were also up-regulated with a concomitant down-regulation of the anti-apoptotic gene, *Bcl211*, in Lin⁺ *Serca2*-deficient BM cells (Figure 41 B). However, anti-apoptotic *Bcl2* was also up-regulated upon conditional *Serca2* inactivation in the BM.

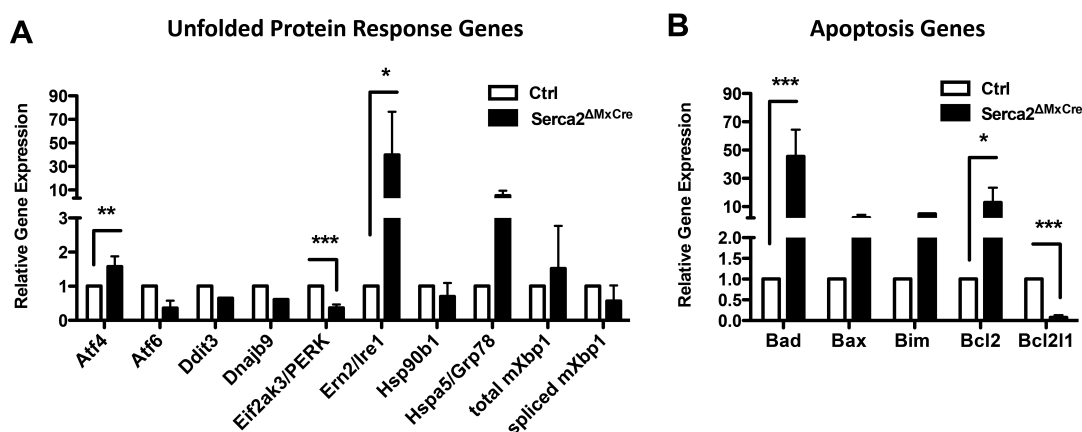


Figure 41: Unfolded Protein Response Genes are deregulated and pro-apoptotic genes up-regulated in *Serca2*-deficient lineage positive BM cells. Quantitative RT-PCR gene expression analysis of UPR candidate genes (A) and apoptosis-related genes (B) in sorted *Serca2* Δ MxCre versus *Serca2*^{lox/lox} (Ctrl) lineage positive BM cells. Error bars represent mean \pm SD, n = 3 (*Serca2* Δ MxCre) and n = 3 (Ctrl).

In summary, we demonstrated that the calcium ATPase *Serca2* is crucial for maintaining calcium levels within hematopoietic cells. This imbalance in calcium flux likely contributes to ER stress and activation of the UPR in hematopoietic cells, leading to the induction of apoptosis.

5.3.3 Genetic Ablation of *Serca2* negatively affects the HSC compartment

Serca2 conditional ablation in the BM led to a severe reduction in BM, thymic and splenic cellularity. This was likely due to ER stress and induction of UPR, resulting in subsequent activation of the apoptosis cascade in mature hematopoietic lineages. We then wondered, whether loss of both alleles of *Serca2* may equally affect cells within the HSC compartment. Upon analysis of the BM over a time course of 1, 4 and 8 weeks post MxCre induction, CD45.2⁺ donor-derived BM cells were rapidly outcompeted by residual CD45.1⁺ host cells with a maximal decrease in CD45.2⁺ reconstitution observed at 8 weeks post induction, as shown by phenotypic flow cytometric analysis (Figure 42 A). These data support the progressive loss of CD45.2⁺ cells in PBLs of *Serca2*-deficient mice compared to Ctrl (Figure 33). When analysing the HSC compartment, relative numbers of *Serca2*^{ΔMxCre} KLS cells were significantly enriched at 1, 4 and at 8 weeks post induction compared to control (Figure 42 B). Subfractionation into HSCs (KLSCD150-CD48⁺), MPP2 (KLSCD150+CD48⁺) and MPP3-MPP4 (KLSCD150-CD48⁺) cells demonstrated an accumulation of MPP2s and MPP3-MPP4s in percentages (Figures 42 C), accounting for the overall enrichment of the KLS compartment in *Serca2*-deficient chimeras. In contrast, relative HSC numbers (Figure 42 C) were strongly reduced in these mice at all time points of analysis.

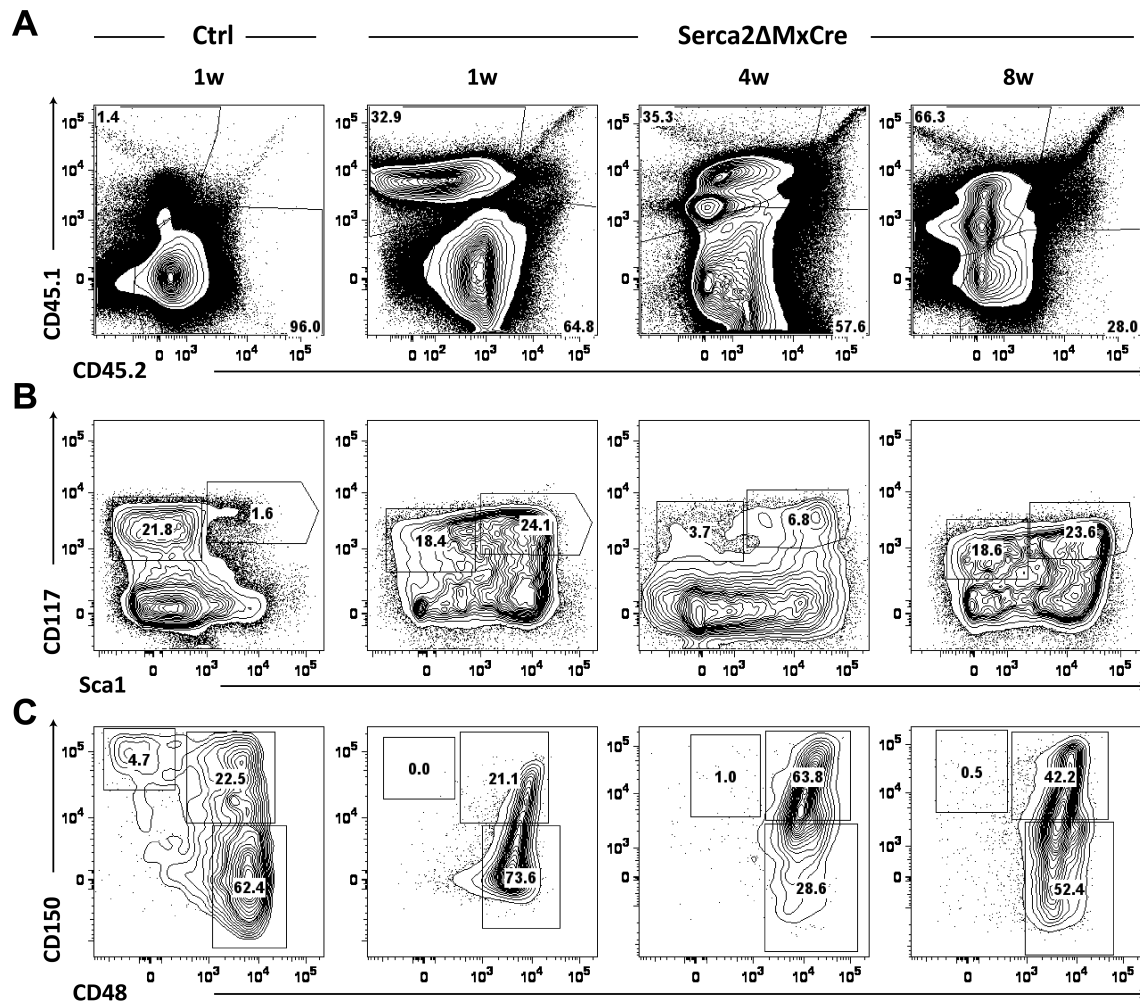


Figure 42: *Serca2* deficiency leads to an enrichment of KLS cells with concomitant loss of LT-HSCs. Bone marrow of *Serca2*^{ΔMxCre} and *Serca2*^{lox/lox} (Ctrl) chimeras was analysed at 1, 4 and 8 weeks post MxCre induction. **A**, Representative FACS plots showing cell surface expression of congenic markers CD45.1 and CD45.2 in Ctrl and *Serca2*^{ΔMxCre} chimeric mice. **B**, Representative FACS plots showing cell surface expression of CD117 and Sca1 gated on CD45.2⁺Lin⁻ cells and **C**, CD150 and CD48 cell surface expression to identify HSCs (CD150⁺CD48⁻), MPP2 (CD150⁺CD48⁺) and MPP3-MPP4 cells (CD150⁻CD48⁺), gated on CD45.2⁺Lin⁻KLS, in Ctrl and *Serca2*^{ΔMxCre} chimeric mice.

Upon *Serca2* inactivation in the BM, donor-derived CD45.2⁺ were continuously outcompeted by residual CD45.1⁺ WT cells from the recipient. This effect was evident at all time points of analysis, as the percentage of CD45.2⁺ cells was significantly reduced in *Serca2*^{ΔMxCre} chimeras compared to controls at 1w (Figure 43 D, left), 4w (Figure 43 E, left) and 8w (Figure 43 F, left) post MxCre induction.

When analysing the HSC compartment, absolute numbers of *Serca2*^{ΔMxCre} KLS cells were significantly enriched at 1 week ($108.20 \pm 33.41 \times 10^6$ versus Ctrl = $9.86 \pm 0.36 \times 10^6$, Figure 43 D), 4 weeks ($10.60 \pm 1.55 \times 10^6$ versus Ctrl = $3.08 \pm 0.31 \times 10^6$, Figure 43 E) and at 8 weeks post induction ($13.81 \pm 5.31 \times 10^6$ versus Ctrl = $2.09 \pm 0.49 \times 10^6$, Figure 43 F) compared to controls. This was due to an accumulation of MPP2 and MPP3-MPP4 cells at all given time points with a

concomitant reduction in HSC numbers as shown for all analysed time points (Figure 43 D-F, right).

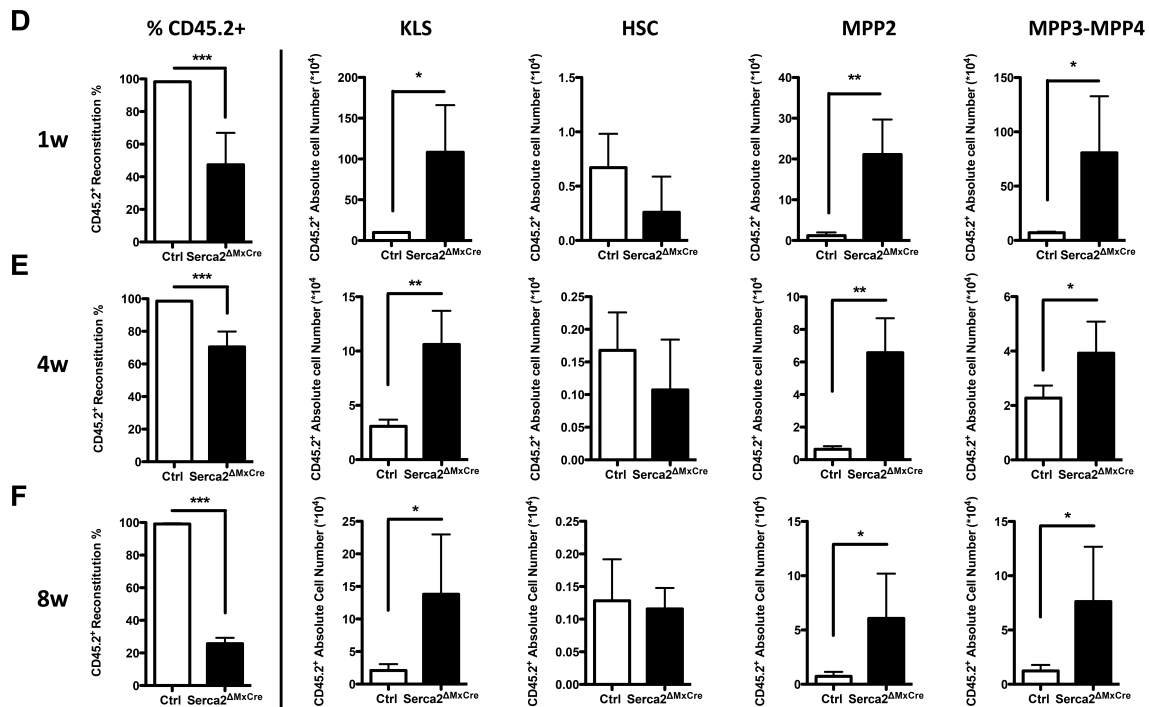


Figure 43: *Serca2* deficiency leads to an enrichment of KLS cells with concomitant loss of LT-HSCs. Left, Percentage of CD45.2⁺ cells in the BM of *Serca2*^{ΔMxCre} and Ctrl chimeras analysed 1 w (D), 4w (E) and 8w (F) post MxCre induction. **Right,** Corresponding absolute cell numbers for HSCs, MPP2 and MPP3-MPP4 cells are shown for 1 week (D), 4 week (E) and 8 week (F) time points depicted Figure 42. Absolute cell numbers are derived from Ctrl (n = 5) and *Serca2*^{ΔMxCre} (n = 5) mice. Error bars represent mean ± SD (* p < 0.05; ** p < 0.01, *** p < 0.001).

In summary, *Serca2* deficiency severely perturbs hematopoietic homeostasis in the BM by enriching the KLS pool with abnormal high numbers of MPP2 and MPP3-MPP4 cells and concomitant reduction of HSCs.

5.3.4 Enrichment of KLS in *Serca2* cKO Animals 1 week post MxCre Induction is not due to Interferon α -induced Mobilization of HSCs

Interferon- α (INF- α) was previously shown to be a potent inducer of HSC mobilization (Essers et al., 2009). Therefore, we investigated whether PIC administration may explain the observed enrichment of KLS cells in *Serca2*-deficient chimeras. We set out to compare the effects of PIC administration on HSCs in interferon-responsive *MxCre* mice and interferon-irresponsible *INF α R*^{KO} animals 16 h after induction and 1 week post induction when *Serca2* deficient chimeras had been analysed.

INFaR_KO and $\Delta MxCre$ chimeric mice were generated by transplanting total BM from *INFaR_KO* (n = 3) or *MxCre* (n = 3) donors into lethally irradiated CD45.1⁺ recipient mice. Upon successful engraftment of donor cells after 4 weeks, 5 injections of PIC were administered every second day and the HSC compartment was analysed (i) 16 h (Figure 44 A) and (ii) 1 week following final PIC injection (Figure 44 B). The percentages (Figure 44 A) and absolute numbers (Figure 44 C) of KLS cells, MPP2 and MPP3-MPP4 cells were significantly increased in $\Delta MxCre$ chimeras in comparison with *INFaR_KO* chimeras 16 h post PIC administration. Phenotypic characterization of the KLS compartment demonstrated significantly lower (i) percentages (Figure 44 A) and (ii) absolute numbers (Figure 44 C) of $\Delta MxCre$ HSCs compared to *INFaR_KO* (n = 5 + 5), while MPP2 and MPP3 - MPP4 cells were significantly enriched accounting for the overall enrichment of the KLS compartment 16 h post PIC administration (Figure 44 C). We demonstrated a similar deregulation of HSC and MPPs numbers in the KLS compartment, when analysing *Serca2* $\Delta MxCre$ chimeras at 1 week post PIC administration.

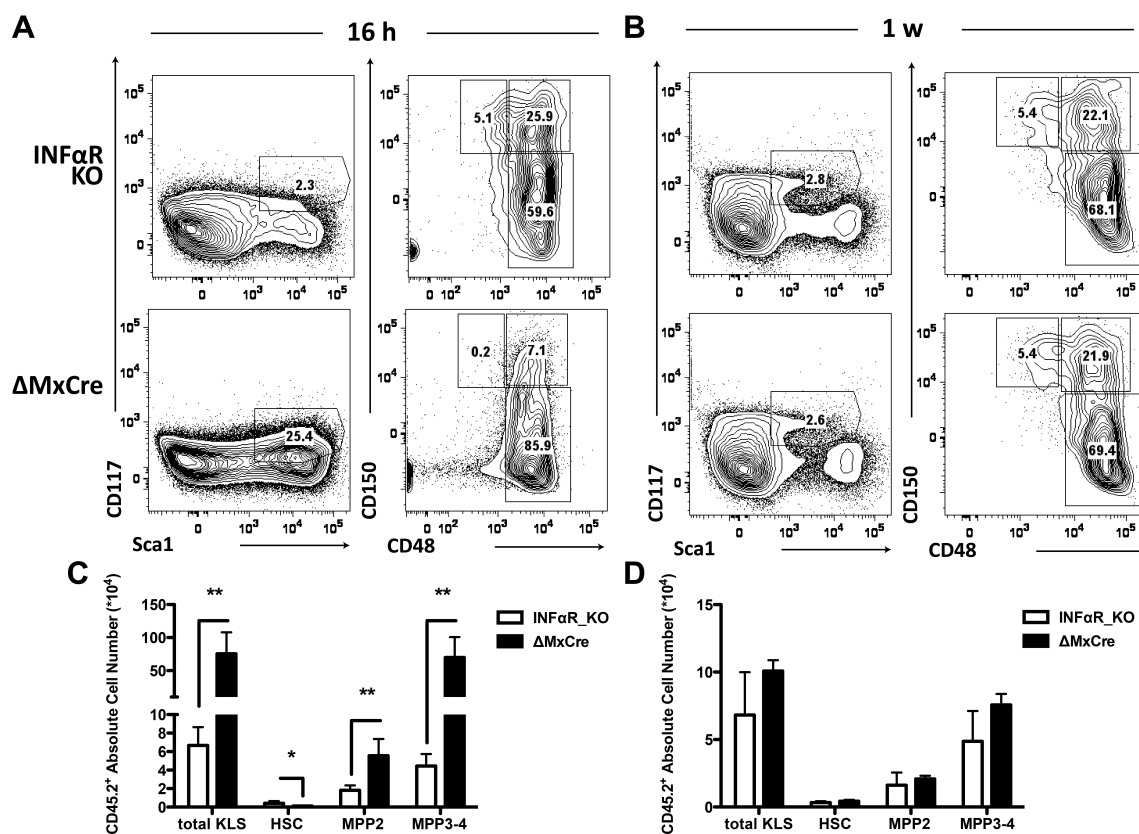


Figure 44: Sixteen hours post PIC treatment hematopoietic stem cells are mobilized but are back to homeostatic state after 1 week in interferon-sensitive $\Delta MxCre$ competitive BM chimeras as compared to *INFaR_KO* controls. *INFaR_KO* and $\Delta MxCre$ -derived BM cells were analysed for the KLS compartment 16 h and 1 week PIC administration. Representative FACS plots depicting staining for CD117 versus Sca1 to identify the overall CD45.2⁺ Lin⁻CD117⁺Sca1⁺ (KLS) population, **upper panel**, further subfractionated into HSCs (KLS, CD150⁺CD48⁻), MPP2, (KLS, CD150⁺CD48⁺) and MPP3-MPP4 cells (KLS, CD150⁺CD48⁺), **lower panel**, for 16 h time point (A) and 1 week time point (B). **C and D**, Absolute cell numbers of donor-derived CD45.2⁺ KLS cells, HSCs, MPP2 and MPP3-MPP4 cells in *INFaR_KO* versus $\Delta MxCre$ competitive BM chimeras (n = 5+5) analysed 16 h or 1 week post last PIC administration. Error bars represent mean \pm SD (\pm SD, * p < 0.05; ** p < 0.011).

In contrast, analysis of the KLS compartment 1 week post PIC administration demonstrated comparable (i) percentages (Figure 45 B) and (ii) absolute numbers of KLS cells, HSCs, MPP2 and MPP3 - MPP4 cells (Figure 45 D) in $\Delta MxCre$ and *INF α R_KO* chimeras. These data indicate that HSC mobilization is rapidly induced in response to INF α treatment (16 h) but is a transient effect since 1 week post PIC administration the KLS compartment is back to normal numbers as under physiologic conditions. This is to some extent comparable to previously published work, in which dormant LT-HSCs (KLS CD150-CD48⁺) were demonstrated to highly proliferate upon INF α stimulation *in vivo* (Essers et al., 2009). Therefore, we speculated that *Serca2*-deficient HSCs may have an intrinsic defect in coping with INF α -induced stress and this until up to 8 weeks post PIC administration.

In addition, we studied the cell cycle kinetics of $\Delta MxCre$ and *INF α R_KO* KLS, HSCs, MPP2 and MPP3 – MPP4 cells at (i) 16 h (Figure 45 A) and (ii) 1 week post PIC administration (Figure 45 A). After 16 h post final PIC injection, the HSC compartment in INF-responsive $\Delta MxCre$ chimeras was significantly deregulated with more KLS cells residing in G₀ phase compared to INF-irresponsive *INF α R_KO* chimeras (Figure 45 B). $\Delta MxCre$ HSCs showed an enrichment of G₁ phase of the cell cycle with a concomitant reduction in the percentage of cells in S/G₂/M phase, while cell cycle kinetics were similar in MPP2s at 16 h post PIC administration (Figure 45 B). In addition, significantly more MPP3 – MPP4 cells were in G₁ phase in $\Delta MxCre$ chimeras compared to *INF α R_KO* chimeras (Figure 45 B). A significant accumulation of KLS cells in G₀ phase was observed in INF-responsive $\Delta MxCre$ chimeras compared to *INF α R_KO* chimeras ($42.16 \pm 3.35\%$ versus $31.46 \pm 1.42\%$, n = 5 +5). Similarly, MPP3 – MPP4 cells were significantly enriched in G₀ ($40.04 \pm 3.37\%$ versus $26.68 \pm 2.13\%$) in $\Delta MxCre$ chimeras compared to *INF α R_KO* chimeras. In addition, a significant increase of HSCs ($58.88 \pm 6.01\%$ versus $39.98 \pm 2.66\%$) in G₁ phase was observed in $\Delta MxCre$ chimeras compared to *INF α R_KO* chimeras. However, the cell cycle distribution of MPP2 cells appeared to be unaffected.

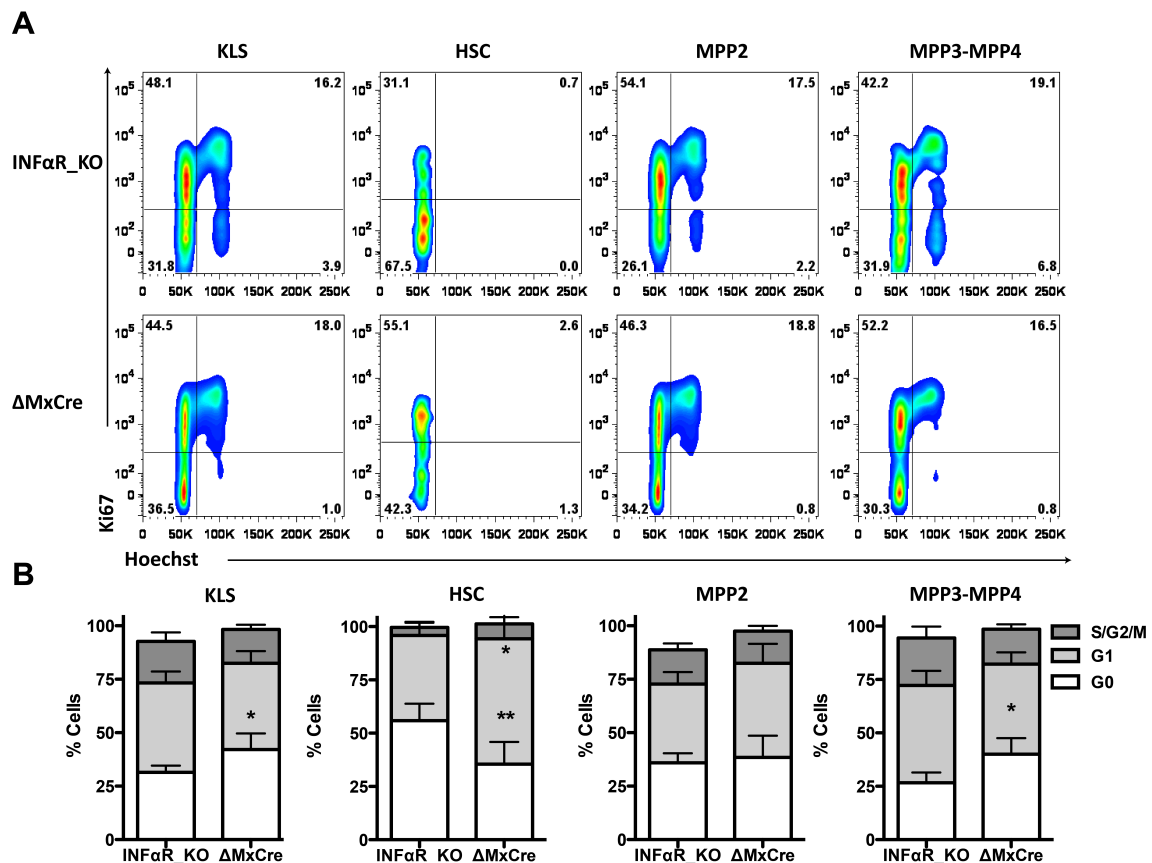


Figure 45: Sixteen hours post PIC treatment cell cycle kinetics are perturbed in $\Delta MxCre$ competitive BM chimeras as compared to *INFαR_KO* controls. *INFαR_KO* and $\Delta MxCre$ -derived HSCs were analysed for cell cycle kinetics 16 h post PIC administration. **A**, Representative FACS plots depicting cell cycle staining for Ki-67 versus Hoechst, gated on the overall CD45.2⁺ KLS population, further subfractionated into HSCs (KLS, CD150⁺CD48⁻), MPP2, (KLS, CD150⁺CD48⁺) and MPP3-MPP4 cells (KLS, CD150⁺CD48⁺) in *INFαR_KO* versus $\Delta MxCre$ competitive BM chimeras. **C**, Percentage of cells in cell cycle phases G₀, G₁ and S/G₂/M for KLS cells, HSCs (KLS, CD150⁺CD48⁻), MPP2, (KLS, CD150⁺CD48⁺) and MPP3-MPP4 cells (KLS, CD150⁺CD48⁺) in *INFαR_KO* versus $\Delta MxCre$ competitive BM chimeras (n = 5 + 5). Error bars represent mean ± SD (* p < 0.05; ** p < 0.011).

Taken together, these data demonstrate that the cell cycle of $\Delta MxCre$ HSCs in response to PIC is significantly affected as early as 16 h post induction, corresponding with the observed enrichment of the KLS population (Figure 44 A).

In this study, the KLS compartment of *Serca2*-deficient chimeras was analysed over a time course with time point 1 week being the earliest time point of analysis. Therefore, we studied INF-responsive ($\Delta MxCre$) and INF-irresponsive (*INFαR_KO*) HSCs at 1 w post final PIC administration and analysed their cell cycle profile (Figure 46 A). $\Delta MxCre$ and *INFαR_KO* HSCs represented with comparable and physiologic numbers 1 week post PIC administration, which is in contrast to the deregulation of HSC numbers in *Serca2*-deficient chimeras observed for the same time point. At 1 week post PIC administration, the rare and quiescent HSCs (KLS⁺CD150⁺CD48⁻) in both $\Delta MxCre$ and *INFαR_KO* cohorts primarily resided in the G₀ phase of the cell cycle. It was shown previously, that approximately 70% of LT-HSCs (KLS⁺CD150⁺

CD48⁺CD34⁻) reside in G₀ phase (Trumpp et al., 2010; Wilson et al., 2008); therefore we can experimentally reproduce these data. Overall, the cell cycle phase distribution of KLS cells, HSCs, MPP2 and MPP3-MPP4 cells was not significantly perturbed when comparing $\Delta MxCre$ with *INFaR_KO* chimeras at 1 week post last PIC injection (Figure 46 B).

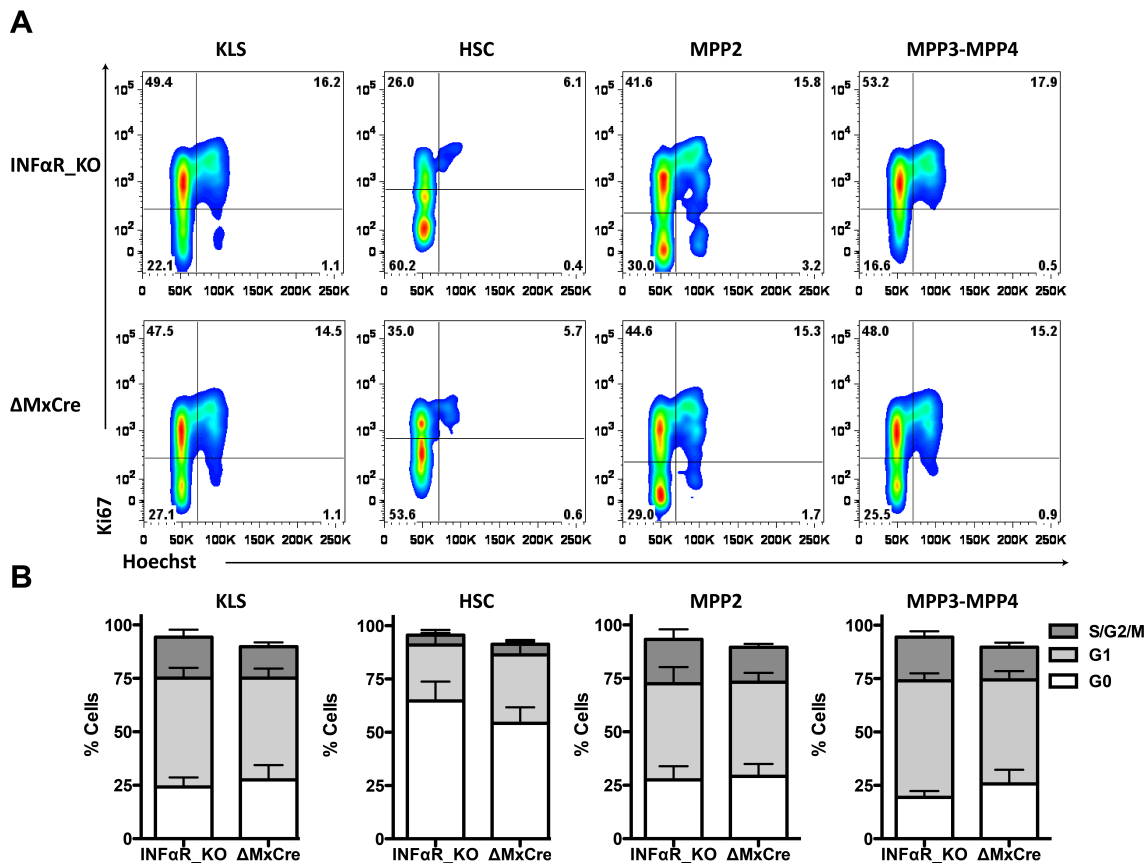


Figure 46: One week post PIC treatment cell cycle kinetics are no longer perturbed in $\Delta MxCre$ competitive BM chimeras as compared to *INFaR_KO* controls. *INFaR_KO* and $\Delta MxCre$ -derived HSCs were analysed for cell cycle kinetics one week post PIC administration. **A**, Representative FACS contour plots depicting cell cycle staining for Ki-67 versus Hoechst, gated on the overall CD45.2⁺ KLS population, further subfractionated into HSCs (KLS, CD150⁺CD48⁻), MPP2 (KLS, CD150⁺CD48⁺) and MPP3-MPP4 cells (KLS, CD150⁻CD48⁺) in *INFaR_KO* versus $\Delta MxCre$ competitive BM chimeras. **C**, Percentage of cells in cell cycle phases G₀, G₁ and S/G₂/M for KLS cells, LT-HSCs (KLS, CD150⁺CD48⁻), ST-HSCs, (KLS, CD150⁺CD48⁺) and MPPs (KLS, CD150⁻CD48⁺) in *INFaR_KO* versus $\Delta MxCre$ competitive BM chimeras (n = 5 + 4). Error bars represent mean ± SD.

In summary, we demonstrated that 16 h post PIC administration, INF-responsive $\Delta MxCre$ chimeras show similar enrichment in the KLS compartment with simultaneous loss of HSCs compared to *Serca2*-deficient chimeras. This was likely due to INF-induced mobilization of the quiescent HSC pool, stimulating altered cell cycle kinetics in these cells at 16 h post final PIC injection. While this effect was only transient in $\Delta MxCre$ chimeras treated with PIC for 16 h and HSCs were back to homeostatic state at 1 week post treatment, *Serca2*-deficient KLS remained enriched for up to 8 weeks post *MxCre* induction (Figure 43). This raised the hypothesis

whether *Serca2*-deficient KLS may harbor other functional defects in addition to the observed impaired long-term reconstitutive capacity.

5.3.5 *Serca2*-deficient KLS form less and smaller CFUs

Hematopoietic stem cells have the potential to self-renew and to differentiate into progenitor cells and all mature lineages of the blood system. The colony forming unit (CFU) assay is a methylcellulose-based assay to study the differentiation potential of HSCs *in vitro* and was used herein to study the impact of *Serca2* ablation on HSC function. *Serca2*^{ΔMxCre} and Ctrl KLS cells were sorted and cultured in methylcellulose containing HSC-specific supplementary growth factors for 1 week. *Serca2*-deficient KLS differentiated into GEMM, monocyte, granulocyte (CFU-G) and granulocyte-macrophage (CFU-GM) colonies *in vitro* (Figure 47 A). However, the numbers and size of these colonies generated from *Serca2*-deficient KLS were significantly reduced compared to those from *Serca2*-competent KLS (Figure 47 B).

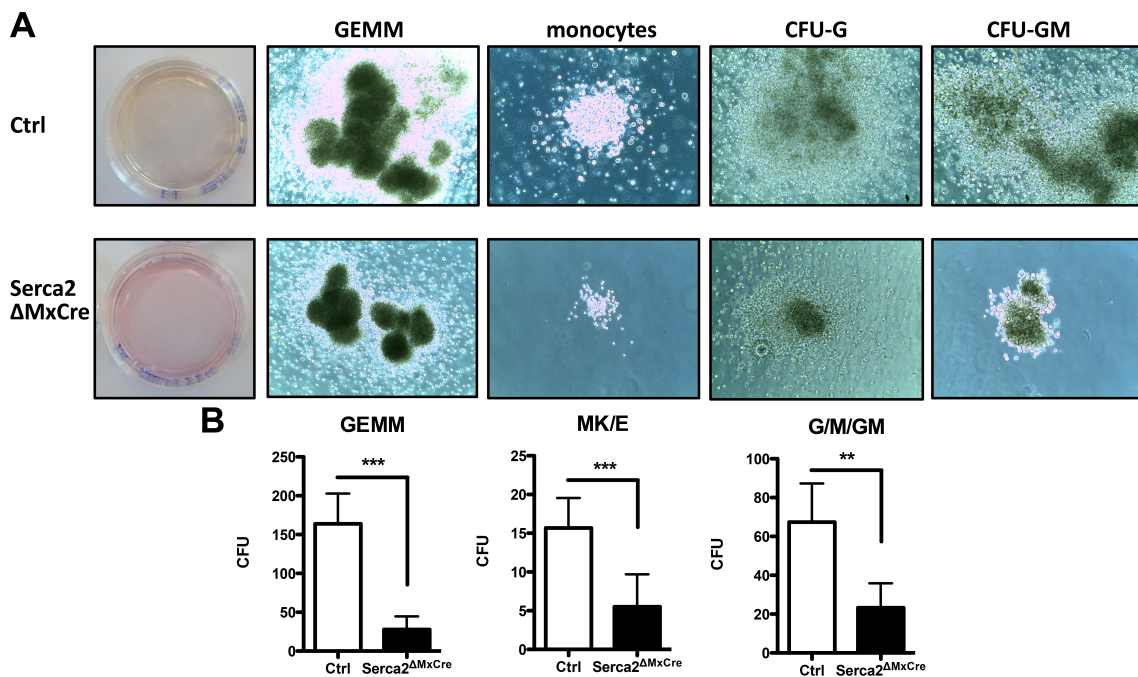


Figure 47: *Serca2*-deficient KLS form less and smaller CFUs *in vitro*. Sorted *Serca2*^{lox/lox} (Ctrl) and *Serca2*^{ΔMxCre} CD45.2⁺ KLS cells were plated in methylcellulose and CFUs were counted following 1 week of culture. **A**, Representative pictures of Ctrl and *Serca2*^{ΔMxCre} GEMM, monocyte, granulocyte (CFU-G) and granulocyte-macrophage (CFU-GM) colonies formed *in vitro*. **B**, Absolute Numbers of GEMM, megakaryocyte erythrocyte (MK/E) and granulocyte (G), macrophage (M) and mixed granulocyte - macrophage colonies. Error bars represent mean ± SD (* p < 0.05, ** p < 0.01, *** p < 0.001), n = 8 (Ctrl) and n = 6 (*Serca2*^{ΔMxCre}).

These results demonstrate that *Serca2* deficiency negatively impacts on HSC function, as the *in vitro* differentiation potential of *Serca2*^{ΔMxCre} KLS cells was significantly reduced compared with

Serca2-competent cells, as demonstrated in the CFU *in vitro* assay. We hence addressed the question whether *Serca2* deficiency may affect the overall survival of HSCs.

5.3.6 *Serca2*-deficient KLS cells are not driven into Apoptosis but have a Cell Cycle Defect

We demonstrated that *Serca2*-deficient lineage committed cells in the BM were apoptotic, likely contributing to the strong reduction in total BM cellularity observed in *Serca2*^{ΔMxCre} chimeras compared to Ctrl chimeras (Figures 34, 39). Given the persistent enrichment of KLS cells in *Serca2*-deficient chimeras up to 8 weeks following MxCre induction with concomitant loss of reconstitutive potential, we hypothesized that HSCs may have a cell intrinsic defect in absence of *Serca2*.

Therefore, apoptosis analysis was performed on 1 week deleted *Serca2* and Ctrl chimeras (Figure 48). *Serca2*-deficient and *Serca2*-competent chimeras had comparably low numbers of apoptotic (Annexin-V+DAPI^{+/-}) cells in the KLS compartment. However, apoptotic cells were slightly but not significantly increased in the KLS population in *Serca2*-deficient chimeras compared to Ctrl (data not shown). This was mainly due to more apoptotic HSCs (Figure 48 B), while MPP2 cells were significantly less apoptotic and MPP3-4 cells remained unaffected upon MxCre-mediated *Serca2* ablation (Figure 48 C). Therefore, we ruled out that *Serca2* deficiency as early as 1 week post MxCre induction triggers massive apoptosis in the HSC compartment of the studied chimeras.

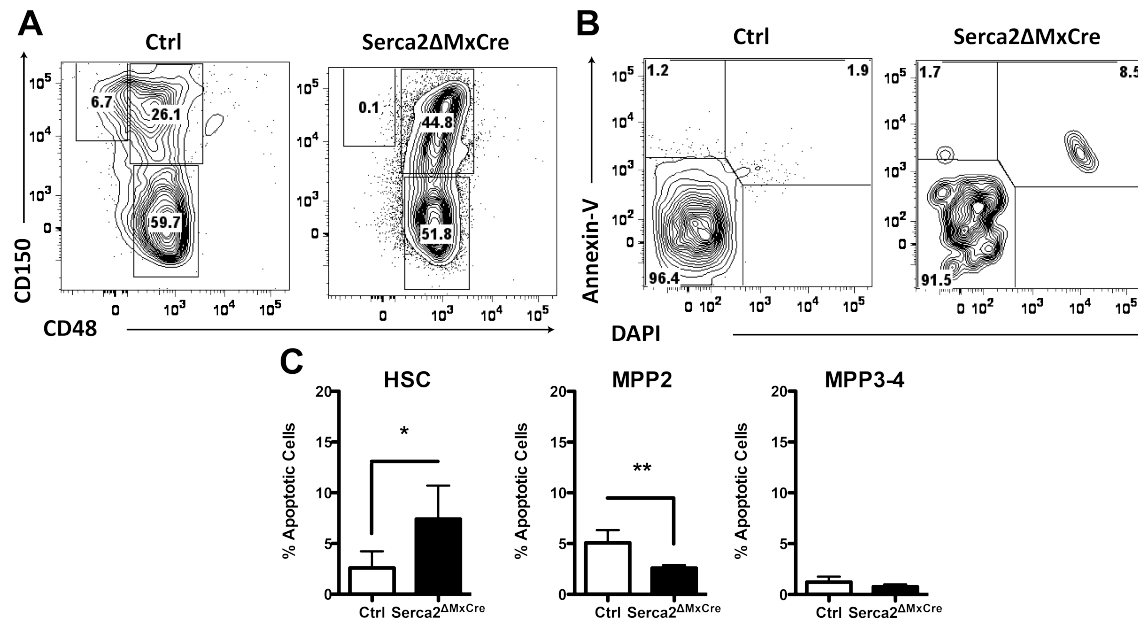


Figure 48: *Serca2*-deficient HSCs are slightly more apoptotic, while MPP subsets less apoptotic or are not affected. *Serca2*-deficient HSCs were analysed for apoptosis one week post MxCre induction. **A**, Representative FACS plots depicting anti-CD150 and anti-CD48 staining, gated on the overall CD45.2⁺ KLS population of *Serca2*^{lox/lox} (Ctrl) versus *Serca2* Δ MxCre animals. **B**, Representative FACS plots depicting apoptosis staining for Annexin-V versus DAPI, gated on the overall CD45.2⁺ HSC population (KLS, CD150⁺CD48⁻) of *Serca2*^{lox/lox} (Ctrl) versus *Serca2* Δ MxCre animals. **C**, Quantification of the percentage of apoptotic cells in CD45.2⁺ HSCs, containing MPP1 cells (KLS, CD150⁺CD48⁻), MPP2 (KLS, CD150⁺CD48⁺) and MPP3-4 (KLS, CD150⁻CD48⁺) populations in *Serca2* Δ MxCre versus *Serca2*^{lox/lox} mice (n = 5+5). Error bars represent mean \pm SD.

These observations nevertheless raised the question whether KLS cells and the rare HSC subpopulations may still resist apoptotic cues up to 8 weeks post MxCre induction, while mature lineages rapidly underwent apoptosis upon *Serca2* inactivation. Therefore, apoptosis analysis was performed on 8 week-long deleted *Serca2* chimeras using AMNIS imaging technology ((McGrath et al., 2008); Figure 49). Strikingly, donor-derived CD45.2⁺ KLS cells did not show significant differences in percentages of (i) live cells (Annexin-V-DAPI-, Figure 49 A), (ii) early apoptotic (Annexin-V⁺) cells (Figure 49 B) or (iii) dead cells (Annexin-V⁺DAPI+, Figure 49 C), while the percentage of KLS cells was still significantly enriched (Figure 49 D) when comparing *Serca2*-deficient with *Serca2*-competent chimeras.

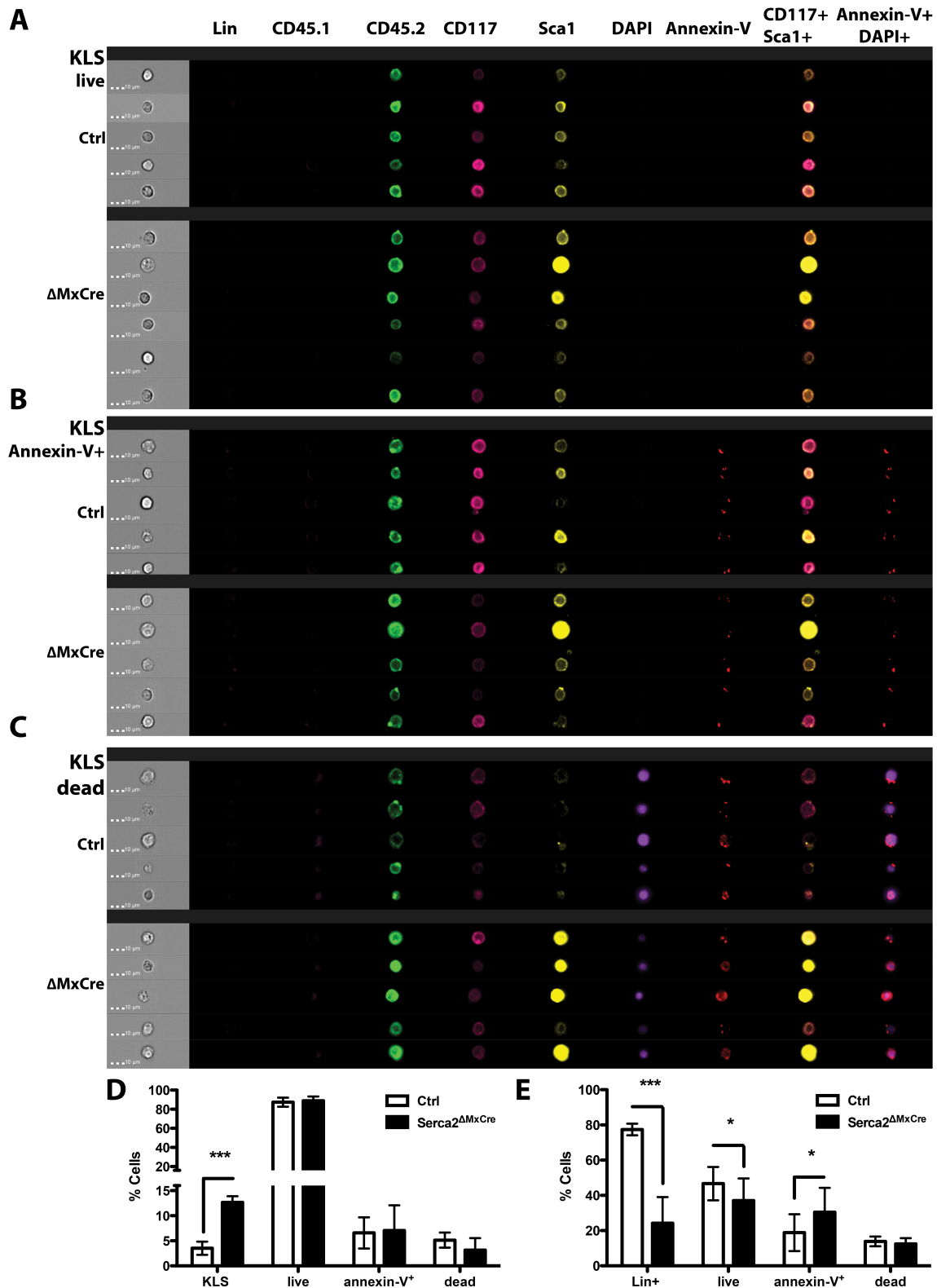


Figure 49: *Serca2*-deficient hematopoietic stem cells are not apoptotic 8 weeks post MxCre induction. *Serca2*^{ΔMxCre} and *Serca2*^{lox/lox} (Ctrl) KLS cells were analysed for apoptosis using AMNIS flow cytometry-imaging technology. Representative images of live (A), Annexin-V+ (B) and dead (C) Ctrl and *Serca2*^{ΔMxCre} single KLS cells, gated on CD45.2⁺, Lin-CD117⁺Sca1⁺ and DAPI versus Annexin-V. D, Percentage of KLS cells and quantification of apoptosis data depicted in (A)-(C.) E, Percentage of CD45.2⁺Lin⁺ cells and apoptosis results. N = 3 mice per

experimental group. Error bars represent mean \pm SD (* $p < 0.05$; ** $p < 0.01$, *** $p < 0.001$). Experiment performed in collaboration with Dr. Stefanie Siegert at the UNIL flow facility.

In contrast, analysis of lineage committed (Lin⁺) BM cells confirmed the previously demonstrated reduction in the total cell numbers and the increased proportions of apoptotic cells (Figure 46 B). Subsequently we set out to analyse the cell cycle of KLS cells, containing HSCs, MPP2 and MPP3-MPP4 subpopulations.

Serca2-deficient total KLS cells, remaining HSCs and MPP3-MPP4 cells showed a deregulated cell cycle with the majority of cells residing in G₀ phase of the cell cycle compared to Ctrl, as depicted in (i) percentages (Figure 50 A) and (ii) in quantified percentages of $n = 5 + 5$ chimeras (Figure 50 B).

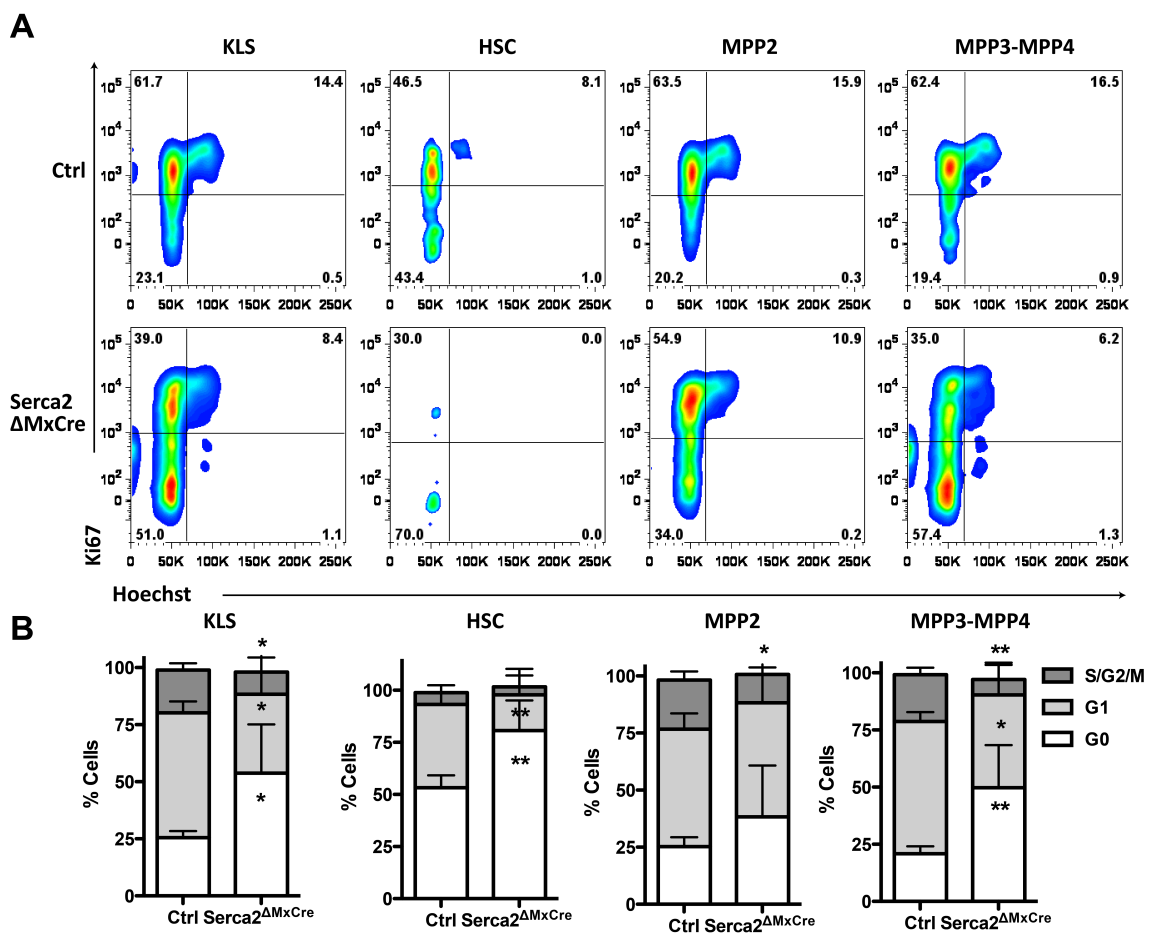


Figure 50: Serca2-deficient hematopoietic stem cells are driven into cell cycle arrest. *Serca2*-deficient HSCs were analysed for cell cycle kinetics 1 week post MxCre induction via PIC administration. **A**, Representative FACS plots depicting cell cycle staining for Ki-67 versus Hoechst, gated on the overall CD45.2⁺KLS population, further subfractionated into HSCs (KLS, CD150⁺CD48⁻), MPP2 (KLS, CD150⁺CD48⁺) and MPP3-MPP4 cells (KLS, CD150⁺CD48⁺) of Ctrl versus *Serca2* Δ MxCre animals. **C**, Percentage of cells in cell cycle phases G₀, G₁ and S/G₂/M for donor-derived CD45.2⁺ KLS cells, HSCs (KLS, CD150⁺CD48⁻), MPP2 (KLS, CD150⁺CD48⁺) and MPP3-MPP4 cells (KLS, CD150⁺CD48⁺) in *Serca2*-deficient versus Ctrl ($n = 5 + 5$). Error bars represent mean \pm SD (* $p < 0.05$; ** $p < 0.01$).

This analysis, however, only captured the cell cycle profile of *Serca2*-deficient versus *Serca2*-competent HSCs at the discrete time point of 1 week post MxCre induction. To further assess whether *Serca2*-deficient KLS cells harbor cell cycle defects, the proliferation capacity of these cells was measured *in vitro*. In contrast to Hoechst-Ki-67 staining, Carboxyfluorescein succinimidyl ester (CFSE) cell division tracking allows quantifying the number of cell divisions made by a given cell type over time. CFSE is a fluorescent dye that labels the totality of a given cell population but washes out with every division the cell undergoes, thereby constantly decreasing in fluorescence intensity (Weston and Parish, 1990). In brief, *Serca2*^{ΔMxCre} or Ctrl Lin⁻ BM cells were labelled with CFSE and analysed by flow cytometry daily over 5 days (Figure 51 A). Total BM cells, containing a mix of about 20-30% Lin⁻ enriched progenitor cells and mature Lin⁺ cells, demonstrated slower cycling kinetics in (i) percentages (Figure 51 B) and in (ii) percentages quantified (Figure 51 C; *Serca2*^{ΔMxCre} (n = 4) and Ctrl (n = 4)) in absence of *Serca2* compared to Ctrl. This effect was more evident when analysing the KLS compartment (Figure 51 D), in which significantly less KLS cells underwent one additional division at day 3 (68.07 ± 5.81% versus 89.98 ± 0.22%, n = 4 + 4) and at day 4 (33.05 ± 9.93% versus 90.40 ± 0.55%, n = 4 + 4) when comparing *Serca2*-deficient with *Serca2*-competent cells.

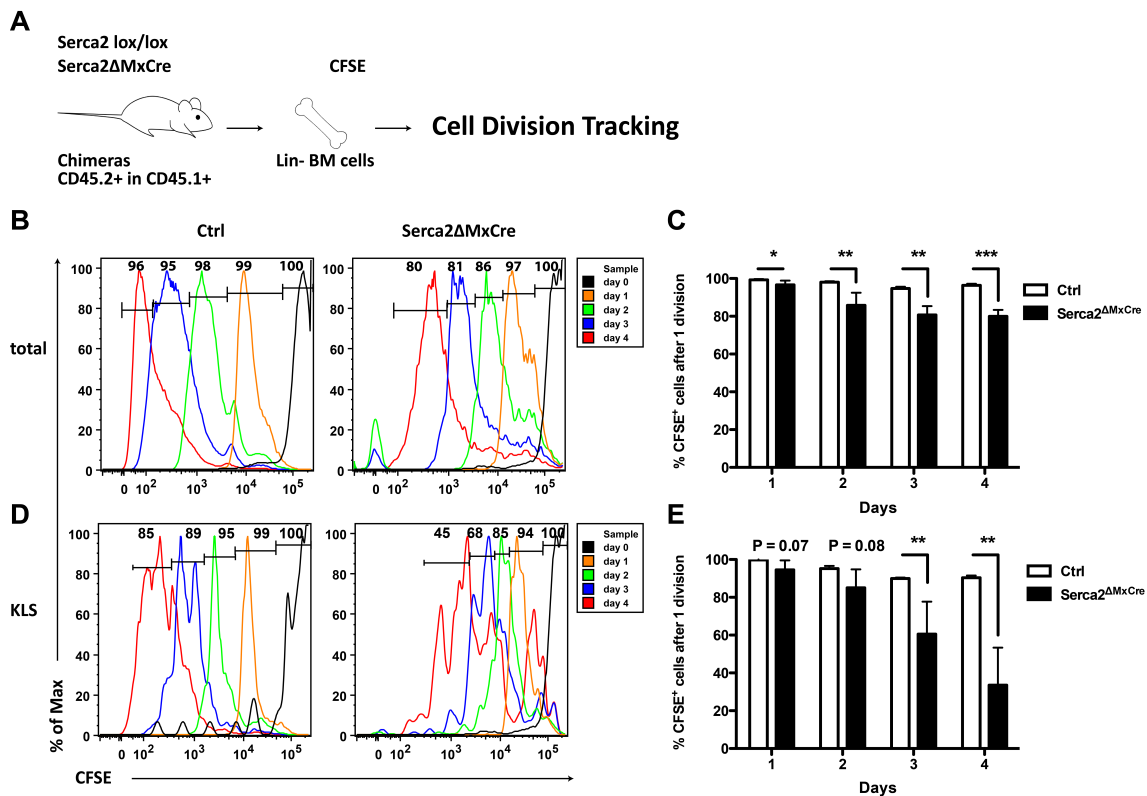


Figure 51: *Serca2*-deficient KLS cells show slower cell cycle kinetics in CFSE cell division assay. A, Experimental set up for CFSE cell division tracking of *Serca2*^{lox/lox} (Ctrl) versus *Serca2*^{ΔMxCre} derived lineage negative BM cells. Representative FACS histograms depicting cell divisions of Ctrl versus *Serca2*^{ΔMxCre} lineage negative BM (**B**) and KLS (**D**) cells measured daily over 5 days. Quantification of cell divisions in total lineage negative cells (**C**) and KLS cells (**E**) of Ctrl and *Serca2*^{ΔMxCre} mice (n = 4 + 4). Error bars represent mean ± SD (* p < 0.05; ** p < 0.01, *** p < 0.001).

In summary, these data demonstrate that *Serca2*-deficient KLS cells have a deregulated cell cycle with cells predominantly enriched G₀ phase, which is likewise reflected in the slower cycling behavior of KLS cells as shown in the CFSE cell division tracking assay. We have shown that *Serca2*-deficient lineage committed BM cells undergo apoptosis most likely due to ER stress and induction of UPR, in line with the up-regulation of pro-apoptotic genes (Figure 41). Therefore, we wanted to validate whether *Serca2*-deficient KLS may be resistant to UPR-mediated induction of apoptosis.

Expression of target genes of the UPR were mildly affected in *Serca2*^{ΔMxCre} KLS compared to Ctrl (Figure 52 A), while expression of the anti-apoptotic genes *Bcl-2* and *Bcl2l1* remained unchanged, whereas pro-apoptotic genes *Bax* and *Bim* were down- or up-regulated, respectively in *Serca2*-deficient KLS cells (Figure 52 B). Overall, expression changes for candidate genes of UPR and apoptosis were not dramatically altered in *Serca2*-deficient KLS cells compared to those in *Serca2*-competent KLS cells.

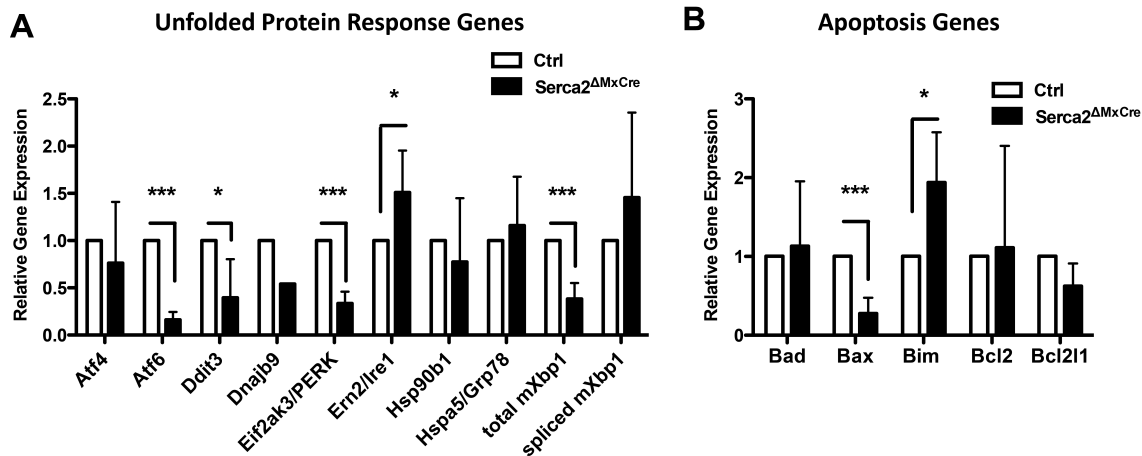


Figure 52: Unfolded Protein Response Genes and apoptosis-related genes are slightly deregulated in *Serca2*-deficient KLS cells. Quantitative RT-PCR gene expression data for UPR candidate genes (A) and apoptosis-related genes (B) of sorted *Serca2*^{ΔMxCre} versus *Serca2*^{lox/lox} (Ctrl) KLS cells. Error bars represent mean ± SD. N= minimum of 3+3.

In addition, we analysed UPR and apoptosis-related gene expression comparing mature hematopoietic lineages to those in KLS cells (set to 1) sorted from *Serca2*^{ΔMxCre} chimeras. Upon *Serca2* conditional inactivation, Lin⁺ cells up-regulated UPR-associated genes (Figure 53 A) with simultaneous up-regulation of pro-apoptotic *Bad*, *Bax* and *Bim* (Figure 53 B). This demonstrates that in our chimeric mice, *Serca2* deficiency primarily affects mature cells compared to the KLS pool, that contains HSC and MPP subpopulations.

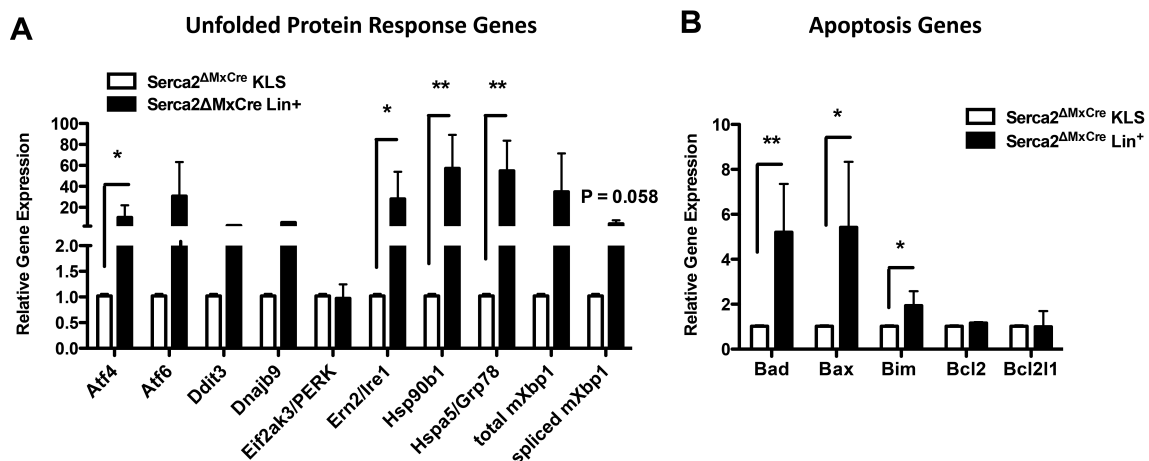


Figure 53: Unfolded Protein Response Genes and pro-apoptotic genes are highly enriched in mature lineages compared to *Serca2*-deficient KLS cells. Quantitative RT-PCR gene expression data for UPR candidate genes (A) and apoptosis-related genes (B) in sorted *Serca2*^{ΔMxCre} Lin⁺ BM compared to *Serca2*^{ΔMxCre} KLS cells (set to 1). Error bars represent mean ± SD. N= minimum of 3+3.

Taken together, we have demonstrated that *Serca2*-deficient KLS are likely resistant to ER stress, which in contrast had a drastic effect on mature lineages by inducing apoptosis. This is to

some extent consistent to the previously published work by the group of John Dick (van Galen et al., 2014), which postulates that human HPSCs (Lin⁻CD117⁺CD59⁺CD34⁺CD38⁻) are more sensitive to ER stress than progenitor cells (Lin⁻CD117⁺CD59⁺CD34⁺CD38⁺), thereby protecting the integrity of the hematopoietic system.

5.4 Thapsigargin treatment mimics Serca2 LOF *in vitro*

The chemical compound thapsigargin (TH) is known to cause calcium imbalance in the cells by specifically blocking the ATPase function of Serca pumps (Thastrup et al., 1990). The group of Kimberly Stegmaier identified TH as potential Notch1 inhibitor in human T-ALL cells and therefore TH represents a drug candidate for the treatment of T-ALL (Roti et al., 2013). TH, a non-competitive ATP-ase inhibitor specifically blocking the action of calcium pumps of the Serca family, was shown to induce ER stress primarily in human HSCs compared to progenitor cells (van Galen et al., 2014). Therefore, we set out to study the effect of TH treatment on BM cells and investigated whether inhibition of Serca2 in BM cells *in vitro* may recapitulate the phenotype observed in *Serca2*-deficient animals. Therefore, BM cells from C57BL6/J WT animals were isolated, enriched for lineage negative cells and treated with 200 nM TH for 1, 6, 24 and 40 h or DMSO (Ctrl) (Figure 54 A). Prolonged TH treatment significantly affected the proliferation of the total population of MACS enriched Lin⁻ BM cells in culture. Absolute cell numbers were dramatically reduced upon 24 h treatment ($0.52 \pm 0.24 \times 10^6$ cells, n = 3) compared to DMSO-treated controls ($3.14 \pm 0.22 \times 10^6$ cells, n = 3) and cell numbers remained equally low at 40 h post treatment (Figure 54 B).

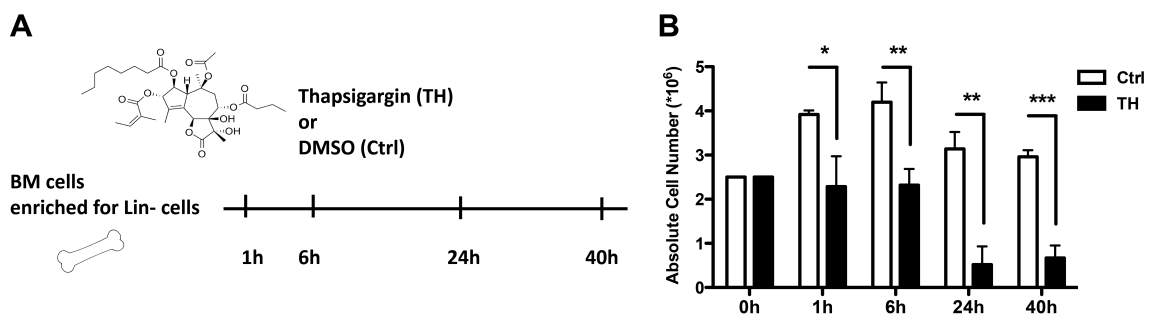


Figure 54: Prolonged thapsigargin treatment inhibits proliferation of total MACS enriched lineage negative BM population cells *in vitro*. A, WT C57BL6/J BM cells were enriched for lineage negative cells and the total population was cultured in presence of 200 nM thapsigargin (TH) or DMSO (Ctrl) over a time course of 1, 6, 24 and 40 h. B, Absolute cell numbers in presence of TH compared to Ctrl over 0, 1, 6, 24 and 40 h (n = 3 + 3). Error bars represent mean ± SD (* p < 0.05; ** p < 0.01, *** p < 0.001).

5.4.1 Thapsigargin induces Apoptosis of Total MACS enriched Lineage negative Cells *in vitro*

Given the significant reduction in absolute cell numbers of TH-treated cells compared to control, we speculated that TH may induce apoptosis as shown for mature BM lineages in *Serca2*-deficient chimeric mice.

Analysis of MACS enriched Lin⁻ total BM cells cultured in the presence of 200 nM TH demonstrated that with increasing treatment duration, TH is a strong apoptosis-inducing agent in these cells (Figure 55 A upper panel). At 24 h post treatment, $51.57 \pm 3.75\%$ of cells ($n = 3$) were apoptotic compared to $13.37 \pm 2.88\%$ in DMSO-treated controls ($n = 3$). The cytotoxic effect of TH was even more striking after 40 h, when $71.67 \pm 4.14\%$ of Lin⁺ BM cells were apoptotic compared to $14.10 \pm 3.77\%$ in control cultures. In contrast, when gating on the Lin⁻ cell fraction in the same culture conditions, we did not observe apoptotic cells (Figure 55 A lower panel), which was consistent until up to 40 h post TH treatment (Figure 55C).

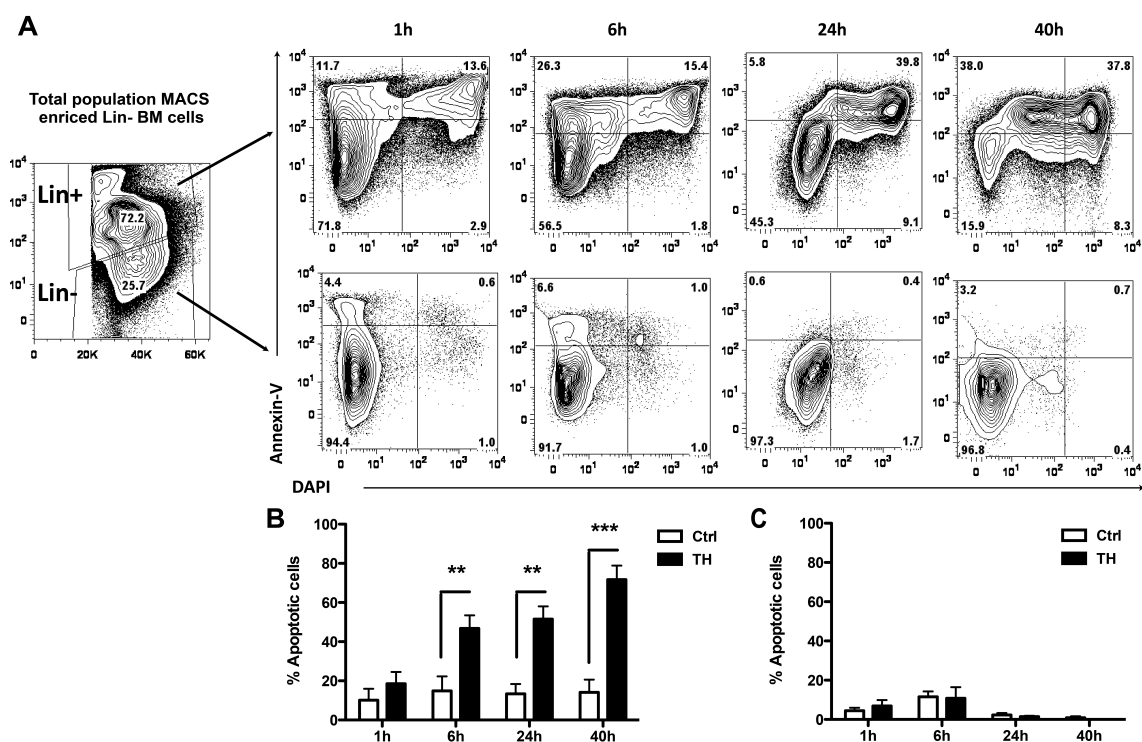


Figure 55: Prolonged thapsigargin treatment induces apoptosis in Lin⁺ but not Lin⁻ MACS enriched BM cells *in vitro*. Total MACS enriched lineage negative BM cells were treated with 200 nM thapsigargin (TH) for 1, 6, 24 or 40 h. **A**, Representative FACS plots depicting apoptosis staining for Annexin-V versus DAPI over the timecourse of thapsigargin treatment for Lin⁺ (**upper panel**) and Lin⁻ fraction (**lower panel**). Quantification of apoptotic cells in presence of thapsigargin compared to DMSO treatment ($n = 3$) for Lin⁺ fraction (**B**) and Lin⁻ cells (**C**). Error bars represent mean \pm SD (* $p < 0.05$; ** $p < 0.01$, *** $p < 0.001$).

These data indicate that *in vitro* inhibition of Serca ATPases in C57BL6/J WT cells via treatment with TH recapitulates the induction of apoptosis we observed in mature lineages of *Serca2* cKO

animals. This observation raised the question whether the KLS compartment may also be affected in response to TH treatment.

5.4.2 Thapsigargin induces an enrichment of the KLS population *in vitro*

We then investigated whether TH-mediated blockage of Serca pumps in WT MACS enriched Lin⁻ BM cells may affect the HSC compartment over time. Phenotypic analysis for cell surface expression of CD117 and Sca1 on Lin⁻ BM cells revealed an enrichment of KLS cells in (i) percentages (Figure 56 A, B) and (ii) absolute cell numbers (Figure 56 C) following TH treatment for 6, 24 and 40 h.

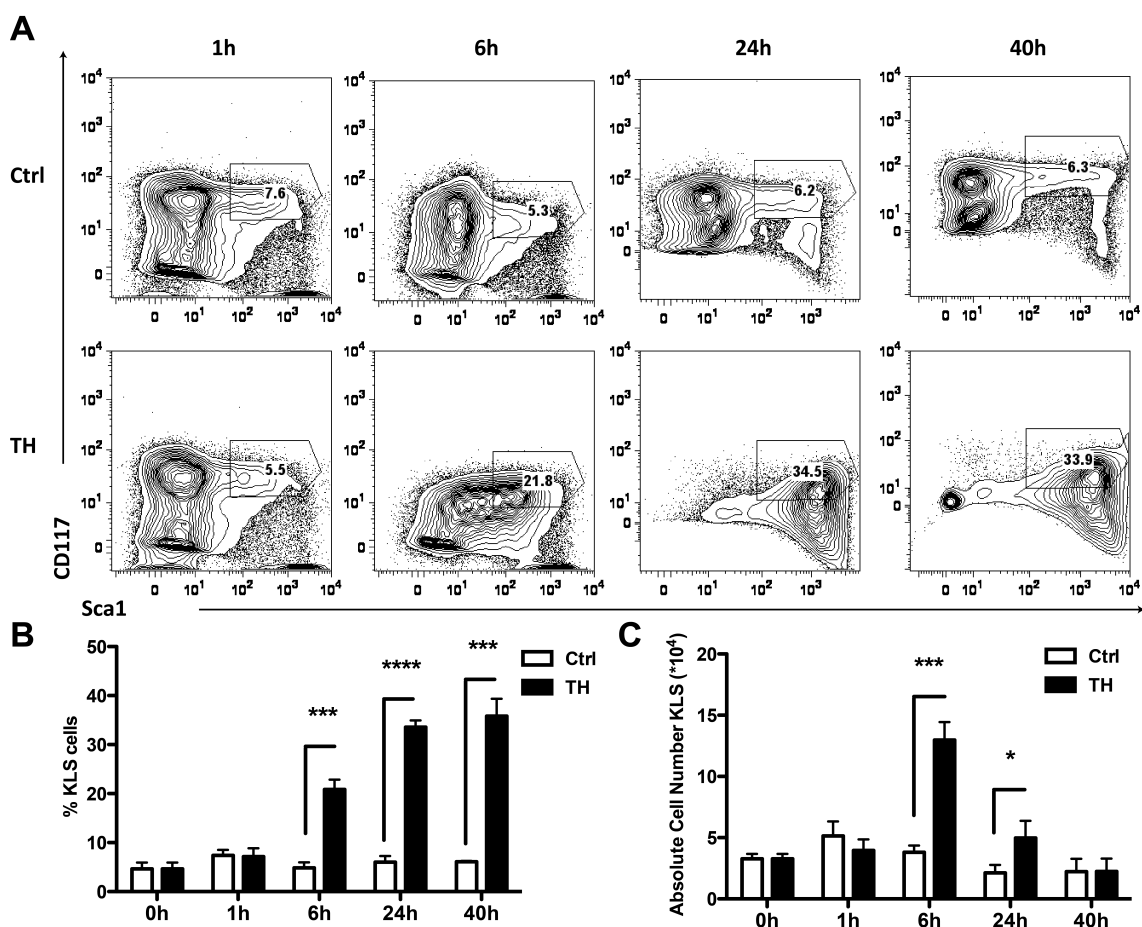


Figure 56: Prolonged thapsigargin treatment induces an enrichment of the KLS population *in vitro*. Total population of MACS enriched lineage negative BM cells were treated with 200 nM thapsigargin (TH) or DMSO (Ctrl) for 1, 6, 24 and 40 h. **A**, Representative FACS plots depicting cell surface staining for CD117 versus Sca1, gated on lineage negative cells, over the time course of TH treatment. Percentage (**B**) and absolute cell numbers (**C**) of KLS cells in presence of TH compared to DMSO (n = 3 + 3). Error bars represent mean \pm SD (* p < 0.05, ** p < 0.01, *** p < 0.001, **** p < 0.0001).

The percentage of KLS cells progressively increased over time in presence of TH, with a maximal enrichment of $35.80 \pm 2.05\%$ KLS cells in TH-treated cultures versus $6.10 \pm 0.10\%$ KLS cells in

DMSO-treated cultures (Figure 56 A). In contrast, the absolute number of KLS cells peaked at 6 h with $12.97 \pm 0.84 * 10^4$ compared to $3.82 \pm 0.31 * 10^4$ for Ctrl (Figure 56 C). Prolonged TH treatment for 24 h still led to increased absolute cell numbers (TH = $4.97 \pm 0.81 * 10^4$ versus Ctrl = $2.13 \pm 0.37 * 10^4$), 40 h treatment in contrast did no longer reflect in more KLS cells compared to Ctrl, which is likely due to the (i) overall strong reduction in proliferation (Figure 56) and (ii) induction of apoptosis (Figure 56) in the total population of MACS enriched Lin⁻ BM cells in response to TH. Overall, these data indicate that KLS cells were persistently enriched in presence of TH, indicating that chemical inhibition of Serca pumps *in vitro* recapitulates the KLS enrichment phenotype observed in *Serca2*^{ΔMxCre} chimeras *in vivo*.

5.4.3 Thapsigargin does not induce Apoptosis in KLS cells but deregulates their Cell Cycle *in vitro*

Upon analysis of TH treated Lin⁻ BM cells we observed an enrichment of KLS cells with simultaneous and progressive apoptosis of lineage-committed cells with increasing treatment duration. We hypothesized that TH treatment, similarly to *Serca2* deficiency *in vivo*, may regulate the survival of KLS cells. Apoptosis analysis of the KLS compartment after 1, 6, 24 and 40 h of treatment demonstrated similarly low levels of apoptotic cells in presence or absence of TH (data not shown). These *in vitro* results were confirmative of the absence of apoptotic KLS cells in *Serca2*-deficient chimeras described earlier (Figures 48, 49) and raised the question whether TH-treated KLS may have a cell cycle defect.

One hour TH treatment did not affect cycling behavior of KLS cells in comparison with DMSO-treated Ctrl (Figure 57 A, B), while 6 h treatment induced an enrichment of KLS cells in G₁ phase at the expense of S/G₂/M phase cells (Figure 57 A, B). Prolonged treatment with TH, however led to a block of KLS cells in G₀ phase of the cell cycle, in which predominantly quiescent HSCs reside under physiologic conditions. This effect was most evident with $87.47 \pm 4.18\%$ TH-treated KLS cells in G₀ phase compared to $27.33 \pm 6.57\%$ Ctrl-treated KLS cells (Figure 57 B) at 40 h post treatment.

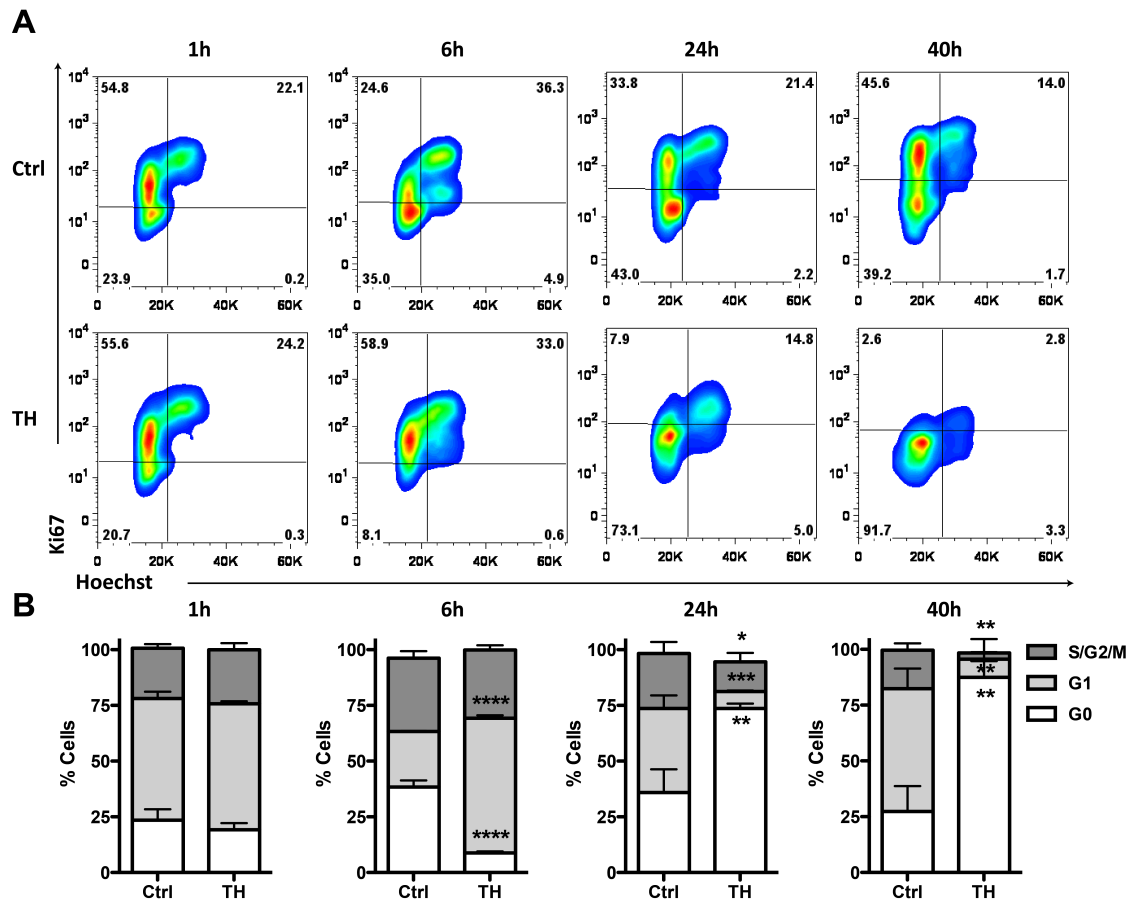


Figure 57: Prolonged thapsigargin treatment induces cell cycle arrest in KLS cells *in vitro*. Lineage negative BM cells were treated with thapsigargin (TH) or DMSO (Ctrl) for 1, 6, 24 and 40 h. **A**, Representative FACS contour plots depicting cell cycle staining for Ki-67 versus Hoechst, gated on KLS cells, over the time course of thapsigargin treatment. **B**, Percentage of cells in cell cycle phases G0, G1 and S/G2/M in presence of thapsigargin compared to DMSO treatment (n = 3+3). Error bars represent mean \pm SD (* p < 0.05; ** p < 0.01, *** p < 0.001, **** p < 0.0001).

In summary, we have demonstrated that inhibition of Serca calcium pumps using the non-competitive ATPase inhibitor TH *in vitro* effectively mimics *Serca2* LOF in the BM *in vivo*. Prolonged TH treatment of BM cells induces apoptosis in the majority of mature hematopoietic cells (Lin⁺), while rare HSCs (KLS) are resistant to apoptosis and rather accumulate in G₀ phase of the cell cycle in presence of TH. These data are somewhat confirmative to previously published data, which claims that HSCs are very sensitive to ER stress. More importantly, these data question the use of TH for the treatment of T-ALL.

6 Discussion Part II: Role of Serca2 in Hematopoiesis

Aberrant Notch pathway activation is frequently linked to T-ALL and therefore the Notch signalling pathway represents a bona fide drug target. Therefore, Rajwinder Lehal and Stegmaier *et al.* set out to identify novel inhibitors of the Notch pathway by performing chemical compound screens (Lehal, 2011; Roti et al., 2013). Co-culture based chemical compound screening in HeLa cells, stably expressing N1 and Dll4 ligand, identified CPA as potent drug to down-regulate Notch pathway activation and downstream target genes such as *Hes1*, *cmyc* and *Deltex1* (Lehal, 2011). Similarly, when screening for chemical inhibitors in Notch-driven DND41 T-ALL cells, Stegmaier *et al.* identified CPA and TH, both compounds inhibiting pumps of the Serca family of calcium ATPases. A complementary cDNA library screen was conducted in parallel in order to identify factors that would potentiate oncogenic Notch. This approach led to the identification of Serca2, thereby confirming previous results (Roti et al., 2013). Although this work shows that Serca2 is indeed regulating N1, the work did not address, whether Serca2 function is specific for Notch, or may have additional function within the hematopoietic system. This is of importance since Serca2 has been suggested as a potential novel drug target to fight Notch-driven T-ALL. Therefore, we set out to study the impact of Serca2 ablation on the hematopoietic system, mainly to address whether i) Serca2 deficiency may recapitulate the Notch LOF effects on T and MZB cell development and ii) to assess whether a Serca2 inhibitor may be an applicable therapeutic target for T-ALL, as previously suggested.

6.1 Functional Characterization of loss of one Serca2 allele in the Hematopoietic system

Missense mutations in the SERCA2 encoding gene *ATP2A2* are strongly linked to Darier's disease in humans (Sakuntabhai et al., 1999). As a result, one SERCA2 allele is functionally inactivated leading to genodermatosis, characterized by an abnormal hyperkeratotic epidermis, nail abnormalities and mucous membrane defects. Interestingly, mice heterozygous for *Serca2* (*Serca2*^{+/-}) develop squamous cell carcinoma of the skin (Prasad et al., 2004), which is confirmative of the identification of *ATP2a2* as the Darier's disease-causing gene. Taken together, these studies demonstrate a gene dosage effect for SERCA2 in regulating skin homeostasis. Therefore, we addressed the question whether *Serca2* haploinsufficiency may

impact on the hematopoietic system and studied conditional ablation of one *Serca2* allele under physiological and competitive conditions (Appendix Section 7.6). We did, however, not observe any lineage specification deficits in these chimeric mice under steady state conditions. Furthermore, *Serca2* haploinsufficiency did not render HSCs less susceptible to 5-FU-induced mobilization and subsequent exhaustion upon prolonged treatment, thereby ablating mature hematopoietic lineages and forcing HSCs to self-renew and differentiate. We also studied *Serca2* haploinsufficiency in competitive BM chimeras and under serial transplantation stress, but did not observe any overt changes in short-term multi-lineage reconstitution capacity in absence of one functional *Serca2* allele. In addition, T cell development was unperturbed when studied in these chimeras under physiological and competitive conditions. *N1* conditional ablation in the BM is crucial for T lineage versus B lineage commitment, however ectopic B cell development in the thymus only occurs when conditionally targeting both *N1* alleles for inactivation (Radtke et al., 1999). Recent studies by Stegmaier *et al.* proposed that *Serca2* regulates *N1* maturation leading to increased NICD protein available for signalling. Consequently, chemical inhibition of *Serca2* with TH, resulted in the accumulation of misfolded Notch receptors within the ER, thereby reducing Notch receptor numbers available for trafficking to the cell membrane (Roti et al., 2013). For our work, this may suggest, that *Serca2* haploinsufficiency does not efficiently induce misfolding of Notch receptors, whereby the trafficking and occurrence of Notch receptors to and at the cell membrane remains unperturbed. Therefore, *Serca2* haploinsufficiency cannot mimic *N1* LOF in the thymus and T cell development remains unaffected. To experimentally prove this hypothesis, target genes of the UPR could be measured in BM cells derived from *Serca2*-haploinsufficient and Ctrl chimeras.

In conclusion, one functional *Serca2* allele can compensate haploinsufficiency during hematopoiesis, suggesting that gene dosage does not majorly impact in this self-renewing organ, which is in contrast to *Serca2* function in the skin.

6.2 Functional Characterization of SERCA2 loss of function in the Hematopoietic System

Serca2 conditional inactivation was studied in chimeras in order to limit *Serca2* deletion to BM cells. Upon transplantation, residual recipient-derived WT CD45.1⁺ cells outnumbered *Serca2*^{ΔMxCre} CD45.2⁺ cells over time, leading to a significant reduction in overall multi-lineage reconstitution in *Serca2*-deficient chimeras. This effect was cell intrinsic as *Serca2* conditional ablation was studied solely in BM chimeras, in which BM niche cells are not targeted for deletion. Upon analysis of the BM, we observed a strong reduction in total BM cellularity, which

was characterized by reduced numbers of mature lineages of myeloid origin (CD11b⁺Gr1⁺), erythroid origin (Ter119⁺CD71⁺) and also affecting B (B220⁺IgM⁺) cell numbers. Further analysis demonstrated that these cells underwent apoptosis in response to Serca2 inactivation. These data indicate that conditional Serca2 ablation in the BM globally affects the survival of mature hematopoietic lineages. Since N1 signaling is crucial for T lineage versus B lineage commitment in the thymus (Radtke et al., 1999) and Serca2 was demonstrated to regulate N1 maturation (Roti et al., 2013), we analysed thymi of *Serca2*^{ΔMxCre} and control chimeras. Similarly to the BM, total thymic cellularity was severely reduced upon conditional *Serca2* inactivation. Upon analysis of T cell maturation stages, we observed reduced numbers of cells passing through all DN1 to DN4 stages of differentiation, which is majorly due to reduced *Serca2*^{ΔMxCre} ETP numbers migrating from the BM into the thymus. Upon closer analysis CD4⁺CD8⁻Lin⁻ thymic progenitors, we did observe an enrichment of CD44^{hi}CD117⁻ cells, similar to the phenotype for N1 LOF previously published (Radtke et al., 1999). These cells, however, were not committed to the B cell lineage as assessed by the markers B220 and IgM. Beyond TCRβ selection, *Serca2*^{ΔMxCre} chimeras had significantly less immature CD4⁺CD8⁺DP cells compared to controls, which may be explained by their higher sensitivity to apoptotic cues than CD4⁺SP or CD8⁺SP cells, which have passed negative and positive selection.

In addition, we studied mature peripheral lineages in the spleen of *Serca2*^{ΔMxCre} and control chimeras. Similarly to the BM and the thymus, absolute cell numbers were reduced in the spleens of *Serca2*-deleted chimeras, affecting all studied cell types of mature B and T cells.

While N1 is crucial for T cell differentiation, N2 regulates MZB cell development in the spleen (Saito et al., 2003). Therefore, we studied MZB cells in *Serca2*-deficient chimeras, which were significantly enriched in relative numbers; however this effect was not reflected in absolute numbers due to the reduced overall cell number of splenocytes. This suggests that either (i) follicular zone B cells are more sensitive to Serca2 ablation and therefore MZBs accumulate or (ii) Serca2 may regulate N2 and as a consequence of Serca2 inactivation N2 signalling is deregulated during MZB development. In contrast, Serca2 was identified to be important for maturation and cleavage of N1, thereby modulating Notch 1 signalling strength (Roti et al., 2013). This work however, solely focussed on N1 and therefore, our *in vivo* studies are complementary, demonstrating that Serca2 inhibition may also impact on N2 signalling. However, *in vitro* studies performed by Rajwinder Lehal, demonstrated, that CPA, targeting Serca ATPases, primarily down-regulates N1-Dll4 mediated Notch signalling, while N2-Dll1-induced signalling was not blocked in response to CPA in the co-culture system (Lehal, 2011). It is possible that global Serca inhibition by CPA treatment may account for these *in vitro* data.

Therefore, further *in vitro* and *in vivo* studies are needed to delineate the potential role of Serca2 in regulating N2 signalling.

In addition, we have studied functional consequences of Serca2 inactivation. Upon calcium flux measurements, *Serca2*^{ΔMxCre} peripheral T and B cells have a higher calcium baseline but lower intracellular Ca²⁺ levels. These results indicate that *Serca2*-deficient hematopoietic cells have indeed a deregulated calcium load characterized by Ca²⁺ store depletion and thereby increasing cytosolic free Ca²⁺. These data are confirmative of previously published work, in which TH-treatment induces Ca²⁺ store depletion in neuronal cells, thereby interfering with protein synthesis (Paschen et al., 1996). In addition, it was shown previously that Notch receptors require Ca²⁺ for proper protein folding in the ER (Aster et al., 1999) and that calcium imbalance within the cell can lead to protein misfolding and induction of the UPR (Ron and Walter, 2007). During UPR, three different signalling branches are activated with the sole aim to resolve ER stress or, if unable to achieve this goal, induce apoptosis. Given the global effect of *Serca2* conditional inactivation in reducing the cellularity of the BM, thymus and spleen and induction of apoptosis, we characterized expression of UPR-target and apoptosis-associated genes in lineage committed BM cells. *Serca2*-deficient cells showed up-regulation of the UPR effectors *ATF4*, *IRE1* and *Grp78* with a concomitant up-regulation of pro-apoptotic genes *Bad*, *Bax* and *Bim*. Therefore, we postulate that mature hematopoietic lineages cannot sufficiently resolve *Serca2*-ablation mediated ER stress and consequently undergo apoptosis supposedly via Bax and Bad. However, there are several means to study UPR activation in mammalian cells. In this work, we were limited in material sorted from the HSC compartment of chimeric mice, and therefore performed qRT-PCR for UPR genes. Western Blot analysis for cleaved caspase-3, caspase-9 or caspase-12 may shed light on downstream effects of *Serca2*-deficiency induced apoptosis in these mice. In addition, flow cytometric analysis for expression of pro- (*Bad*, *Bax*, *Bim*) and anti-apoptotic (*Bcl2*, *Bcl2l1*) proteins on peripheral T and B cell subsets would demonstrate a means to confirm our qRT-PCR data.

Given the dramatic effect of *Serca2* inactivation on mature hematopoietic lineages, we addressed the hypothesis whether HSCs would be equally affected. Upon analysis of the KLS compartment over a time course of 1 w, 4 w and 8 w post MxCre induction, relative and absolute numbers of KLS cells were significantly enriched. This was due to an accumulation of both MPP subsets, MPP2 (KLS, CD150⁺CD48⁺) and MPP3-MPP4 (KLS, CD150⁺CD48⁺), while the KLS, CD150⁺CD48⁺ fraction, enriched for LT-HSCs, was reduced.

In this thesis, *Serca2* was deleted in BM progenitors using MxCre recombinase, which is induced by INF α and INF β . INF α is a potent inducer of HSC mobilization, thereby regulating the cell cycle of these cells in order to induce proliferation (Essers et al., 2009). Therefore, we conducted

complementary studies in INF-responsive *MxCre* and INF-irresponsible *INFaR_KO* chimeras in order to delineate the effect of INF-induced stress in *Serca2*-deficient chimeras. We demonstrated that $\Delta MxCre$ (i) KLS cells are enriched due to (ii) accumulated MMP subsets but (iii) reduced HSC numbers 16h post last PIC administration. This effect was only transient as 1 w post last PIC injection HSCs and MPPs were back to homeostatic numbers. In contrast, PIC administration did not affect *INFaR_KO* HSCs confirming previously published data (Essers et al., 2009). Therefore, we propose that *Serca2*-deficient KLS and HSC subpopulations, analysed at 1 w post PIC administration, may have a cell intrinsic defect and cannot sufficiently cope with INF α -induced mobilization. This may explain the observation that *Serca2* ^{$\Delta MxCre$} KLS cells are enriched until up to 8 w post PIC administration.

In order to delineate the mechanisms by which HSC numbers are deregulated in absence of *Serca2*, we set out to perform functional *in vivo* and *in vitro* studies. Cell cycle analysis at 1 w post *Serca2* ablation revealed that the majority of HSCs and MPP cells resided in G₀ phase of the cell cycle, suggesting that these populations stop proliferating in response to *Serca2* inactivation. These data were confirmed by CFSE cell division tracking, as *Serca2* ^{$\Delta MxCre$} KLS cells displayed slower cycling kinetics compared to controls.

This also translated into impaired “fitness” during the CFU differentiation assay *in vitro*, in which *Serca2* ^{$\Delta MxCre$} KLS cells gave rise to significantly lower and smaller colonies compared to control. Whether *Serca2* ^{$\Delta MxCre$} KLS were still able to form colonies *in vitro* may be due to sort impurity and the potential outgrowth of CD45.1⁺ WT in the sorted cell population. In a future experiment, this potential contamination of host-derived WT cells, while sorting *Serca2* ^{$\Delta MxCre$} KLS cells, needs to be monitored by deletion PCR on DNA from input KLS cells and DNA derived from *Serca2* ^{$\Delta MxCre$} colonies.

Therefore, we conclude that *Serca2* conditional ablation in the BM does not majorly induce apoptosis in the KLS compartment; however apoptosis analysis of the subfractions within the KLS pool demonstrated that HSCs (KLS, CD150⁺CD48⁻) were more apoptotic compared to more differentiated MPP2s (KLS, CD150⁺CD48⁺) or MPP3-MPP4s (KLS, CD150⁻CD48⁺), which is confirmative of previously published work by John Dicks group. In addition, *Serca2* ablation resulted in a deregulation of the cell cycle and fitness of KLS cells. This raised the hypothesis if KLS cells may cope differently with ER stress induced by *Serca2* ablation than MPPs or mature lineages. Human HSCs have previously been studied in the context of ER stress (van Galen et al., 2014). In this study, TH- or tunicamycin-treated human HSC and progenitor cells (HSPC; Lin⁻CD34⁺CD38⁻CD59⁺CD117⁺) have been assessed for UPR activation upon ER stress compared to hematopoietic progenitors (Lin⁻CD34⁺CD38⁺CD59⁺CD117⁺). Interestingly, hHPSCs activate the PERK branch of the UPR and are prone to ER-stress-induced apoptosis, while progenitors can

cope with this stress and are resistant to apoptosis. Therefore, John Dick *et al.* postulate that hHSCs protect themselves and their progeny from potential stress-induced accumulation of mutations by choosing apoptosis over propagation. Our apoptosis analysis on overall KLS, further subfractionated into HSCs, MPP2 and MPP3-MPP4 cells are confirmative of this study, as *Serca2*-deficient HSCs were more apoptotic compared to control, while MPPs were resistant to apoptotic cues.

We set out to study ER stress in our chimeras and discovered that *Serca2*^{ΔMxCre} KLS did not majorly up-regulate genes of the UPR or pro-apoptotic genes in response to *Serca2* ablation. This is in contrast to the work by John Dicks laboratory and may be due to the fact that we studied the mixed pool of KLS cells compared to lineage committed mature (Lin⁺) cells. The hHPSCs studied were compared to progenitors, which correspond to the KLSCD150-CD48⁺ pool of HSCs and MPP1 cells compared to MPP2 cells (KLS, CD150⁺CD48⁺) in the mouse. We did, however, not include the markers CD150, CD48, CD34 to enrich for the rare and pure LT-HSCs and cannot state, at the molecular level, whether true HSCs are less resistant to *Serca2*^{ΔMxCre}-induced ER stress compared to MPPs in general. Experimentally, it will be challenging to purify the HSC and MPP subpopulations for downstream qRT-PCR analysis, as the HSC containing KLSCD150-CD48⁺ fraction is severely reduced in absence of *Serca2*. Therefore, we cannot truly compare our experimental system with the one studied by Van Galen *et al.* and it is difficult to draw concrete conclusions. In order to so, *Serca2*^{ΔMxCre} HSCs and different MPP subsets within the KLS pool need to be sorted and analysed for UPR target gene expression using single cell PCR technology. Nevertheless, our work demonstrates that HSCs are more prone to ER-stress induced apoptosis, while MPPs are more resistant; but the overall KLS cells preferentially reside in a somewhat “frozen” state, in which they exist the cell cycle.

In summary, *Serca2* conditional ablation severely affects hematopoiesis by driving mature lineages into apoptosis through activation of the UPR, while KLS cells are not overly apoptotic but show a deregulated cell cycle and impaired “fitness”. Therefore, we question targeting *Serca2* as potential treatment of T-ALL in patients as *Serca2* inhibition will cause dramatic side effects on normal hematopoietic cells and will not specifically target T-ALL cells, as previously postulated (Roti *et al.*, 2013).

6.3 Thapsigargin treatment mimics *Serca2* LOF *in vitro*

The chemical compounds CPA and TH, targeting *Serca* ATPases, were identified as putative Notch inhibitors by Rajwinder Lehal and Roti *et al.* (Lehal, 2011; Roti *et al.*, 2013). TH treatment of Notch-driven T-ALL cell lines negatively affected their proliferation, induced apoptosis and

led to a deregulation of the cell cycle *in vitro*, while TH *in vivo* marginally but significantly slowed down T-ALL in Xenograft models. Therefore, TH treatment was postulated as novel therapeutic approach to dampen oncogenic Notch1 in T-ALL through modulation of Ca²⁺ levels by Serca2 inhibition (Roti et al., 2013). However, this work did not address potential function of Serca2 regulating hematopoiesis. We therefore investigated the effect of conditional Serca2 inactivation in the BM and demonstrated that (i) mature hematopoietic lineages are apoptotic in response to Serca2 LOF, while (ii) KLS cells accumulate and (iii) LT-HSCs and the most HSC-like MMP1 subset are severely reduced, leading to a concomitant increase in other further differentiated MPP cells.

Being clinically more relevant, we set out to study the effect of TH on BM progenitor cells *in vitro*. Upon enrichment of Lin⁻ cells from BM of WT animals and treatment over a time course over 1, 6, 24 and 40 h, we observed a strong reduction in proliferation of the overall mixed cell population (Lin⁻ and Lin⁺ fractions) in response to TH.

Calcium imbalance in the cell and chemical blockage of Serca pumps was shown to induce accumulation of unfolded proteins in the ER, consequently leading to induction of chaperone/stress proteins in an effort to increase the impaired folding capacity. In case of “unresolved” ER stress the cell however decides to undergo apoptosis (Kim et al., 2008). Therefore, we hypothesized TH-mediated Serca inhibition may induce apoptosis in these cells and assessed their viability at the indicated time points of treatment. Lineage committed cells were highly apoptotic with increasing treatment duration, while KLS cells were viable at all assessed time points. This suggests, that similar to the results achieved in *Serca2*^{ΔMxCre} chimeras, mature lineages are more sensitive to calcium imbalance-induced ER stress and induction of apoptosis. Interestingly, upon TH-treatment, KLS cells were significantly enriched *in vitro*. As early as 6 h post treatment, KLS cells accumulated and were maximal enriched at 40 h post treatment. We reasoned that this may be due to enhanced proliferation of KLS cells. Upon cell cycle analysis, however, TH-treatment caused a predominant block of KLS cells in G₀ phase of the cell cycle. Within the KLS pool, there are quiescent HSCs (>70% in G₀ phase) and the different MPP subsets (<10% in G₀ phase) (Wilson et al., 2008). It would be interesting to include the cell surface markers CD34, CD48 and CD150 in our analysis in order to characterize whether Serca inhibition predominantly enriches for the rare dormant HSC (KLSCD34-CD150-CD48⁺) or whether HSCs and MPPs are equally affected upon TH treatment *in vitro*.

These data indicate that Serca inhibition *in vitro*, renders lineage committed cells more sensitive to TH-induced ER stress and induction of apoptosis than KLS cells. This may be an adaptive response of KLS cells to cope with this intrinsic stress signals, in order to protect their genetic information from mutations, which would consequently be passed on to their progeny. However,

long-term reconstitutive potential of MPPs is limited and if HSCs within the KLS pool rapidly undergo apoptosis upon TH treatment, then MPPs cannot account for multilineage differentiation over unlimited time. These results demonstrate that low doses of TH in the nanomolar range (200 nM) significantly affect total MACS enriched Lin⁻ BM cells *in vitro* by (i) inducing apoptosis in the overall population, while (ii) inducing an enrichment of KLS cells, that (iii) primarily reside in G₀ phase of the cell cycle, when treated for 6 h or longer.

These observations closely mimic *Serca2* conditional inactivation in the BM as described during this work. However, TH is a non-competitive ATPase inhibitor blocking the function of all *Serca* family members. In order to confirm *Serca2* specificity in these *in vitro* studies, it would be worth targeting WT BM progenitors for CRISPR- mediated *Serca2* KD.

However, comparison of genetic *Serca2* LOF studies in *Serca2*^{AMxCre} chimeras with TH studies performed *in vitro* strongly suggests that the effect is *Serca2*-specific. In addition, it is tempting to hypothesize whether other ER stress-inducing agents may induce similar downstream effects in BM progenitors as TH.

In conclusion, we demonstrate that TH treatment induces apoptosis in the overall MACS enriched Lin⁻ population, while leading to a deregulated cell cycle of KLS cells. Therefore, treatment of N1-induced T-ALL with TH may result in severe side effects and needs to be carefully monitored and controlled. Taken together, we question the applicability of *Serca2* inhibition as treatment regimen to fight Notch1-activated T-ALL.

7 Material and Methods

7.1 Mouse Work

7.1.1 Experimental Mice

Multiple genetically modified mouse strains were used in this work. *RosaNotch1C* (RNIC) mice were generated by L.C. Murtaugh and kindly provided by Prof. D. Melton, Harvard University, MA. These mice harbor the intracellular domain of the mouse Notch1 receptor lacking the PEST domain (NICD aa 1749-2293), which is preceded by a stop cassette flanked by loxP sites. This allows the over-expression of NICD from the Rosa26 locus upon activation of Cre recombinase. NICD is fused to an internal ribosomal entry site (IRES) and the enhanced green fluorescent protein (eGFP). Therefore, detection of eGFP expressing cells can be used as an indirect means of monitoring NICD expression. In this work, RNIC mice were crossed onto the *Chd7^{lox/lox}* background in combination with either the Mx1Cre (Kuhn et al., 1995) or the LckCre (Orban et al., 1992) deleter strain. Experimental animals were heterozygous for the RNIC locus and homozygous for the *Chd7* locus.

Chd7^{lox/lox} mice (Hurd et al., 2010) were kindly provided by Prof. D.M. Martin, University of Michigan, MI. In these mice, the ATG-containing exon 2 of *Chd7* is flanked by loxP sites, allowing the excision of the translation initiation site upon Cre recombinase activation, which results in a *Chd7 null* allele. In this study *Chd7^{lox/lox}* mice were intercrossed with the Mx1Cre as well as with the CD4Cre transgenic mice to obtain *Chd7^{lox/lox} ± Mx1Cre* or *Chd7^{lox/lox} ± CD4Cre* experimental mice.

Serca2^{lox/lox} mice (Andersson et al., 2009) were kindly provided by Prof. Christensen, University of Oslo, Norway. In these mice, the ATG-containing exon 2 and exon 3 of *Serca2* are flanked by loxP sites, hence resulting in a *Serca2 null* allele upon Cre recombinase activation. *Serca2^{lox/lox}* mice were bred onto the MxCre background in order to generate *Serca2^{lox/+} ± MxCre* as well as *Serca2^{lox/lox} ± MxCre* experimental mice.

Animal husbandry and experimental procedures were conducted according to Swiss national guidelines under the licence 1099.5. Animals were kept in individual cages at $23 \pm 1^\circ\text{C}$ with a 12 h light/dark cycle in the EPFL animal facility. Food and water were supplied *ad libitum*.

For genotyping of transgenic animals a standard PCR program of denaturation for 5 min at 95° , * cycles of: 95°C for 30 s, annealing at # $^\circ\text{C}$ for 30 s, extension at 72°C for 30 s, and a final

extension at 72°C for 5 min was followed. Gene specific primers and PCR conditions for the above mentioned transgenic animals are depicted in Table Appendices 1.

Efficient Cre recombinase activation and hence generation of either *Chd7* or *Serca2 null* allele was confirmed by deletion PCR, for which primer sequences and conditions are depicted in Table Appendices 2.

7.1.2 Poly(I)-poly(C): Preparation and Administration

The double-stranded RNA analogue polyinosinic:polycytidylic acid (Poly(I)-poly(C); Invivogen, Toulouse, France) was administered *in vivo* in order to activate the interferon-inducible Mx1Cre recombinase. Therefore, Poly(I)-poly(C) was dissolved in physiological water at a concentration of 2 mg/ml for 10 min at 65°C followed by cooling down to RT to enable annealing single stranded RNA molecules. Poly(I)-poly(C) stock was further diluted in sterile PBS to a final concentration of 0.2 mg/ml. Five Poly(I)-poly(C) injections of 2 µg/g body weight were administered intraperitoneally (i.p.) at 2-day intervals.

7.1.3 5-FU: Preparation and Administration

The pyrimidine analogue 5-fluorouracil (5-FU, Invitrogen, CA, USA) was administered in order to deplete all cycling cells within the BM, stimulating HSC proliferation. A 5-FU stock concentration of 15 mg/ml was prepared in sterile PBS for 10 min at 65°C. 150 mg/kg body weight was administered i.p. 3 days prior to HSC isolation.

7.1.4 Generation of Single Cell Suspensions from Isolated Organs

Experimental mice were sacrificed under carbon dioxide conditions. Single BM cell suspensions were prepared from 2 femurs and 2 tibiae per mouse by crushing bones in ice-cold staining medium (SM; HBSS containing 2% fetal calf serum (FCS), 12.5 mM HEPES and 2mM EDTA) using a pestle and mortar. Cell suspensions from other organs such as spleen, thymus and lymph nodes were prepared by disaggregating the appropriate tissues using a nylon mesh in cold SM. Filtration through a 70 µm filter removed debris as well as non-dissociated fat or conjunctive tissue.

7.1.5 Generation of Bone Marrow Chimeras

7.1.5.1 Preparation of T cell Depleted Bone Marrow Cells for Transplantation (ATBM)

Femurs and tibiae of 3 donor mice were pooled per experimental group and BM cell suspensions were prepared in SM as previously described. Cells were counted and pelleted by centrifugation at 1700 rpm for 10 min at 4°C. Cells were then resuspended at a concentration of 1×10^6 cells/ml and incubated with anti-Thy 1.2 mAb (clone AT83; rat IgG) at a 1:20 dilution for 30 min on ice. Rabbit complement was added at a 1:40 dilution and cells were incubated for an additional 60 min at 37°C. One hundred μ l DNase (0.01% w/v) was added per 10 ml cell suspension and cells were mixed gently every 10 min in order to prevent clumping. Cells were then filtered through a 70 μ m filter and washed three times with excessive volumes of SM to remove residual traces of antibody and complement. T-cell depleted BM was counted and resuspended in sterile PBS at a concentration of $5-10 \times 10^6$ cells/100 μ l and subsequently injected retro-orbitally. Input BM was assessed for contribution of HSCs by flow cytometric analysis and genomic DNA from BM samples was prepared to monitor for unspecific activation of Mx1Cre.

7.1.5.2 Treatment of Recipient Mice prior to ATBM

Two days prior to ATBM, recipient C57BL6/J_CD45.1 mice were each injected with 100 μ g purified anti-NK1.1 mAb (clone PK1.36) to deplete radio-resistant host-derived NK cells. One day prior to ATBM, mice were lethally irradiated using a split dose of 2 x 450 Gy.

7.1.5.3 Treatment of Chimeric Mice post ATBM

Upon ATBM, reconstituted mice were kept on drinking water containing antibiotics (3 ml Baytril/250 ml) and painkiller (Dafalgan 500 mg/250 ml). Donor reconstitution was monitored by flow cytometric analysis of peripheral blood lymphocytes (PBL) 4 weeks post transplantation.

7.1.6 Isolation of Peripheral Blood Lymphocytes (PBL)

Fifty μ l total blood was collected from the retro-orbital vein of anaesthetised mice using haematocrit capillaries. Blood samples were incubated in 3 ml erythrocyte lysis buffer for 10 min at RT to lyse erythrocytes. Samples were then centrifuged and washed twice in cold SM prior to cell surface staining.

7.1.7 White Blood Cell Count

White blood cell counts were determined from cell suspensions diluted 1:30 in SM using the automated ViCell Cell Counter (Beckman Coulter).

7.2 Flow Cytometry Analysis

7.2.1 Cell Surface Staining

For flow cytometric analysis, cells were stained with specific antibodies prepared in Fc blocking staining buffer containing the clone 2.4G2. Following incubation on ice, cells were washed in SM and resuspended in 100-500 μ l SM (depending on cell concentration) for further analysis. Fluorophore-conjugated monoclonal antibodies were purchased from eBiosciences (San Diego, CA) and are listed in Table 3 (Appendix). Biotin-conjugated antibodies were purified from hybridoma supernatants and produced in house following standard laboratory techniques.

7.2.2 Cell Sorting

Fluorescence activated cell sorting (FACS) was performed on either a FACS Aria II (BD Biosciences) at the EPFL or UNIL Flow Cytometry Core Facility or on a MoFlo Astrios^{EQ} (Beckman Coulter Life Sciences) at the CHUV site of the UNIL Core Facility. Cell sorting was performed under sterile conditions at 4°C and cells were collected in pure FCS for further analysis.

7.2.3 Automated Cell Sorting using Magnetic Beads (AutoMACS)

AutoMACS technology was used in order to enrich for lineage negative cells using the Lineage Cell Depletion Kit (Miltenyi Biotec, Germany). Volumes are indicated for 1×10^7 cells. In brief, BM cells were resuspended in 20 μ l SM followed by addition of 5 μ l biotin-conjugated antibody following incubation for 20 min at 4°C. Fifteen μ l SM and 10 μ l anti-biotin Microbeads were added to each sample for a further 30 min incubation. Following washing in SM, cells were filtered through a 30 μ m nylon mesh and pelleted at 1700 rpm for 10 min. Cells were then resuspended in 1-2 ml SM for magnetic bead separation on an AutoMacs Pro Separator (Miltenyi Biotec, Germany). Enrichment of lineage negative cells was assessed by flow cytometric analysis of labelled cells pre- and post-AutoMACS.

7.2.4 Cell Cycle Analysis (Ki67 vs. Hoechst)

Cell cycle status was assessed by intracellular staining of the nuclear cell proliferation-associated antigen, Ki67, and the DNA-intercalating agent, Hoechst. Ki67 was detected using FITC mouse anti-human Ki-67 set (BD Pharmingen™). Volumes are indicated per 5×10^5 cells. Following cell surface staining, cells were washed in SM and then permeabilized and fixed in 100 μ l Cytofix/Cytoperm solution for 30 min on ice. Cells were then washed in 2 ml Permwash solution and pelleted at 1700 rpm for 5 min. FITC mouse anti-human Ki-67 antibody was diluted 1:10 in Permwash solution and intracellular staining was performed in 100 μ l per sample at 4°C overnight. The following day, cells were stained in 100 μ l Permwash containing 1:250 dilution of Hoechst 33342 for 10 min at 4°C. Cells were washed once in 1 ml Permwash, pelleted by centrifugation and then resuspended in SM for flow cytometric analysis.

7.2.5 CFSE Cell Division Assay

The CFSE cell division assay enables monitoring of individual cell divisions over time. Bone marrow cells enriched for lineage negative cells were labelled with 1 μ M CFSE (Ebioscience) in PBS for 10 min at 37°C. CFSE signal was quenched twice by addition of 45 ml RPMI medium containing 10% FCS followed by centrifugation at 1700 rpm for 10 min at 4°C. Cells were then maintained in HSC culture medium (see 7.3.1) in 5% CO₂ at 37°C and flow cytometric analysis was performed each day over a period of 5 days.

7.2.6 Apoptosis Analysis (Annexin V vs. 7-AAD or DAPI)

Apoptosis analysis was performed by staining cells with Annexin V-Cy5, followed by the DNA intercalating fluorescent dyes 7-aminoactinomycin D (7-AAD) or 4',6-diamidino-2-phenylindole (DAPI). Cells were washed twice in PBS and incubated with anti-Annexin V-Cy5 antibody (Biolegend) diluted 1:100 and 7-AAD diluted 1:20 in Annexin V binding buffer for 15 min on ice. Annexin V binding buffer was added to a final volume of 500 μ l shortly before acquisition on the flow cytometer. 7-AAD was replaced by DAPI at a dilution of 1:50 in staining combinations that exceeded 9 colours.

7.2.7 Calcium Flux Assay

Indo1-AM is a cell permeable ratiometric Ca²⁺ indicator used to monitor changes in intracellular calcium levels. Following cell surface staining, cells were incubated with 1 μ M Indo1-AM (Molecular Probes, Invitrogen) in cell loading medium (CLM; HBSS, 2mM MgCl₂, 2mM CaCl₂) for 30 min at 37°C in the dark. Following washing in SM, cells were resuspended in CLM and kept on

ice. Cell suspensions were incubated at 37°C shortly before and during flow cytometric analysis and the ratio of Indo-violet against Indo-blue was acquired at a 70° angle over time. After 30-60 s of acquisition 10 µl ionomycin (1 mg/ml) was added per 500 µl cells to induce calcium flux. 2 mM EGTA was added to the cells 5 min before acquisition to bind all free extracellular calcium present in the CLM allowing to measure intracellular calcium levels. The addition of 2 mM EGTA with the cell permeable form EGTA-AM (Molecular Probes, Invitrogen) served as negative control to bind both extra- as well as intracellular free Ca²⁺.

7.3 Cell Culture/*In vitro* Experiments

7.3.1 Culture of Lineage Negative Bone Marrow Cells

Lineage depleted cells were cultured at 1-2 * 10⁶ cells per well of a 24 well plate in Iscove's medium supplemented with 20% FCS, 25 mM Hepes, β-mercaptoethanol (ME), 2 mM glutamine, 1 mM non-essential amino acids, 1 mM sodium pyruvate, 100 ng/ml Flt3 ligand, 10 ng/ml IL1, 6 ng/ml IL3 and 100 ng/ml stem cell factor hereafter, referred to as HSC culture medium.

7.3.2 Retroviral Infection of Bone Marrow Cells

In this work, lineage depleted BM cells were infected with the MigR1-NICD-IRES-NGFR expression vector, which allows expression of NICD fused to IRES followed by the Nerve Growth Factor Receptor (NGFR) encoding cDNA. Therefore, detection of NGFR expressing cells can be used as an indirect means of monitoring NICD expression. In brief, 1-2 * 10⁵ BM cells were transferred into a 5 ml round-bottom tube; viral particles were added to achieve a final multiplicity of infection (MOI) of 10 and infection was performed during spin oculation at 1700 rpm at 42°C for 45 min. Cells were then resuspended in HSC culture medium and maintained at 5% CO₂ at 37°C for 48 h prior to transplantation.

7.3.3 Thapsigargin Treatment

The ATPase inhibitor Thapsigargin (Enzo Lifesciences) was dissolved at a stock concentration of 1 mM in DMSO and stored in aliquots at -20°C. Lineage depleted BM cells were treated with a final concentration of 200 nM or 1 µM Thapsigargin for 1, 6, 24 and 40 h. DMSO treatment served as internal control.

7.3.4 Colony Forming Unit (CFU) Assay

The colony forming unit (CFU) assay enables measurement of HSC differentiation potential under *in vitro* conditions. In brief, 500-700 sorted KLS cells were resuspended in 100 μ l Iscove's Modified Dulbecco's Medium supplemented with 20% FCS and Gentamycin. 1 ml of MethoCult GF M3434 methylcellulose based medium, supplemented with cytokines and erythropoietin (Stemcell Technologies) was added and the sample vigorously mixed. Cells, suspended in methylcellulose, were seeded into a 6-well dish using a 16 gauge-blunt ended needle. Six-well dishes were then placed in 10 cm dishes, which contained one open 6-well dish with sterile water. Following incubation at 5% CO₂ at 37°C for one week, colonies were scored under the microscope using a 60 mm gridded scoring dish (Stemcell Technologies).

7.3.5 Culture of murine and human T-ALL cells

Murine T-ALL cell lines established from primary Notch1-induced tumors were cultured in RPMI containing 10% FCS, 12.5 mM HEPES, Gentamycin (1/1000 dilution) and 2 mM ME. Human T-ALL cell lines were cultured in the same medium in absence of ME.

7.3.6 Lentiviral Infection of T-ALL cell lines

Murine and human T-ALL cell lines were infected with viral particles encoding either non-inducible pLKO.1 small hairpin RNA (shRNA) or inducible pTripz shRNA targeting CHD7 mRNA for degradation. The clones pLKO.1_shCHD7 (RHS3979-958410) and Tripz_shCHD7 (RHS4696-99634943) were purchased from Open Biosystems. Control vectors pLKO.1_shCtrl (Sigma, SHC002) and pTripz_shCtrl (RHS4743) encoding scrambled hairpin sequences were used as internal controls for off-target effects of lentiviral insertion into the genome. Lentiviral infection of cells was performed by spin oculation as previously described (see 7.3.2). Infected cells were selected and maintained *in vitro* in the presence of 2 μ g/ml puromycin (pLKO.1 expressing cells) or 0.5 μ g/ml puromycin (pTripz expressing cells) for at least 1 week prior to experimentation. pTripz_shRNA vector expression was induced by addition of 1 mg/ml Doxycyclin resulting in concomitant expression of red fluorescent protein (RFP).

7.4 Molecular Biology Techniques

7.4.1 DNA Preparation from Cells and Tissues

Five to 10 * 10⁶ cells were resuspended in 200 μ l extraction buffer DNA A (10 mM Tris-HCl, 10 mM EDTA, 10 mM NaCl, pH 7.5) and 200 μ l DNA B (DNA A containing 2% SDS). Two μ l

proteinase K (15 mg/ml in Tris-HCl, pH 7.6) was added and samples were incubated at 500 rpm overnight at 56°C. The following day, 100 µl 8 M potassium acetate (KOAc) and 500 µl chloroform were added sequentially and samples were then vortexed for 2 min at RT. Following phase separation via centrifugation at 13000 rpm for 10 min at RT, the upper phase, containing DNA, was transferred into a fresh tube and precipitated in 800 µl 100% ethanol (EtOH). DNA pellets were then washed in 800 µl 75% EtOH and resuspended in 50-100 µl TE buffer (10 mM Tris, 1 mM EDTA, pH 8.0) for 20 min at 37°C.

7.4.2 RNA Isolation from Cells and Tissues

Five to 10×10^6 cells were washed in 1 x PBS, pelleted by centrifugation at 1700 rpm at 4°C and resuspended in 50 µl 1 x PBS before careful addition of 1 ml PeqGOLD TriFast (PeqLab, VWR) per sample. Samples were kept at RT for 5 min to allow dissociation of nucleotide complexes and then stored at -80°C until further processing. Two hundred µl chloroform was added to each sample and then mixed by inversion. Following phase separation via centrifugation at 13000 rpm for 15 min at 4°C, the upper phase containing RNA was transferred into a fresh tube. Each RNA sample was precipitated with 1 ml ice-cold 100% isopropanol and 1 µl of glycerol (1 mg/ml, Invitrogen) overnight at -20°C. RNA samples were centrifuged at 13000 rpm for 15 min at 4°C and washed twice in ice-cold 80% EtOH. RNA pellets were then air-dried for 10 min at RT and dissolved in 10-20 µl RNase-free water for 10 min at 55°C.

7.4.3 Reverse Transcription

During reverse transcription the RNA-dependent DNA polymerase, Reverse Transcriptase transcribes single-stranded RNA into complementary double-stranded DNA called cDNA. In this work, cDNA was generated using the SuperScript II reverse transcriptase (Life Technologies) and random hexamer primers to guarantee reverse transcription from randomized starting points in the RNA molecule. In brief, a maximum of 2 µg total RNA was transcribed per single reaction. RNA was heated to 65°C for 5 min in presence of 10 mM dNTPs and 250 ng random primers. Following cooling at 4°C, 2 µl of 0.1 mM DTT, 4 µl of 5 x First-Strand buffer and 1 µl RNase-free H₂O were added per reaction mix and incubated for 2 min at 25°C. One µl of SuperScript II reverse transcriptase was added per reaction and reverse transcription was performed for 10 min at 25°C followed by incubation for 50 min at 42°C and then for 15 min at 70°C. cDNA was stored at -20°C until further analysis.

7.4.4 Quantitative Real Time RT-PCR

During quantitative Real-Time PCR (qRT-PCR), fluorescent reporter molecules are incorporated into newly generated DNA strands. This allows monitoring of the amplification of PCR products during each cycle in real time. Power SYBR Green Master mix (Life Technologies) was used to amplify 5-10 ng total cDNA in a reaction mix of 10 μ l. Initial denaturation was performed for 10 min at 95°C followed by 40 cycles of each 15 s denaturation at 95°C and a 1 min annealing/extension step at 60°C. Melting curve analysis was included in the qRT-PCR run in order to monitor for specific amplification of the gene of interest. Relative expression of the gene of interest was normalized against the expression of the housekeeping gene HPRT. The $\Delta\Delta$ Ct method was used to compare relative gene expression levels between two different groups, e.g. WT versus cKO. Primer sequences for the housekeeping gene hypoxanthine-guanine phosphoribosyltransferase (HPRT) are the following: Fwd: 5'- GTT GGA TAC AGG CCA GAC TTT GTT G-3' and Rev: 5'- GAT TCA ACT TGC GCT CAT CTT AGG C-3'. Gene-specific qRT-PCR primers used in this work are shown in Tables 4-9 in Appendices.

7.5 Protein Methods

7.5.1 Preparation of Whole Cell Extracts

Following washing in cold 1 x PBS, cells were supplemented with 100 μ l RIPA buffer (150 mM NaCl, 0.1% SDS, 0.5% sodium deoxycholate, 1% NP40, 50 mM Tris, pH 8) containing protease inhibitors (Roche) and incubated on ice for 30 min. Samples were then centrifuged at 13000 rpm for 30 min at 4°C and supernatant containing extracted protein was transferred into a fresh tube on ice. Protein extracts were stored at -80°C until further analysis.

7.5.2 Preparation of Nuclear Extracts

Preparation of nuclear protein extracts was performed according to the protocol provided by PhD Amandine Hurbin (INSERM U823, France). In brief, cell pellet were resuspended in hypotonic extraction buffer (10 mM Tris-HCl, pH 7.5, 10 mM KCl, 1.5 mM MgCl₂, 0.2 mM DTT) supplemented with protease inhibitors and incubated for 30 min on ice. Following centrifugation at 2000 rpm for 5 min at 4°C, the supernatant was carefully discarded and each cell pellet was resuspended in hypotonic extraction buffer containing 1% NP40 and protease inhibitors. Following incubation for 10 min on ice, cells were centrifuged at 3000 rpm for 15 min at 4°C and washed once in ice-cold 1 x PBS. Nuclear proteins were extracted in RIPA buffer by sonication at 200 W followed by centrifugation at 13000 rpm for 15 min at 4°C. Protein extracts

were stored at -80°C until further analysis. Protein concentration was measured using the Bradford Assay on an Ultraspec 3000 spectrophotometer (GE Healthcare)

7.5.3 SDS-Polyacrylamide Gel Electrophoresis & Western Blot Analysis

Protein samples were resuspended in 5 x SDS loading buffer (0.25% Bromophenol blue, 0.5 M DTT, 50% glycerol, 10% SDS, 0.25 M Tris-HCl) and incubated for 5 min at 95°C for denaturation. Samples were then loaded on a SDS gel comprised of an upper 5% stacking gel and a lower 6% separation gel (Table 10 in Appendix) and gel electrophoresis was performed in Tris glycine buffer (25 mM Tris base, 190 mM glycine, 0.1% SDS) for 1 h at 200 V at 4°C.

Separated proteins were transferred onto the methanol-activated PVDF membrane in transfer buffer containing 48 mM Tris, 39 mM glycine, 0.04% SDS and 20% fresh methanol at 25 V overnight at 4°C. Membranes were blocked in 5% non-fat milk solution prepared in TBS buffer containing 2% Tween-20 (TBS-T) for 1 h at RT. Membranes were incubated with primary antibodies (1:2000 dilution) at 4°C overnight and with corresponding horseradish peroxidase (HRP)-conjugated secondary antibodies (1:5000 dilution) for 1 h at RT. Antibody incubation was separated by 3 washes in TBS-T for 10 min.

Murine Chd7 protein was detected using the rabbit polyclonal anti-Chd7 antibody (ab31824, Abcam), which binds to residues 2950 within the C-terminus of the protein. Human CHD7 protein was detected using the rabbit polyclonal anti-CHD7 antibody from Bethyl laboratories (A301-223A). Tata-box binding protein (TBP; ab51841, Abcam) was used as loading control for nuclear extracts. Immunoblots were exposed using ECL western blotting substrate (Thermo Scientific) and X ray films (Kodak).

Appendices

Microarray Validation *RNIC*⁺/ Δ LckCre late-stage versus *RNIC*⁺/ Δ MxCre early-stage T-ALL – Up-regulated Candidate Genes

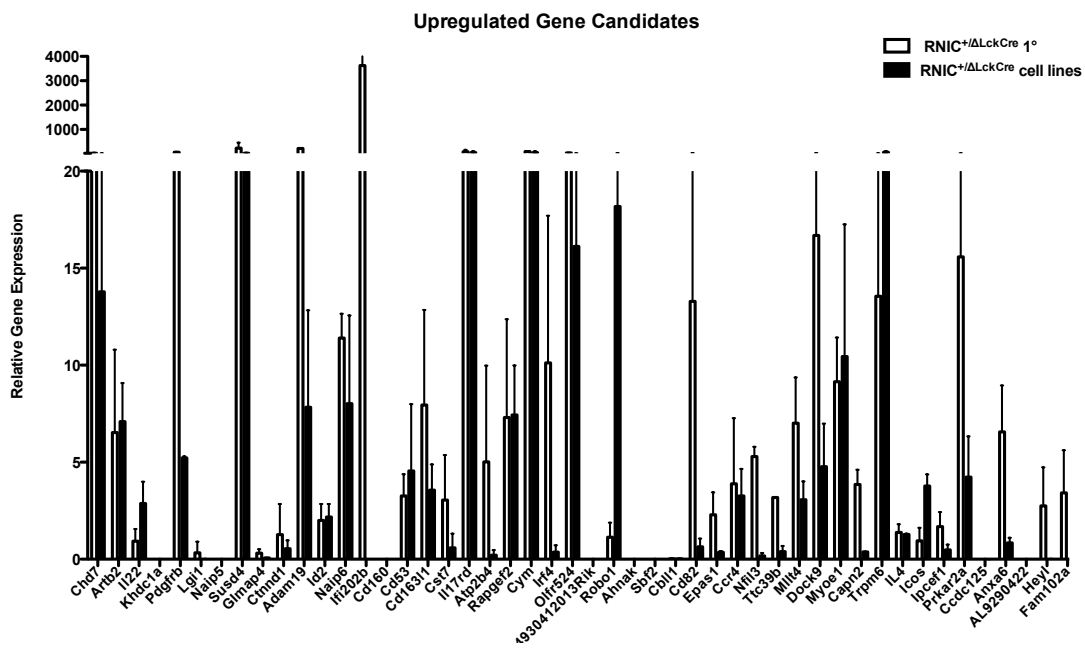


Figure Appendix 1: Top Up-regulated Gene Candidates Validated.

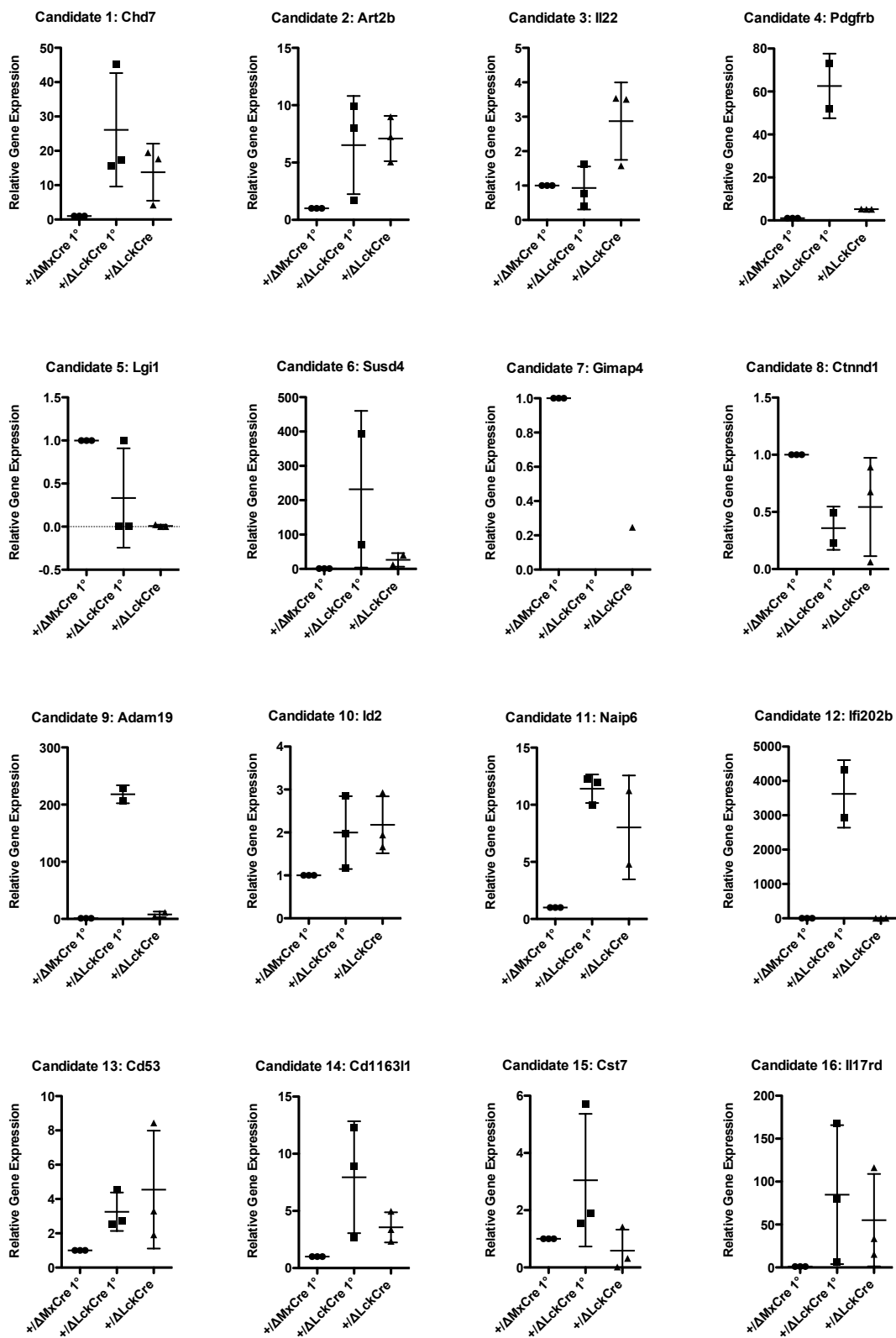


Figure Appendix 2: qRT-PCR Validation Of Top Up-regulated Gene Candidates 1-16.

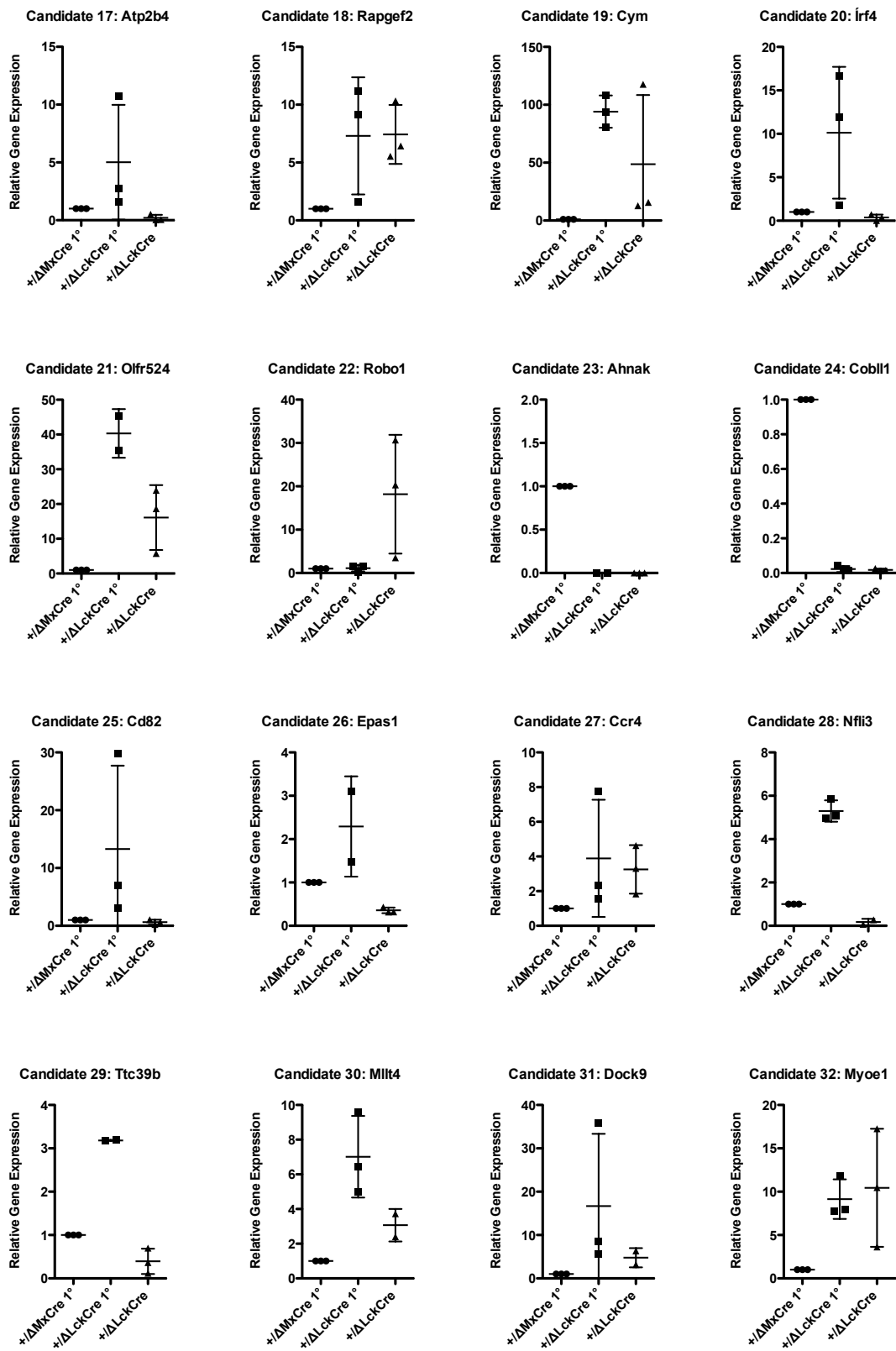


Figure Appendix 3: qRT-PCR Validation Of Top Up-regulated Gene Candidates 17-32.

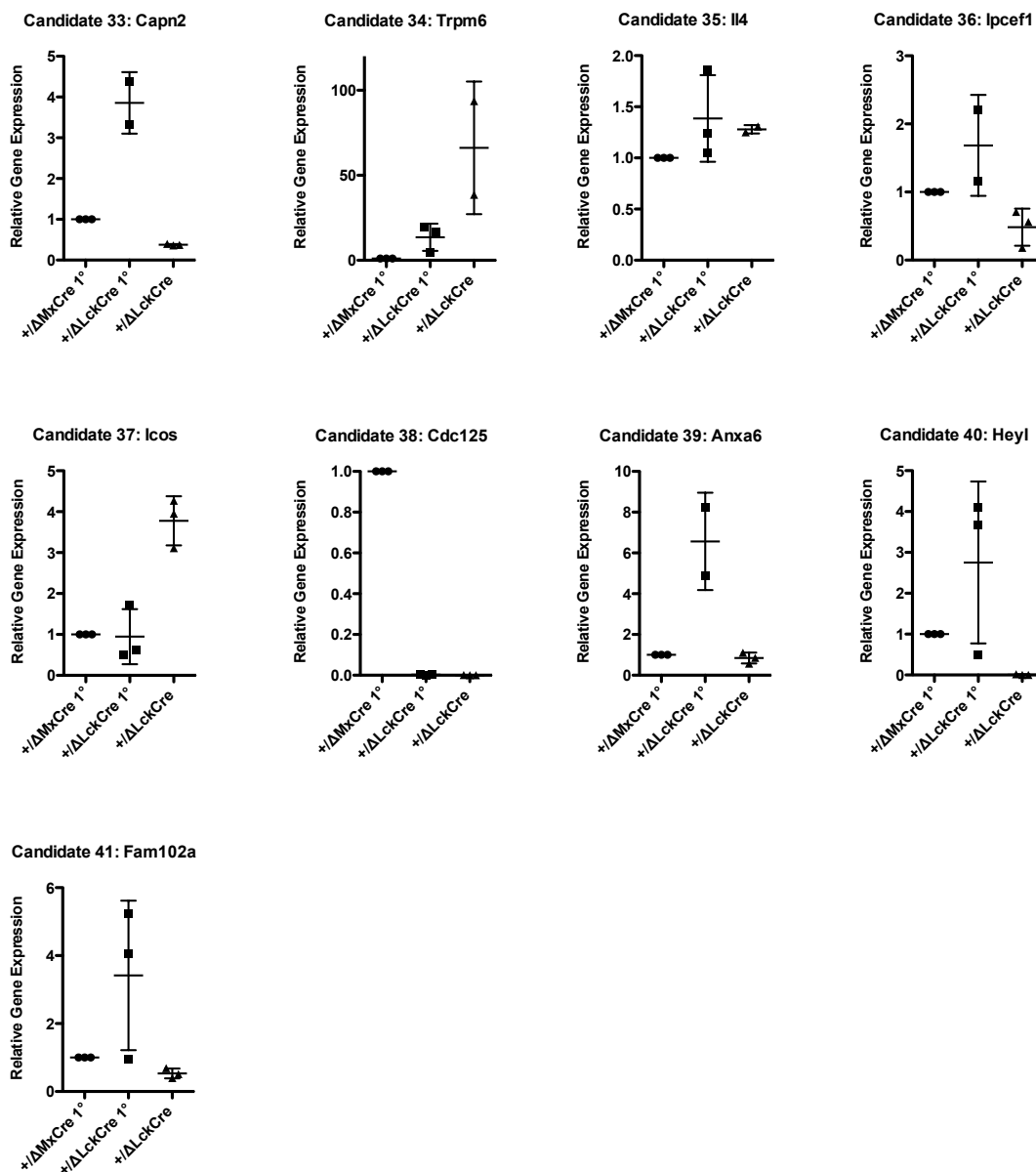


Figure Appendix 4: qRT-PCR Validation Of Top Up-regulated Gene Candidates 33-41.

Microarray Validation *RNIC*⁺/ Δ LckCre late-stage versus *RNIC*⁺/ Δ MxCre early-stage T-ALL - Down-regulated Candidate Genes

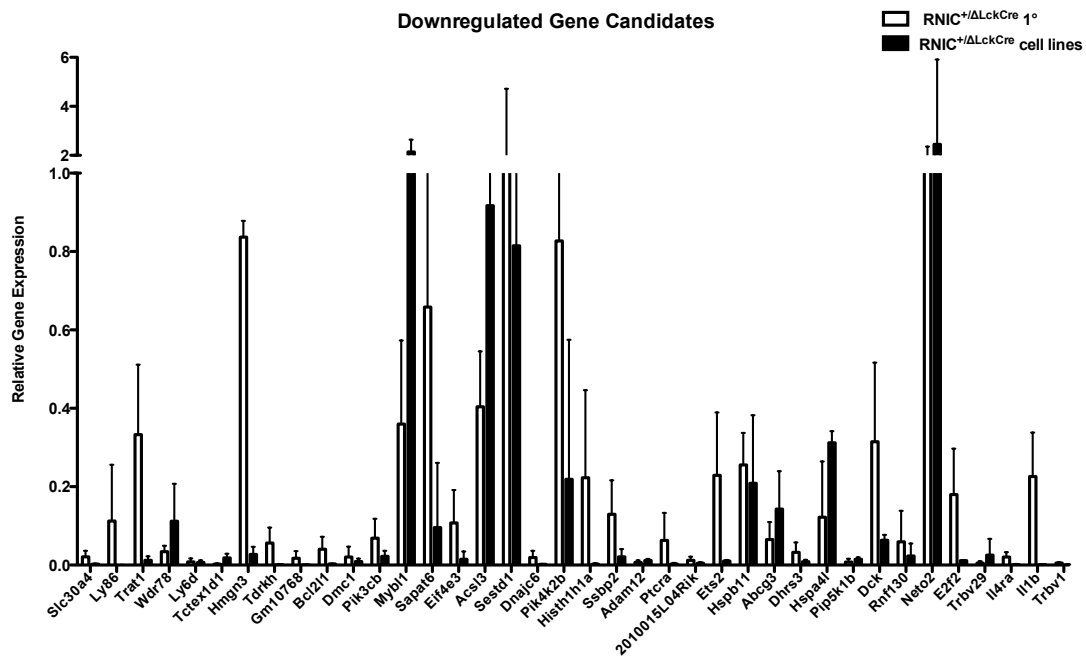


Figure Appendix 5: Top Down-regulated Gene Candidates Validated.

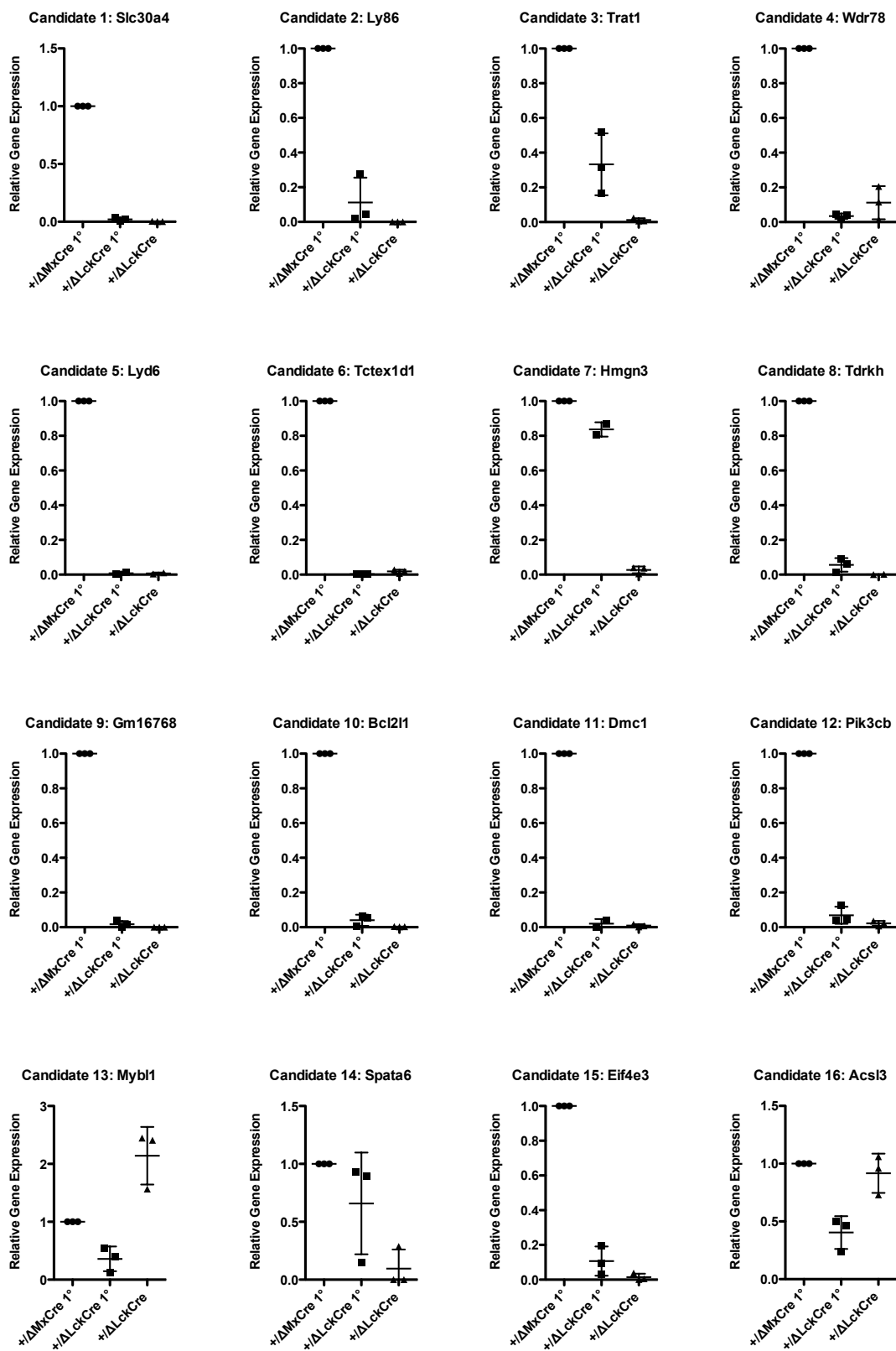


Figure Appendix 6: qRT-PCR Validation Of Top Down-regulated Gene Candidates 1-16.

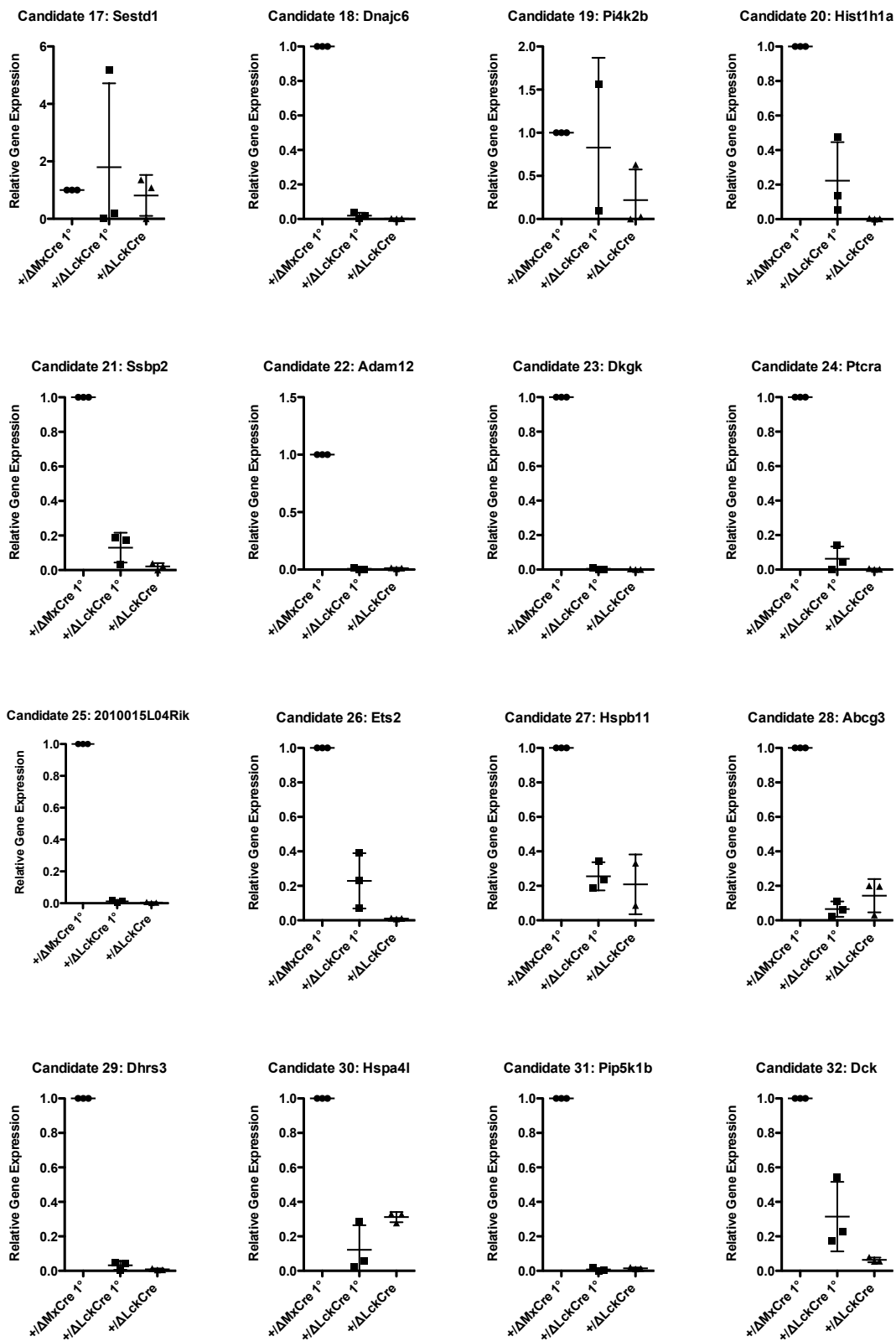


Figure Appendix 7: qRT-PCR Validation Of Top Down-regulated Gene Candidates 17-32.

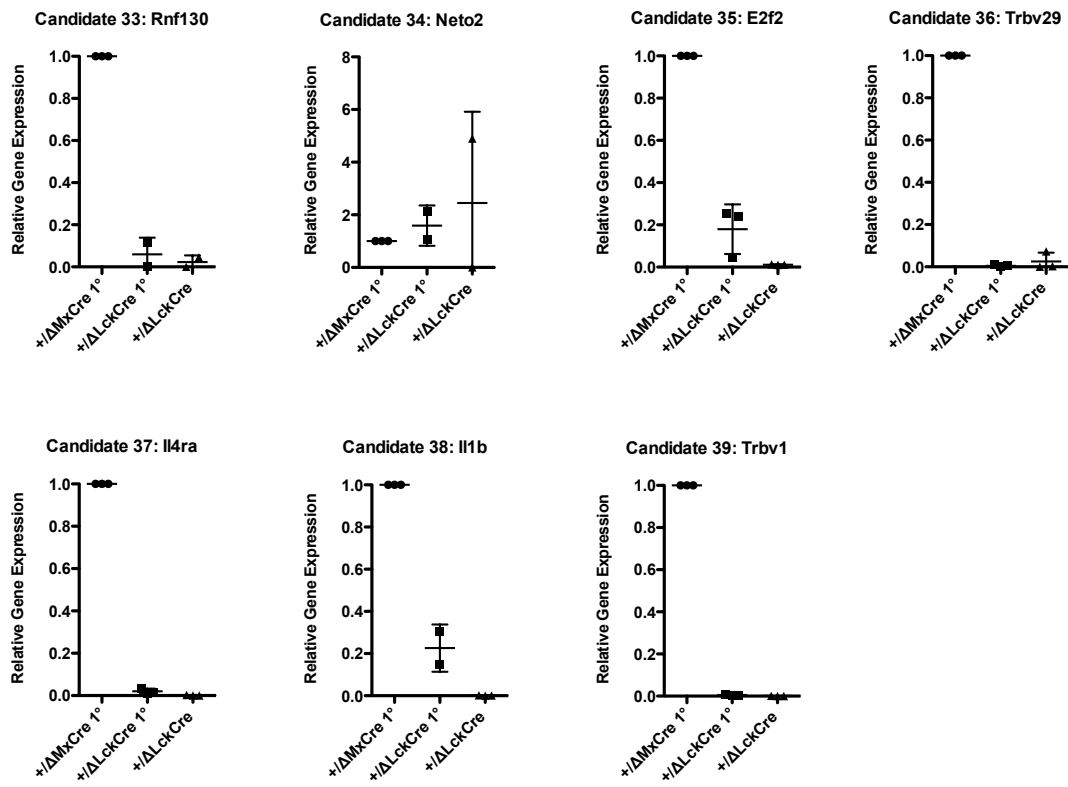


Figure Appendix 8: qRT-PCR Validation Of Top Down-regulated Gene Candidates 33-39.

7.6 Functional Characterization of Loss of one *Serca2* Allele in the Hematopoietic System

Since *Serca2* was proposed to be a therapeutic target in Notch-driven T-ALL (Roti et al., 2013), we set out to study the physiological role of *Serca2* in the hematopoietic system via conditional deletion in the MxCre background. In *Serca2* cKO mice, the translational start site containing exon 2 as well as exon 3 are flanked by loxP sites, resulting in a *Serca2 null* allele upon Cre recombinase activation following administration of PIC (Figure 58 A).

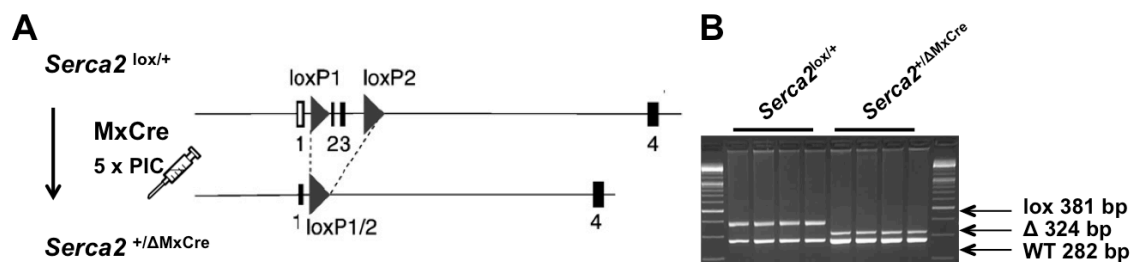


Figure 58: Strategy for *in vivo* conditional inactivation of *Serca2* in the BM. A, Schematic representation of the genetically modified murine *Serca2* locus, in which the ATG-encoding exon 2 and exon 3 are flanked by loxP sites. Activation of the efficient BM-deleter strain MxCre recombinase by administration of PIC leads to the generation of a *Serca2 null* allele in BM cells. B, Deletion PCR analysis demonstrating a 381 bp lox band, a 324 bp deletion band and a 282 bp WT band amplified from genomic DNA isolated from *Serca2*^{lox/+} or *Serca2*^{+/ Δ MxCre} BM cells.

Efficient (> 90%) conditional *Serca2* deletion was confirmed by PCR analysis: MxCre-mediated excision of exon 2 and 3 out of the murine *Serca2* locus led to amplification of a 324 bp deletion band (Δ), whereas the genetically modified *Serca2*^{lox/lox} locus would yield in a 381 bp band (lox) and WT murine *Serca2* locus a smaller 282 bp amplicon (Figure 58 B).

7.6.1 *Serca2* Haploinsufficiency does not affect Hematopoiesis under Steady State Conditions

First, we investigated whether loss of a single allele of *Serca2* may affect hematopoiesis given its gene dosage effect in other diseases such as Darier's disease (Ji et al., 2000; Muller et al., 2006). *Serca2*^{+/ Δ MxCre} mice were generated by crossing the *Serca2*^{lox/lox} cKO strain (Andersson et al., 2009) with the MxCre Tg mice to study the effect of conditional loss of one *Serca2* allele on hematopoiesis. Experiments were performed in BM chimeras in order to specifically limit *Serca2* deletion to BM cells as MxCre is active within all INF α - and INF β -responsive cell types such as in the skin, liver and kidney, as well as the BM.

Upon analysis of the HSC compartment, no significant differences in (i) percentages (Figure 59 A) and absolute numbers of KLS, ST-HSC and LT-HSCs were found between *Serca2*-competent and *Serca2*-haploinsufficient cells (Figure 59 B).

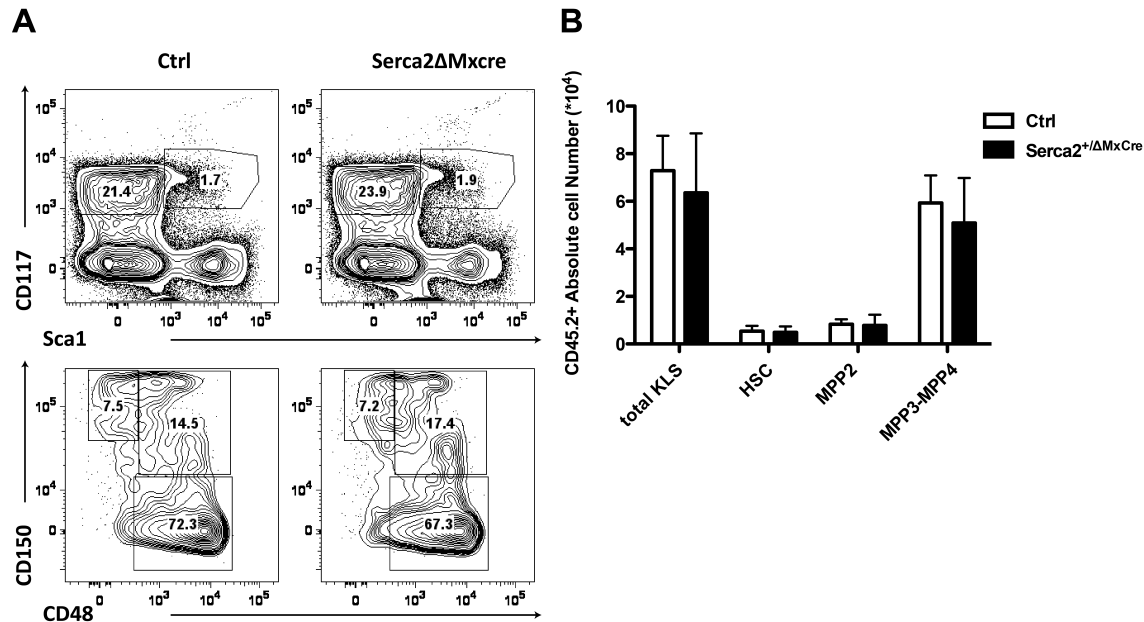


Figure 59: *Serca2* haploinsufficiency does not perturb hematopoietic development. KLS compartment of *Serca2* $^{+/\Delta}$ MxCre and *Serca2* $^{lox/+}$ (Ctrl) BM cells was analysed 5 weeks post MxCre induction. **A**, Representative FACS plots depicting staining of donor-derived CD45.2 $^{+}$ Lin $^{-}$ CD117 $^{+}$ Sca1 $^{+}$ (KLS) population, **upper panel**. This was further subfractionated into HSCs (KLS, CD150 $^{+}$ CD48 $^{-}$), MPP2s, (KLS, CD150 $^{+}$ CD48 $^{+}$) and MPP3-MPP4s (KLS, CD150 $^{-}$ CD48 $^{+}$), **lower panel**, in Ctrl and *Serca2* $^{+/\Delta}$ MxCre BM chimeras. **B**, Absolute cell numbers of CD45.2 $^{+}$ KLS cells, LT-HSCs, ST-HSCs and MPPs in *Serca2* $^{+/\Delta}$ MxCre and Ctrl BM chimeras (n= 5 + 5). Error bars represent mean \pm SD.

Furthermore, *Serca2* $^{+/\Delta}$ MxCre hematopoietic progenitors gave rise to normal numbers of T cell progenitors in double negative stages DN1-DN4 (Figure 60 A) as wells as immature CD4 $^{+}$ CD8 $^{+}$ DP, CD4 $^{+}$ and CD8 $^{+}$ SP cells (Figure 60 B) and TCR $\gamma\delta$ T cells (Figure 60 C), indicating that *Serca2* haploinsufficiency does not recapitulate the *N1* LOF function phenotype in T lineage commitment.

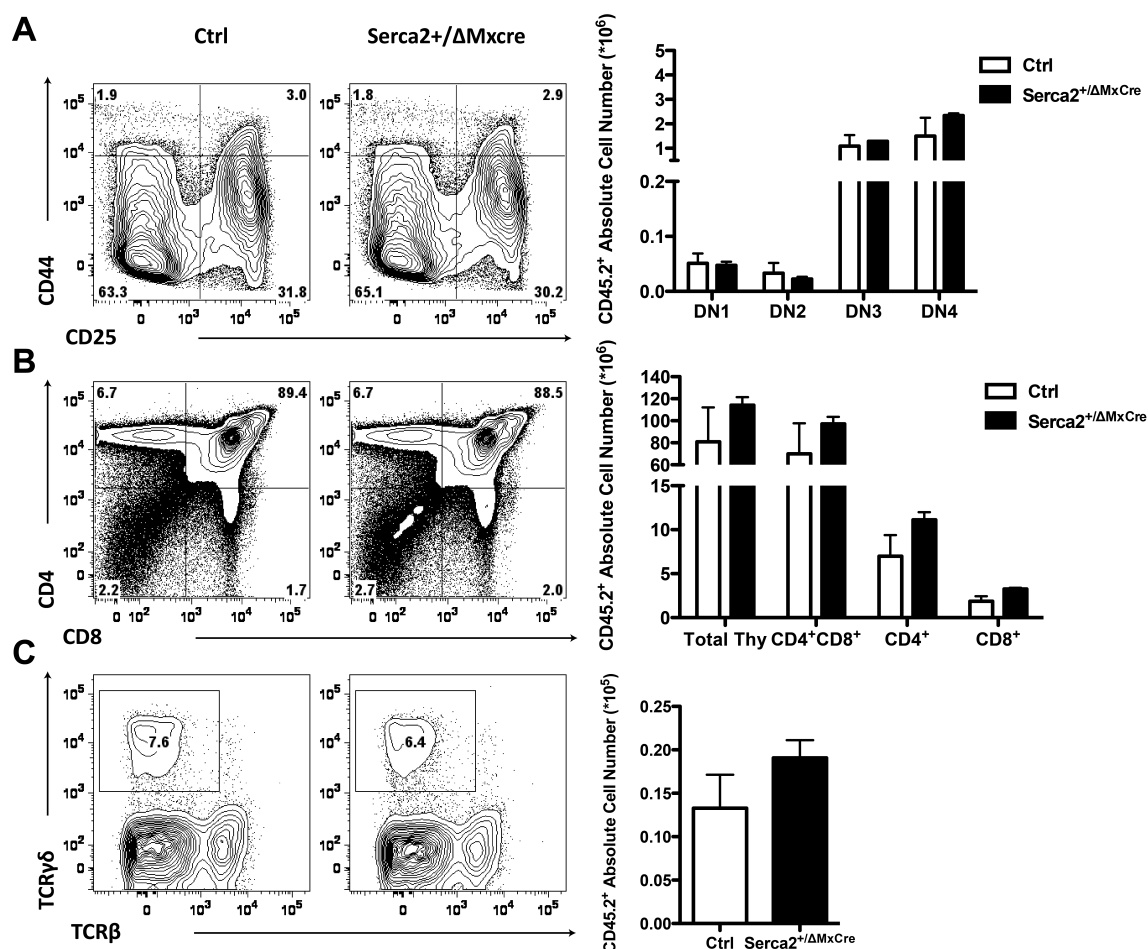


Figure 60: *Serca2* haploinsufficiency does not affect T cell development in the thymus. Thymi of *Serca2*^{+/ΔMxCre} and *Serca2*^{lox/+} (Ctrl) chimeric mice were analysed 5 weeks post MxCre induction. **A**, Representative FACS analysis of Ctrl and *Serca2*^{+/ΔMxCre} CD4-CD8-Lin- thymocytes stained with anti-CD25 and anti-CD44 to distinguish DN1 (CD44⁺CD25⁻), DN2, (CD44⁺CD25⁺), DN3 (CD44⁻CD25⁺) and DN4 (CD44⁻CD25⁻) stages of maturation and **left panel** corresponding absolute cell numbers, **right panel**. **B**, Representative FACS analysis showing cell surface expression of CD4 and CD8 in thymi of Ctrl and *Serca2*^{+/ΔMxCre} chimeric mice and **left panel** corresponding absolute cell numbers, **right panel**. **C**, Representative FACS plots showing cell surface expression of TCRγδ and TCRβ, on CD4-CD8⁻ thymocytes, **left panel** and corresponding absolute cell numbers, **right panel**. Error bars represent mean ± SD, n = 5 (Ctrl) and n = 5 (*Serca2*^{+/ΔMxCre}).

Percentages (Figure 61 A) and absolute numbers (Figure 61 B) of mature peripheral B220⁺IgM⁺ B cells were also unaffected by *Serca2* deficiency in these chimeras (n = 5 + 5).

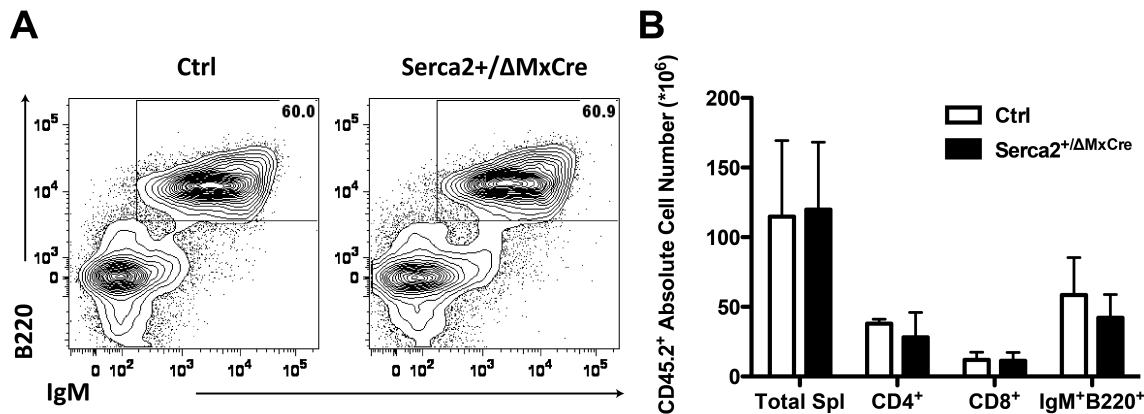


Figure 61: *Serca2* haploinsufficiency does not affect B or T cell numbers in the periphery. *Serca2*^{+/ΔMxCre} and *Serca2*^{lox/+} (Ctrl) spleens from chimeric mice were analysed 5 weeks post MxCre induction. **A**, Representative FACS plots of Ctrl and *Serca2*^{+/ΔMxCre} mature B220⁺IgM⁺ B cells. **B**, Absolute cell numbers of total splenic cellularity, mature T cells (TCRb⁺, CD4⁺, CD8⁺) and mature B cells (B220⁺IgM⁺) in the spleens of Ctrl (n = 5) and *Serca2*^{+/ΔMxCre} (n=5) mice. Error bars represent mean ± SD.

In summary, *Serca2* haploinsufficiency does not impact on the hematopoietic system under steady state conditions.

7.6.2 *Serca2* Haploinsufficiency does not affect Hematopoiesis under Stress

7.6.2.1 *Serca2* Haploinsufficiency does not render Hematopoietic Stem Cells more susceptible to 5-FU-mediated Exhaustion

Hematopoietic stem cells possess the capacity to self-renew but also to maintain homeostasis via differentiation in order to replenish the pool of mature hematopoietic cell types in response to injury. The chemotherapeutic agent 5-FU depletes all cycling cells, including hematopoietic cells, thereby stimulating HSC proliferation (Lerner and Harrison, 1990). Therefore, 5-FU is frequently administered to study HSC mobilization in response to stress *in vivo*. 5-FU was administered bi-weekly in *Serca2*-haploinsufficient and *Serca2*-competent chimeras over a period of 14 days. *Serca2*-haploinsufficient BM chimeras (n = 7) had a median survival of 12.5 days as compared to 13 days in Ctrl chimeras (n = 6) (Figure 62 A). This demonstrates that *Serca2* haploinsufficiency does not confer any survival advantage to HSCs following 5-FU challenge. In response to 5-FU treatment, total BM cellularity (Figure 62 B) and the percentage of mobilized donor-derived CD45.2⁺Lin⁻CD117⁻Sca1⁺ HSCs (Figure 62 C) in *Serca2*-haploinsufficient (n = 3) and Ctrl (n = 3) chimeras were comparable.

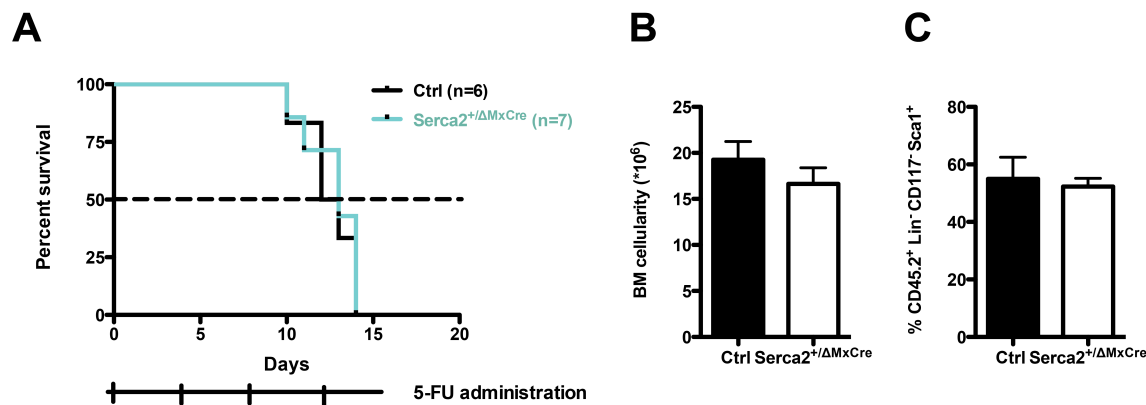


Figure 62: *Serca2* haploinsufficiency does not render hematopoietic stem cells more susceptible to exhaustion. Four weeks post MxCre induction *Serca2*^{lox/+} (Ctrl) and *Serca2*^{+/-ΔMxCre} mice were treated with 5-FU twice per week over 14 days. **A**, Kaplan-Meier survival curve of 5-FU treated BM chimeras with *Serca2*^{+/-ΔMxCre} (n = 7) mice depicted in blue and Ctrl (n = 6) mice depicted in black. Arrows indicate 5-FU injections. Median survival was calculated using Log-rank Mantel-Cox test. **B**, Absolute number of total BM cells and **C**, Percentage of HSCs (KLS; Lin⁻CD117⁺Sca1⁺) from control and indicated cKO mice. Error bars represent mean ± SD.

Taken together, these data indicate that *Serca2* haploinsufficiency does not render HSCs more susceptible to exhaustion upon 5-FU mediated stress.

7.6.2.2 *Serca2* Haploinsufficiency does not render Hematopoietic Stem Cells less competent in Secondary Bone Marrow Chimeras

We demonstrated that *Serca2*-haploinsufficient HSCs retain their full reconstitutive potential and that mature lineages are also unaffected by haploinsufficiency of *Serca2* under steady state conditions (Figures 59-61). However, these conditions and the 5-FU challenging system do not address whether long-term reconstitution of the hematopoietic system may be affected by the loss of one *Serca2* allele. To address this question, secondary BM chimeras were generated by serially transplanting BM pooled from similarly reconstituted *Serca2*^{+/-ΔMxCre} (n = 3) and Ctrl (n = 3) chimeras into lethally irradiated CD45.1⁺ recipient mice (Figure 63 A). Reconstitution by donor-derived CD45.2⁺ HSCs was comparable between *Serca2*-competent and *Serca2*-haploinsufficient secondary chimeras (Figure 63 B). (i) total BM cellularity (Figure 63 C), (ii) percentages and (iii) absolute cell numbers of KLS (Figure 63 D, E) and HSCs, MPP2 and MPP3-MPP4 cells (Figure 63 F, G) were also not significantly altered by *Serca2* haploinsufficiency.

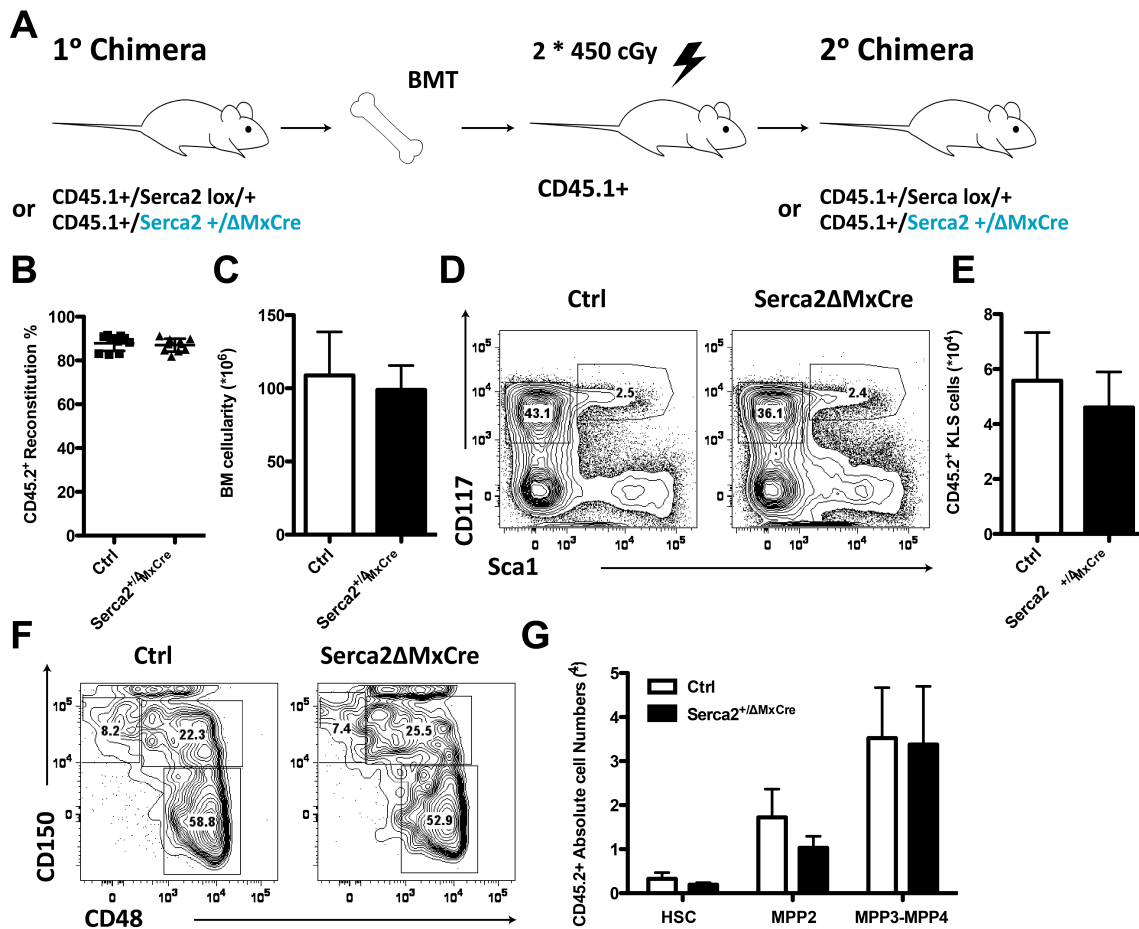


Figure 63: Serca2 haploinsufficiency does not alter the long-term repopulation capacity of HSCs in secondary BM chimeras. **A**, Schematic representation of the generation of *Serca2*^{+/ΔMxCre} and *Serca2*^{lox/+} (Ctrl) secondary BM chimeras. **B**, Relative percentage of CD45.2⁺ cells in PBLs 4 weeks post ATBM. **C**, Total BM cellularity in secondary chimeras. **D**, Representative FACS plots of Ctrl and *Serca2*^{+/ΔMxCre} KLS cells with corresponding absolute cell numbers depicted (**E**). **F**, Representative FACS counter plots of Ctrl and *Serca2*^{+/ΔMxCre} HSCs (CD150⁺CD48⁻), MPP2 (CD150⁺CD48⁺) and MPP3-MPP4 cells (CD150⁻CD48⁺) with absolute cell numbers depicted in **G**. *Serca2*^{+/ΔMxCre} (n = 5) and Ctrl (n = 5) BM cells were analysed 10 weeks post MxCre induction. Error bars represent mean ± SD.

In addition, we addressed whether *Serca2* haploinsufficiency under conditions of stress may mimic *Notch1* LOF in the thymus. Overall, (i) total thymic cellularity (Figure 64 B) and (ii) the absolute numbers of immature DN and DP thymocytes (Figure 64 A, B), mature CD4⁺ and CD8⁺ SPs (Figure 64 C) and intra-thymic B cells were comparable between the serially transplanted cohorts (n = 5 + 5).

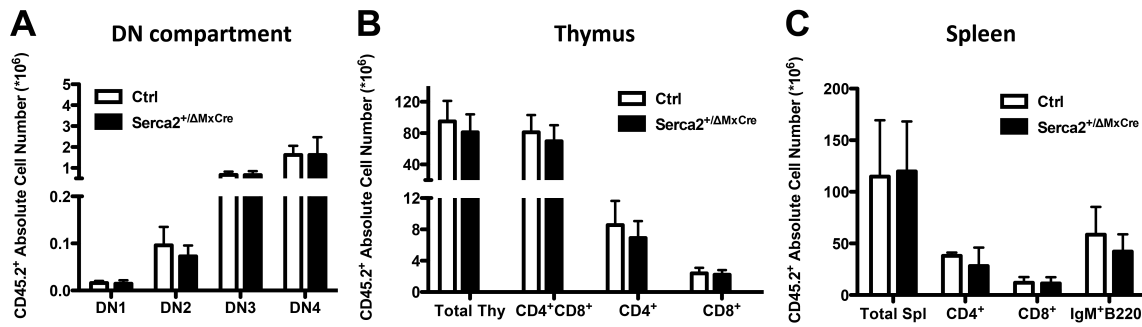


Figure 64: *Serca2* haploinsufficiency does not affect peripheral T or B cell numbers in secondary BM chimeras. Secondary BM chimeras were analysed 10 weeks post MxCre induction. **A**, Absolute cell numbers for DN1, DN2, DN3 and DN4 thymic progenitor cells. **B**, Total thymic cellularity and absolute cell numbers of immature CD4⁺CD8⁺ DP, CD4⁺ and CD8⁺ SP T cells. **C**, Total splenic cellularity and absolute cell numbers of mature CD4⁺ and CD8⁺ T cells and IgM⁺B220⁺ B cells. Error bars represent mean ± SD, n = 5 (Ctrl) and n = 5 (*Serca2*^{+/ΔMxCre}).

Overall, *Serca2* haploinsufficiency did not impact on hematopoiesis under stress conditions in the serial transplantation setting.

7.6.2.3 *Serca2* Haploinsufficiency does not impact on HSC function in 3:1 competitive BM Chimeras

In order to assess the long-term repopulation capacity of *Serca2*-haploinsufficient HSCs under stress conditions, competitive mixed BM chimeras were generated by mixing either CD45.2⁺ *Serca2*^{+/ΔMxCre} or *Serca2*^{lox/+} (Ctrl) with CD45.1⁺ WT C57BL6/J BM cells in a 3:1 ratio, followed by transplantation into lethally irradiated CD45.1⁺ recipients (Figure 65 A). The 3:1 ratio of *Serca2*-competent or *Serca2*-haploinsufficient versus WT hematopoietic reconstitution was maintained long-term post transplantation (Figure 65 B) as indicated by the persistence of CD45.2⁺ cells in PBL of chimeric mice.

When analysing *Serca2*^{+/ΔMxCre} competitive BM chimeras, we first focussed on the HSC compartment. Overall, the total BM cellularity of *Serca2*-competent and *Serca2*-haploinsufficient mixed BM chimeras was comparable (Ctrl = $152.3 \pm 8.70 \times 10^6$ cells; *Chd7*^{ΔMxCre} = $162.9 \pm 5.13 \times 10^6$ cells, 65 C). Similarly, the percentages and absolute numbers of KLS (Lin⁻CD117⁺Sca1⁺) remained comparable between these cohorts (65 D). Subfractionation of the KLS compartment into HSCs (CD150⁺CD48⁻), MPP2 (CD150⁺CD48⁺) and MPP3-MPP4 cells (CD150⁻CD48⁺) also demonstrated no apparent effect of *Serca2* haploinsufficiency on these subpopulations of the stem cell pool (65 E).

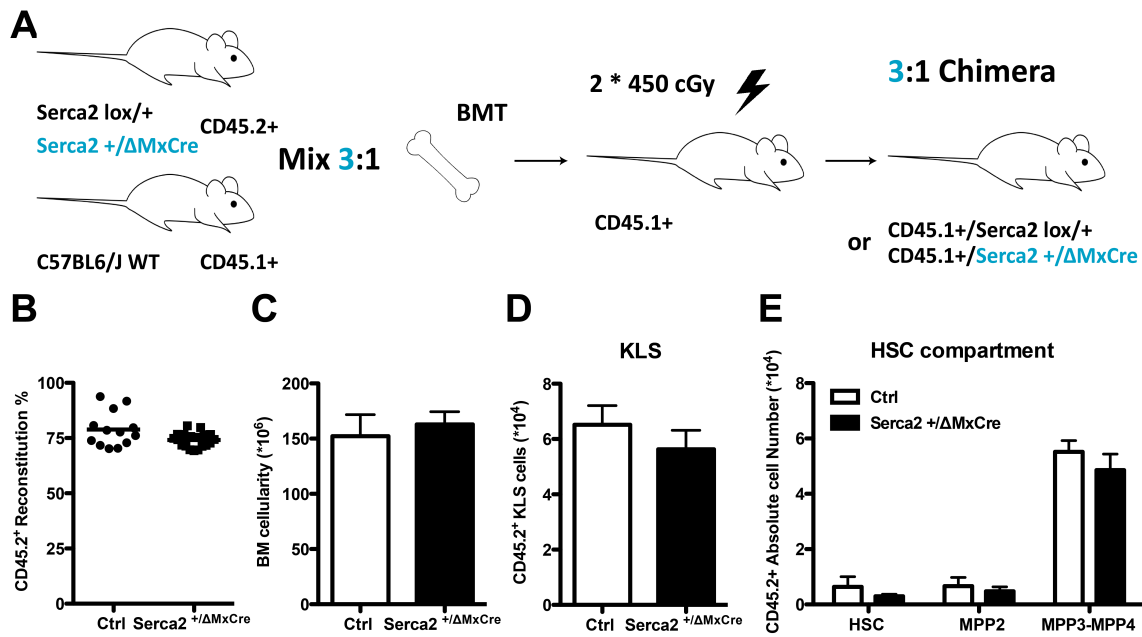


Figure 65: *Serca2* haploinsufficiency does not alter the long-term repopulation capacity of HSCs in 3:1 competitive BM chimeras. **A**, Schematic representation of the generation of *Serca2*^{+/ Δ MxCre} and *Serca2*^{lox/+} (Ctrl) 3:1 competitive BM chimeras. **B**, Percentage CD45.2⁺ reconstitution in PBLs 4 weeks post ATBM. **C**, Total BM cellularity of 3:1 mixed BM chimeras. **D**, Absolute cell numbers of Ctrl and *Serca2*^{+/ Δ MxCre} CD45.2⁺ KLS cells. **E**, Absolute numbers of Ctrl and *Serca2*^{+/ Δ MxCre} HSCs (KLSCD150+CD48⁻), MPP2 (KLSCD150+CD48⁺) and MPP3-MPP4 (KLSCD150-CD48⁺) cells. *Serca2*^{+/ Δ MxCre} (n = 5) and Ctrl (n = 5) BM cells were analysed 10 weeks post MxCre induction. Error bars represent mean \pm SD.

In addition, we addressed whether *Serca2* haploinsufficiency under conditions of stress may mimic *Notch1* LOF in the thymus. Overall, (i) total thymic cellularity (Figure 66 B) and (ii) the absolute numbers of immature DN and DP thymocytes (Figure 66 A, B), mature CD4⁺ and CD8⁺ SPs (Figure 66 C) and intra-thymic B cells were comparable between the serially transplanted cohorts (n = 5 + 5).

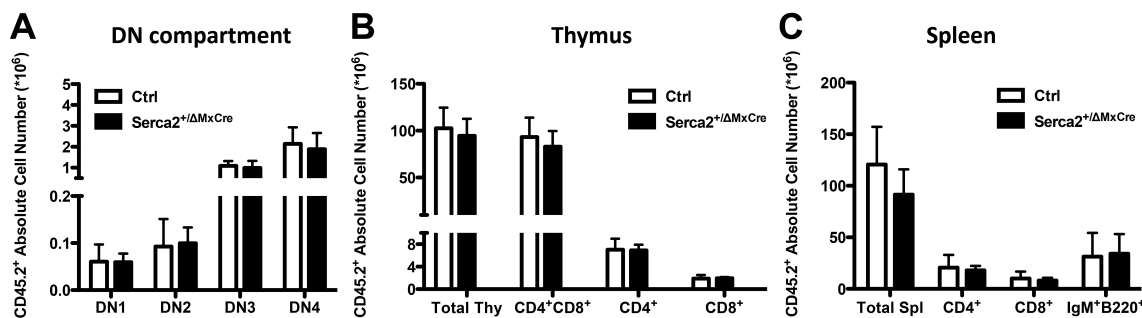


Figure 66: *Serca2* haploinsufficiency does not affect peripheral T or B cell numbers in 3:1 mixed BM chimeras. Competitive BM chimeras were analysed 10 weeks post MxCre induction. **A**, Absolute cell numbers for DN1, DN2, DN3 and DN4 thymocytes. **B**, Total thymic cellularity and absolute cell numbers of immature CD4⁺CD8⁺ DP, mature CD4⁺ and CD8⁺ SP T cells. **C**, Total splenic cellularity and absolute cell numbers of mature CD4⁺ and CD8⁺ T cells and IgM⁺B220⁺ B cells. Error bars represent mean \pm SD, n = 5 (Ctrl : CD45.1⁺) and n = 5 (*Serca2*^{+/ Δ MxCre} : CD45.1⁺).

In summary, these data indicate that *Serca2* haploinsufficiency does not affect the long-term repopulation of HSCs in 3:1 competitive BM chimeras. Therefore, we can rule out a gene dosage effect of *Serca2* in the regulation of hematopoiesis under steady state and under conditions of stress. Overall, these results collectively indicate that *Serca2* haploinsufficiency in the BM does not lead to any overt phenotype, not under physiological, nor under stress conditions.

Tables of Primer Sequences, Antibodies & PCR conditions

Table Appendix 1: Genotyping Primers And PCR Conditions For Experimental Animals.

Gene/ Transgene	Primer sequences [5´-3´]	PCR conditions	Expected PCR product
Cre Recombinase	Fwd: CTA GAG CCT GTT TTG CAC GTT C Rev: GTT CGC AAG AAC CTG ATG GAC A	17.5 mM MgCl ₂ ; #60°C; *30 cycles	Tg+: 339 bp
RosaNICD	Fwd: AAA GTC GCT CTG AGT TGT TAT Rev-Neo: GCG AAG AGT TTG TCC TCA ACC Rev: GGA GCG GGA GAA ATG GAT ATG	17.5 mM MgCl ₂ ; #60°C; *35 cycles; DMSO 1/10	WT: 600 bp Tg+: 200 bp
Chd7	P458: ATT TTT CTG AAT GCA TCT TCA CCT P459: AGGCAAAGCCTTTCCTT CA	17.5 mM MgCl ₂ ; #56°C; *35 cycles	WT: 568 bp Lox: 306 bp
Serca2	OL86 Fwd: TCT TCA TAA CAC ACG CCA ATT T OL87 Rev: CCC TTT GCT GCC AAT TAA CTA TT	17.5 mM MgCl ₂ ; #56°C; *35 cycles	Lox: 381 bp WT: 282 bp

Table Appendix 2: Deletion PCR Primers And PCR Conditions For Experimental Animals.

Gene/ Transgene	Primer sequences [5´-3´]	PCR conditions	Expected PCR product
Chd7	P152: CAG CAG CCA TCT TTC CAG CAG TTG P434: GTT CCC ACT TCC TGT TGC TCA CC P435: GCC CAG AGC CAT GAG TGA GTG AAA T	15 mM MgCl ₂ ; #58°C; *38 cycles	WT: 1249 bp Lox: 987 bp Δ: 324 bp
Serca2	OL86 Fwd: TCT TCA TAA CAC ACG CCA ATT T OL88 Fwd: ACC TCT AGG GGT CTC GAA TCA OL87 Rev: CCC TTT GCT GCC AAT TAA CTA TT	17.5 mM MgCl ₂ ; #56°C; *35 cycles	Lox: 381 bp Δ: 324 bp WT: 282 bp

Table Appendix 3: Monoclonal Antibodies Used For Flow Cytometric Analysis.

Antibody	Clone	Conjugate
AnnexinV		Cy5
B220	RA3-6B2	FITC, PECy7, PE-TexasRED, Alexa700
CD4	GK1.5	FITC, PE, PECy7, Alexa700
CD8	α-subunit; YTS 168.4 or 53-6.7	FITC, PECy5, Alexa700, Alexa647
CD11b/Mac1	M1/70	FITC, PECy5, Alexa700
CD16/32	93	PE, PECy7
CD21	eBio8D9	FITC
CD23	B3B4	PE
CD25/IL2Rα	PC61.5	PacificBlue, APCeF780
CD34	RAM34	FITC, eF660/APC
CD44/Pgp1	IM7	PE
CD45.1/Ly5.1	A20	APCeF780

CD45.2/Ly5.2	A104	PE, PacificBlue, BrilliantViolet650
CD48	HM48-1	PacificBlue, Biotin
CD71	R17217	PE
CD117/c-kit	2B8	APC, PECy7
CD135/Flt3	A2F10	PE
CD150	TC15-12F12.2	PECy5
Gr1/Ly6G	RB6-8C5	PECy7, Alexa647
IgM	II/41	APC
Sca1/Ly6A/E	D7	PE, PacificBlue, PECy7
Ki67		FITC, PE
TCR β	H57-597	APCeF780
TCR $\gamma\delta$	eBioGL3	PE
Ter119/Ly6		APCeF780

Table Appendix 4: qRT-PCR Primer Sequences Used For Microarray Validation.

Gene name	Forward primer [5' -3']	Reverse primer [5' -3']	Amplicon length
Robo1	CCA CGG CCA CTC TCA CCC CT	CTG CCG CCT CCT GTC TGG TG	107 bp
Dkge	TGG CTT ACT GGA AAT CGT TGG CGT	AAG TCA GCC GCA CTG TGT GCG	110 bp
Dgkg	CGC GCC ATG CTG ATG GGT GT	CGC ATG CTG CAT CAC CTC GC	150 bp
Il4	CCC CCA GCT AGT TGT CAT CCT GC	GTG CAT GGC GTC CCT TCT CCT G	132 bp
Pdgfrb	CCT GCA GAG ACC TCA AAA GTA GGT G	GCA GGC GCA GTG TGC TCA C	147 bp
Il22	TGC TCC CCC AGT CAG ACA GGT TC	GGT CGT CAC CGC TGA TGT GAC AGG A	105 bp
Trat1	CTG CAC AGG TAC CGG CTG AAG CT	TTT CCT GGG CCT TCT GCG TTT CC	83 bp
Adam19	CCC AGG GCA AGC GAA AGG TGA C	AGG TGG CGA TTC AAC GCG CA	104 bp
Art2b	ACC CAG CAG GTG ACT GGC CTT	CAG CTG GGG TGC CTT TTT CTC CA	114 bp
Susd4	ACA GCT CAC GGG TGG GTT CG	AAC TCC TCC GCT GGG GGT CC	88 bp
Id2	GGA CAG AAC CAG GCG TCC AGG A	GAA TTC AGA TGC CTG CAA GGA CAG G	81 bp

Slc30a4	CGC CTA GAG GTT TTG TCG GCC A	TGC AAC TCC AAC AGC TGC AGT GA	150 bp
Ly86	CCT GGA CTT GAT GTT CCA CAG GGA G	TGG CAC AAG CCA CAG TAG CAC G	82 bp
Trbv29	ACC ACA GGC CTT GTG GAC ATG	AGC TGT AGC CCC AGA CCA GGG	149 bp
Ly6d	ACG TGT GCA CCA ACA GTG CCA A	GAG GCT CCA CTG AGG TGA CGG TT	90 bp
Wdr78	AAC CCC ATG TGG CCA GAG CGT	ATC GCA ACG GTG CCA TTG TGG	116 bp
Notch1	GTG TTT ATG GGC CTT GGG AGT	GCG AGT CCA CAA TGC ACA TTG G	243 bp
Notch3	TGC CAG AGT TCA GTG GTG G	CAC AGG CAA ATC GGC CAT C	157 bp
Dll1	GGA TAC ACA CAG CAA ACG TGA	CGC TTC CAT CTT ACA CCT CAG	215 bp
Deltex	ATC AGT TCC GGC AAG ACA CAG	CGA TGA GAG GTC GAG CCA C	194 bp
Chd7	CTT TTC ATG AGC CAC AAA CG	TCT TCT TCA AAA GCT TTG GTC AC	71 bp
Cd53	GGG ACT TCA TCC AGA CAC AAC TGC A	TGG GCA GGA AGA TGG TGG ACC A	83 bp
Crr4	GCC GCC GAC CAG TGG GTT TT	ATA CCG CGT GCA CGA TGG CC	136 bp
Il17rd	GAA CAC GGG CCT GTG ACC TGT	GTT CTG CGG GGC ATG GTC GA	131 bp
Ifi202b	CCT CAA GCC TCT CCT GGA CCT AAC A	TGG GTT TCT CAT GAA GAA CAG CAC C	85 bp
Gm1676 8	AAT CAA GGA GGG TCT GCG AAG CTC	CTC ACT GTC AGC TTT GTC CCC TCC	56 bp
Pik3cb	GAA AAC CGG CCA GCT CTT CCA CA	TTC ACA GCA CTG GCG GAA TCT GC	178 bp
Il4ra	TTC AGC CCC AGT GGT AAT GTG AAG C	ATT CCA GGT CAG CAG CCA TTC GTC	90 bp
Pip5k1b	AGA CTG CCG GGT TCT GGA AAG CTT	CCG CTT TGC ATC AGG CAC GT	127 bp

Lgi1	ACA CCA TCG CTG CAG CTC TTG TTA	TCA AAG ACT TGA GTC CCC GGA AAG T	157 bp
Ptcra	ACC ATC AGG CAT CGC TGG CAC	GTG CCG CAT CGA GGA CCA GG	110 bp
Adam12	CCA CGG GGT TCC CAT TCC CC	CAC TTC CGG CCC CCA AAG GC	133 bp
Rapgef2	ACC AAG GGA CTC ATC GCA CGG A	CGC TGC AGG GCC ACG TTG TA	149 bp
Hmgn3	CCA CAA GAC GGT CGG CCA GG	TCC TTC TTC CCC TTA GCA CCT CTG C	127 bp
Tctex 1d1	ACC GTG TCC CAC GCG GAT GA	GAC AGT GGC CAC GGG GAA AGG	114 bp
Acs13	ATG CTA CTC TGG GAG GTC CAG CC	TAT GCC GCA GAC GTG GGA CCA	132 bp
Bcl211	GAA CGG CGG CTG GGA CAC TTT	CCC GTC AGG AAC CAG CGG TTG	99 bp
E2f2	TTG TGC GAT GTG CAC CCG CA	TTG GGG GTT TTG GGG CTT GGC	145 bp
Hspa4l	AGG TGC ACG CCG GCC TGT ATA	TGG GGT CAT CAA ATG ATC GCC CAT G	139 bp
Mybl1	TGG GCA CCA CAC CAA GAA CTC CTA	AAA AGG CAA GTG GCT GGG ACA CA	102 bp
Spata6	TTT CCG AAG ACA CTC GGC GGC	TGG GAC TCG GGG GAT CAA CAT GTC	114 bp
Eif4e3	AGA GGC GAC CAC TTT GGG AGG AG	CGC ACA CTC ACG CTG ACT CCG	178 bp
Tdrkh	CGA GCC CGG GTT CTT GGA ACC	CCA CTC TTC ACC TGT GGG GGC A	180 bp
Sestd1	GGA CAC ATT CTG GCT CAC GCT TCC	TCA GGC ATC TCG GGG CTG TCA TA	179 bp
Dmc1	CGA CGG AGG GGT CTC GTG GT	GCC AGT TCA CAA CCT GCA TCA CCT	101 bp
Dnajc6	ACA GCC GGG TCT CAG AGT GCA	CAG GAT TGA CGA CGC GGC CC	158 bp
Hist1h1a	CGA AAG CAT CCG GGG CTG CTA AG	CCT TCG CCT TGG CAG GGC TTT T	180 bp

Ssbp2	GTG CAG CTC CAG AGA GAC GGG A	TGG GAC ACC TCC AAG TGC CTG G	143/233 bp
2010015 L04Rik	GAC CTT GTG GAC AAC TTC CCT CCC A	TCG CTG AAC TGT GGC TGC CTT C	118 bp
Ets2	GCT GAC CCC GAT GAG GTT GCC	ACA CGT AGC GCT TGC CCG AAG	139 bp
Hspb11	AGC CAT TGG ATT TTG AGC AGT GGG T	GCG TAG CCA TCT CGT GCC ACA A	94 bp
Dhrs3	GGC CAA TTC TGG ACC ACC AAG GC	GCA GTA GTC GAT GGC GCC AGG	120 bp
Abcg3	TGT CAC CCC TTT CTG CCA TCA GCT	TGT CAC CCC TTT CTG CCA TCA GCT	180 bp
Atp2b4	ACA GCC AAG AGG GGC TCG ACA	TGA TCA GAC CCG CCT TCC CGA	129 bp
Cym	CCA CCG CAG GAG TTC ACC GTG	AAA ACG GTG GTG GTT TCG GCA CA	102 bp
Irf4	TGA CGT TTG GCC CAC GAG GC	CAG CCG GCA GTC TGA GAG CG	170 bp
Olf1r524	AGT GCG CGC TCT TGG GTG TC	AGG AGG CTG CAG AGA CCG GG	100 bp
Hey1	AAA CGG CGC AGA GAC CGC AT	CGG GCA TCA AAG AAC CCT GTG CC	173 bp
Cd163l1	GCT TGG CTG CCT TCT GGG CA	CCC CAA CAT GCC AGC ACC CAT	91 bp
Cst7	CAG GAG TGC TTA AGG CCG CCA G	AGG CCT TTC ACC ACC TGT ACC AGG	118 bp
Myo1e	ATG CAG AGC AGT GAG CTG CCT TTT	TTT GCT TCC TGC GGT CGT TGG G	93 bp
Icos	ACA ACC CAG ACA GCT CCC AGG G	CTG GCA GCA GAG CTG GGA TTC ATA	128 bp
Ipcef1	TCT CCT GTG GCT GCA CAG TGG G	CCG AGG AAG AAA ACT GGC TGG GT	115 bp
Prkar2a	TAA CGA TCC AAG GGT GGT TCA TCC C	CCG TCG TCG CCT TGG TCA ATG A	180 bp
Cd82	CGG GGT GTG GAT TCT TGC AGA CA	ACA AAG TAC AGA CCC AGC AAG CAG C	180 bp

Cobll1	CAC AGA GGG GCA AGG GCC GTA T	CTC CTG GTT TGG GCC CAG TGT CT	106 bp
Epas1	GAC GTG TCC ACC GAG CGT GA	CGG TGC AGT GCA GGA CCT TCC	109 bp
Ccdc125	TGG AAA TAA ATG CCT TGC AGT GGG A	TGC ATT GTC ACA GTT TAG CCT GTC A	107 bp
Nfli3	TCG GCG TGT CGG AGA AAA CGG	GCG GCG CTT CTC CCG AGA TC	114 bp
Ttc39b	TTG CTA CGT CCA TGG GCC AAG G	GCT GCT CGA AGG TCA TGA CAG CC	91 bp
Dock9	TCT GAG GTC TGC CTG CAC CAG TT	GCC TCT GAG TGG CCG TAG CTG TG	140/209/2 43 bp
Capn2	GCT TCG GCA TCT ATG AGG TTC CAG A	CAT ACT CTC CCG GGG GCA GCT T	159 bp
Trpm6	GCA GAG CCA GGA GAA ACT AAC ACC A	TCT CGG TTC TCT TGT GGC TGC CT	176 bp
Anxa6	TAA AGA CGC CAT CTC GGG CGT TG	TCT TTG TAT GCG GCC ACC AGC TG	105 bp
Fam102 a	CAC CGT CCG CTG CTG CCT AT	GCG GTA GAC GGT GGC GTC TT	132 bp
Neto2	GTG ATC CGG ATG TGG GCA GAC G	GCT GCT TGT ACA GGG AGG TTC CAC	90 bp
Trbv1	CTG TGG CTA CAG ACC CCA CAG TGA	ACT CCG CAG AGT GAA CAG CCA CT	176 bp
Il1b	TCT GGG ATC CTC TCC AGC CAA GC	AGC AGC CCT TCA TCT TTT GGG GTC	153/685 bp
Dck	TCG GAC TCT GAA AAC CAG CTT	CGC TGG CTC CTG TAC AAT CA	147 bp
Rnf130	CCT GCA AGC ATG TTT TCC ACA	CTT GGG TTC TGG TCA GCC TT	165 bp
Pi4k2b	CAT CAG GAA CAC AGA CAG GGG	ATG CTA GCC CAT TAT CAA TTG CAG	149 bp

Ahnak	GGT TCT GAA CAC GGT ACA ACC T	TCT TCC TGG CCA CTG CTA CA	130/222/2 79 bp
Gimap4	AGT TAG CAG CTC AGC AGG TG	GGC AGA AGC AGC ATG ATT GG	151 bp
Ctnnd1	CAC ATT TGA GCT CTC TCC TTC CT	AGT AGG TCC CCT CAC TTC ACA	149 bp
Milt4	CCC AGC AGG ACC AAA CTC TTA	AAC TGC CAG GTA AGT CTG CG	119 bp
Sbf2	CGA AAC ACC AGC TGC GAT AC	ATA CTT TGG GGC TCC CAT GC	119 bp
Olfir524	TGC CCT CTA CTC CTT CGA CT	GCT TGA CCT CTT GGT TCC GA	107 bp
Gm1549 8	GCC GCA GCC TGT GTC CGT AG	GGT CAC TGC CTC CTG GGC CT	172 bp
AC12667 6-1	GAT CCT TCT TCA AGC CCT GGG	GTG TGG GCA GCT TGA CCT AT	
Armcx3	AAG AGC TGA CGT GTG CAG AA	GTT GTA CCG CAA CCT ACG GA	163 bp
Gm9766	CAG CGT GGA AGA TCA TTC AAC TT	ATC ACA TGG GCA GTG GGA AG	87 bp
Trdv5	CTT CTG TTT GCC TAC AAG GAT GTG	TCT GGG TTT GGA GAA TCC GC	125 bp
Atxn1	GAG AAT CGA GGA GAG CCA CAG	CAA GAC TTC GAC ACT GAC CTG	88/112 bp
Trav15-1	GTG GAA ATT TCC AGG AGT ATG TTC ATG	GCC AGG TAT AGT CAG AGT GCC	

Table Appendix 5: qRT-PCR Primer Sequences Used For Expression Of Chd Family Members.

Gene name	Forward primer [5´-3´]	Reverse primer [5´-3´]	Amplicon length
Chd1	GGA TCC GAA GAA GAC TCG TCC	CCC GTC GCA GCT GCT TTT A	171 bp
Chd2	CAC TAT CCT TTC CAG CGC CT	CGT GTG GAG AGC AGG AAA CA	113 bp
Chd3	CGG GCT CGT GTG CTT TTC A	TTC AGC TTC TTG GCA CGG AC	127 bp
Chd4	CTT CGC TGA GGT GGA GTG TT	CCA GCT GTT TCA GGA CTT TGT G	110 bp
Chd5	ATG TGG GCG CCT GAC TTT TA	GCA CTT CCT TCT TCA TGC GG	139 bp

Chd6	CTC CCC GCA TGG AAA GAT GA	CAC GGA CTT TCC TCA GCA GT	115 bp
Chd7	CTT TTC ATG AGC CAC AAA CG	TCT TCT TCA AAA GCT TTG GTC AC	71 bp
Chd8	CAC CTA CCC AGG GTG AAT CG	GCT AGC TGG TTG CCC TGT AA	133 bp
Chd9	GAG AAG GCA CGC CTC ACA G	TCA TTA CCC GGT CCT TTG GC	177 bp

Table Appendix 6: qRT-PCR Primer Sequences Used For Expression Of Serca Family Members.

Gene name	Forward primer [5'-3']	Reverse primer [5'-3']	Amplicon length
Serca1	AGC TAC CAT CAG CTG ACT CAT TT	CCG CAG TAG GGA CTG GTT C	177 bp
Serca2ab	ACC TTT GCC GCT CAT TTT CC	CGG GTT GTT CCA GGT AGT T	134 bp
Serca3	TGA AAT GTG CAA CGC CCT CA	GAA AAA TGA GAG GCA GAG GTG G	152 bp

Table Appendix 7: qRT-PCR Primer Sequences Used For Apoptosis-Related Genes.

Gene name	Forward primer [5'-3']	Reverse primer [5'-3']	Amplicon length
Bcl2l1	GAA CGG CGG CTG GGA CAC TTT	CCC GTC AGG AAC CAG CGG TTG	99 bp
Bcl2	GCC TTC TTT GAG TTC GGT GG	ATA TAG TTC CAC AAA GGC ATC CCA G	162 bp
Bax	AAA CTG GTG CTC AAG GCC C	TTG GAT CCA GAC AAG CAG CC	105 bp
Bim	GCC AGG CCT TCA ACC ACT AT	TGC AAA CAC CCT CCT TGT GT	152 bp
Bad	AAA TGG GAA CCC CAA AGC AG	GAA CAT ACT CTG GGC TGC TGG	134 bp

Table Appendix 8: qRT-PCR Primer Sequences Used For Unfolded Protein Response-Related Genes.

Gene name	Forward primer [5'-3']	Reverse primer [5'-3']	Amplicon length
Atf6	GAA GAC TGG GAG TCG ACG TT	ATG TCT GAG CAG AAG TGG CT	179 bp
Ern2/Ire1	ATT TCC TTG TCC TCC GCT GG	ACA GTG TCA TCA AAA GCT GGG	105 bp
Atf4	CGG CAA GGA GGA TGC CTT T	TCT GGC ATG GTT TCC AGG TC	111 bp

Hsp90b1	TCA AAT CGA ACA CGG CTT GC	AGA TTC CGC CTC CTT TCT GC	153 bp
Eif2ak3/PE RK	CGC CGA TGG GAT AGT GAT GA	CAC TGA AAT TCC ACT TCT CAC TGC	118 bp
Total Xbp1	AAG AAC ACG CTT GGG AAT GG	ACT CCC CTT GGC CTC CAC	67 bp
spliced Xbp1	GAG TCC GCA GCA GGT G	GTG TCA GAG TCC ATG GGA	
Hspa5/Grp 78	GAC CAC CTA TTC CTG CGT CG	CCA ATC AGA CGC TCC CCT TC	123 bp
Dnajb9	GAG ATT GCA GAA GCG TAT GAA ACA C	CTC CCA TTG CCT CTT TGT CCT	110 bp
Ddit3	ACC TGA GGA GAG AGT GTT CCA	CAA GGT GAA AGG CAG GGA CT	112 bp

Table Appendix 9: qRT-PCR Primer Sequences Used For Cell Cycle-Related Genes.

Gene name	Forward primer [5´-3´]	Reverse primer [5´-3´]	Amplicon length
Ccnd1	TGC AAA TGG AAC TGC TTC TGG	ATG AAC TTC ACA TCT GTG GCA	175 bp
Ccnd3	ATG GCA GTT GCG GGA GT	TTT TTG ACC AAA GCC TGC CG	138 bp
p16	AAA GCG AAC TCG AGG AGA GC	TCA TCA TCA CCT GAA TCG GGG	169 bp
p21	TTG CAC TCT GGT GTC TGA GC	GGA GTG ATA GAA ATC TGT CAG GC	103 bp
p27	CAA ACT CTG AGG ACC GGC AT	AGA AGA ATC TTC TGC AGC AGG	116 bp
p57	AGG ACG AGA ATC AAG AGC AGC	CGA AGA AGT CGT TCG CAT TGG	111 bp
p107	ACC ATA TAA TGG ATG CTC CCC C	CTT AGA AGG GCT GCC GTT GA	173 bp

Table Appendix 10: Solutions for Preparing Stacking and Separation gel for SDS-PAGE.

Solution components	Volumes per 5% stacking gel	Volumes per 6% separation gel
H ₂ O	1.4ml	5.3ml
30% acrylamide mix	330µl	2.0ml
1M Tris-HCl (pH 6.8)	250µl	-
1.5M Tris-HCl (pH 8.8)	-	2.5ml
10% SDS	20µl	100µl
10% APS	20µl	100µl
TEMED	2µl	8µl

References

- Adams, G. B., Chabner, K. T., Alley, I. R., Olson, D. P., Szczepiorkowski, Z. M., Poznansky, M. C., Kos, C. H., Pollak, M. R., Brown, E. M., and Scadden, D. T. (2006). Stem cell engraftment at the endosteal niche is specified by the calcium-sensing receptor. *Nature* *439*, 599-603.
- Andersson, K. B., Finsen, A. V., Sjaland, C., Winer, L. H., Sjaastad, I., Odegaard, A., Louch, W. E., Wang, Y., Chen, J., Chien, K. R., *et al.* (2009). Mice carrying a conditional *Serca2*(flox) allele for the generation of Ca(2+) handling-deficient mouse models. *Cell Calcium* *46*, 219-225.
- Aster, J. C., Simms, W. B., Zavala-Ruiz, Z., Patriub, V., North, C. L., and Blacklow, S. C. (1999). The folding and structural integrity of the first LIN-12 module of human Notch1 are calcium-dependent. *Biochemistry* *38*, 4736-4742.
- Bagchi, A., Papazoglu, C., Wu, Y., Capurso, D., Brodt, M., Francis, D., Bredel, M., Vogel, H., and Mills, A. A. (2007). CHD5 is a tumor suppressor at human 1p36. *Cell* *128*, 459-475.
- Bajpai, R., Chen, D. A., Rada-Iglesias, A., Zhang, J., Xiong, Y., Helms, J., Chang, C. P., Zhao, Y., Swigut, T., and Wysocka, J. (2010). CHD7 cooperates with PBAF to control multipotent neural crest formation. *Nature* *463*, 958-962.
- Bashir, R., Munro, C. S., Mason, S., Stephenson, A., Rees, J. L., and Strachan, T. (1993). Localisation of a gene for Darier's disease. *Hum Mol Genet* *2*, 1937-1939.
- Becker, P. B., and Horz, W. (2002). ATP-dependent nucleosome remodeling. *Annu Rev Biochem* *71*, 247-273.
- Berridge, M. J., Bootman, M. D., and Roderick, H. L. (2003). Calcium signalling: dynamics, homeostasis and remodelling. *Nat Rev Mol Cell Biol* *4*, 517-529.
- Bryder, D., Rossi, D. J., and Weissman, I. L. (2006). Hematopoietic stem cells: the paradigmatic tissue-specific stem cell. *Am J Pathol* *169*, 338-346.
- Buckley, B. J., and Whorton, A. R. (1997). Tunicamycin increases intracellular calcium levels in bovine aortic endothelial cells. *Am J Physiol* *273*, C1298-1305.
- Calvi, L. M., Adams, G. B., Weibrecht, K. W., Weber, J. M., Olson, D. P., Knight, M. C., Martin, R. P., Schipani, E., Divieti, P., Bringhurst, F. R., *et al.* (2003). Osteoblastic cells regulate the haematopoietic stem cell niche. *Nature* *425*, 841-846.
- Chan, S. W., and Egan, P. A. (2005). Hepatitis C virus envelope proteins regulate CHOP via induction of the unfolded protein response. *Faseb J* *19*, 1510-1512.
- Chen, X., Shen, J., and Prywes, R. (2002). The luminal domain of ATF6 senses endoplasmic reticulum (ER) stress and causes translocation of ATF6 from the ER to the Golgi. *J Biol Chem* *277*, 13045-13052.

- Chopra, C., Baretto, R., Duddridge, M., and Browning, M. J. (2009). T-cell immunodeficiency in CHARGE syndrome. *Acta Paediatr* *98*, 408-410.
- Clapier, C. R., and Cairns, B. R. (2009). The biology of chromatin remodeling complexes. *Annu Rev Biochem* *78*, 273-304.
- Colbert, L. E., Petrova, A. V., Fisher, S. B., Pantazides, B. G., Madden, M. Z., Hardy, C. W., Warren, M. D., Pan, Y., Nagaraju, G. P., Liu, E. A., *et al.* (2014). CHD7 expression predicts survival outcomes in patients with resected pancreatic cancer. *Cancer Res* *74*, 2677-2687.
- Craddock, N., Dawson, E., Burge, S., Parfitt, L., Mant, B., Roberts, Q., Daniels, J., Gill, M., McGuffin, P., Powell, J., and *et al.* (1993). The gene for Darier's disease maps to chromosome 12q23-q24.1. *Hum Mol Genet* *2*, 1941-1943.
- Daubresse, G., Deuring, R., Moore, L., Papoulas, O., Zakrajsek, I., Waldrip, W. R., Scott, M. P., Kennison, J. A., and Tamkun, J. W. (1999). The *Drosophila* *kismet* gene is related to chromatin-remodeling factors and is required for both segmentation and segment identity. *Development* *126*, 1175-1187.
- De Craene, B., and Berx, G. (2013). Regulatory networks defining EMT during cancer initiation and progression. *Nat Rev Cancer* *13*, 97-110.
- de Kruijf, E. J., van Pel, M., Hagoort, H., Kruysdijk, D., Molineux, G., Willemze, R., and Fibbe, W. E. (2007). Repeated hematopoietic stem and progenitor cell mobilization without depletion of the bone marrow stem and progenitor cell pool in mice after repeated administration of recombinant murine G-CSF. *Hum Immunol* *68*, 368-374.
- Dhitavat, J., Fairclough, R. J., Hovnanian, A., and Burge, S. M. (2004). Calcium pumps and keratinocytes: lessons from Darier's disease and Hailey-Hailey disease. *Br J Dermatol* *150*, 821-828.
- Domen, J., and Weissman, I. L. (1999). Self-renewal, differentiation or death: regulation and manipulation of hematopoietic stem cell fate. *Mol Med Today* *5*, 201-208.
- Durr, H., Flaus, A., Owen-Hughes, T., and Hopfner, K. P. (2006). Snf2 family ATPases and DExx box helicases: differences and unifying concepts from high-resolution crystal structures. *Nucleic Acids Res* *34*, 4160-4167.
- Egan, C. M., Nyman, U., Skotte, J., Streubel, G., Turner, S., O'Connell, D. J., Rraklli, V., Dolan, M. J., Chadderton, N., Hansen, K., *et al.* (2013). CHD5 is required for neurogenesis and has a dual role in facilitating gene expression and polycomb gene repression. *Dev Cell* *26*, 223-236.
- Ellisen, L. W., Bird, J., West, D. C., Soreng, A. L., Reynolds, T. C., Smith, S. D., and Sklar, J. (1991). TAN-1, the human homolog of the *Drosophila* notch gene, is broken by chromosomal translocations in T lymphoblastic neoplasms. *Cell* *66*, 649-661.
- Ema, H., and Nakauchi, H. (2000). Expansion of hematopoietic stem cells in the developing liver of a mouse embryo. *Blood* *95*, 2284-2288.
- Ema, H., Sudo, K., Seita, J., Matsubara, A., Morita, Y., Osawa, M., Takatsu, K., Takaki, S., and Nakauchi, H. (2005). Quantification of self-renewal capacity in single hematopoietic stem cells from normal and Lnk-deficient mice. *Dev Cell* *8*, 907-914.

- Engelen, E., Akinci, U., Bryne, J. C., Hou, J., Gontan, C., Moen, M., Szumska, D., Kockx, C., van Ijcken, W., Dekkers, D. H., *et al.* (2011). Sox2 cooperates with Chd7 to regulate genes that are mutated in human syndromes. *Nat Genet* *43*, 607-611.
- Essers, M. A., Offner, S., Blanco-Bose, W. E., Waibler, Z., Kalinke, U., Duchosal, M. A., and Trumpp, A. (2009). IFN α activates dormant haematopoietic stem cells in vivo. *Nature* *458*, 904-908.
- Esteller, M. (2007). Cancer epigenomics: DNA methylomes and histone-modification maps. *Nat Rev Genet* *8*, 286-298.
- Felli, M. P., Maroder, M., Mitsiadis, T. A., Campese, A. F., Bellavia, D., Vacca, A., Mann, R. S., Frati, L., Lendahl, U., Gulino, A., and Screpanti, I. (1999). Expression pattern of notch1, 2 and 3 and Jagged1 and 2 in lymphoid and stromal thymus components: distinct ligand-receptor interactions in intrathymic T cell development. *Int Immunol* *11*, 1017-1025.
- Fiorini, E., Merck, E., Wilson, A., Ferrero, I., Jiang, W., Koch, U., Auderset, F., Laurenti, E., Tacchini-Cottier, F., Pierres, M., *et al.* (2009). Dynamic regulation of notch 1 and notch 2 surface expression during T cell development and activation revealed by novel monoclonal antibodies. *J Immunol* *183*, 7212-7222.
- Flaus, A., Martin, D. M., Barton, G. J., and Owen-Hughes, T. (2006). Identification of multiple distinct Snf2 subfamilies with conserved structural motifs. *Nucleic Acids Res* *34*, 2887-2905.
- Gaspar-Maia, A., Alajem, A., Polesso, F., Sridharan, R., Mason, M. J., Heidersbach, A., Ramalho-Santos, J., McManus, M. T., Plath, K., Meshorer, E., and Ramalho-Santos, M. (2009). Chd1 regulates open chromatin and pluripotency of embryonic stem cells. *Nature* *460*, 863-868.
- Gelebart, P., Martin, V., Enouf, J., and Papp, B. (2003). Identification of a new SERCA2 splice variant regulated during monocytic differentiation. *Biochem Biophys Res Commun* *303*, 676-684.
- Hoover-Fong, J., Savage, W. J., Lisi, E., Winkelstein, J., Thomas, G. H., Hoefsloot, L. H., and Loeb, D. M. (2009). Congenital T cell deficiency in a patient with CHARGE syndrome. *J Pediatr* *154*, 140-142.
- Hotamisligil, G. S. (2010). Endoplasmic reticulum stress and atherosclerosis. *Nat Med* *16*, 396-399.
- Hozumi, K., Negishi, N., Suzuki, D., Abe, N., Sotomaru, Y., Tamaoki, N., Mailhos, C., Ish-Horowicz, D., Habu, S., and Owen, M. J. (2004). Delta-like 1 is necessary for the generation of marginal zone B cells but not T cells in vivo. *Nat Immunol* *5*, 638-644.
- Hsu J, L. C., Gerber S, Yu S, Speck NA (2011). Runx1-Cbfb Interacts with CHD7, a Chromatin Modifying Enzyme with a Potential Role in Hematopoiesis In Gordon Conference: Hematopoietic Stem and Progenitor Biology.
- Hsuan-Ting Huang, K. K., Ph.D., Yue-Hua Huang, Zachary Gitlin, Abby Barton, Anhua Song, Yi Zhou, Ph.D. and Leonard I. Zon (2010). Chd7 Is a Cell Autonomous Regulator of Chromatin In Hematopoietic Stem Cells. In Gordon Conference: Hematopoietic Stem and Progenitor Biology.
- Huang HT, K. K., Huang YH, Gitlin Z, Barton A, Song A, Zhou Y, Zon LI (2010). Chd7 Is a Cell Autonomous Regulator of Chromatin In Hematopoietic Stem Cells. In Gordon Conference - Session Hematopoietic Stem and Progenitor Biology.

- Hurd, E. A., Capers, P. L., Blauwkamp, M. N., Adams, M. E., Raphael, Y., Poucher, H. K., and Martin, D. M. (2007). Loss of Chd7 function in gene-trapped reporter mice is embryonic lethal and associated with severe defects in multiple developing tissues. *Mamm Genome* *18*, 94-104.
- Hurd, E. A., Micucci, J. A., Reamer, E. N., and Martin, D. M. (2012). Delayed fusion and altered gene expression contribute to semicircular canal defects in Chd7 deficient mice. *Mech Dev* *129*, 308-323.
- Hurd, E. A., Poucher, H. K., Cheng, K., Raphael, Y., and Martin, D. M. (2010). The ATP-dependent chromatin remodeling enzyme CHD7 regulates pro-neural gene expression and neurogenesis in the inner ear. *Development* *137*, 3139-3150.
- Jarriault, S., Brou, C., Logeat, F., Schroeter, E. H., Kopan, R., and Israel, A. (1995). Signalling downstream of activated mammalian Notch. *Nature* *377*, 355-358.
- Jarriault, S., Le Bail, O., Hirsinger, E., Pourquie, O., Logeat, F., Strong, C. F., Brou, C., Seidah, N. G., and Israel, A. (1998). Delta-1 activation of notch-1 signaling results in HES-1 transactivation. *Molecular and cellular biology* *18*, 7423-7431.
- Jenuwein, T., and Allis, C. D. (2001). Translating the histone code. *Science* *293*, 1074-1080.
- Ji, Y., Lalli, M. J., Babu, G. J., Xu, Y., Kirkpatrick, D. L., Liu, L. H., Chiamvimonvat, N., Walsh, R. A., Shull, G. E., and Periasamy, M. (2000). Disruption of a single copy of the SERCA2 gene results in altered Ca²⁺ homeostasis and cardiomyocyte function. *J Biol Chem* *275*, 38073-38080.
- Jiang, S., Chow, S. C., Nicotera, P., and Orrenius, S. (1994). Intracellular Ca²⁺ signals activate apoptosis in thymocytes: studies using the Ca(2+)-ATPase inhibitor thapsigargin. *Exp Cell Res* *212*, 84-92.
- Kidd, S., and Young, M. W. (1986). Transposon-dependent mutant phenotypes at the Notch locus of *Drosophila*. *Nature* *323*, 89-91.
- Kiel, M. J., Yilmaz, O. H., Iwashita, T., Terhorst, C., and Morrison, S. J. (2005). SLAM family receptors distinguish hematopoietic stem and progenitor cells and reveal endothelial niches for stem cells. *Cell* *121*, 1109-1121.
- Kim, I., Xu, W., and Reed, J. C. (2008). Cell death and endoplasmic reticulum stress: disease relevance and therapeutic opportunities. *Nat Rev Drug Discov* *7*, 1013-1030.
- Kim, M. S., Chung, N. G., Kang, M. R., Yoo, N. J., and Lee, S. H. (2011). Genetic and expressional alterations of CHD genes in gastric and colorectal cancers. *Histopathology* *58*, 660-668.
- Kitsos, C. M., Sankar, U., Illario, M., Colomer-Font, J. M., Duncan, A. W., Ribar, T. J., Reya, T., and Means, A. R. (2005). Calmodulin-dependent protein kinase IV regulates hematopoietic stem cell maintenance. *J Biol Chem* *280*, 33101-33108.
- Koch, U., Fiorini, E., Benedito, R., Besseyrias, V., Schuster-Gossler, K., Pierres, M., Manley, N. R., Duarte, A., Macdonald, H. R., and Radtke, F. (2008). Delta-like 4 is the essential, nonredundant ligand for Notch1 during thymic T cell lineage commitment. *The Journal of experimental medicine* *205*, 2515-2523.

- Kuhlbrandt, W. (2004). Biology, structure and mechanism of P-type ATPases. *Nat Rev Mol Cell Biol* 5, 282-295.
- Kuhn, R., Schwenk, F., Aguet, M., and Rajewsky, K. (1995). Inducible gene targeting in mice. *Science* 269, 1427-1429.
- Lam, B. S., Cunningham, C., and Adams, G. B. (2011). Pharmacologic modulation of the calcium-sensing receptor enhances hematopoietic stem cell lodgment in the adult bone marrow. *Blood* 117, 1167-1175.
- Laurenti, E., Doulatov, S., Zandi, S., Plumb, I., Chen, J., April, C., Fan, J. B., and Dick, J. E. (2013). The transcriptional architecture of early human hematopoiesis identifies multilevel control of lymphoid commitment. *Nat Immunol* 14, 756-763.
- Lehal, R. (2011) Identification and Preclinical Validation of Novel Inhibitors of the Notch Pathway, Doctoral, EPFL, Lausanne.
- Lerner, C., and Harrison, D. E. (1990). 5-Fluorouracil spares hemopoietic stem cells responsible for long-term repopulation. *Exp Hematol* 18, 114-118.
- Luger, K., and Richmond, T. J. (1998). The histone tails of the nucleosome. *Curr Opin Genet Dev* 8, 140-146.
- Lund, A. H., and van Lohuizen, M. (2004). Epigenetics and cancer. *Genes & development* 18, 2315-2335.
- MacLennan, D. H., Brandl, C. J., Korczak, B., and Green, N. M. (1985). Amino-acid sequence of a Ca²⁺ + Mg²⁺-dependent ATPase from rabbit muscle sarcoplasmic reticulum, deduced from its complementary DNA sequence. *Nature* 316, 696-700.
- Mai, A., Massa, S., Rotili, D., Cerbara, I., Valente, S., Pezzi, R., Simeoni, S., and Ragno, R. (2005). Histone deacetylation in epigenetics: an attractive target for anticancer therapy. *Med Res Rev* 25, 261-309.
- Maillard, I., Koch, U., Dumortier, A., Shestova, O., Xu, L., Sai, H., Pross, S. E., Aster, J. C., Bhandoola, A., Radtke, F., and Pear, W. S. (2008). Canonical notch signaling is dispensable for the maintenance of adult hematopoietic stem cells. *Cell Stem Cell* 2, 356-366.
- Mancini, S. J., Mantei, N., Dumortier, A., Suter, U., MacDonald, H. R., and Radtke, F. (2005). Jagged1-dependent Notch signaling is dispensable for hematopoietic stem cell self-renewal and differentiation. *Blood* 105, 2340-2342.
- Matsuno, K., Diederich, R. J., Go, M. J., Blaumueller, C. M., and Artavanis-Tsakonas, S. (1995). Deltex acts as a positive regulator of Notch signaling through interactions with the Notch ankyrin repeats. *Development* 121, 2633-2644.
- Matsuzaki, Y., Kinjo, K., Mulligan, R. C., and Okano, H. (2004). Unexpectedly efficient homing capacity of purified murine hematopoietic stem cells. *Immunity* 20, 87-93.
- McCulloch, E. A., Till, J. E., and Siminovitch, L. (1965). The role of independent and dependent stem cells in the control of hemopoietic and immunologic responses. *Wistar Inst Symp Monogr* 4, 61-68.

- McCullough, K. D., Martindale, J. L., Klotz, L. O., Aw, T. Y., and Holbrook, N. J. (2001). Gadd153 sensitizes cells to endoplasmic reticulum stress by down-regulating Bcl2 and perturbing the cellular redox state. *Molecular and cellular biology* 21, 1249-1259.
- McGrath, K. E., Bushnell, T. P., and Palis, J. (2008). Multispectral imaging of hematopoietic cells: where flow meets morphology. *J Immunol Methods* 336, 91-97.
- Micucci, J. A., Layman, W. S., Hurd, E. A., Sperry, E. D., Frank, S. F., Durham, M. A., Swiderski, D. L., Skidmore, J. M., Scacheri, P. C., Raphael, Y., and Martin, D. M. (2014). CHD7 and retinoic acid signaling cooperate to regulate neural stem cell and inner ear development in mouse models of CHARGE syndrome. *Hum Mol Genet* 23, 434-448.
- Mokarram, P., Kumar, K., Brim, H., Naghibalhossaini, F., Saberi-firoozi, M., Nourai, M., Green, R., Lee, E., Smoot, D. T., and Ashktorab, H. (2009). Distinct high-profile methylated genes in colorectal cancer. *PLoS One* 4, e7012.
- Morgan, T. H. (1917). Goodale's Experiments on Gonadectomy of Fowls. *Science* 45, 483-484.
- Morrison, S. J., and Weissman, I. L. (1995). Heterogeneity of hematopoietic stem cells: implications for clinical applications. *Proc Assoc Am Physicians* 107, 187-194.
- Mulero-Navarro, S., and Esteller, M. (2008). Chromatin remodeling factor CHD5 is silenced by promoter CpG island hypermethylation in human cancer. *Epigenetics* 3, 210-215.
- Muller, A. M., Medvinsky, A., Strouboulis, J., Grosveld, F., and Dzierzak, E. (1994). Development of hematopoietic stem cell activity in the mouse embryo. *Immunity* 1, 291-301.
- Muller, E. J., Caldelari, R., Kolly, C., Williamson, L., Baumann, D., Richard, G., Jensen, P., Girling, P., Delprincipe, F., Wyder, M., *et al.* (2006). Consequences of depleted SERCA2-gated calcium stores in the skin. *J Invest Dermatol* 126, 721-731.
- Nagarajan, P., Onami, T. M., Rajagopalan, S., Kania, S., Donnell, R., and Venkatachalam, S. (2009). Role of chromodomain helicase DNA-binding protein 2 in DNA damage response signaling and tumorigenesis. *Oncogene* 28, 1053-1062.
- Nakagawa, T., and Yuan, J. (2000). Cross-talk between two cysteine protease families. Activation of caspase-12 by calpain in apoptosis. *J Cell Biol* 150, 887-894.
- Niggli, V., and Sigel, E. (2008). Anticipating antiport in P-type ATPases. *Trends Biochem Sci* 33, 156-160.
- Nishiyama, M., Oshikawa, K., Tsukada, Y., Nakagawa, T., Iemura, S., Natsume, T., Fan, Y., Kikuchi, A., Skoultchi, A. I., and Nakayama, K. I. (2009). CHD8 suppresses p53-mediated apoptosis through histone H1 recruitment during early embryogenesis. *Nat Cell Biol* 11, 172-182.
- Orban, P. C., Chui, D., and Marth, J. D. (1992). Tissue- and site-specific DNA recombination in transgenic mice. *Proc Natl Acad Sci U S A* 89, 6861-6865.
- Orrenius, S., Zhivotovsky, B., and Nicotera, P. (2003). Regulation of cell death: the calcium-apoptosis link. *Nat Rev Mol Cell Biol* 4, 552-565.

- Osawa, M., Hanada, K., Hamada, H., and Nakauchi, H. (1996). Long-term lymphohematopoietic reconstitution by a single CD34-low/negative hematopoietic stem cell. *Science* 273, 242-245.
- Palomero, T., Lim, W. K., Odom, D. T., Sulis, M. L., Real, P. J., Margolin, A., Barnes, K. C., O'Neil, J., Neuberg, D., Weng, A. P., *et al.* (2006). NOTCH1 directly regulates c-MYC and activates a feed-forward-loop transcriptional network promoting leukemic cell growth. *Proc Natl Acad Sci U S A* 103, 18261-18266.
- Pan, Z. Z. (2003). Kappa-opioid receptor-mediated enhancement of the hyperpolarization-activated current (I_h) through mobilization of intracellular calcium in rat nucleus raphe magnus. *J Physiol* 548, 765-775.
- Paschen, W., Doutheil, J., Gissel, C., and Treiman, M. (1996). Depletion of neuronal endoplasmic reticulum calcium stores by thapsigargin: effect on protein synthesis. *J Neurochem* 67, 1735-1743.
- Pazin, M. J., and Kadonaga, J. T. (1997). SWI2/SNF2 and related proteins: ATP-driven motors that disrupt protein-DNA interactions? *Cell* 88, 737-740.
- Pear, W. S., Aster, J. C., Scott, M. L., Hasserjian, R. P., Soffer, B., Sklar, J., and Baltimore, D. (1996a). Exclusive development of T cell neoplasms in mice transplanted with bone marrow expressing activated Notch alleles. *J Exp Med* 183, 2283-2291.
- Pear, W. S., Aster, J. C., Scott, M. L., Hasserjian, R. P., Soffer, B., Sklar, J., and Baltimore, D. (1996b). Exclusive development of T cell neoplasms in mice transplanted with bone marrow expressing activated Notch alleles. *The Journal of experimental medicine* 183, 2283-2291.
- Periasamy, M., Reed, T. D., Liu, L. H., Ji, Y., Loukianov, E., Paul, R. J., Nieman, M. L., Riddle, T., Duffy, J. J., Doetschman, T., *et al.* (1999). Impaired cardiac performance in heterozygous mice with a null mutation in the sarco(endo)plasmic reticulum Ca²⁺-ATPase isoform 2 (SERCA2) gene. *J Biol Chem* 274, 2556-2562.
- Pleasance, E. D., Stephens, P. J., O'Meara, S., McBride, D. J., Meynert, A., Jones, D., Lin, M. L., Beare, D., Lau, K. W., Greenman, C., *et al.* (2010). A small-cell lung cancer genome with complex signatures of tobacco exposure. *Nature* 463, 184-190.
- Poisson, C. (2011) *The Cell Differentiation Status Influences the Outcome of Notch-Induced Malignancy*, Doctoral, EPFL, Lausanne.
- Prasad, V., Okunade, G. W., Miller, M. L., and Shull, G. E. (2004). Phenotypes of SERCA and PMCA knockout mice. *Biochem Biophys Res Commun* 322, 1192-1203.
- Radtke, F., Schweisguth, F., and Pear, W. (2005). The Notch 'gospel'. *EMBO Rep* 6, 1120-1125.
- Radtke, F., Wilson, A., Stark, G., Bauer, M., van Meerwijk, J., MacDonald, H. R., and Aguet, M. (1999). Deficient T cell fate specification in mice with an induced inactivation of Notch1. *Immunity* 10, 547-558.
- Radzioch, D. (2013).

- Rangarajan, A., Talora, C., Okuyama, R., Nicolas, M., Mammucari, C., Oh, H., Aster, J. C., Krishna, S., Metzger, D., Chambon, P., *et al.* (2001). Notch signaling is a direct determinant of keratinocyte growth arrest and entry into differentiation. *The EMBO journal* *20*, 3427-3436.
- Reynolds, T. C., Smith, S. D., and Sklar, J. (1987). Analysis of DNA surrounding the breakpoints of chromosomal translocations involving the beta T cell receptor gene in human lymphoblastic neoplasms. *Cell* *50*, 107-117.
- Riccio, O., van Gijn, M. E., Bezdek, A. C., Pellegrinet, L., van Es, J. H., Zimmer-Strobl, U., Strobl, L. J., Honjo, T., Clevers, H., and Radtke, F. (2008). Loss of intestinal crypt progenitor cells owing to inactivation of both Notch1 and Notch2 is accompanied by derepression of CDK inhibitors p27Kip1 and p57Kip2. *EMBO Rep* *9*, 377-383.
- Robert-Moreno, A., Guiu, J., Ruiz-Herguido, C., Lopez, M. E., Ingles-Esteve, J., Riera, L., Tipping, A., Enver, T., Dzierzak, E., Gridley, T., *et al.* (2008). Impaired embryonic haematopoiesis yet normal arterial development in the absence of the Notch ligand Jagged1. *EMBO J* *27*, 1886-1895.
- Ron, D., and Walter, P. (2007). Signal integration in the endoplasmic reticulum unfolded protein response. *Nat Rev Mol Cell Biol* *8*, 519-529.
- Roti, G., Carlton, A., Ross, K. N., Markstein, M., Pajcini, K., Su, A. H., Perrimon, N., Pear, W. S., Kung, A. L., Blacklow, S. C., *et al.* (2013). Complementary genomic screens identify SERCA as a therapeutic target in NOTCH1 mutated cancer. *Cancer Cell* *23*, 390-405.
- Saito, T., Chiba, S., Ichikawa, M., Kunisato, A., Asai, T., Shimizu, K., Yamaguchi, T., Yamamoto, G., Seo, S., Kumano, K., *et al.* (2003). Notch2 is preferentially expressed in mature B cells and indispensable for marginal zone B lineage development. *Immunity* *18*, 675-685.
- Sakuntabhai, A., Ruiz-Perez, V., Carter, S., Jacobsen, N., Burge, S., Monk, S., Smith, M., Munro, C. S., O'Donovan, M., Craddock, N., *et al.* (1999). Mutations in ATP2A2, encoding a Ca²⁺ pump, cause Darier disease. *Nature genetics* *21*, 271-277.
- Schmitt, T. M., Ciofani, M., Petrie, H. T., and Zuniga-Pflucker, J. C. (2004). Maintenance of T cell specification and differentiation requires recurrent notch receptor-ligand interactions. *The Journal of experimental medicine* *200*, 469-479.
- Schnetz, M. P., Bartels, C. F., Shastri, K., Balasubramanian, D., Zentner, G. E., Balaji, R., Zhang, X., Song, L., Wang, Z., Laframboise, T., *et al.* (2009). Genomic distribution of CHD7 on chromatin tracks H3K4 methylation patterns. *Genome Res* *19*, 590-601.
- Schnetz, M. P., Handoko, L., Akhtar-Zaidi, B., Bartels, C. F., Pereira, C. F., Fisher, A. G., Adams, D. J., Flicek, P., Crawford, G. E., Laframboise, T., *et al.* (2010). CHD7 targets active gene enhancer elements to modulate ES cell-specific gene expression. *PLoS Genet* *6*, e1001023.
- Scorrano, L., Oakes, S. A., Opferman, J. T., Cheng, E. H., Sorcinelli, M. D., Pozzan, T., and Korsmeyer, S. J. (2003). BAX and BAK regulation of endoplasmic reticulum Ca²⁺: a control point for apoptosis. *Science* *300*, 135-139.
- Shannon, T. R., and Bers, D. M. (1997). Assessment of intra-SR free [Ca] and buffering in rat heart. *Biophys J* *73*, 1524-1531.

- Sidrauski, C., Chapman, R., and Walter, P. (1998). The unfolded protein response: an intracellular signalling pathway with many surprising features. *Trends Cell Biol* 8, 245-249.
- Sims, J. K., and Wade, P. A. (2011). SnapShot: Chromatin remodeling: CHD. *Cell* 144, 626-626 e621.
- Siu, K. T., Xu, Y., Swartz, K. L., Bhattacharyya, M., Gurbuxani, S., Hua, Y., and Minella, A. C. (2014). Chromosome instability underlies hematopoietic stem cell dysfunction and lymphoid neoplasia associated with impaired Fbw7-mediated cyclin E regulation. *Molecular and cellular biology* 34, 3244-3258.
- Strahl, B. D., and Allis, C. D. (2000). The language of covalent histone modifications. *Nature* 403, 41-45.
- Szyf, M., and Detich, N. (2001). Regulation of the DNA methylation machinery and its role in cellular transformation. *Prog Nucleic Acid Res Mol Biol* 69, 47-79.
- Takemura, H., Hughes, A. R., Thastrup, O., and Putney, J. W., Jr. (1989). Activation of calcium entry by the tumor promoter thapsigargin in parotid acinar cells. Evidence that an intracellular calcium pool and not an inositol phosphate regulates calcium fluxes at the plasma membrane. *J Biol Chem* 264, 12266-12271.
- Tanigaki, K., Han, H., Yamamoto, N., Tashiro, K., Ikegawa, M., Kuroda, K., Suzuki, A., Nakano, T., and Honjo, T. (2002). Notch-RBP-J signaling is involved in cell fate determination of marginal zone B cells. *Nat Immunol* 3, 443-450.
- Thastrup, O., Cullen, P. J., Drobak, B. K., Hanley, M. R., and Dawson, A. P. (1990). Thapsigargin, a tumor promoter, discharges intracellular Ca²⁺ stores by specific inhibition of the endoplasmic reticulum Ca²⁺(+)-ATPase. *Proc Natl Acad Sci U S A* 87, 2466-2470.
- Todd, D. J., Lee, A. H., and Glimcher, L. H. (2008). The endoplasmic reticulum stress response in immunity and autoimmunity. *Nat Rev Immunol* 8, 663-674.
- Trumpp, A., Essers, M., and Wilson, A. (2010). Awakening dormant haematopoietic stem cells. *Nat Rev Immunol* 10, 201-209.
- Tsai, S., Fero, J., and Bartelmez, S. (2000). Mouse Jagged2 is differentially expressed in hematopoietic progenitors and endothelial cells and promotes the survival and proliferation of hematopoietic progenitors by direct cell-to-cell contact. *Blood* 96, 950-957.
- Uchida, N., and Weissman, I. L. (1992). Searching for hematopoietic stem cells: evidence that Thy-1.1^{lo} Lin⁻ Sca-1⁺ cells are the only stem cells in C57BL/Ka-Thy-1.1 bone marrow. *The Journal of experimental medicine* 175, 175-184.
- Urano, F., Wang, X., Bertolotti, A., Zhang, Y., Chung, P., Harding, H. P., and Ron, D. (2000). Coupling of stress in the ER to activation of JNK protein kinases by transmembrane protein kinase IRE1. *Science* 287, 664-666.
- van Galen, P., Kreso, A., Mbong, N., Kent, D. G., Fitzmaurice, T., Chambers, J. E., Xie, S., Laurenti, E., Hermans, K., Eppert, K., *et al.* (2014). The unfolded protein response governs integrity of the haematopoietic stem-cell pool during stress. *Nature* 510, 268-272.

- Vissers, L. E., van Ravenswaaij, C. M., Admiraal, R., Hurst, J. A., de Vries, B. B., Janssen, I. M., van der Vliet, W. A., Huys, E. H., de Jong, P. J., Hamel, B. C., *et al.* (2004). Mutations in a new member of the chromodomain gene family cause CHARGE syndrome. *Nature genetics* *36*, 955-957.
- Wang, L. D., and Wagers, A. J. (2011). Dynamic niches in the origination and differentiation of haematopoietic stem cells. *Nat Rev Mol Cell Biol* *12*, 643-655.
- Wendorff, A. A., Koch, U., Wunderlich, F. T., Wirth, S., Dubey, C., Bruning, J. C., MacDonald, H. R., and Radtke, F. (2010). *Hes1* is a critical but context-dependent mediator of canonical Notch signaling in lymphocyte development and transformation. *Immunity* *33*, 671-684.
- Weng, A. P., Ferrando, A. A., Lee, W., Morris, J. P. t., Silverman, L. B., Sanchez-Irizarry, C., Blacklow, S. C., Look, A. T., and Aster, J. C. (2004). Activating mutations of NOTCH1 in human T cell acute lymphoblastic leukemia. *Science* *306*, 269-271.
- West, S. C. (1997). Processing of recombination intermediates by the RuvABC proteins. *Annu Rev Genet* *31*, 213-244.
- Weston, S. A., and Parish, C. R. (1990). New fluorescent dyes for lymphocyte migration studies. Analysis by flow cytometry and fluorescence microscopy. *J Immunol Methods* *133*, 87-97.
- Wharton, K. A., Yedvobnick, B., Finnerty, V. G., and Artavanis-Tsakonas, S. (1985). *opa*: a novel family of transcribed repeats shared by the Notch locus and other developmentally regulated loci in *D. melanogaster*. *Cell* *40*, 55-62.
- Wilson, A., Laurenti, E., Oser, G., van der Wath, R. C., Blanco-Bose, W., Jaworski, M., Offner, S., Dunant, C. F., Eshkind, L., Bockamp, E., *et al.* (2008). Hematopoietic stem cells reversibly switch from dormancy to self-renewal during homeostasis and repair. *Cell* *135*, 1118-1129.
- Wilson, A., and Trumpp, A. (2006). Bone-marrow haematopoietic-stem-cell niches. *Nat Rev Immunol* *6*, 93-106.
- Witzl, K., Cale, C. M., Pierce, C. M., Wilson, L. C., and Hennekam, R. C. (2007). Immunological abnormalities in CHARGE syndrome. *Eur J Med Genet* *50*, 338-345.
- Wu, L., Maillard, I., Nakamura, M., Pear, W. S., and Griffin, J. D. (2007). The transcriptional coactivator *Maml1* is required for Notch2-mediated marginal zone B-cell development. *Blood* *110*, 3618-3623.
- Zhang, Y., LeRoy, G., Seelig, H. P., Lane, W. S., and Reinberg, D. (1998). The dermatomyositis-specific autoantigen Mi2 is a component of a complex containing histone deacetylase and nucleosome remodeling activities. *Cell* *95*, 279-289.

Acknowledgements

I thank Prof. Freddy Radtke for his support, guidance and the opportunity to work in his laboratory for the last 5 years thanks to the extensions he granted me in order to finish the second fruitful and challenging PhD project about Serca2. This opportunity fuelled me with motivation and a passion to finish this chapter during my scientific career with positive results. I also want to use this opportunity to thank Prof. Oliver Hantschel, Prof. Matthias Lutolf, Prof. Markus Manz and Dr. Anne Wilson for reading this manuscript and being on my PhD committee. Special thanks to Dr. Ute Koch, who has guided me in experimental design, mouse handling and has introduced me to the colourful world of flow cytometry. Ute is the heart of the lab, without her things would fall out of place. I want to thank Caroline Poisson and especially Rajwinder Lehal who provided the basis for the projects studied during my thesis.

I want to thank Fabian Junker a.k.a. FJ for his limitless friendship, his support in scientific questions and for having made my time in UPRAD and in Lausanne a special experience worth doing again. Without you things would have been different.

I thank all current and former lab members for their scientific, physical but also moral support throughout the last five years. I have made good friends and will remember my time at EPFL with a good spirit.

I dedicate this work to the three most important women in my life, my grandmother Gisela - the panther, my mother Christiane and my aunt and foster mother Angelika. Thank you for guiding me through life with your unconditional love, wisdom and support. I value the limited time we spend together and appreciate all discussions we have over the phone.

Curriculum Vitae



Personal Details

Name Monique Coersmeyer
Date of Birth 13.01.1984
Nationality German
Marital status Single
Home address Rue de l'Aurore 2, c/o Hassina Zekrya, 1005 Lausanne, Switzerland
Work address EPFL-SV-ISREC UPRAD, SV2533, Station 19, 1015 Lausanne
Email monique.coersmeyer@epfl.ch
Phone +41 (0) 78 850 98 18

Education

2010-present **PhD in Molecular Life Sciences** (defense April 2015)
École Polytechnique Fédérale de Lausanne (EPFL), Switzerland in the laboratory of Professor Freddy Radtke, Swiss Institute for Cancer Research (ISREC)

2003-2009 **M.Sc. in Biology** (German *Diploma*)
Ruhr-Universität-Bochum, Bochum. Diploma project at the Max-Planck-Institute of Molecular Physiology in Dortmund, Diploma project: „The epigenetic regulation of the Wnt target gene *LEF-1*” in the lab of Prof. Dr. A. Wittinghofer

2003 **Abitur** (University entrance qualification)
Archigymnasium, Soest, Germany

Research Experience

PhD project **The chromatin remodeler Chd7 & the calcium ATPase Serca2 – adding new facets to Notch in Hematopoiesis and T-ALL**
Notch1 has been shown to be a key driver in pediatric T-ALL. The chromatin-remodelling enzyme Chd7 was identified as potential regulator of T-ALL, in concert with Notch1, as it was highly over-expressed comparing aggressive versus pre-malignant T-ALL. In a chemical compound screen, the Notch inhibiting compounds CPA and thapsigargin, targeting the calcium ATPase Serca2, were identified. The aim of this thesis was to study Chd7 and Serca2 in the context of hematopoiesis and in T-ALL.

Professional Skills

In vivo Murine bone marrow transplantation (tail-vein/retro-orbital injections); intra peritoneal injections, acquisition of peripheral blood samples (tail vein bleedings)
Flow cytometric analysis of hematopoietic cells (up to 12 colors)
Breeding and characterization of transgenic mouse strains

<i>In vitro</i>	Histological tissue analysis (OCT / paraffin embedded) Culturing and transfection / transduction of primary cells and cell lines Molecular cloning of expression vectors and lentiviruses Retro- and lentivirus production and titration PCR and qPCR on cDNA Western Blotting
-----------------	---

Doctoral Courses and Teaching

Bioinformatics	Bioinformatics analysis of differential gene expression , 2011, Apr 04-08, Swiss Institute of Bioinformatics, Lausanne
Animal Work	Course in laboratory animal science (RESAL1) , 2010, June 18-27, EPFL
Teaching	Biotechnology Laboratory II , summer 2011, Prof. Florian Wurm / Dr. David Hacker, laboratory of cellular biotechnology Supervision of Bachelor students , spring 2010 and spring 2012
Doctoral Courses	Notch in vascular development and pathology , 2012, Sept 19-20, Faculté de Médecine, Paris, France Workshop on stem cell biology , 2011, Feb 03-04, EPFL, Lausanne Notch and hematopoiesis , 2010, Oct 24-26, Edinburgh University, UK Model systems in heart development , 2010, Jun 28-30, CNIC, Madrid, Spain NF-κB, inflammation and cancer 2010, Feb-May, UNIL

Conferences with Poster Presentation

2013, Feb 08	9th Annual SSCN Meeting , Inselspital, Bern, Switzerland (poster)
2011, Oct 02-06	The Notch Meeting V Athens , Athens, Greece (poster)
2011, Sept 07-10	ISREC Symposium on cancer , EPFL (poster)
2011, July 1	1st Life Science Symposium by Doctoral Students , EPFL (poster)
2011, Feb 04	7th Annual SSCN Meeting , EPFL (poster)

Internships / Studies abroad

2008, April-May	Drug treatment of non-small cell lung cancer , group of Dr. J.-L. Coll, <i>Institute Albert Bonniot, Grenoble, France</i>
2008, Jan-June	Exchange semester at the <i>Université Joseph Fourier, Grenoble, France</i>
2007, July-Sept	Serotonin signaling and depression , group of Dr. M. Panicker, <i>National Centre for Biological Sciences, Bangalore, India</i>
2006, June-July	Voluntary work , <i>Healesville Sanctuary, Victoria, Australia</i>
2006, Jan-Feb	DNA sequencing techniques & finger printing , <i>Institute of Forensic Medicine, Essen, Germany</i>
2005, Oct-Dec	Biofermentation techniques , <i>Pharma-Zentrale GmbH, Herdecke, Germany</i>

Grants

2010-2013	Fellow of the NotchIT 7th Framework Initial Training Programme / Marie Curie Actions
2008 Jan-June	Erasmus Mobility Grant in collaboration with <i>Université Joseph Fourier, Grenoble, France</i>
2007 July-Sept	German Academic Exchange Service Travel Grant to visit the <i>National Centre of</i>

Biological Sciences in Bangalore, India as research trainee

Scientific Publications

Götze S, Coersmeyer M, Müller O, Sievers S (2014). Histone deacetylase inhibitors induce attenuation of Wnt signaling and TCFL2 depletion in colorectal carcinoma cells. *Int J Oncol.* Oct;45(4):1715-23.

Languages

German	Mother tongue
English	Fluent written and spoken
French	Fluent written and spoken

References

Prof. Dr. Freddy Radtke	Mail address: EPFL SV ISREC UPRAD, SV 2534, Station 19, 1015 Lausanne, Switzerland Email address: freddy.radtke@epfl.ch Tel.: +41 21 693 07 71
Dr. Ute Koch	Mail address: EPFL SV ISREC UPRAD, SV 2534, Station 19, 1015 Lausanne, Switzerland Email address: ute.koch@epfl.ch Tel.: +41 21 693 07 75